

Copyright  
by  
Yunseong Cho  
2023

The Dissertation Committee for Yunseong Cho  
certifies that this is the approved version of the following dissertation:

**Towards Power-Efficient and Intelligent  
Wireless Communication Systems**

Committee:

---

Brian L. Evans, Supervisor

---

Jeffrey G. Andrews

---

Grani A. Hanasusanto

---

Hyeji Kim

---

Aryan Mokhtari

**Towards Power-Efficient and Intelligent  
Wireless Communication Systems**

by

**Yunseong Cho**

**DISSERTATION**

Presented to the Faculty of the Graduate School of  
The University of Texas at Austin  
in Partial Fulfillment  
of the Requirements  
for the Degree of

**DOCTOR OF PHILOSOPHY**

The University of Texas at Austin

August 2023

Dedicated to my wife Su Hyun Lee and my family.

## Acknowledgments

I would like to express my sincere appreciation to my supervisor Prof. Brian L. Evans. His constructive feedback, thoughtful insights, and encouragement have helped me become a better researcher and a better person. His mentorship has been invaluable, and I will always cherish the lessons I have learned from him.

I also wish to express my gratitude to the rest of my Ph.D. dissertation committee. Prof. Jeffery Andrews' extensive knowledge in wireless communications, Prof. Grani Hanasusanto's constructive feedback, Prof. Hyeji Kim's comprehensive knowledge in machine learning-based communications, and Prof. Aryan Mokhtari's optimization theories and skills have helped me explore challenging topics in a timely manner.

I want to thank my colleague Jinseok Choi as one of my academic mentors. His expertise and commitment to helping me succeed have made a tremendous impact on me. I would like to thank my talented colleagues from ESPL, WNCG, and 6G@UT and the affiliated industry leaders as well.

I would like to express my deep appreciation to my loving and supportive family members: my father, Kwangjun Cho, my mother, Mikyoung Ha, and my younger brother, Yunyeong Cho. Your passion, support, and unconditional love guide me throughout my life.

Last but not least, I appreciate my wife, Su Hyun Lee, more than words can express. Thank you for being my spouse and my best friend. You always have a warm embrace, and I feel incredibly lucky to have you by my side. Your kindness and understanding never cease to amaze me, and I am forever grateful for the way you make our environment a place of love and comfort.

# **Towards Power-Efficient and Intelligent Wireless Communication Systems**

Publication No. \_\_\_\_\_

Yunseong Cho, Ph.D.

The University of Texas at Austin, 2023

Supervisors: Brian L. Evans

With the growing demand for higher data rates and more reliable service capabilities, wireless communication systems continue to grow in popularity and importance. In order to enable higher data rate via broader bandwidth, millimeter wave (mmWave) systems are deployed for modern and future communication systems. Due to the high transmission loss of the mmWave frequency bands, a massive number of antennas are employed to focus transmitted power in narrow radio frequency (RF) beams. However, associating one RF chain with two high-resolution data converters for each antenna element would consume a prohibitively large amount of power. Furthermore, challenging service requirements can be handled by machine learning techniques in a variety of application spaces.

The goal of this dissertation is to propose communication systems that are not only reliable and high-performing, but also power-efficient as well as intelligent. Two possible ways to alleviate the huge power consumption problem

are 1) low-resolution data converters, and 2) hybrid analog-digital beamforming architectures since the former tries to reduce the power consumption of each individual RF chain and the latter directly scales down the number of RF chains. Additionally, intelligent communication systems that can adapt to changing network conditions and user requirements are crucial for ensuring reliable and efficient communication. In either case, these solutions introduce severe non-convexity and non-linearity to the entire system. In this regard, I propose new solutions that can respond to future communication systems requiring a fundamental re-design of current communication systems based on a power-efficient and intelligent framework.

First, I investigate a coordinated multipoint (CoMP) beamforming and power control problem for base stations (BSs) with a massive number of antenna arrays under coarse quantization by low-resolution analog-to-digital converters (ADCs) and digital-to-analog converters (DACs). I first formulate total power minimization problems of both uplink (UL) and downlink (DL) systems subject to signal-to-quantization-plus-interference-and-noise ratio (SQINR) constraints. I then show strong duality for the UL and DL problems under the coarse quantization condition when channel reciprocity holds with time-division duplexing (TDD) assumption. Leveraging the duality, I propose a framework that is directed toward a twofold aim: to discover the optimal transmit powers in UL by developing iterative algorithm in a distributed manner and to obtain the optimal precoder in DL as a scaled instance of UL combiner. Under homogeneous transmit power and SQINR constraints per



cell, I further derive a deterministic solution for the UL CoMP problem by analyzing the lower bound of the SQINR. Lastly, I extend the derived result to wideband orthogonal frequency-division multiplexing (OFDM) systems to optimize transmit power and beamformer for all subcarriers. Simulation results validate the theoretical results and proposed algorithms in terms of total transmit power, duality gap, and convergence.

Second, I aim to find the DL beamformer that minimizes the maximum power on transmit antenna array of each BS under received SQINR constraints while minimizing per-antenna transmit power for a more realistic deployment. I first formulate formulating the quantized DL OFDM antenna power minimax problem and deriving its associated dual problem. With proving strong duality, I use the associated UL dual solution to compute the DL beamformer. Subsequently, the DL beamformer is used in updating the covariance matrix of the uplink noise signals. The series of processes builds an efficient algorithm to find a numerical solution. Simulations validate the proposed algorithm in terms of the maximum antenna transmit power and peak-to-average-power ratio.

Third, I propose a learning-based maximum likelihood detection framework with an acceptable learning length for uplink massive multiple-input-multiple-output (MIMO) systems with one-bit ADCs. The learning-based detection only requires counting the occurrences of the quantized outputs at each antenna. The learning in the high signal-to-noise ratio (SNR) regime, however, needs excessive training to estimate the extremely small likelihood

probabilities. To address this drawback, I utilize a dithering signal to artificially decrease the SNR and then remove the impact of the dithering noise via post processing. I evolve the technique by developing an adaptive dither-and-learning method that updates the dithering power according the patterns observed in the quantized dithered signals. Lastly, the computed likelihood probabilities are utilized in deriving log-likelihood ratio to enable state-of-the-art channel coding schemes. I compare the uncoded and coded detection performance of the proposed algorithm with other learning-based frameworks and show that the proposed algorithm shows the performance closest to optimal performance.

Fourth, I propose a deep reinforcement learning (DRL)-based solution for joint hybrid beamforming (HB) and power control problems when multiple massive MIMO BSs are communicating with multiple users in the uplink mmWave band. The HB method requires both digital and analog beamformers, with the latter using discrete phase shifters to project high-dimensional antenna ports to low-dimensional logical ports and scale down the number of RF chains. However, this results in non-convexity, making the problem difficult to solve using existing algorithms. In multicell uplink communication systems, I aim to jointly design the HB at each BS and transmit power control of the associated users while ensuring that the received signal-to-interference-and-noise ratio (SINR) constraints are satisfied. Considering the use of the DRL-based approach and the primal problem, I formulate the RL basics. To handle the combination of discrete and continuous inputs, I use the DDPG RL

algorithm, which outputs a valid action that maps to the design factors. In particular, I aim to control each phase shifter individually by introducing an intermediate vector and applying a differentiable argmax function to estimate the phase angle index. The proposed method is evaluated through simulation results based on the achieved SINR.

The four contributions could make a worthwhile enhancement to the development of power-efficient and intelligent wireless communication systems by meeting the communication needs of modern society while minimizing energy consumption and maximizing the use of available resources.

# Table of Contents

<b>Acknowledgments</b>	<b>5</b>
<b>Abstract</b>	<b>7</b>
<b>List of Tables</b>	<b>17</b>
<b>List of Figures</b>	<b>18</b>
<b>Chapter 1. Introduction</b>	<b>21</b>
1.1 Background . . . . .	22
1.1.1 Wireless Communication Systems . . . . .	22
1.1.2 Multiple-Input Multiple-Output System . . . . .	23
1.1.3 Millimeter Wave Signals . . . . .	24
1.1.4 Low-Resolution Data Converters . . . . .	25
1.1.5 Hybrid Analog-Digital Beamforming Architecture . . . . .	26
1.1.6 Machine Learning . . . . .	27
1.2 Motivation . . . . .	29
1.3 Dissertation Summary . . . . .	30
1.3.1 Thesis Statement . . . . .	31
1.3.2 Overview of Contributions . . . . .	31
1.4 Notation and Abbreviations . . . . .	34
1.4.1 Notation . . . . .	34
1.4.2 Abbreviations . . . . .	35
<b>Chapter 2. Coordinated Beamforming and Power Control for Low-Resolution Systems: Total Power Minimization</b>	<b>39</b>
2.1 Introduction . . . . .	40
2.1.1 Prior Work . . . . .	41

2.1.2	Contributions . . . . .	45
2.2	System Model . . . . .	47
2.2.1	Uplink Narrowband System . . . . .	48
2.2.2	Downlink Narrowband System . . . . .	50
2.3	Uplink and Downlink Joint Beamforming and Power Control . . . . .	51
2.3.1	Uplink and Downlink Duality . . . . .	53
2.3.2	Distributed Iterative Algorithm . . . . .	54
2.3.3	Deterministic Solution for Homogeneous Transmit Power and SQINR Constraint per Cell . . . . .	57
2.4	Extension to Wideband OFDM Systems . . . . .	59
2.4.1	Uplink OFDM System with Low-resolution ADCs . . . . .	59
2.4.2	Downlink OFDM System with Low-resolution DACs . . . . .	63
2.4.3	Joint Beamforming and Power Control for Wideband OFDM Systems . . . . .	65
2.5	Simulation Results . . . . .	67
2.5.1	Covariance Estimation . . . . .	73
2.5.2	Complexity and Convergence . . . . .	74
2.5.3	Wideband OFDM Communications . . . . .	76
2.6	Conclusion . . . . .	77
2.7	Proof of Theorem 1 . . . . .	78
2.8	Proof of Corollary 1 . . . . .	81
2.9	Proof of Corollary 2 . . . . .	82
2.10	Proof of Corollary 3 . . . . .	83
2.11	Proof of Corollary 4 . . . . .	84
2.12	Proof of Theorem 2 . . . . .	85
2.13	Proof of Corollary 5 . . . . .	88
2.14	Proof of Corollary 6 . . . . .	88
<b>Chapter 3. Coordinated Per-Antenna Maximum Power Minimization for Low-Resolution Systems</b>		<b>93</b>
3.1	Introduction . . . . .	94
3.1.1	Prior Work . . . . .	95
3.1.2	Contributions . . . . .	100

3.2	System Model . . . . .	101
3.2.1	Network and Signal Model . . . . .	101
3.2.2	Problem Formulation . . . . .	105
3.3	Duality between Downlink and Uplink . . . . .	106
3.3.1	Dual UL OFDM Systems with Low-Resolution ADCs . . . . .	107
3.3.2	Downlink-Uplink Duality . . . . .	109
3.4	Proposed Solution for Joint Beamforming . . . . .	110
3.4.1	Optimal Downlink Precoder . . . . .	110
3.4.2	Iterative Algorithm via Dual Uplink Solution . . . . .	111
3.4.3	Convergence of Sub-problems . . . . .	115
3.4.4	Computational Complexity . . . . .	116
3.5	Simulation Results . . . . .	116
3.5.1	Wideband OFDM Communications . . . . .	117
3.5.2	Narrowband Communications . . . . .	121
3.5.3	Convergence . . . . .	122
3.5.4	Channel Estimation Error . . . . .	123
3.5.5	Peak-to-Average-Power Ratio (PAPR) . . . . .	125
3.6	Conclusion . . . . .	126
3.7	Proof of Theorem 3 . . . . .	127
3.8	Proof of Corollary 7 . . . . .	132
3.9	Proof of Corollary 8 . . . . .	134
3.10	Proof of Corollary 9 . . . . .	136
3.11	Proof of Corollary 10 . . . . .	136
3.12	Proof of Corollary 11 . . . . .	137

**Chapter 4. Learning-Based Maximum Likelihood Detection with One-Bit ADCs 142**

4.1	Introduction . . . . .	143
4.1.1	Prior Works . . . . .	144
4.1.2	Contributions . . . . .	147
4.2	System Model . . . . .	149
4.2.1	Signal Model . . . . .	149
4.2.2	One-Bit ML Detection with CSI . . . . .	151

4.3	Preliminary: Naive One-bit ML Detection without CSI . . . . .	153
4.4	Adaptive Statistical Learning without CSI . . . . .	156
4.4.1	Dithering-and-Learning . . . . .	157
4.4.2	Adaptive Dithering Power Update . . . . .	159
4.4.3	SNR Estimation . . . . .	161
4.5	Extension to Channel Coding . . . . .	162
4.5.1	Frame Structure . . . . .	163
4.5.2	Soft Metric . . . . .	164
4.6	Simulation Results . . . . .	166
4.6.1	Under-trained Likelihood Functions . . . . .	166
4.6.2	Uncoded System: Symbol Error Rate . . . . .	168
4.6.3	Coded System: Frame Error Rate . . . . .	173
4.7	Conclusion . . . . .	176

**Chapter 5. Joint Hybrid Beamforming and Power Control Using Deep Reinforcement Learning 177**

5.1	Introduction . . . . .	178
5.2	Prior Works . . . . .	179
5.3	Preliminaries . . . . .	181
5.3.1	Signal Model . . . . .	182
5.3.2	Channel Model . . . . .	184
5.3.3	Deep Reinforcement Learning . . . . .	185
5.4	Hybrid Beamforming and Power Control via Reinforcement Learning: Action Space . . . . .	187
5.4.1	Digital Beamformer . . . . .	187
5.4.2	Analog Beamformer . . . . .	187
5.4.3	Power Control . . . . .	190
5.4.4	Action Vector . . . . .	190
5.5	Hybrid Beamforming and Power Control via Reinforcement Learning: State and Reward . . . . .	191
5.5.1	State Space . . . . .	191
5.5.2	Reward . . . . .	191
5.6	Policy Gradient Deep Reinforcement Learning . . . . .	192

5.6.1	Critic Network . . . . .	193
5.6.2	Actor Network . . . . .	194
5.6.3	Replay Buffer . . . . .	194
5.6.4	Network Update . . . . .	194
5.7	Simulation Results . . . . .	196
5.8	Conclusion . . . . .	198
<b>Chapter 6. Concluding Remarks</b>		<b>199</b>
6.1	Summary and contributions . . . . .	199
6.2	Future work . . . . .	202
<b>Bibliography</b>		<b>207</b>
<b>Vita</b>		<b>225</b>



## List of Tables

2.1	Quantization Gain $\alpha$ For ADC Quantization Bits $b \leq 5$ . . . .	50
3.1	Comparison of peak-to-average power ratio (PAPR) for selected target SQINR values $\gamma$ . . . . .	141

## List of Figures

1.1	A receiver with low-resolution analog-to-digital converter and/or digital-to-analog converter. . . . .	26
1.2	A receiver with hybrid analog-digital beamforming architecture.	27
1.3	An agent-environment feedback loop of a generic reinforcement learning. . . . .	30
2.1	Multicell multiuser-MIMO network which is incorporated with low-resolution ADCs and DACs at the BS. . . . .	48
2.2	CDFs of the SQINRs of users in all cells for $\gamma = 0$ dB target SQINR, $b = 3$ quantization bits, and $N_b = 64$ BS antennas with (a) $N_c = 2$ cells with $N_u = 4$ users per cell and with (b) $N_c = 7$ cells with $N_u = 4$ users per cell. . . . .	68
2.3	UL total transmit power versus the target SQINR for $N_b = 64$ BS antennas, $N_c = 2$ cells and $N_u = 2$ users per cell. . . . .	70
2.4	Total transmit power versus the target SQINR for (a) the UL network with $N_b \in \{16, 128\}$ antennas, $N_c = 7$ cells, and $N_u = 4$ users per cell. . . . .	71
2.5	Total transmit power versus the target SQINR for the UL and DL networks with $N_b \in \{16, 32, 64\}$ BS antennas, $N_c = 3$ cells, $N_u = 3$ users per cell, and $b \in \{3, \infty\}$ quantization bits. The overlapped lines and markers can demonstrate the derived strong duality. . . . .	72
2.6	CDFs of the SQINRs of users in all cells for $\gamma = 0$ dB target SQINR, $b = 3$ quantization bits, $N_b = 64$ BS antennas, $N_c = 7$ cells, and $N_u = 4$ users per cell. . . . .	74
2.7	Convergence results for $N_b = 64$ antennas, $N_c = 4$ cells, $N_u = 3$ per cell, and $b = 3$ quantization bits. (a) shows total transmit power with respect to the number of iterations and (b) shows the total number of iterations for convergence with respect to time for channel realization. . . . .	90
2.8	UL total transmit power versus the target SQINR for $N_b = 16$ BS antennas, $N_c = 2$ cells, $N_u = 2$ users per cell, $b \in \{2, 3, 4, \infty\}$ quantization bits, and 64 subcarriers. . . . .	91

3.1	Multicell and multiuser MIMO communication configuration when each base station (BS) is equipped with low-resolution ADCs and DACs. The power amplifier causes nonlinear distortion in the high input power regime. . . . .	102
3.2	Maximum transmit antenna power versus the target SQINR for the multicell wideband network with $N_b = 16$ BS transmit antennas, $N_c = 4$ cells, $N_u = 2$ users per cell, $K = 32$ subcarriers, and $b \in \{2, 3, \infty\}$ bits. . . . .	118
3.3	Empirical CDFs of BS antennas with respect to antenna transmit power in the multicell network with $N_b = 32$ BS antennas, $N_c = 4$ cells, $N_u = 2$ users per cell, $K = 64$ subcarriers, $b = 3$ quantization bits, and $\gamma = -1$ dB target SQINR. . . . .	119
3.4	Maximum transmit antenna power versus target SQINR for the communication network with $N_b = 32$ transmit antennas per BS, $N_c = 4$ cells, $N_u = 2$ users per cell, $b \in \{2, 3, \infty\}$ bits, and $K = 1$ . . . . .	121
3.5	Empirical CDF of the transmit power of all BS transmit antennas in the network with $N_b = 32$ transmit antennas per BS, $N_c = 5$ cells, $N_u = 2$ users per cell, $b = 3$ quantization bits, $\gamma = 2$ dB target SQINR, and $K = 1$ . . . . .	123
3.6	Convergence behavior for $N_b = 32$ antennas, $N_c = 2$ cells, $N_u = 3$ users per cell, $b = 3$ bits, $K = 64$ subcarriers, and $\gamma \in \{-3, 0, 3\}$ dB. . . . .	124
3.7	CDFs of the SQINRs of users in all cells for $\gamma = 3$ dB target SQINR, $b = 3$ quantization bits, $N_b = 32$ BS antennas, $N_c = 4$ cells, and $N_u = 3$ users per cell with channel estimation error factor $e \in \{0, 0.1, 0.2\}$ . . . . .	125
4.1	Symbol error rate simulation results of the optimal one-bit ML detection with full CSI against naive learning-based one-bit ML detection for $N_r = 32$ receive antennas, $N_u = 3$ users, 4-QAM, and $N_{tr} \in \{10, 100, 1000\}$ pilot signals. . . . .	154
4.2	A receiver architecture for the pilot transmission phase with dithering signal added before quantization. Based on the feedback information, the variance of the dithering signal is updated.	156
4.3	Communication data frame with a pilot transmission and a data transmission phases. . . . .	157
4.4	Illustration of the SNR offline training via deep neural networks.	163

4.5	The number of under-trained likelihood functions among $2N_r$ likelihood functions for $N_u = 4$ users, 4-QAM, $N_r = 32$ antennas, and $N_{\text{tr}} = 45$ pilot signals with Rayleigh channels. The proposed adaptive dither-and-learning (ADL) method divides the training period into $N_s \in \{1, 3, 5\}$ sub-blocks for the feedback-driven update of dithering power. . . . .	167
4.6	Symbol error rate results with $N_u = 4$ users, $N_r = 32$ BS antennas, $N_{\text{tr}} = 45$ pilot signals, and 4-QAM constellation. The proposed adaptive dither-and-learning (ADL) uses $N_s \in \{1, 3\}$ split factors. . . . .	169
4.7	Symbol error rate results with $N_u = 4$ users, $N_r = 32$ BS antennas, $N_{\text{tr}} \in \{45, 90\}$ pilot signals, and 4-QAM constellation. The proposed adaptive dither-and-learning (ADL) uses $N_s \in \{1, 3\}$ split factors. . . . .	170
4.8	Symbol error rate results with $N_u = 3$ users, $N_r = 64$ BS antennas, $N_{\text{tr}} = 45$ pilot signals, and 16-QAM constellation. The proposed adaptive dither-and-learning (ADL) method divides the training period into $N_s \in \{1, 3\}$ sub-blocks. . . . .	172
4.9	Frame error rate results for $N_u = 4$ users, $N_r = 32$ BS antennas, $N_{\text{tr}} = 45$ , 4-QAM constellation, and a polar code of rate $1/2$ where $(\kappa, \eta) = (64, 128)$ . The proposed adaptive dither-and-learning (ADL) method learns the likelihood probability with split factor $N_s \in \{1, 3\}$ . The one-bit successive-cancellation soft-output (OSS) detector is valid in case of perfect CSI. . . . .	175
5.1	Illustration of hybrid beamforming architecture in a cell. . . . .	179
5.2	Illustration of deep reinforcement learning frame work via deep deterministic policy gradient approach. . . . .	182
5.3	The progress of the achieved SINRs and the reward. . . . .	197
6.1	Syetem model with reconfigurable intelligent surfaces. . . . .	206

# Chapter 1

## Introduction

As the need for faster data rates and more dependable service features increases, wireless communication systems are becoming increasingly popular and significant. The potential of the mmWave frequency band lies in the development of communication systems that can facilitate high-speed data transmission in wireless local area networks and fifth-generation (5G) cellular networks. The mmWave holds promise for achieving its potential via its large transmission bandwidths and the small carrier wavelengths that make it possible to create an array of antennas that features a substantial number of antenna elements. These arrays can generate the required array gain for establishing high-quality communication links and achieve huge beamforming gain by creating a narrow beam to a desired direction. The employment of massive antenna arrays, however, gets into trouble due to high power consumption caused by a number of radio frequency (RF) components. In this regard, low-power solutions need to be explored while maintaining challenging requirements. In this dissertation, I present prospective solutions for the design of communication functions such as beamforming, power control, and data detection when considering non-linear yet non-convex system distortion caused by the low-power system architecture.

In this introductory chapter, I provide relevant information, the motivation behind the research problems handled in this dissertation, and a summary of my contributions. In Section 1.1, I start with providing an overview of the contextual information that pertains to my research. In Section 1.2, I present the motivation behind the proposed research. Section 1.3 summarizes the contributions of the proposed research. In Section 1.4, the notation and abbreviations are provided for clarity and ease of understanding.

## **1.1 Background**

In this section, I provide a brief overview of the background that is relevant to my research.

### **1.1.1 Wireless Communication Systems**

A cellular network is based on the concept of dividing the geographic area into smaller regions where user devices in each region are covered by at least one base station (BS). Cellular networks consist of numerous users who utilize mobile devices, such as tablets and mobile phones, and a vast number of fixed BSs that are organized to provide users with coverage within their respective cells. The wireless link that enables data transmission from a BS to mobile users is referred to as the downlink system, while the signal directed from mobile users to the BS is called the uplink system. To divide the uplink and downlink in wireless communication, two methods are used: time division duplex (TDD) and frequency division duplex (FDD). TDD separates

the two domains in the time domain, while FDD separates them using different frequency bands.

Wireless communications encounter two major issues, namely fading and interference, which are not present in wireline communications. Fading is caused by fluctuations in channel strengths over time, which result from the effects of multi-path fading, path loss, and shadowing. Unlike thermal noise, interference appears when signals are disrupted or weakened by the presence of other wireless signals. Inter-symbol interference occurs at the receiver due to delays caused by multiple paths from the transmitter to the receiver, resulting in interference for subsequent transmissions. When multiple users communicate with the same BS using the same time and frequency resource, there exists a significant amount of interference in the link, which is referred to as inter-user interference. In a wireless communication environment with multiple coexisting cells, incoming signals from neighboring cells can cause interference with the co-channel signals of the current cell, known as inter-cell interference. Designing wireless communication systems that effectively manage interference is one of the most significant challenges.

### **1.1.2 Multiple-Input Multiple-Output System**

The typical error event occurs when the channel is in a deep fade. As one of the techniques that combat deep fading, multiple antennas are employed at the transmitters and/or receivers to achieve spatial diversity. When having multiple antenna ports at both transmitters and receivers, the system

is called a multiple-input-multiple-output (MIMO) system. By leveraging the full potential of many antennas, MIMO communication systems can achieve increased data rates via multiplexing gain and increased reliability via enhanced diversity gain.

Employing many antennas can also provide beamforming gain. Beamforming is a technique used in wireless communications to enhance signal strength in a specific direction by having individually controllable phase and amplitude. By focusing the signal in a specific direction, beamforming can improve signal quality, reduce interference, and increase the coverage of the wireless signal. Channel State Information (CSI) is typically used to help the antenna arrays form the beam pointing at the transceiver. This information includes the strength and quality of the received signal, as well as the distance and location of the receiver. Beamforming is a key technology in modern wireless communication systems and can be used in a variety of applications, including cellular networks, Wi-Fi, and satellite communications.

### **1.1.3 Millimeter Wave Signals**

Modern and future wireless communication systems regard a millimeter wave (mmWave) spectrum that extends from 10 to 300 GHz as a promising technology to provide a remarkable increase in both data rates and energy-efficiency [4, 91]. However, radio signals with high frequencies are known to experience significant power attenuation as propagation distance increases. In comparison to traditional MIMO communication systems that operate at



sub-3 GHz frequencies and have a limited number of antennas, mmWave systems can accommodate a larger number of antennas in the transceivers due to the smaller wavelength of the mmWave spectrum. Large antenna arrays in mmWave systems can enable the use of directional beamforming, which is crucial in achieving high beamforming gain. This is necessary to overcome the significant free-space pathloss of mmWave signals and achieve an adequate strength of received signal-to-noise ratio (SNR).

#### 1.1.4 Low-Resolution Data Converters

Increasing the number of antenna chains results in the increased number of RF chains, thereby locating a plethora of analog-to-digital converters (ADCs) and digital-to-analog converters (DACs). ADCs and DACs are the power-hungry component in the transceiver. Since the power consumption of an RF chain exponentially increases with the number of quantization bits  $b$ , i.e.,  $P \propto 2^b$  [94], replacing high-resolution data converters with low-resolution data converters (typically 1-4 bits) can significantly reduce power consumption. The general illustration of low-resolution systems is shown in Fig. 1.1. However, the reduction in resolution results in non-negligible and non-linear quantization error which degrades the overall performance and makes it difficult to directly apply existing methods. It is unavoidable to experience performance degradation when using coarse quantization; however, lots of recent efforts show that the loss can be reduced by carefully analyzing and designing low-resolution systems.

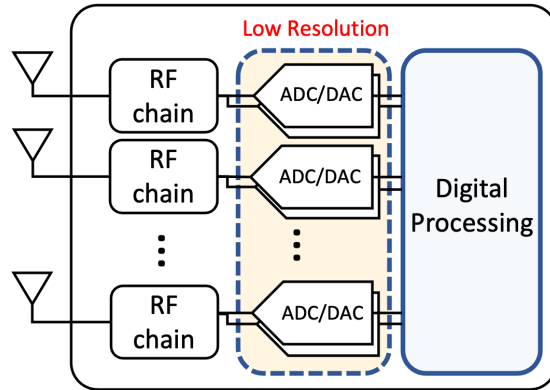


Figure 1.1: A receiver with low-resolution analog-to-digital converter and/or digital-to-analog converter.

In order to properly handle the severe nonlinearities in low-resolution ADCs, many studies have re-engineered essential wireless communication functions such as channel estimation and data detection [17, 22, 39, 89, 97, 98]. For downlink transmission, a number of works have reduced hardware cost using low-resolution DACs [38, 51, 71].

### 1.1.5 Hybrid Analog-Digital Beamforming Architecture

In conventional MIMO communication systems, each antenna element is connected to its dedicated RF chain which owns two power-hungry data converters. This architecture is called an all-digital beamforming architecture, which is highly flexible but also expensive and power-intensive. Therefore, the power consumption generally scales with the number of antennas at a BS. Because of the problem caused by having too many RF chains, the notion of hybrid analog-digital beamforming architecture (HB) appears. As shown in Fig. 1.2, the HB aims to cut down the number of RF chains by separating the

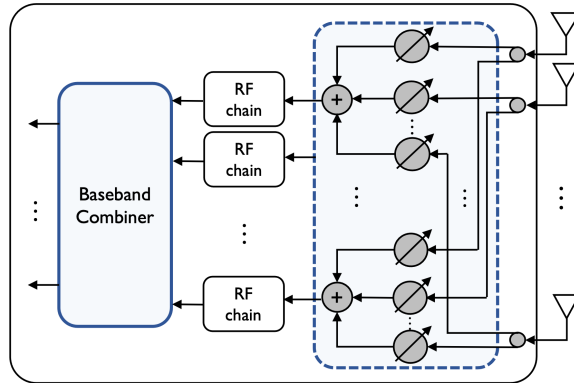


Figure 1.2: A receiver with hybrid analog-digital beamforming architecture.

combining process into two parts: analog beamforming and digital beamforming. To produce high beamforming gain and immunize against large free-space pathloss, the analog beamformer manipulates directional propagation paths via the array of phase shifters. Afterward, the digital beamformer carries out multi-stream baseband processing on the low-dimensional input produced by the analog beamformer. The analog beamformer is newly introduced considering the propagation characteristics of mmWave systems; however, the analog beamformer introduces non-convex behavior due to the unit-modulus constraint of the phase shifters. Therefore, beamforming-related signal processing functions need to be revised for the HB systems.

### 1.1.6 Machine Learning

Machine learning is a method of data analysis that automates analytical model building by enabling machines to learn and estimate complex functions on specific tasks, without requiring explicit one-on-one programming. Machine

learning algorithms aim to build a black box using sampled data points, to make decisions or predictions of new observations. Although machine learning is related to computational statistics, mathematical optimization also plays a vital role in this field. The learner splits all available data points into three disjoint groups, which are the training dataset, validation dataset, and test dataset. The training dataset is the collection of data points which are directly used to fit the model. The validation dataset is the sample of data to be utilized to offer an assessment of the trained model while tuning model hyperparameters and modifying model complexity. The test dataset is private during the training stage to provide a final evaluation of the trained model. There exist three types of machine learning strategies: 1) supervised learning, 2) unsupervised learning, and 3) reinforcement learning.

Supervised learning can be applied to problems where labeled data, i.e., ground truth, is included in the training data set along with feature vectors. The primary objective of supervised learning algorithms is to learn a function that can successfully infer an estimated label using a given feature vector. A supervised classification problem aims to predict the probability or likelihood that the test data belongs to one of the predefined discrete categories. In contrast, a supervised regression problem tries to plot a best-fit curve of the training data set and to predict the continuous outcome of feature vectors. Typically, the learning stage of supervised learning is minimizing or optimizing a loss function where binary cross-entropy and mean-squared error are used for the classification problem and the regression problem, respectively.

Unsupervised learning is a type of data-driven problem that involves examining unlabeled datasets and identifying hidden patterns or clusters without the involvement of human intervention. The primary feature that sets unsupervised learning apart is the absence of ground truth. For example, clustering and autoencoder fall under this category. Clustering refers to the task of organizing a set of similar data points into the same cluster. Autoencoder aims to encode high-dimensional unlabeled data into a low-dimensional latent space and use the compressed feature to decode the original data. This framework needs to make sure that the encoded latent representation is rich enough to minimize reconstruction error.

Last but not least, reinforcement learning (RL) is a machine learning technique that facilitates an agent's learning in an interactive environment by utilizing trial and error and feedback derived from its own actions and experiences. The objective is to develop an effective action model that maximizes the agent's total cumulative reward. The agent-environment feedback loop of a generic RL model is illustrated in Fig. 1.3. Since the RL approach learns from experiences and mistakes, it is crucial to strike a balance between exploitation and exploration.

## 1.2 Motivation

There exist two potential low-power architectures: 1) low-resolution data converters and 2) HB architecture. The implementation of wireless communication systems using low-power architectures necessitates modifications

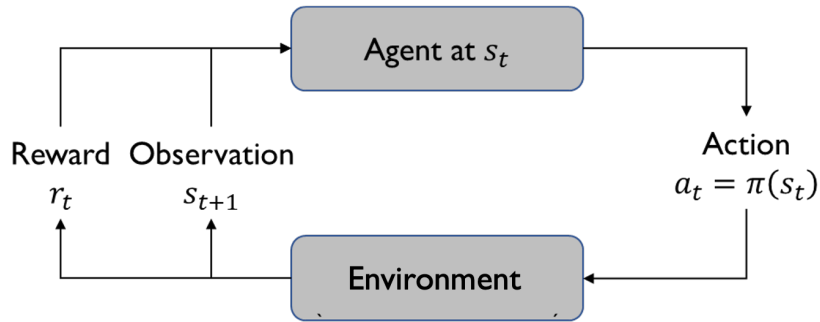


Figure 1.3: An agent-environment feedback loop of a generic reinforcement learning.

to core signal processing operations. The low-power structures naturally introduce severe impairments to the system due to the coarse quantization and the analog beamformer of the HB. However, it is unclear whether the previous findings in prior research are still applicable in low-resolution ADC and DAC systems or the HB due to these impairments. Therefore, I take into account those negative impacts for the thorough investigation of key communication functions such as beamformer, power control, and data detection when considering either low-resolution data converters or the HB.

### 1.3 Dissertation Summary

In summary, I have made a commitment to the development of advanced power-efficient and intelligent solutions for beamforming and detection, which in turn minimize power consumption, enable near-optimal error probability, and guarantee signal strength requirements.

### 1.3.1 Thesis Statement

In this dissertation, I define the following statement:

*Advanced power-efficient and intelligent communication techniques have the ability to satisfy challenging requirements and improve key performance indicators despite the presence of severe distortion and non-linearity caused by low-power architectures.*

### 1.3.2 Overview of Contributions

The main contributions of this dissertation are summarized as follows:

- **Chapter 2: Coordinated Beamforming and Power Control for Low-Resolution Systems: Total Power Minimization**

1. I propose an optimal coordinated multipoint (CoMP) beamforming algorithm for the wireless communication systems equipped with low-resolution ADCs or DACs to achieve the desired signal-to-quantization-and-interference-plus-noise ratio (SQINR) with minimum total transmit power.
2. I formulate total power minimization problems for both uplink (UL) and downlink (DL) systems, while taking into account non-negligible quantization noise and interference, subject to SQINR constraints. I derive strong duality between the UL and DL problems, with coarse quantization systems being taken into consideration.

3. I propose a framework that aims to determine the optimal UL transmit power and DL precoder using the aforementioned duality. Moreover, I extend the results obtained to wideband orthogonal frequency-division multiplexing (OFDM) systems.
4. I derive a deterministic solution for the UL CoMP problem by analyzing the lower bound of the SQINR under homogeneous transmit power and SQINR constraints per cell.

- **Chapter 3: Coordinated Per-Antenna Maximum Power Minimization for Low-Resolution Systems**

1. I propose a multicell-coordinated beamforming solution for the maximum power minimization problem with per-antenna power constraints to place less burden on power amplifiers and other electronics.
2. I formulate the quantized DL OFDM antenna power minimax problem with per-antenna constraints and deriving its associated dual problem which is interpreted as a virtual UL OFDM problem powered by unknown yet tunable covariance matrices. I manipulate the constraints to show that strong duality holds between the aforementioned DL and UL problems.
3. I develop an iterative minimax algorithm to identify a feasible solution for the dual problem. This particular problem involves the



joint optimization of virtual UL transmit power and noise covariance matrices To tackle this issue, I begin by determining the optimal dual solution of the UL problem for given noise covariance matrices. I then utilize the solution to compute the associated DL beamformer. Finally, the UL noise covariance matrices are updated using subgradient projection based on the DL beamformer.

- **Chapter 4: Learning-Based Maximum Likelihood Detection with One-Bit ADCs**

1. I propose a learning-based maximum likelihood detection framework for the uplink systems with one-bit ADCs to complete the learning stage within acceptable training length.
2. To facilitate the acquisition of the small probabilities that appear at the high SNR regime, I propose a dither-and-learning technique that adds a dithering signal with known statistics to artificially decrease the SNR and removes the impact of the artificial noise from the inferred likelihood functions.
3. I propose how to adjust the dithering power according to the observed patterns of the quantized and dithered signals. I compute a bit-wise and user-wise log-likelihood ratio from the refined likelihood probabilities to enable state-of-the-art channel coding schemes.

- **Chapter 5: Joint Hybrid Beamforming and Power Control Using Deep Reinforcement Learning:**

1. I propose a DRL-based solution for joint hybrid beamforming and power control problems when multiple massive MIMO BSs with hybrid beamforming architecture are communicating with multiple users in the uplink mmWave band.
2. I formulate the main problem that jointly design the HB at each BS and transmit power control of the associated users in a way that the total power is minimized while ensuring that the signal-to-interference-plus-noise ratio constraints are satisfied.
3. I utilize the DDPG RL algorithm to address the combination of discrete and continuous inputs. This algorithm produces an appropriate action that corresponds to the design factors. Specifically, I aim to exert individual control over each phase shifter by introducing an intermediate vector and employing a differentiable argmax function to estimate the phase angle index.

## 1.4 Notation and Abbreviations

### 1.4.1 Notation

$\mathbf{A}$  denotes a matrix and  $\mathbf{a}$  represents a column vector.  $\mathbf{A}^H$  and  $\mathbf{A}^T$  denote conjugate transpose and transpose, respectively.  $[\mathbf{A}]_i$  and  $\mathbf{a}_i$  indicate the  $i$ th column vector of  $\mathbf{A}$ .  $[\mathbf{A}]_{i,:}$  and  $\mathbf{a}_{i,:}$  indicates the  $i$ th row vector of  $\mathbf{A}$ . I denote  $a_{i,j}$  as the  $\{i,j\}$ th element of  $\mathbf{A}$  and  $a_i$  as the  $i$ th element of  $\mathbf{a}$ . With mean  $\mu$  and variance  $\sigma^2$ , a real Gaussian distribution and a complex Gaussian distribution using  $\mathcal{N}(\mu, \sigma^2)$  and  $\mathcal{CN}(\mu, \sigma^2)$  are generated, respectively.

The diagonal matrix  $\text{diag}(\mathbf{A})$  has  $\{a_{i,i}\}$  as its diagonal entries, and  $\text{diag}(\mathbf{a})$  or  $\text{diag}(\mathbf{a}^T)$  creates a diagonal matrix with  $\{a_i\}$  as its diagonal entries. A block diagonal matrix is denoted as  $\text{blkdiag}(\mathbf{A}_1, \dots, \mathbf{A}_N)$ . A block circulant matrix is denoted as  $\text{blkcirc}(\mathbf{A}_1, \dots, \mathbf{A}_N)$  with a first block-row of  $\mathbf{A}_1, \dots, \mathbf{A}_N$ .  $\text{eig}_M(\mathbf{A})$  and  $\text{eig}_m(\mathbf{A})$  denote the maximum and minimum eigenvalues of  $\mathbf{A}$ , respectively. The vectorization operation of a matrix  $\mathbf{A}$  with  $n$  columns is defined as  $\text{vec}(\mathbf{A}) = [\mathbf{A}]_1^T, \dots, [\mathbf{A}]_n^T]^T$ .  $\mathbf{1}_N$  and  $\mathbf{0}_N$  are a  $N \times 1$  one vector and zero vector, respectively.  $\mathbf{I}_N$  denotes the  $N \times N$  identity matrix.  $\text{Re}\{\mathbf{A}\}$  and  $\text{Im}\{\mathbf{A}\}$  take the real and imaginary part of  $\mathbf{A}$ , respectively.  $\mathbb{1}_{\{A\}}$  denotes the indicator function which outputs 1 if  $A$  is true, and 0 otherwise.  $\otimes$  is used to denote Kronecker product operator.  $\|\mathbf{A}\|$  represents  $L_2$  norm. Matrix inequality is denoted by  $\preceq$ .  $\mathbb{P}[\cdot]$  and  $\mathbb{E}[\cdot]$  are the probability and expectation operators, respectively.

#### 1.4.2 Abbreviations

**5G** fifth-generation

**ADC** analog-to-digital converter

**ADL** adaptive dither-and-learning

**AoA** angle of arrival

**APP** a posteriori probability

**AQNM** additive quantization noise model

**AWGN** additive white Gaussian noise

**BER** bit error rate

**BS** base station

**CDF** cumulative density function

**CoMP** coordinated multipoint

**CP** cyclic prefix

**CSI** channel state information

**DAC** digital-to-analog converter

**DDPG** deep deterministic policy gradient

**DFT** discrete Fourier transformation

**DL** downlink

**DNN** deep neural network

**DRL** deep reinforcement learning

**FER** frame error rate

**GoB** grid-of-beams

**KKT** Karush-Kuhn-Tucker

**LLR** log-likelihood ratio

**LS** least-square

**MCD** minimum-center-distance

**MIMO** multiple-input-multiple-output

**ML** maximum-likelihood

**MMSE** minimum mean-squared-error

**mmWave** millimeter wave

**NGoB** none-grid-of-beams

**OFDM** orthogonal frequency division multiplexing

**OSS** one-bit successive cancellation soft-output

**PAPR** peak-to-average power ratio

**QAM** quadrature-amplitude-modulation

**Q-CoMP** quantization-aware CoMP

**Q-CoMP-PA** quantized CoMP under per-antenna power constraints

**Q-dCoMP** quantization-aware deterministic CoMP

**Q-iCoMP** quantization-aware iterative CoMP

**Q-PerCell** quantization-aware per-cell

**RF** radio frequency

**RL** reinforcement learning

**SER** symbol error rate

**SNR** signal-to-noise ratio

**SOCP** second-order cone program

**SQINR** signal-to-quantization-and-interference-plus-noise ratio

**TDD** time-division duplexing

**UL** uplink

**ULA** uniform linear array

**ZF** zero-forcing

## Chapter 2

# Coordinated Beamforming and Power Control for Low-Resolution Systems: Total Power Minimization

In this chapter<sup>1</sup>, I investigate a coordinated multipoint (CoMP) beamforming and power control problem for BSs with a massive number of antenna arrays under coarse quantization at low-resolution analog-to-digital converters (ADCs) and digital-to-analog converters (DACs). Unlike high-resolution ADC and DAC systems, non-negligible quantization noise that needs to be considered in CoMP design makes the problem more challenging. I first formulate total power minimization problems of both uplink (UL) and downlink (DL) systems subject to signal-to-quantization-and-interference-plus-noise ratio (SQINR) constraints considering non-negligible quantization noise and interference. I then derive strong duality for the UL and DL problems under coarse quantization systems. Leveraging the duality, I propose a framework

---

<sup>1</sup>This chapter is based on the work published in the following journal paper: J. Choi, Y. Cho, and B. L. Evans, “Quantized Massive MIMO Systems With Multicell Coordinated Beamforming and Power Control,” in *IEEE Transactions on Communications*, vol. 69, no. 2, pp.946-961, Dec. 2020. This work was published in part in the following conference paper: Y. Cho, J. Choi, and B. L. Evans, “Coordinated Multicell Beamforming and Power Allocation for Massive MIMO with Low-Resolution ADC/DAC,” in *IEEE International Conference on Communications (ICC)*, Jun. 14-23, 2021. This work was supervised by Prof. Brian L. Evans.

that is directed toward finding the optimal UL transmit power and the optimal DL precoder. I also extend the derived result to wideband orthogonal frequency-division multiplexing systems to optimize transmit power and beamformer for all subcarriers. Under homogeneous transmit power and SINR constraints per cell, I further derive a deterministic solution for the UL CoMP problem by analyzing the lower bound of the SQINR.

## 2.1 Introduction

Employing large-scale antenna arrays at the BS has been widely studied in last decades as a potential future wireless communication technology because of its significant gain in spectral efficiency [56]. Due to the large number of antennas followed by power-demanding high-resolution ADCs and DACs, however, significant power consumption becomes one of the primary practical challenges in realizing the system. Accordingly, employing low-resolution quantizers has attracted the most interest as a low-power solution in recent years [22, 38, 48, 89]. In multicell systems, non-negligible quantization error due to the low-resolution quantizers is a function of not only the in-cell channels and beamformers but also the inter-cell channels and beamformers. In this regard, I investigate CoMP beamforming and power control problems in low-resolution massive multiple-input and multiple-output (MIMO) systems to take into account the effect of the quantization error to the beamformer design and power control in the multicell communications.



### 2.1.1 Prior Work

As modern cellular systems operate on the interference-limited regime, the coordination between base stations (BSs) or users has shown large gain in communication performance [8, 23, 36, 44, 65, 80, 85, 87, 88]. Due to the difficulty in designing DL BF, the DL beamforming was derived by exploiting a virtual UL concept based on the duality between UL single-input and multiple-output and DL multiple-input and single-output systems. In [8], relaxing and casting the DL beamforming problem into a semidefinite optimization problem, a DL beamforming solution was efficiently computed by using interior point methods. In addition to the semidefinite relaxation optimization for the beamforming design, BS allocation and congestion control were further investigated in [88], providing substantial increase in the system performance. Assuming interference only from adjacent cells, a Kalman smoothing based beamforming method was developed by recasting the DL beamforming problem to a virtual minimum mean-squared error (MMSE) estimation problem to design network-wide MMSE beamforming without requiring a central processing unit [65]. Linear programming-based network duality for MIMO UL and DL with a single layer was leveraged in [87] to develop more efficient beamforming algorithms both in convergence and performance. Lagrangian based duality for multiuser MIMO systems was further derived in [23] and used to propose an distributed algorithm, requiring less synchronization and complexity burden on users and BSs. Practical constraints such as limited backhaul capacity was considered in [80], and a CoMP beamforming system was imple-

mented in a real field testbed in [36], showing its benefits in spectral efficiency especially for cell edge users. Improving the data rates of cell-edge users, a CoMP beamforming problem based on interference alignment was also studied in a non-orthogonal multiple access system [85]. Recently, understanding the benefit of employing a large antenna arrays at the BS, the performance gain from using massive antenna arrays jointly with CoMP beamforming was demonstrated by providing a more robust link and more localized interference [44]. The authors in [81] proposed the efficient and reliable multiplexing scheme in case of multi-user connectivity. Although prior findings in MIMO CoMP systems can be naturally extended to massive MIMO systems with high-resolution ADCs and DACs, employing low-resolution ADCs and DACs further needs to be considered to address the excessive power consumption problem.

Problems of minimizing transmit power for given quality of service constraints were often investigated [37, 76, 77]. In case of single MIMO systems, the authors in [37] presented the generic class of optimization problems that can embrace many wireless communication problems subject to power constraints. In [77], a multicell CoMP UL beamforming and power control method was developed by utilizing a fixed point iteration method. In addition, a multicell CoMP DL beamforming and power control method was further proposed in [76].

To achieve power-efficient communications, low-resolution ADC architectures have been extensively investigated in recent years [17–19, 22, 39, 41,

52, 69, 89, 97, 98, 104, 110]. As an effort to realize low-resolution ADC systems, essential wireless communication techniques such as channel estimation and detection have been developed in low-resolution ADC systems [17, 22, 39, 41, 52, 89, 97, 98]. Unified frameworks for channel estimation and symbol detection were developed for 1-bit ADC systems by using 1-bit maximum likelihood estimation [22]. Quantized maximum a-posteriori channel estimation and data detection were also developed by showing that 4-bit ADCs yield no performance loss from infinite-resolution ADCs [89]. For orthogonal frequency-division multiplexing (OFDM) systems, a generalized turbo estimator was utilized for channel estimation and symbol detection with over-the-air experiments, showing reasonable reliability when using low-resolution ADCs [97, 98]. In [17, 41], learning-based detectors were proposed without requiring explicit channel estimation. As a special low-resolution ADC system, a detector for mixed-ADC systems was proposed in [110]. In addition, a resolution-adaptive ADC system was proposed with near optimal bit-allocation solutions [18]. For tractability, linear quantization models such as Bussgang decomposition [39, 52] and an additive quantization noise model (AQNM) [19, 69, 104] were utilized by providing insightful analytical results.

Low-resolution DAC systems have also been studied in many literatures [38, 48, 95]. Achievable rates with linear precoders were derived in low-resolution DAC systems, and a nonlinear precoder was developed for 1-bit DAC systems, showing that using 3-4 bits offers comparable performance to infinite-resolution DACs and that the proposed 1-bit precoder causes only 3 dB loss

from infinite-resolution DACs [38]. A universal precoding approach was further developed in [95] by improving the performance and complexity trade-off from [38]. The rate analysis in [51] showed that using  $2.5\times$  more antennas can compensate for performance loss due to using 1-bit DACs. In addition, a constructive interference approach was adopted in [48] to develop a low-complexity precoder for 1-bit DAC systems. For orthogonal frequency-division multiplexing (OFDM) systems, the rate and bit-error-rate (BER) analysis in [40] demonstrated that using 3-4 bits can achieve the BER comparable to that of infinite-resolution DAC systems. A mixed-DAC as well as mixed-ADC system was also considered in [108] for relaying channels. Bussgang decomposition was adopted in [38, 51, 103] to linearize the low-resolution DAC system to develop precoder and analyze system performance. Interestingly, it was shown in [103] that employing low-resolution DACs can offer more reliable secure communication depending on system configuration. The AQNM was also used in [24, 78]. In [78], numerical comparison among digital beamforming and hybrid analog and digital beamforming with fully-connected and partially-connected phase shifter networks was provided. In [24], using low-resolution ADCs and DACs provided benefits in reducing power consumption while maintaining achievable rate in full duplex systems.

The prior works on low-resolution ADCs and DACs disclose that using low-resolution quantizers can significantly reduce the power consumption at the BSs while maintaining desirable spectral efficiency. Given the benefit of using low-resolution ADCs and DACs in the spectral efficiency and energy effi-

ciency trade-off, it is indispensable to consider coarse quantization systems for CoMP beamforming with massive antenna arrays. However, the non-negligible quantization error that is a function of channels, beamformers and transmit power makes the CoMP problem more challenging to solve. Due to the quantization error, it is unknown whether previous findings in the prior works can still be valid in the low-resolution ADC and DAC systems. Regarding the OFDM system, the quantization effect involves the OFDM modulations as well as beamforming and channels, which leads to highly complicated problems. Therefore, comprehensive study on CoMP for massive MIMO systems with low-resolution ADCs and DACs is desirable.

### 2.1.2 Contributions

In this work, I investigate joint beamforming and power control problems in coordinated multicell networks with BSs equipped with a large number of antenna arrays. I focus on coarse quantization systems where the BSs are equipped with low-resolution ADCs and DACs to achieve energy-efficient communications. Accordingly, the non-negligible quantization error which involves various system functions needs to be properly manipulated. For tractability, I adopt the AQNM for modeling the quantization system. The contributions are summarized as follows:

- First of all, I formulate the minimum total transmit power problem subject to individual SQINR constraints for both DL and UL. Then I prove the duality between the DL and UL problems under the coarse quanti-

zation systems by showing that the Lagrangian dual problem of the DL problem is equivalent to the UL problem with MMSE combiners. I further demonstrate that there is no duality gap, i.e., strong duality holds, by casting the DL problem into a standard second order conic problem and by showing strict feasibility with respect to the beamformer.

- Leveraging the strong duality, I propose a fixed point iterative algorithm to jointly solve the DL and UL problems. Using the properties of a standard function, I show that the algorithm converges to a unique optimal set of transmit powers for the UL problem. I further show that the optimal DL beamformers can be obtained by scaling the UL MMSE combiner that includes the optimal transmit powers. I also remark that the proposed algorithm can be implemented in a distributed manner with in-cell channel knowledge and without requiring explicit estimation of inter-cell channels.
- Assuming homogeneous transmit powers and SQINR constraints per cell, a deterministic algorithm is developed to provide a closed-form solution for the UL beamforming and power control problem. To this end, I consider an MMSE equalizer and derive a lower bound of the minimum SQINR for each cell. Then the solution is derived as a linear function of the SQINR constraints and maximum eigenvalues of matrices that are composed of channels.
- I extend the CoMP beamforming and power control problem to a wide-

band OFDM system. I first derive DL and UL system models by incorporating the coarse quantization effect into the OFDM modulation. Then I formulate the minimum total transmit power problems for UL and DL to find the optimal beamformer and transmit power for each user and subcarrier subject to the SQINR constraints for each user and subcarrier. Manipulating the quantization error that is intertwined with not only the channels, beamformers, and transmit power but also the OFDM modulation, I show that the strong duality also holds for the wideband OFDM systems and the similar results as the narrowband system can be applied.

- Simulation results validate the derived theoretical results and demonstrate that the proposed iterative CoMP algorithm achieves the target SQINR. The algorithm also outperforms a conventional per-cell method in terms of accuracy and minimizing total transmit power.

## 2.2 System Model

I consider a multicell multiuser-MIMO network with  $N_c$  cells,  $N_u$  single-antenna users per cell. Users are served by an associated BS with  $N_b$  antennas ( $N_b \gg N_u$ ), i.e., users in cell  $i$  are served by a BS in cell  $i$ . I assume that the BSs for all  $N_c$  cells are equipped with low-resolution ADCs and DACs with equal bits, i.e.,  $b$ -bit ADCs and DACs for all BSs and all BSs cooperate as shown in Fig. 2.1. Time-division duplexing (TDD) is considered in the system.

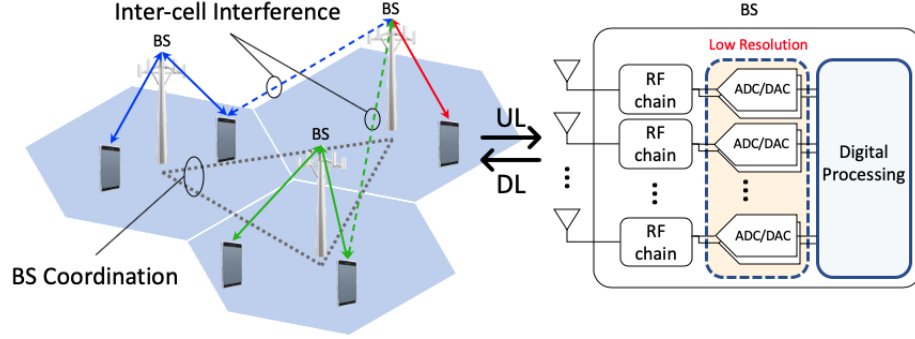


Figure 2.1: Multicell multiuser-MIMO network which is incorporated with low-resolution ADCs and DACs at the BS.

### 2.2.1 Uplink Narrowband System

Each user  $u$  in cell  $i$  transmits signal  $x_{i,u}^{\text{ul}} = \sqrt{\lambda_{i,u}} s_{i,u}^{\text{ul}}$  over a narrowband channel, where  $\lambda_{i,u}$  and  $s_{i,u}^{\text{ul}}$  are transmit power and a symbol, respectively. The narrowband channel vector between user  $u$  in cell  $j$  and the BS in cell  $i$  ( $\text{BS}_i$ ) is represented as  $\mathbf{h}_{i,j,u} \in \mathbb{C}^{N_b}$ . Then, the received baseband analog signal at  $\text{BS}_i$  is expressed as

$$\begin{aligned}
 \mathbf{r}_i^{\text{ul}} &= \mathbf{H}_{i,i} \mathbf{x}_i^{\text{ul}} + \sum_{j \neq i}^{N_c} \mathbf{H}_{i,j} \mathbf{x}_j^{\text{ul}} + \mathbf{n}_i^{\text{ul}} \\
 &= \mathbf{H}_{i,i} \mathbf{\Lambda}_i^{1/2} \mathbf{s}_i^{\text{ul}} + \sum_{j \neq i}^{N_c} \mathbf{H}_{i,j} \mathbf{\Lambda}_j^{1/2} \mathbf{s}_j^{\text{ul}} + \mathbf{n}_i^{\text{ul}}
 \end{aligned} \tag{2.1}$$

where  $\mathbf{H}_{i,j} \in \mathbb{C}^{N_b \times N_u}$  is the channel matrix between  $\text{BS}_i$  and users in cell  $j$  whose  $u$ th column is  $\mathbf{h}_{i,j,u}$ ,  $\mathbf{x}_i^{\text{ul}} \in \mathbb{C}^{N_u}$  and  $\mathbf{s}_i^{\text{ul}} \in \mathbb{C}^{N_u}$  are the transmit signal and symbol vectors of the  $N_u$  users in cell  $i$ , whose  $u$ th entries are  $x_{i,u}^{\text{ul}}$  and  $s_{i,u}^{\text{ul}}$ , respectively,  $\mathbf{\Lambda}_i = \text{diag}(\lambda_{i,1}, \dots, \lambda_{i,N_u})$  is the transmit power matrix of the users in cell  $i$ , and  $\mathbf{n}_i^{\text{ul}} \in \mathbb{C}^{N_b}$  is the additive white Gaussian noise (AWGN)



vector at BS<sub>*i*</sub>. Throughout this chapter, I consider a normalized variance for AWGN without loss of generality, i.e,  $\mathbf{n}_i^{\text{ul}} \sim \mathcal{CN}(\mathbf{0}, \mathbf{I}_{N_b})$ . I further consider that  $\mathbf{s}_i^{\text{ul}}$  has a zero mean and unit variance. I can rewrite the analog received signal (2.1) in a more compact expression as

$$\mathbf{r}_i = \mathbf{H}_i \mathbf{\Lambda}^{1/2} \mathbf{s}^{\text{ul}} + \mathbf{n}_i^{\text{ul}}$$

where  $\mathbf{H}_i = [\mathbf{H}_{i,1}, \dots, \mathbf{H}_{i,N_c}] \in \mathbb{C}^{N_b \times N_c N_u}$ ,  $\mathbf{s}^{\text{ul}} = [(\mathbf{s}_1^{\text{ul}})^T, \dots, (\mathbf{s}_{N_c}^{\text{ul}})^T]^T \in \mathbb{C}^{N_c N_u}$ , and  $\mathbf{\Lambda} = \text{blkdiag}(\mathbf{\Lambda}_1, \dots, \mathbf{\Lambda}_{N_c}) \in \mathbb{C}^{N_c N_u \times N_c N_u}$ .

I consider that each ADC has *b* quantization bits. I adopt the AQNM [29, 69] to obtain a linearized approximation of the quantization process derived from assuming a scalar MMSE quantizer. Under the AQNM, the quantized signal vector can be given as [29]

$$\begin{aligned} \mathcal{Q}(\mathbf{r}_i) &\approx \mathbf{r}_{\text{q},i} \\ &= \alpha \mathbf{H}_{i,i} \mathbf{\Lambda}_i^{1/2} \mathbf{s}_i^{\text{ul}} + \alpha \sum_{j \neq i}^{N_c} \mathbf{H}_{i,j} \mathbf{\Lambda}_j^{1/2} \mathbf{s}_j^{\text{ul}} + \alpha \mathbf{n}_i^{\text{ul}} + \mathbf{q}_i^{\text{ul}} \end{aligned} \quad (2.2)$$

where  $\mathcal{Q}(\cdot)$  is an element-wise quantizer applied to the real and imaginary parts. The quantization gain  $\alpha$  is a function of the number of ADC bits and defined as  $\alpha = 1 - \beta$ , where  $\beta = \frac{\mathbb{E}[|r - r_q|^2]}{\mathbb{E}[|r|^2]}$  [28, 29]. Assuming that  $\mathbf{s}_i^{\text{ul}}$  is Gaussian distributed, i.e.,  $\mathbf{s}_i^{\text{ul}} \sim \mathcal{CN}(\mathbf{0}, \mathbf{I}_{N_u})$ ,  $\forall i$ , the values of  $\beta$  are listed in Table 2.1 for  $b \leq 5$ , and  $\beta$  is approximated as  $\beta \approx \frac{\pi\sqrt{3}}{2} 2^{-2b}$  for  $b > 5$  [31]. The quantization noise  $\mathbf{q}_i^{\text{ul}}$  is uncorrelated with  $\mathbf{r}_i$  [29] and considered to follow the complex Gaussian distribution with a zero mean and covariance of [29, 69]

$$\mathbf{C}_{\mathbf{q}_i^{\text{ul}} \mathbf{q}_i^{\text{ul}}} = \alpha(1 - \alpha) \text{diag}(\mathbf{H}_i \mathbf{\Lambda} \mathbf{H}_i^H + \mathbf{I}_{N_b}). \quad (2.3)$$

Table 2.1: Quantization Gain  $\alpha$  For ADC Quantization Bits  $b \leq 5$

$b$	1	2	3	4	5
$\beta$	0.3634	0.1175	0.03454	0.009497	0.002499

Once the received signals are quantized, they are combined with  $\mathbf{F}_i$  at BS $_i$ . Then I have

$$\begin{aligned} \mathbf{y}_i^{\text{ul}} &= \mathbf{F}_i^H \mathbf{r}_{q,i} \\ &= \alpha \mathbf{F}_i^H \mathbf{H}_{i,i} \mathbf{\Lambda}_i^{\frac{1}{2}} \mathbf{s}_i^{\text{ul}} + \alpha \sum_{j \neq i}^{N_c} \mathbf{F}_i^H \mathbf{H}_{i,j} \mathbf{\Lambda}_j^{\frac{1}{2}} \mathbf{s}_j^{\text{ul}} + \alpha \mathbf{F}_i^H \mathbf{n}_i^{\text{ul}} + \mathbf{F}_i^H \mathbf{q}_i^{\text{ul}}. \end{aligned}$$

Accordingly, the quantized and combined received signal for user  $u$  in cell  $i$  is given as

$$\begin{aligned} y_{i,u}^{\text{ul}} &= \alpha \sqrt{\lambda_{i,u}} \mathbf{f}_{i,u}^H \mathbf{h}_{i,i,u} s_{i,u}^{\text{ul}} + \alpha \sum_{v \neq u}^{N_u} \sqrt{\lambda_{i,v}} \mathbf{f}_{i,u}^H \mathbf{h}_{i,i,v} s_{i,v}^{\text{ul}} \\ &\quad + \alpha \sum_{\substack{j \neq i \\ v}}^{N_c, N_u} \sqrt{\lambda_{j,v}} \mathbf{f}_{i,u}^H \mathbf{h}_{i,j,v} s_{j,v}^{\text{ul}} + \alpha \mathbf{f}_{i,u}^H \mathbf{n}_i^{\text{ul}} + \mathbf{f}_{i,u}^H \mathbf{q}_i^{\text{ul}} \\ &= \alpha \sqrt{\lambda_{i,u}} \mathbf{f}_{i,u}^H \mathbf{h}_{i,i,u} s_{i,u}^{\text{ul}} + \alpha \sum_{(j,v) \neq (i,u)}^{(N_c, N_u)} \sqrt{\lambda_{j,v}} \mathbf{f}_{i,u}^H \mathbf{h}_{i,j,v} s_{j,v}^{\text{ul}} \\ &\quad + \alpha \mathbf{f}_{i,u}^H \mathbf{n}_i^{\text{ul}} + \mathbf{f}_{i,u}^H \mathbf{q}_i^{\text{ul}} \end{aligned}$$

where  $\mathbf{f}_{i,u}$  is the  $u$ th column of  $\mathbf{F}_i$ .

### 2.2.2 Downlink Narrowband System

Similarly to the UL quantized signals, the transmit signal vector quantized at low-resolution DACs of BS $_i$  with a precoder  $\mathbf{W}_i \in \mathbb{C}^{N_b \times N_u}$  is expressed

as [24, 78, 108]

$$\mathbf{x}_i^{\text{dl}} = \alpha \mathbf{W}_i \mathbf{s}_i^{\text{dl}} + \mathbf{q}_i^{\text{dl}} \in \mathbb{C}^{N_b},$$

where  $\mathbf{s}_i^{\text{dl}} \sim \mathcal{CN}(\mathbf{0}, \mathbf{I}_{N_u})$  denotes the transmit symbol vector for the  $N_u$  users in cell  $i$ , and  $\mathbf{q}_i^{\text{dl}} \in \mathbb{C}^{N_b}$  is a quantization noise vector with a covariance [24]

$$\mathbf{C}_{\mathbf{q}_i^{\text{dl}} \mathbf{q}_i^{\text{dl}}} = \alpha(1 - \alpha) \text{diag}(\mathbf{W}_i \mathbf{W}_i^H). \quad (2.4)$$

The same assumptions are made for the quantization as the UL system and  $\alpha$  is also identical to the one in the UL system with the equal quantization resolution as the ADCs. Under TDD, the channel vector between BS $_j$  and user  $u$  in cell  $i$  is  $\mathbf{h}_{j,i,u}^H$ . The received signal at user  $u$  is

$$y_{i,u}^{\text{dl}} = \alpha \mathbf{h}_{i,i,u}^H \mathbf{w}_{i,u} \mathbf{s}_{i,u}^{\text{dl}} + \alpha \sum_{(j,v) \neq (i,u)}^{(N_c, N_u)} \mathbf{h}_{j,i,v}^H \mathbf{w}_{j,v} \mathbf{s}_{j,v}^{\text{dl}} + \sum_{j=1}^{N_c} \mathbf{h}_{j,i,u}^H \mathbf{q}_j^{\text{dl}} + n_{i,u}^{\text{dl}}$$

where  $\mathbf{w}_{i,u}$  is the  $u$ th column of  $\mathbf{W}_i$  and  $n_{i,u}^{\text{dl}}$  is the AWGN distributed as  $n_{i,u}^{\text{dl}} \sim \mathcal{CN}(0, 1)$ .

### 2.3 Uplink and Downlink Joint Beamforming and Power Control

In this section, I formulate transmit power minimization problems for the UL and DL systems subject to SQINR constraints and propose algorithms that solve the problems. Throughout this dissertation,  $\mathcal{P}_a b$  denotes the  $b$ th problem defined in Chapter  $a$ . First, the UL problem is formulated to minimize the transmit power of the users in  $N_c$  cells with an individual user SQINR

constraint as

$$\mathcal{P}_2 1 : \min_{\mathbf{f}_{i,u}, \lambda_{i,u}} \sum_{i,u}^{N_c, N_u} \lambda_{i,u} \quad \text{s.t.} \quad \max_{\mathbf{f}_{i,u}} \Gamma_{i,u}^{\text{ul}} \geq \gamma_{i,u}, \quad \forall i, u \quad (2.5)$$

where  $\Gamma_{i,u}^{\text{ul}}$  is the UL SQINR of user  $u$  in cell  $i$ , which is computed as

$$\Gamma_{i,u}^{\text{ul}} = \frac{\alpha^2 \lambda_{i,u} |\mathbf{f}_{i,u}^H \mathbf{h}_{i,i,u}|^2}{\alpha^2 \sum_{(j,v) \neq (i,u)}^{(N_c, N_u)} \lambda_{j,v} |\mathbf{f}_{i,u}^H \mathbf{h}_{i,j,v}|^2 + \alpha^2 \|\mathbf{f}_{i,u}\|^2 + \mathbf{f}_{i,u}^H \mathbf{C}_{\mathbf{q}_i \mathbf{q}_i} \mathbf{f}_{i,u}}. \quad (2.6)$$

Unlike the perfect quantization system (no quantization error),  $\Gamma_{i,u}^{\text{ul}}$  has the additional term associated with quantization error,  $\mathbf{f}_{i,u}^H \mathbf{C}_{\mathbf{q}_i \mathbf{q}_i} \mathbf{f}_{i,u}$ , which is a function of the channel and the transmit power  $\lambda_{i,u}$ . In addition, it is also involved with the combiner  $\mathbf{f}_{i,u}$ . Accordingly, the effect of coarse quantization needs to be incorporated when solving  $\mathcal{P}_2 1$ .

Now the DL problem is formulated to minimize the transmit power of the BSs in  $N_c$  cells with an individual user SQINR constraint as

$$\mathcal{P}_2 2 : \min_{\mathbf{w}_{i,u}} \alpha \sum_{i,u}^{N_c, N_u} \mathbf{w}_{i,u}^H \mathbf{w}_{i,u} \quad \text{s.t.} \quad \Gamma_{i,u}^{\text{dl}} \geq \gamma_{i,u}, \quad \forall i, u \quad (2.7)$$

where

$$\Gamma_{i,u}^{\text{dl}} = \frac{\alpha^2 |\mathbf{w}_{i,u}^H \mathbf{h}_{i,i,u}|^2}{\alpha^2 \sum_{(j,v) \neq (i,u)}^{(N_c, N_u)} |\mathbf{w}_{j,v}^H \mathbf{h}_{j,i,u}|^2 + \sum_{j=1}^{N_c} \mathbf{h}_{j,i,u}^H \mathbf{C}_{\mathbf{q}_j^{\text{dl}} \mathbf{q}_j^{\text{dl}}} \mathbf{h}_{j,i,u} + 1}. \quad (2.8)$$

Note that  $\alpha$  in the objective function is a fixed scalar which does not change the solution of  $\mathcal{P}_2 2$ . The solution of  $\mathcal{P}_2 2$  also needs to incorporate the effect of the coarse quantization, i.e., quantization noise covariance  $\mathbf{C}_{\mathbf{q}_j^{\text{dl}} \mathbf{q}_j^{\text{dl}}}$  as it is a function of  $\mathbf{W}_j$  and involved with channels  $\mathbf{h}_{j,i,u}$ .

### 2.3.1 Uplink and Downlink Duality

In this subsection, I extend the duality of the UL and DL power minimization problems for infinite-resolution quantizer systems [23] to low-resolution quantizer systems by incorporating the quantization error terms. Exploiting the duality, I propose an iterative algorithm based on the fixed-point iteration [105] and further prove optimality and convergence of the algorithm.

**Theorem 1** (Duality). *The uplink transmit power minimization problem  $\mathcal{P}_2 1$  in (2.5) is equivalent to a Lagrangian dual problem of the downlink transmit minimization problem  $\mathcal{P}_2 2$  in (2.7).*

*Proof.* See Section 2.7. □

This result generalizes the UL-DL beamforming duality derived in [23] to any quantization resolution since the  $\mathcal{P}_2 1$  and  $\mathcal{P}_2 2$  become equivalent to the UL and DL power minimization problem without quantization error, i.e.,  $b \rightarrow \infty$  (equivalently,  $\alpha \rightarrow 1$ ). To propose an algorithm which solves  $\mathcal{P}_2 1$  and  $\mathcal{P}_2 2$ , and to prove its optimality, I first show strong duality between  $\mathcal{P}_2 1$  and  $\mathcal{P}_2 2$ .

**Corollary 1** (Strong duality). *Strong duality holds for  $\mathcal{P}_2 2$  and its Lagrangian dual problem.*

*Proof.* See Section 2.8. □

### 2.3.2 Distributed Iterative Algorithm

In this subsection, I characterize solutions by exploiting the strong duality between  $\mathcal{P}_2 1$  and  $\mathcal{P}_2 2$ , and develop an iterative algorithm that finds the solutions for  $\mathcal{P}_2 1$  and  $\mathcal{P}_2 2$  simultaneously.

**Corollary 2.** *The optimal transmit power for the uplink minimization problem (2.5) is derived as*

$$\lambda_{i,u} = \frac{1}{\alpha \left(1 + \frac{1}{\gamma_{i,u}}\right) \mathbf{h}_{i,i,u}^H \mathbf{K}_i^{-1}(\boldsymbol{\Lambda}) \mathbf{h}_{i,i,u}} \quad (2.9)$$

where  $\mathbf{K}_i(\boldsymbol{\Lambda}) = \mathbf{I}_{N_b} + \alpha \sum_{j,v} \lambda_{j,v} \mathbf{h}_{i,j,v} \mathbf{h}_{i,j,v}^H + (1 - \alpha) \text{diag}(\mathbf{H}_i \boldsymbol{\Lambda} \mathbf{H}_i^H)$  with the MMSE receiver as

$$\mathbf{f}_{i,u} = \left( \alpha^2 \sum_{(j,v) \neq (i,u)} \lambda_{j,v} \mathbf{h}_{i,j,v} \mathbf{h}_{i,j,v}^H + \alpha \mathbf{I}_{N_b} + \alpha(1 - \alpha) \text{diag}(\mathbf{H}_i \boldsymbol{\Lambda} \mathbf{H}_i^H) \right)^{-1} \mathbf{h}_{i,i,u}. \quad (2.10)$$

*Proof.* See Section 2.9. □

The solution in (2.9), however, is a function of all transmit powers including itself. Hence the solution does not fully solve the problem; I develop an algorithm to find an optimal set of transmit power by utilizing the solution. Once I find the optimal transmit power, I can compute the MMSE combiner  $\mathbf{F}_i$  based on the transmit power. In addition, I show the linear relationship between the optimal UL MMSE combiner and the optimal DL precoder.

**Corollary 3** (DL precoder). *With the scaling factor, an optimal downlink precoder can be linearly proportional to the uplink MMSE receiver, i.e.,  $\mathbf{w}_{i,u} =$*

$\sqrt{\tau_{i,u}}\mathbf{f}_{i,u} \forall i, u$ , and  $\tau_{i,u}$  is derived as  $\boldsymbol{\tau} = \boldsymbol{\Sigma}^{-1}\mathbf{1}$ , where  $\mathbf{1}$  is a  $N_u N_c \times 1$  column vector with entries of all ones,  $\boldsymbol{\tau} = [\boldsymbol{\tau}_1^T, \boldsymbol{\tau}_2^T, \dots, \boldsymbol{\tau}_{N_c}^T]^T$  with  $\boldsymbol{\tau}_i^T = [\tau_{i,1}, \tau_{i,2}, \dots, \tau_{i,N_u}]^T$ , and

$$\boldsymbol{\Sigma} = \begin{pmatrix} \boldsymbol{\Sigma}_{1,1} & \boldsymbol{\Sigma}_{1,2} & \cdots & \boldsymbol{\Sigma}_{1,N_c} \\ \boldsymbol{\Sigma}_{2,1} & \boldsymbol{\Sigma}_{2,2} & \cdots & \boldsymbol{\Sigma}_{2,N_c} \\ \vdots & \vdots & \ddots & \vdots \\ \boldsymbol{\Sigma}_{N_c,1} & \boldsymbol{\Sigma}_{N_c,2} & \cdots & \boldsymbol{\Sigma}_{N_c,N_c} \end{pmatrix}. \quad (2.11)$$

Each element of  $\boldsymbol{\Sigma}_{i,j} \in \mathbb{R}^{N_u \times N_u}$  is defined as (2.12)

$$[\boldsymbol{\Sigma}_{i,j}]_{u,v} = \begin{cases} \frac{\alpha^2}{\gamma_{i,u}} |\mathbf{f}_{i,u}^H \mathbf{h}_{i,i,u}|^2 - \alpha(1-\alpha) \mathbf{f}_{i,u}^H \text{diag}(\mathbf{h}_{i,i,u} \mathbf{h}_{i,i,u}^H) \mathbf{f}_{i,u} \\ \text{if } i = j \text{ and } u = v, \\ -\alpha^2 |\mathbf{f}_{j,v}^H \mathbf{h}_{j,i,u}|^2 - \alpha(1-\alpha) \mathbf{f}_{j,v}^H \text{diag}(\mathbf{h}_{j,i,u} \mathbf{h}_{j,i,u}^H) \mathbf{f}_{j,v} \\ \text{otherwise.} \end{cases} \quad (2.12)$$

*Proof.* See Section 2.10. □

Now, I use an iterative standard power control algorithm [23, 102, 105] to find the optimal UL transmit power by exploiting (2.9), which allows us to compute the optimal UL MMSE combiner and DL precoder; let  $\lambda_{i,u}^{(n)}$  be the UL transmit power at  $n$ th iteration. The algorithm is as follows:

**Step 1.** Initialize  $\lambda_{i,u}^{(0)}$ ,  $\forall i, u$ .

**Step 2.** Iteratively update the transmit power  $\lambda_{i,u}^{(n+1)}$  until converges, using (2.9) as

$$\lambda_{i,u}^{(n+1)} = \frac{1}{\alpha \left(1 + \frac{1}{\gamma_{i,u}}\right) \mathbf{h}_{i,i,u}^H \mathbf{K}_i^{-1}(\boldsymbol{\Lambda}^{(n)}) \mathbf{h}_{i,i,u}}, \quad \forall i, u. \quad (2.13)$$

**Step 3.** Find the UL MMSE combiner  $\mathbf{f}_{i,u}$  in (2.10) with  $\lambda_{i,u}$  obtained from the Step 1 and 2.

**Step 4.** Compute the DL precoder  $\mathbf{w}_{i,u}$  based on Corollary 3.

As remarked in [23],  $\mathbf{K}_i$  may be estimated locally at each BS $_i$ , the fixed-point iteration in Step 2 for the optimal UL transmit power only requires the user channel information in the associated cell at the BS without the need for the explicit out-of-cell channel knowledge. In addition, the scaling coefficient  $\tau_{i,u}$  for each user can be considered as a DL transmit power on the effective channel that achieves the target SQINR. According to [30], the transmit power (equivalently,  $\tau_{i,u}$ ) can be obtained using a per-user power update algorithm, whose convergence is guaranteed [105]; each step of the algorithm computes  $\tau_{i,u}$  that satisfies its target SQINR while assuming other  $\tau_{i',u'}$ 's are fixed. Therefore, the proposed algorithm can be implemented in a distributed manner.

**Corollary 4** (Convergence). *For any initial points  $\lambda_{i,u}^{(0)}$ ,  $\forall i, u$ , the proposed fixed-point iterative algorithm converges to a unique fixed point at which total transmit power is minimized.*

*Proof.* See Section 2.11. □

Therefore, the fixed-point iteration in Step 2 always converges to an unique fixed point that is the optimal transmit power, and the optimal solutions for  $\mathcal{P}_2 1$  and  $\mathcal{P}_2 2$  can be obtained.



### 2.3.3 Deterministic Solution for Homogeneous Transmit Power and SQINR Constraint per Cell

In this subsection, I derive a deterministic transmit power solution for a special case in which transmit powers and SQINR constraints are homogeneous within each cell for UL, i.e.,  $\lambda_{i,u} = \lambda_i$  and  $\gamma_{i,u} = \gamma_i, \forall u$ . I solve this problem by forcing the minimum SQINR to satisfy the SQINR constraint;  $\min_u \Gamma_{i,u} \geq \gamma_i, \forall i, u$ , and by relaxing the problem with the lower bound of the minimum SQINR. With the MMSE equalizer  $\mathbf{F}_i$ , the matrix of MSE for UL in cell  $i$  becomes

$$\mathbf{E}_i^{\text{mmse}} = \left( \alpha^2 \lambda_i \mathbf{H}_{i,i}^H \left( \alpha^2 \sum_{j \neq i}^{N_c} \lambda_j \mathbf{H}_{i,j} \mathbf{H}_{i,j}^H + \alpha^2 \mathbf{I}_{N_b} + \mathbf{C}_{\mathbf{q}_i^{\text{ul}} \mathbf{q}_i^{\text{ul}}} \right)^{-1} \mathbf{H}_{i,i} + \mathbf{I}_{N_u} \right)^{-1}. \quad (2.14)$$

Consequently, the SQINR of user  $u$  in cell  $i$  can be expressed as  $\Gamma_{i,u} = 1/[\mathbf{E}_i^{\text{mmse}}]_{u,u} - 1$ . As shown in [11], the minimum SQINR in cell  $i$  is given as

$$\begin{aligned} \min_u \Gamma_{i,u} &= \frac{1}{\max_u [\mathbf{E}_i^{\text{mmse}}]_{u,u}} - 1 \\ &\geq \frac{1}{\text{eig}_M(\mathbf{E}_i^{\text{mmse}})} - 1 \\ &= \text{eig}_m \left( \alpha \lambda_i \mathbf{H}_{i,i}^H \left( \alpha \sum_{j \neq i}^{N_c} \lambda_j \mathbf{H}_{i,j} \mathbf{H}_{i,j}^H + \mathbf{I}_{N_b} + (1-\alpha) \text{diag}(\mathbf{H}_i \mathbf{\Lambda} \mathbf{H}_i^H) \right)^{-1} \mathbf{H}_{i,i} \right). \end{aligned} \quad (2.15)$$

Let  $\mathbf{H}_{i,i}^\dagger = (\mathbf{H}_{i,i}^H \mathbf{H}_{i,i})^{-1} \mathbf{H}_{i,i}^H$ ,  $A_{i,j} = \text{eig}_M(\mathbf{H}_{i,i}^\dagger \mathbf{H}_{i,j} \mathbf{H}_{i,j}^H \mathbf{H}_{i,i}^\dagger)$ ,  $B_i = \text{eig}_M((\mathbf{H}_{i,i}^H \mathbf{H}_{i,i})^{-1})$ , and  $C_{i,j} = \text{eig}_M(\mathbf{H}_{i,i}^\dagger \text{diag}(\mathbf{H}_{i,j} \mathbf{H}_{i,j}^H) \mathbf{H}_{i,i}^\dagger)$ . Then (2.15) further becomes (2.16) where (a) comes from Corollary 1 in [11], and (b) is from  $\text{diag}(\mathbf{H}_i \mathbf{\Lambda} \mathbf{H}_i^H) = \sum_j \lambda_j \text{diag}(\mathbf{H}_{i,j} \mathbf{H}_{i,j}^H)$  due to  $\mathbf{\Lambda}_i = \lambda_i \mathbf{I}_{N_u}, \forall i$  and Corollary 1 in [11].

$$\begin{aligned}
& \frac{\alpha \lambda_i}{\text{eig}_M \left( \mathbf{H}_{i,i}^\dagger \left( \alpha \sum_{j \neq i} \lambda_j \mathbf{H}_{i,j} \mathbf{H}_{i,j}^H + \mathbf{I}_{N_b} + (1 - \alpha) \text{diag}(\mathbf{H}_i \mathbf{\Lambda} \mathbf{H}_i^H) \right) \mathbf{H}_{i,i}^{\dagger H} \right)} \\
& \stackrel{(a)}{\geq} \frac{\alpha \lambda_i}{\text{den}} \\
& \stackrel{(b)}{\geq} \frac{\alpha \lambda_i}{\alpha \sum_{j \neq i} \lambda_j A_{i,j} + B_i + (1 - \alpha) \sum_j \lambda_j C_{i,j}}, \tag{2.16}
\end{aligned}$$

where  $\text{den} = \alpha \sum_{j \neq i} \lambda_j \text{eig}_M \left( \mathbf{H}_{i,i}^\dagger \mathbf{H}_{i,j} \mathbf{H}_{i,j}^H \mathbf{H}_{i,i}^{\dagger H} \right) + \text{eig}_M \left( \mathbf{H}_{i,i}^\dagger \mathbf{H}_{i,i}^{\dagger H} \right) + (1 - \alpha) \text{eig}_M \left( \mathbf{H}_{i,i}^\dagger \text{diag}(\mathbf{H}_i \mathbf{\Lambda} \mathbf{H}_i^H) \mathbf{H}_{i,i}^{\dagger H} \right)$

---

By setting (2.16) equal to  $\gamma_i$  for all  $i$ , the following equation can be established:

$$\boldsymbol{\lambda} = \frac{1}{\alpha} \boldsymbol{\Gamma} (\boldsymbol{\Omega} \boldsymbol{\lambda} + \mathbf{b})$$

where  $\boldsymbol{\lambda} = [\lambda_1, \dots, \lambda_{N_c}]^T$ ,  $\boldsymbol{\Gamma} = \text{diag}(\gamma_1, \dots, \gamma_{N_c})$ ,  $\mathbf{b} = [B_1, \dots, B_{N_c}]^T$ , and the  $(i, j)$ th element of  $\boldsymbol{\Omega}$  is given as

$$\omega_{i,j} = \begin{cases} (1 - \alpha) C_{i,i} & \text{if } i = j \\ \alpha A_{i,j} + (1 - \alpha) C_{i,j} & \text{otherwise.} \end{cases}$$

Finally, the deterministic UL transmit power is derived as

$$\boldsymbol{\lambda} = \frac{1}{\alpha} (\mathbf{I}_{N_c} - \frac{1}{\alpha} \boldsymbol{\Gamma} \boldsymbol{\Omega})^{-1} \boldsymbol{\Gamma} \mathbf{b}. \tag{2.17}$$

I note that the deterministic solution in (2.17) may have negative  $\lambda_i$  when the target SQINRs become high, i.e., the problem may easily become

infeasible since the deterministic approach has a reduced feasible set by assuming homogeneous transmit powers per cell and by solving the problem for the SQINR lower bound. I briefly introduce a possible approach to manage this issue. Since the communication often operates in the interference-limited regime in the multicell system, changing the signs of all transmit powers only causes a marginal change in the SQINR according to (2.6). In this regard, if  $\lambda_i < 0, \forall i$ , I simply take the absolute value of  $\lambda_i$  as a solution. If there exists  $\lambda_i < 0$  only for a subset of the cells, I can set the largest  $\lambda_i$  to zero and re-compute (2.17) until I have  $\lambda_i \geq 0, \forall i$ , because the cell with the large  $\lambda_i$  can be considered to have weak channels. As a result, some of the cells can be assigned with zero transmit power. Then those cells can be scheduled in different time or frequency resources.

## 2.4 Extension to Wideband OFDM Systems

In this section, I extend the total transmit power minimization problem to wideband OFDM systems under coarse quantization at the BSs. I first need to derive signal models for multicell OFDM systems by taking into account quantization error coupled with OFDM modulations.

### 2.4.1 Uplink OFDM System with Low-resolution ADCs

Let  $\mathbf{s}_i^{\text{ul}}(k) \in \mathbb{C}^{N_u}$  denote the vector of symbols of  $N_u$  users in cell  $i$  at subcarrier  $k$ , and let

$$\mathbf{u}_i^{\text{ul}}(k) = \mathbf{\Lambda}_i(k)^{1/2} \mathbf{s}_i^{\text{ul}}(k),$$

where  $\mathbf{\Lambda}_i(k) = \text{diag}(\lambda_{i,1}(k), \dots, \lambda_{i,N_u}(k))$  is the diagonal matrix of transmit power. Let  $\mathbf{x}_i(k)^{\text{ul}} \in \mathbb{C}^{N_u}$  be the vector of OFDM symbols of  $N_u$  users in cell  $i$  at time  $k$ . The OFDM symbol vectors are stacked as  $\underline{\mathbf{x}}_i^{\text{ul}} = [\mathbf{x}_i^{\text{ul}}(0)^T, \dots, \mathbf{x}_i^{\text{ul}}(K-1)^T]^T \in \mathbb{C}^{KN_u}$ . Then  $\underline{\mathbf{x}}_i^{\text{ul}}$  can be represented as

$$\underline{\mathbf{x}}_i^{\text{ul}} = (\mathbf{W}_{\text{DFT}}^H \otimes \mathbf{I}_{N_u}) \underline{\mathbf{u}}_i^{\text{ul}} = \mathbf{\Psi}_{N_u}^H \underline{\mathbf{\Lambda}}_i^{1/2} \underline{\mathbf{s}}_i^{\text{ul}}$$

where  $\underline{\mathbf{s}}_i^{\text{ul}} = [\mathbf{s}_i^{\text{ul}}(0)^T, \dots, \mathbf{s}_i^{\text{ul}}(K-1)^T]^T$ ,  $\underline{\mathbf{u}}_i^{\text{ul}} = [\mathbf{u}_i^{\text{ul}}(0)^T, \dots, \mathbf{u}_i^{\text{ul}}(K-1)^T]^T$ ,  $\underline{\mathbf{\Lambda}}_i = \text{blkdiag}(\mathbf{\Lambda}_i(0), \dots, \mathbf{\Lambda}_i(K-1))$ ,  $\mathbf{\Psi}_{N_u} = (\mathbf{W}_{\text{DFT}} \otimes \mathbf{I}_{N_u})$ , and  $\mathbf{W}_{\text{DFT}}$  is a normalized discrete Fourier transform (DFT) matrix.

Let  $\mathbf{r}_i^{\text{ul}}(k) \in \mathbb{C}^{N_b}$  be the received baseband analog signal at time  $k$  after cyclic prefix (CP) removal at BS $_i$ . Staking for  $K$ -symbol time as  $\underline{\mathbf{r}}_i^{\text{ul}} = [\mathbf{r}_i^{\text{ul}}(0)^T, \dots, \mathbf{r}_i^{\text{ul}}(K-1)^T]^T \in \mathbb{C}^{KN_b}$ , the stacked received baseband analog signals at BS $_i$  is expressed as

$$\underline{\mathbf{r}}_i^{\text{ul}} = \underline{\mathbf{H}}_{i,i} \underline{\mathbf{x}}_i^{\text{ul}} + \sum_{j \neq i}^{N_c} \underline{\mathbf{H}}_{i,j} \underline{\mathbf{x}}_j^{\text{ul}} + \underline{\mathbf{n}}_i^{\text{ul}}$$

where  $\underline{\mathbf{H}}_{i,j} = \text{blkcirc}(\mathbf{H}_{i,j,0}, \mathbf{0}, \dots, \mathbf{0}, \mathbf{H}_{i,j,L-1}, \dots, \mathbf{H}_{i,j,1}) \in \mathbb{C}^{KN_b \times KN_u}$  represents the block circulant channel matrix,  $\mathbf{H}_{i,j,\ell}$  denotes the time domain channel matrix between BS $_i$  and users in cell  $j$  for  $\ell$ th tap,  $L$  is the channel delay spread, and  $\underline{\mathbf{n}}_i^{\text{ul}}$  is the stacked AWGN vector  $\underline{\mathbf{n}}_i^{\text{ul}} = [\mathbf{n}_i^{\text{ul}}(0)^T, \dots, \mathbf{n}_i^{\text{ul}}(K-1)^T]^T \sim \mathcal{CN}(\mathbf{0}, \mathbf{I}_{KN_b})$ .

The received signals are quantized and expressed under the AQNM as

$$\mathcal{Q}(\underline{\mathbf{r}}_i^{\text{ul}}) \approx \underline{\mathbf{r}}_{q,i}^{\text{ul}} = \alpha \underline{\mathbf{H}}_{i,i} \underline{\mathbf{x}}_i^{\text{ul}} + \alpha \sum_{j \neq i}^{N_c} \underline{\mathbf{H}}_{i,j} \underline{\mathbf{x}}_j^{\text{ul}} + \alpha \underline{\mathbf{n}}_i^{\text{ul}} + \underline{\mathbf{q}}_i^{\text{ul}}$$

where  $\underline{\mathbf{q}}_i^{\text{ul}} = [\mathbf{q}_i^{\text{ul}}(0)^T, \dots, \mathbf{q}_i^{\text{ul}}(K-1)^T]^T \in \mathbb{C}^{KN_b} \sim \mathcal{CN}(\mathbf{0}, \mathbf{C}_{\underline{\mathbf{q}}_i^{\text{ul}}})$  is the stacked quantization noise vector for the received signal at BS<sub>*i*</sub>, whose covariance matrix is [29]

$$\begin{aligned} \mathbf{C}_{\underline{\mathbf{q}}_i^{\text{ul}}} & \\ &= \alpha(1 - \alpha)\text{diag}\left(\sum_{j=1}^{N_c} \underline{\mathbf{H}}_{i,j} \underline{\Psi}_{N_u}^H \underline{\Lambda}_j \underline{\Psi}_{N_u} \underline{\mathbf{H}}_{i,j} + \mathbf{I}_{KN_b}\right). \end{aligned} \quad (2.18)$$

Now the quantized signals go through DFT operation and become

$$\begin{aligned} \underline{\mathbf{y}}_i^{\text{ul}} &= (\mathbf{W}_{\text{DFT}} \otimes \mathbf{I}_{N_b}) \underline{\mathbf{r}}_i^{\text{ul}} \\ &= \alpha \underline{\Psi}_{N_b} \underline{\mathbf{H}}_{i,i} \underline{\Psi}_{N_u}^H \underline{\Lambda}_i^{1/2} \underline{\mathbf{s}}_i^{\text{ul}} + \alpha \sum_{j \neq i} \underline{\Psi}_{N_b} \underline{\mathbf{H}}_{i,j} \underline{\Psi}_{N_u}^H \underline{\Lambda}_j^{1/2} \underline{\mathbf{s}}_j^{\text{ul}} \\ &\quad + \underline{\Psi}_{N_b} \underline{\mathbf{n}}_i^{\text{ul}} + \underline{\Psi}_{N_b} \underline{\mathbf{q}}_i^{\text{ul}} \\ &= \alpha \underline{\mathbf{G}}_{i,i} \underline{\Lambda}_i^{1/2} \underline{\mathbf{s}}_i^{\text{ul}} + \alpha \sum_{j \neq i} \underline{\mathbf{G}}_{i,j} \underline{\Lambda}_j^{1/2} \underline{\mathbf{s}}_j^{\text{ul}} + \tilde{\underline{\mathbf{n}}}_i^{\text{ul}} + \tilde{\underline{\mathbf{q}}}_i^{\text{ul}} \end{aligned}$$

where  $\underline{\Psi}_{N_b} = \mathbf{W}_{\text{DFT}} \otimes \mathbf{I}_{N_b}$ ,  $\underline{\mathbf{G}}_{i,j} = \underline{\Psi}_{N_b} \underline{\mathbf{H}}_{i,j} \underline{\Psi}_{N_u}^H = \text{blkdiag}(\mathbf{G}_{i,j}(0), \dots, \mathbf{G}_{i,j}(K-1)) \in \mathbb{C}^{KN_b \times KN_u}$  where  $\mathbf{G}_{i,j}(k) = \sum_{\ell=0}^{L-1} \mathbf{H}_{i,j,\ell} e^{-\frac{j2\pi k\ell}{K}}$  is the frequency domain UL channel matrix for subcarrier  $k$  between BS<sub>*i*</sub> and users in cell  $j$ ,  $\tilde{\underline{\mathbf{n}}}_i^{\text{ul}} = [\tilde{\mathbf{n}}_i^{\text{ul}}(0)^T, \dots, \tilde{\mathbf{n}}_i^{\text{ul}}(K-1)^T]^T = \underline{\Psi}_{N_b} \underline{\mathbf{n}}_i^{\text{ul}}$ , and  $\tilde{\underline{\mathbf{q}}}_i^{\text{ul}} = [\tilde{\mathbf{q}}_i^{\text{ul}}(0)^T, \dots, \tilde{\mathbf{q}}_i^{\text{ul}}(K-1)^T]^T = \underline{\Psi}_{N_b} \underline{\mathbf{q}}_i^{\text{ul}}$ .

The received signal at subcarrier  $k$  is then given as

$$\begin{aligned} \mathbf{y}_i^{\text{ul}}(k) &= \alpha \mathbf{G}_{i,i}(k) \underline{\Lambda}_i(k) \mathbf{s}_i^{\text{ul}}(k) + \alpha \sum_{j \neq i}^{N_c} \mathbf{G}_{i,j}(k) \underline{\Lambda}_j(k) \mathbf{s}_j^{\text{ul}}(k) \\ &\quad + \alpha \tilde{\mathbf{n}}_i^{\text{ul}}(k) + \tilde{\mathbf{q}}_i^{\text{ul}}(k) \end{aligned} \quad (2.19)$$

$$\Gamma_{i,u}^{\text{ul}}(k) = \frac{\alpha^2 \lambda_{i,u}(k) |\mathbf{f}_{i,u}^H(k) \mathbf{g}_{i,i,u}(k)|^2}{\alpha^2 \sum_{(j,v) \neq (i,u)}^{N_c, N_u} \lambda_{j,v}(k) |\mathbf{f}_{i,u}^H(k) \mathbf{g}_{i,j,v}(k)|^2 + \alpha^2 |\mathbf{f}_{i,u}(k)|^2 + \mathbf{f}_{i,u}^H(k) \mathbf{C}_{\tilde{\mathbf{q}}_i^{\text{ul}}(k)} \tilde{\mathbf{q}}_i^{\text{ul}}(k) \mathbf{f}_{i,u}(k)} \quad (2.20)$$

and  $\mathbf{y}_i^{\text{ul}}(k)$  is combined with an equalizer  $\mathbf{F}_i(k)$ . The combined signal for user  $u$  at subcarrier  $k$  is now given as

$$\begin{aligned} \mathbf{f}_{i,u}^H(k) \mathbf{y}_i^{\text{ul}}(k) &= \alpha \lambda_{i,u}^{1/2}(k) \mathbf{f}_{i,u}^H(k) \mathbf{g}_{i,i,u}(k) s_{i,u}^{\text{ul}}(k) \\ &\quad + \alpha \sum_{(j,v) \neq (i,u)}^{N_c, N_u} \lambda_{j,v}^{1/2}(k) \mathbf{f}_{i,u}^H(k) \mathbf{g}_{i,j,v}(k) s_{i,v}^{\text{ul}}(k) \\ &\quad + \alpha \mathbf{f}_{i,u}^H(k) \tilde{\mathbf{n}}_i(k) + \mathbf{f}_{i,u}^H(k) \tilde{\mathbf{q}}_i^{\text{ul}}(k), \end{aligned}$$

where  $\mathbf{f}_{i,u}^H(k)$  is the  $u$ th column of  $\mathbf{F}_i(k)$  and  $\mathbf{g}_{i,j,v}(k)$  is the  $v$ th column of  $\mathbf{G}_{i,j}(k)$ . I note that  $\tilde{\mathbf{n}}_i^{\text{ul}} \sim \mathcal{CN}(\mathbf{0}, \mathbf{I}_{KN_b})$ . The SQINR for user  $u$  in cell  $i$  at subcarrier  $k$  is computed accordingly as (2.20) which is on top of the next page. Based on (2.18),  $\mathbf{C}_{\tilde{\mathbf{q}}_i^{\text{ul}}(k)}$  is expressed as

$$\begin{aligned} \mathbf{C}_{\tilde{\mathbf{q}}_i^{\text{ul}}(k)} &= \alpha(1 - \alpha) \mathbf{\Psi}_{N_b}(k) \\ &\quad \times \text{diag} \left( \sum_{j=1}^{N_c} \mathbf{H}_{i,j} \mathbf{\Psi}_{N_u}^H \mathbf{\Lambda}_j \mathbf{\Psi}_{N_u} \mathbf{H}_{i,j} + \mathbf{I}_{KN_b} \right) \mathbf{\Psi}_{N_b}^H(k) \end{aligned} \quad (2.21)$$

where  $\mathbf{\Psi}_{N_b}(k) = ([\mathbf{W}_{\text{DFT}}]_{k+1,:} \otimes \mathbf{I}_{N_b})$ . Finally, using (2.20), the UL OFDM transmit power minimization problem is formulated as

$$\begin{aligned} \mathcal{P}_2 3 : \quad & \min_{\mathbf{f}_{i,u}(k), \lambda_{i,u}(k)} \sum_{i,u,k} \lambda_{i,u}(k) \\ \text{s.t.} \quad & \max_{\mathbf{f}_{i,u}(k)} \Gamma_{i,u}^{\text{ul}}(k) \geq \gamma_{i,u,k}, \quad \forall i, u, k. \end{aligned} \quad (2.22)$$

In addition to all users in all cells, the maximization needs to be performed for all subcarriers.

### 2.4.2 Downlink OFDM System with Low-resolution DACs

The DL OFDM system with low-resolution DACs can be modeled by following similar steps as the UL OFDM system with low-resolution ADCs. Accordingly, I briefly explain the system model by pointing out the key differences such as precoding and DAC quantization, and definitions of symbols are the same as the ones used in Sec. 2.4.1 unless mentioned otherwise. Similarly to the UL OFDM system, the stacked OFDM symbol vector at BS<sub>*i*</sub> over *K*-symbol time,  $\underline{\mathbf{x}}_i^{\text{dl}} \in \mathbb{C}^{KN_b}$ , is expressed as

$$\underline{\mathbf{x}}_i^{\text{dl}} = (\mathbf{W}_{\text{DFT}}^H \otimes \mathbf{I}_{N_b}) \underline{\mathbf{u}}_i^{\text{dl}} = \underline{\Psi}_{N_b}^H \underline{\mathbf{W}}_i \underline{\mathbf{s}}_i^{\text{dl}}$$

where the block diagonal precoding matrix is  $\underline{\mathbf{W}}_i = \text{blkdiag}(\mathbf{W}_i(0), \dots, \mathbf{W}_i(K-1)) \in \mathbb{C}^{KN_b \times KN_u}$ . Before being transmitted,  $\underline{\mathbf{x}}_i^{\text{dl}}$  is quantized at the low-resolution DACs as [29, 108]

$$\underline{\mathbf{x}}_{\mathbf{q},i}^{\text{dl}} = \alpha \underline{\mathbf{x}}_i^{\text{dl}} + \underline{\mathbf{q}}_i^{\text{dl}}$$

where  $\underline{\mathbf{q}}_i^{\text{dl}} \sim \mathcal{CN}(\mathbf{0}, \mathbf{C}_{\underline{\mathbf{q}}_i^{\text{dl}} \underline{\mathbf{q}}_i^{\text{dl}}})$  is the stacked quantization noise vector at BS<sub>*i*</sub> and its covariance matrix is computed as [29]

$$\mathbf{C}_{\underline{\mathbf{q}}_i^{\text{dl}} \underline{\mathbf{q}}_i^{\text{dl}}} = \alpha(1 - \alpha) \text{diag}(\underline{\Psi}_{N_b}^H \underline{\mathbf{W}}_i \underline{\mathbf{W}}_i^H \underline{\Psi}_{N_b}). \quad (2.23)$$

After transmitting  $\underline{\mathbf{x}}_i^{\text{dl}}$ ,  $N_u$  users in cell *i* receive signals from all BSs. Stacking over *K* subcarriers after CP removal and DFT, the received signals

$$\begin{aligned}
\Gamma_{i,u}^{\text{dl}}(k) &= \frac{\alpha^2 |\mathbf{g}_{i,i,u}^H(k) \mathbf{w}_{i,u}(k)|^2}{\text{den}} \tag{2.25} \\
\text{den} &= \alpha^2 \sum_{\substack{N_c, N_u \\ (j,v) \neq (i,u)}} |\mathbf{g}_{j,i,u}^H(k) \mathbf{w}_{j,v}(k)|^2 \\
&\quad + \alpha(1 - \alpha) \sum_{j=1}^{N_c} \mathbf{g}_{j,i,u}^H(k) \mathbf{\Psi}_{N_b} \text{diag}(\mathbf{\Psi}_{N_b}^H \mathbf{W}_j \mathbf{W}_j^H \mathbf{\Psi}_{N_b}) \mathbf{\Psi}_{N_b}^H \mathbf{g}_{j,i,u}(k) + 1 \tag{2.26}
\end{aligned}$$


---

at the users in cell  $i$  becomes

$$\begin{aligned}
\underline{\mathbf{y}}_i^{\text{dl}} &= \alpha \underline{\mathbf{G}}_{i,i}^H \underline{\mathbf{W}}_i \underline{\mathbf{s}}_i^{\text{dl}} + \alpha \sum_{j \neq i}^{N_c} \underline{\mathbf{G}}_{j,i}^H \underline{\mathbf{W}}_j \underline{\mathbf{s}}_j^{\text{dl}} + \sum_{j=1}^{N_c} \underline{\mathbf{G}}_{j,i}^H \mathbf{\Psi}_{N_b} \underline{\mathbf{q}}_j^{\text{dl}} + \mathbf{\Psi}_{N_u} \underline{\mathbf{n}}_i^{\text{dl}} \\
&= \alpha \underline{\mathbf{G}}_{i,i}^H \underline{\mathbf{W}}_i \underline{\mathbf{s}}_i^{\text{dl}} + \alpha \sum_{j \neq i}^{N_c} \underline{\mathbf{G}}_{j,i}^H \underline{\mathbf{W}}_j \underline{\mathbf{s}}_j^{\text{dl}} + \tilde{\underline{\mathbf{q}}}_i^{\text{dl}} + \tilde{\underline{\mathbf{n}}}_i^{\text{dl}}
\end{aligned}$$

where  $\tilde{\underline{\mathbf{q}}}_j^{\text{dl}} = \sum_{j=1}^{N_c} \underline{\mathbf{G}}_{j,i}^H \mathbf{\Psi}_{N_b} \underline{\mathbf{q}}_j^{\text{dl}}$  and  $\tilde{\underline{\mathbf{n}}}_i^{\text{dl}} = \mathbf{\Psi}_{N_u} \underline{\mathbf{n}}_i^{\text{dl}}$ . Recall that the UL block-diagonal frequency domain channel matrix between BS $_i$  and users in cell  $i$  is defined as  $\underline{\mathbf{G}}_{j,i} = \text{blkdiag}(\mathbf{G}_{j,i}(0), \dots, \mathbf{G}_{j,i}(K-1)) \in \mathbb{C}^{KN_b \times KN_u}$ . Accordingly, the DL frequency domain channel matrix is its conjugate  $\underline{\mathbf{G}}_{j,i}^H$  in the TDD system. The received signal at user  $u$  in cell  $i$  for subcarrier  $k$  is given as

$$\begin{aligned}
y_{i,u}^{\text{dl}}(k) &= \alpha \mathbf{g}_{i,i,u}^H(k) \mathbf{w}_{i,u}(k) s_{i,u}^{\text{dl}}(k) \\
&\quad + \alpha \sum_{\substack{N_c, N_u \\ (j,v) \neq (i,u)}} \mathbf{g}_{j,i,u}^H(k) \mathbf{w}_{j,v}(k) s_{j,v}^{\text{dl}}(k) + \tilde{q}_{i,u}^{\text{dl}}(k) + \tilde{n}_{i,u}^{\text{dl}}(k). \tag{2.24}
\end{aligned}$$

Based on (2.23) and (2.24), the DL SQINR for user  $u$  in cell  $i$  at subcarrier  $k$  is computed as (2.25) which is on the top of the next page, where



$\underline{\mathbf{g}}_{j,i,u}(k)$  denotes the  $(kN_u + u)$ th column of  $\underline{\mathbf{G}}_{j,i}$ , i.e., the entire column of  $\underline{\mathbf{G}}_{j,i}$  that corresponds to the channel for  $k$ th subcarrier of user  $u$ . Using (2.25), the DL OFDM transmit power minimization problem is formulated as

$$\begin{aligned} \mathcal{P}_2 4 : \quad & \min_{\mathbf{w}_{i,u}(k)} \alpha \sum_{i,u,k} \mathbf{w}_{i,u}^H(k) \mathbf{w}_{i,u}(k) \\ & \text{s.t. } \Gamma_{i,u}^{\text{dl}}(k) \geq \gamma_{i,u,k}, \quad \forall i, u, k. \end{aligned} \quad (2.27)$$

### 2.4.3 Joint Beamforming and Power Control for Wideband OFDM Systems

Unlike the narrowband system, the quantization noise terms coupled with not only beamformers and transmit power but also OFDM modulation are the main challenge for showing the duality. In the following theorem, I prove the duality by handling this issue.

**Theorem 2** (Duality). *The duality holds between  $\mathcal{P}_2 3$  and  $\mathcal{P}_2 4$ .*

*Proof.* See Section 2.12. □

**Corollary 5** (Strong duality). *Strong duality holds for  $\mathcal{P}_2 4$  and its Lagrangian dual problem.*

*Proof.* See Section 2.13. □

Since I have shown that the duality between  $\mathcal{P}_2 3$  and  $\mathcal{P}_2 4$  exists without duality gap, the optimal solutions can be characterized via the duality. Here I briefly describe the overall procedures as they are similar to the narrowband

case; solving Karush-Kuhn-Tucker (KKT) conditions, I can show that the UL ODFM problem  $\mathcal{P}_2 3$  can be solved by the distributed iterative algorithm that is proposed in Sec. 2.3.2 with the following solution:

$$\lambda_{i,u}(k) = \frac{1}{\alpha \left(1 + \frac{1}{\gamma_{i,u,k}}\right) \mathbf{g}_{i,i,u}^H(k) \bar{\mathbf{K}}_{i,k}^{-1}(\underline{\mathbf{\Lambda}}) \mathbf{g}_{i,i,u}(k)}. \quad (2.28)$$

Note that (2.28) needs to be computed over not only users but also subcarriers at each BS. Now let  $\lambda_{i,u}^{(n+1)} = f_{i,u,k}(\underline{\mathbf{\Lambda}}^{(n)})$ . Then, as in the proof of Corollary 11, the convergence of the iterative method can be proved by showing that  $f_{i,u,k}(\underline{\mathbf{\Lambda}}^{(n)})$  is a standard function. Using the obtained optimal UL transmit power  $\lambda_{i,u}(k)$  from the standard fixed-point iteration, the MMSE equalizer  $\mathbf{F}_i(k)$  for the received signal at each subcarrier  $\mathbf{y}_i^{\text{ul}}(k)$  is computed as  $\mathbf{F}_i(k) = \mathbf{C}_{\mathbf{z}_{i,u}(k)\mathbf{z}_{i,u}(k)}^{-1} \mathbf{g}_{i,i,u}(k)$  where  $\mathbf{C}_{\mathbf{z}_{i,u}(k)\mathbf{z}_{i,u}(k)}^{-1}$  is given in (2.47). Based on  $\mathbf{F}_i(k)$ , I can also obtain the optimal precoder  $\mathbf{W}_i(k)$  for  $\mathcal{P}_2 4$  from appropriate scaling of  $\mathbf{F}_i(k)$  as shown in Corollary 6.

**Corollary 6** (Precoder). *With the proper scaling coefficient in wideband case, an optimal DL precoder can be proportional to the uplink MMSE receiver, i.e.,  $\mathbf{w}_{i,u}(k) = \sqrt{\tau_{i,u}(k)} \mathbf{f}_{i,u}(k) \forall i, u, k$ , and  $\tau_{i,u}$  is derived as  $\underline{\boldsymbol{\tau}} = \underline{\boldsymbol{\Sigma}}^{-1} \mathbf{1}$ , where  $\mathbf{1}$  is a  $N_u N_c K \times 1$  column vector,  $\underline{\boldsymbol{\tau}} = [\underline{\boldsymbol{\tau}}^T(0), \dots, \underline{\boldsymbol{\tau}}^T(K-1)]^T$  with  $\underline{\boldsymbol{\tau}}(k) = [\underline{\boldsymbol{\tau}}_1^T(k), \underline{\boldsymbol{\tau}}_2^T(k), \dots, \underline{\boldsymbol{\tau}}_{N_c}^T(k)]^T$  and  $\underline{\boldsymbol{\tau}}_i^T(k) = [\tau_{i,1}(k), \tau_{i,2}(k), \dots, \tau_{i,N_u}(k)]^T$ , and  $\underline{\boldsymbol{\Sigma}} = \text{blkdiag}(\underline{\boldsymbol{\Sigma}}(0), \dots, \underline{\boldsymbol{\Sigma}}(K-1))$  whose submatrix is composed as*

$$\underline{\boldsymbol{\Sigma}}(k) = \begin{pmatrix} \underline{\boldsymbol{\Sigma}}_{1,1}(k) & \underline{\boldsymbol{\Sigma}}_{1,2}(k) & \cdots & \underline{\boldsymbol{\Sigma}}_{1,N_c}(k) \\ \underline{\boldsymbol{\Sigma}}_{2,1}(k) & \underline{\boldsymbol{\Sigma}}_{2,2}(k) & \cdots & \underline{\boldsymbol{\Sigma}}_{2,N_c}(k) \\ \vdots & \vdots & \ddots & \vdots \\ \underline{\boldsymbol{\Sigma}}_{N_c,1}(k) & \underline{\boldsymbol{\Sigma}}_{N_c,2}(k) & \cdots & \underline{\boldsymbol{\Sigma}}_{N_c,N_c}(k) \end{pmatrix}, \quad (2.29)$$

and

$$[\underline{\Sigma}_{i,j}(k)]_{u,v} = \begin{cases} \frac{\alpha^2}{\gamma_{i,u}(k)} |\mathbf{g}_{i,i,u}^H(k) \mathbf{f}_{i,u}(k)|^2 - \alpha(1-\alpha) \sum_n \mathbf{f}_{i,u}^H(n) \mathbf{\Psi}_{N_b}(n) \\ \times \text{diag}(\mathbf{\Psi}_{N_b}^H \underline{\mathbf{g}}_{i,i,u}(k) \underline{\mathbf{g}}_{i,i,u}^H(k) \mathbf{\Psi}_{N_b}) \mathbf{\Psi}_{N_b}^H(n) \mathbf{f}_{i,u}(n) \\ \text{if } i = j, u = v, \\ -\alpha^2 |\mathbf{g}_{j,i,u}^H(k) \mathbf{f}_{j,v}(k)|^2 - \alpha(1-\alpha) \sum_n \mathbf{f}_{j,v}^H(n) \mathbf{\Psi}_{N_b}(n) \\ \times \text{diag}(\mathbf{\Psi}_{N_b}^H \underline{\mathbf{g}}_{j,i,u}(k) \underline{\mathbf{g}}_{j,i,u}^H(k) \mathbf{\Psi}_{N_b}) \mathbf{\Psi}_{N_b}^H(n) \mathbf{f}_{j,v}(n) \\ \text{otherwise.} \end{cases} \quad (2.30)$$

*Proof.* See Section 2.14. □

Therefore, since the strong duality also holds between the UL and DL wideband OFDM systems with low-resolution ADCs and low-resolution DACs, respectively, I have shown that  $\mathcal{P}_2 4$  can also be solved by using the distributed iterative algorithm as the narrowband case.

## 2.5 Simulation Results

In this section, I validate the derived theoretical results and the proposed quantization-aware iterative CoMP (Q-iCoMP) algorithm and deterministic CoMP (Q-dCoMP) algorithm. I also simulate the quantization-aware per-cell (Q-PerCell) based iterative algorithm by adapting the per-cell algorithm in [76] to low-resolution ADC systems based on the derived SQINR with quantization noise in (2.6). For the Q-PerCell algorithm, each BS first finds its optimal solution based on the iterative algorithm in [76] by considering the inter-cell interference as noise and assuming it to be fixed. Once the BSs derive solutions for the given noise power, they update the noise power and

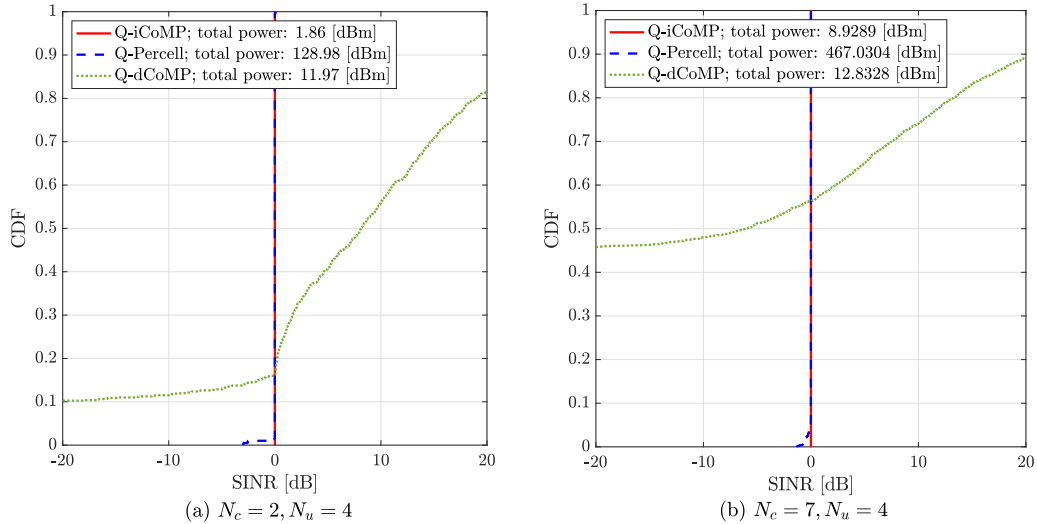


Figure 2.2: CDFs of the SQINRs of users in all cells for  $\gamma = 0$  dB target SQINR,  $b = 3$  quantization bits, and  $N_b = 64$  BS antennas with (a)  $N_c = 2$  cells with  $N_u = 4$  users per cell and with (b)  $N_c = 7$  cells with  $N_u = 4$  users per cell.

find solutions again. These steps are repeated until the solutions converge. For simulations, I use networks with  $N_c \in \{2, 3, 4, 7\}$  hexagonal cells. Assuming narrowband communications, I assume Rayleigh channels with a zero mean and unit variance or small scale fading. For large scale fading, I adopt the log-distance pathloss model in [27]. The distance between adjacent BSs is 2 km. The minimum distance between BSs and users is 100 m. Considering a 2.4 GHz carrier frequency with 10 MHz bandwidth, I use 8.7 dB lognormal shadowing variance and 5 dB noise figure. For simplicity, I assume that the target SQINR  $\gamma$  is equal for all users.

Fig. 2.2 shows the cumulative density function (CDF) of the UL SQINR

of all users for  $\gamma = 0$  dB,  $b = 3$ , and  $N_b = 64$  with (a) ( $N_c = 2, N_u = 4$ ) and (b) ( $N_c = 7, N_u = 4$ ). The proposed Q-iCoMP algorithm shows a step function-like CDF at 0 dB SQINR with the least total transmit power among the evaluated algorithms for both (a) and (b). This verifies the performance of the Q-iCoMP algorithm that provides an optimal solution for the UL and DL problems. Although the Q-Percell algorithm shows similar CDF, about 4% of users cannot achieve the target SQINR and the total transmit power becomes excessive. Accordingly, the Q-Percell algorithm is only feasible when the numbers of cooperating BSs and associated users are small. Regarding the deterministic approach, more than 85% of users meet the target SQINR for (a). For (b), however, about 55% of users cannot achieve the target SQINR, and most of them have zero transmit power. Although the Q-Percell algorithm shows better performance in satisfying the target SQINR than the Q-dCoMP algorithm, its total transmit power easily diverges when the network becomes denser. Therefore, the Q-iCoMP algorithm provides the best performance and the Q-dCoMP algorithm can be more practical than the Q-Percell algorithm for dense networks.

Fig. 2.3 shows the UL total transmit power versus the target SQINRs for  $N_b = 64$ ,  $N_c = 2$ ,  $N_u = 2$ , and  $b \in \{2, 3, \infty\}$ . For the considered target SQINR range, the Q-iCoMP algorithm shows the minimum total transmit power. The increment in the transmit power due to the increased quantization error is also small. Despite that the Q-Percell algorithm also achieves similar performance at the low to medium target SQINR, the transmit power of the

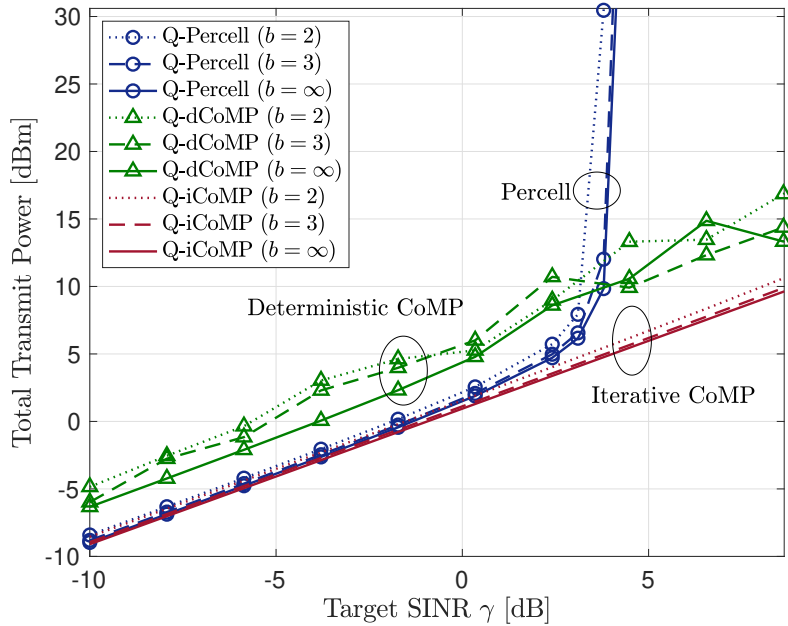


Figure 2.3: UL total transmit power versus the target SQINR for  $N_b = 64$  BS antennas,  $N_c = 2$  cells and  $N_u = 2$  users per cell.

algorithm diverges in the medium to high target SQINR range. The Q-dCoMP algorithm shows a larger gap between different quantization resolutions than that in the iterative algorithms. I note that as the target SQINR increases, the total transmit power curves of the Q-dCoMP algorithm show larger fluctuation, and there are crossing points between different resolutions; as the target SQINR increases, more BSs are likely to assign with zero transmit power to reduce interference to the other cells, which happens more often with a less number of quantization bits.

In Fig. 2.4, the UL network with  $N_c = 7$  and  $N_u = 4$  is considered for various  $b$  and  $N_b$ . For  $N_b = 16$ , the Q-Percell algorithm is almost infeasible

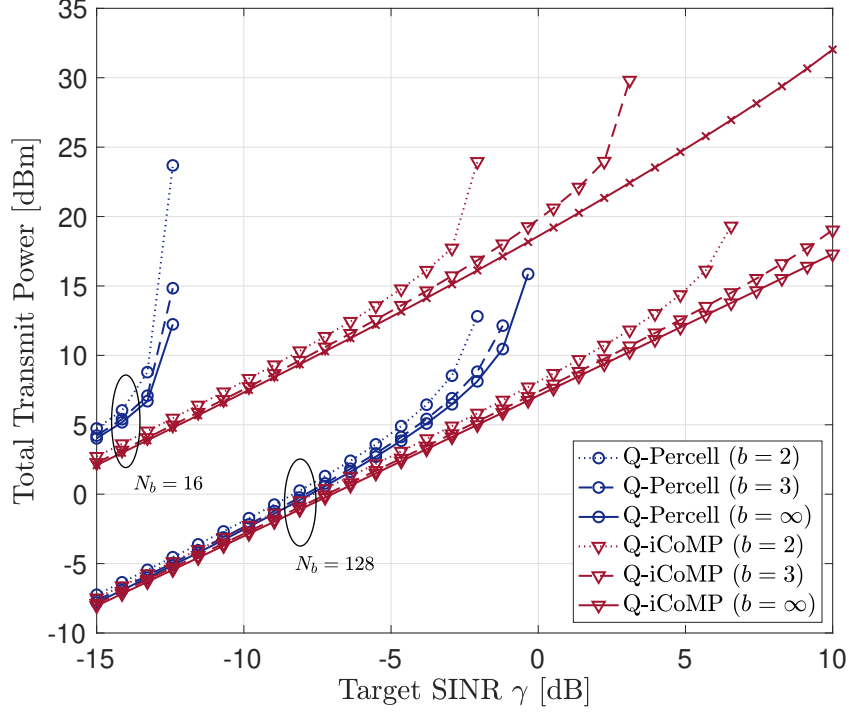


Figure 2.4: Total transmit power versus the target SQINR for (a) the UL network with  $N_b \in \{16, 128\}$  antennas,  $N_c = 7$  cells, and  $N_u = 4$  users per cell.

and the Q-iCoMP algorithm also shows divergence in the total transmit power at the medium to high target SQINRs with a small number of quantization bits. Increasing  $N_b$  from 16 to 128 provides more than 10 dB SQINR gain. Accordingly, for  $N_b = 128$  which is considered as a massive MIMO system, the Q-iCoMP algorithm achieves the target SQINRs for all users without divergence even with  $b = 3$ , whereas the Q-Percell algorithm still suffers from excessive power consumption in the medium to high target SQINR range. Therefore, in massive MIMO systems, the coordinated joint beamforming and

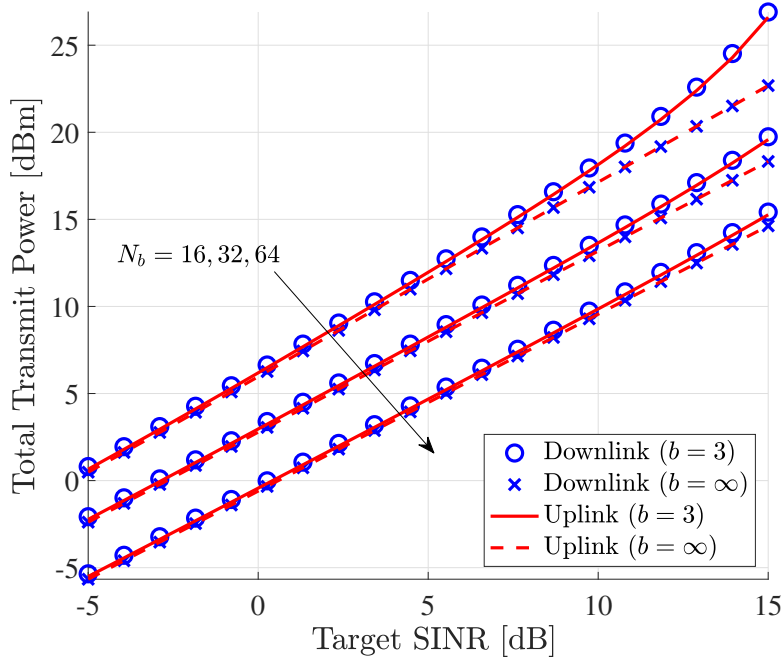


Figure 2.5: Total transmit power versus the target SQINR for the UL and DL networks with  $N_b \in \{16, 32, 64\}$  BS antennas,  $N_c = 3$  cells,  $N_u = 3$  users per cell, and  $b \in \{3, \infty\}$  quantization bits. The overlapped lines and markers can demonstrate the derived strong duality.

power control can provide reliable and power-efficient communications even with a coarse quantizer.

Fig. 2.5 shows the total transmit power over a wide range of target SQINR for both UL and DL for  $N_b \in \{16, 32, 64\}$ ,  $N_c = 3$ ,  $N_u = 3$ , and  $b \in \{3, \infty\}$ . I note that the total transmit power consumed by the DL case in Fig. 2.5 matches the UL transmit power consumption, which validates the derived theoretical results.



### 2.5.1 Covariance Estimation

In this subsection, I show how  $\mathbf{K}_i$  in (2.13) can be estimated without the explicit inter-cell channel knowledge and its impact. I note that  $\mathbf{K}_i$  is indeed a scaled covariance matrix of the quantized signal  $\mathbf{r}_{q,i}$  by  $1/\alpha$  in the uplink direction. Accordingly, I can estimate  $\mathbf{K}_i$  as follows: the BSs compute  $\lambda_{i,u}^{(n-1)}$ ,  $\forall i, u$  at  $(n-1)$ th iteration of the algorithm, and each BS $_i$  requests the associated users to transmit pilots  $\mathbf{s}_i^{\text{ul}}$  with the updated  $\lambda_{i,u}^{(n-1)}$ , where  $|s_{i,k}| = 1$  and  $\mathbb{E}[s_{i,k}] = 0$ . Then each user transmits  $N_p$  pilots per iteration and BS $_i$  estimates  $\hat{\mathbf{K}}_i^{(n)}$ ,  $\forall i$  as  $\hat{\mathbf{K}}_i^{(n)} = \frac{1}{\alpha N_p} \sum_{t=1}^{N_p} \mathbf{r}_{q,i}^{(n)}(t) \left( \mathbf{r}_{q,i}^{(n)}(t) \right)^H$ . BS $_i$  only requires local observations  $\mathbf{r}_{q,i}$  and in-cell channel knowledge  $\mathbf{H}_{i,i}$  to compute  $\lambda_{i,u}$ . To reduce the pilot overhead, I leverage the correlation with the estimated  $\hat{\mathbf{K}}_i^{(m)}$ ,  $m = 1, \dots, n-1$ . Since the change in  $\lambda_{i,u}$  tends to rapidly decrease as the algorithm proceeds, it is reasonable to accentuate the recent estimates when exploiting the correlation. In this regard, I compute a weighted average of the estimates as

$$\hat{\mathbf{K}}_i^{(n)} = \frac{\sum_{m=1}^{n-1} m \hat{\mathbf{K}}_i^{(m)} + \frac{n}{\alpha N_p} \sum_{t=1}^{N_p} \mathbf{r}_{q,i}^{(n)}(t) \left( \mathbf{r}_{q,i}^{(n)}(t) \right)^H}{\sum_{m=1}^n m},$$

which is used for computing  $\lambda_{i,u}^{(n)}$  in (2.9).

Fig. 2.6 shows the CDF of the SQINR including the results with estimated  $\hat{\mathbf{K}}_i$  for  $\gamma = 0$  dB,  $b = 3$ ,  $N_b = 64$ ,  $N_c = 7$ , and  $N_u = 4$ . The  $\mathbf{K}_i$  estimation cases with  $N_p = 5$  and  $N_p = 20$  are evaluated. The estimation cases achieve the target SQINR with less than  $-0.5$  dB margin. The result with 20 pilots achieves the target SQINR with higher probability compared

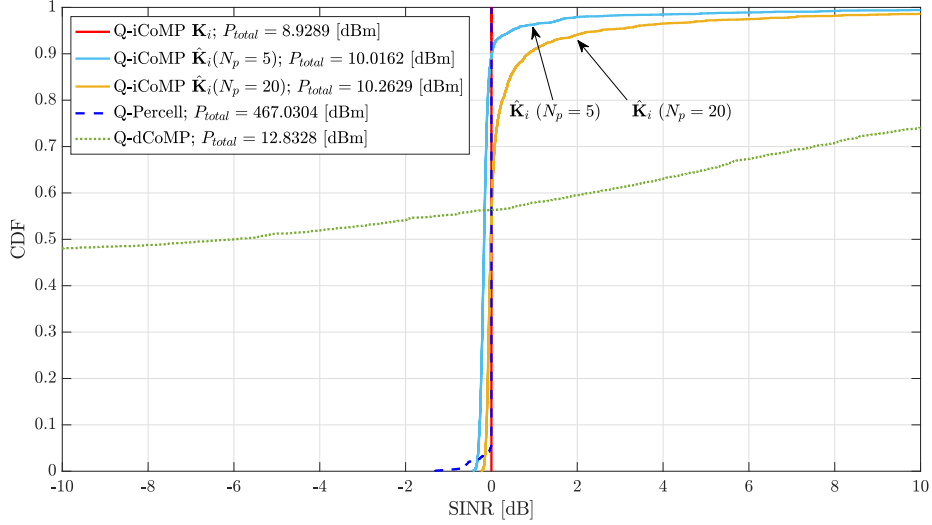


Figure 2.6: CDFs of the SQINRs of users in all cells for  $\gamma = 0$  dB target SQINR,  $b = 3$  quantization bits,  $N_b = 64$  BS antennas,  $N_c = 7$  cells, and  $N_u = 4$  users per cell.

to the estimation with 5 pilots. In addition, the total transmit powers for the  $\mathbf{K}_i$  estimation cases show a marginal increase compared to the perfect  $\mathbf{K}_i$  case, whereas the Q-PerCell algorithm requires excessive total transmit power to meet the target SQINR. Here, I exploit the correlation among  $\hat{\mathbf{K}}_i^{(n)}$ 's to derive a more accurate estimate as one of the possible approaches. I remark that channel time correlation and in-cell channel knowledge can be further leveraged for improvement.

### 2.5.2 Complexity and Convergence

I compare complexity of the proposed and per-cell algorithm. In the massive MIMO regime, the inversion of  $\mathbf{K}_i(\mathbf{\Lambda})$  dominates the complexity for

computing  $\lambda_{i,u}$ . Consequently, the total complexity becomes  $O(TN_uN_b^3)$  where  $T$  is the number of iterations of the proposed algorithm. In addition, the per-cell algorithm also requires  $O(T_pN_uN_b^3)$  where  $T_p$  denotes the number of iterations of the per-cell algorithm. I remark that since  $\mathbf{K}_i(\mathbf{\Lambda})$  is a Hermitian symmetric and positive semi-definite matrix, the number of floating point operations for the inversion of  $\mathbf{K}_i(\mathbf{\Lambda})$  can be reduced by exploiting a Cholesky factorization approach [45].

Fig. 2.7 shows the convergence results of the proposed method and the per-cell method for  $\gamma \in \{-5, 0, 5\}$  dB,  $b = 3$ ,  $N_b = 64$ ,  $N_c = 4$ , and  $N_u = 3$ . Fig. 2.7(a) shows the efficiency of the proposed algorithm by showing that the convergence of the proposed method is faster than that of the per-cell algorithm. In addition, a meaningful transmit power can be achieved within 3 to 10 iterations depending on the target SQINR, which is much smaller than the per-cell algorithm.

In Fig. 2.7(b), I evaluate the proposed algorithm over time-variant channels to show how the algorithm can improve the convergence rate. Assuming a block fading model, the channel is time-invariant during the channel coherence time  $T_c$ . A channel realization within  $n$ th channel coherence block, i.e.,  $t \in [nT_c, (n+1)T_c)$ , is denoted as  $\mathbf{h}_{i,j,u}(n), \forall i, j, u$ . I consider that the channel model is written as  $\mathbf{h}_{i,j,u}(n) = \rho_{i,j,u}\boldsymbol{\xi}_{i,j,u}(n)$  where  $\boldsymbol{\xi}_{i,j,u}(n)$  and  $\rho_{i,j,u}$  denote small scale fading at  $n$ th block and large scale fading, respectively. For Fig. 2.7(b), I assume that  $\rho_{i,j,u}$  is invariant as it is the long-term characteristics of the channels while changing  $\boldsymbol{\xi}_{i,j,u}(n)$  at each channel coherence

time. To model the time varying small scale fading  $\xi_{i,j,u}(n)$ , I use the first-order Gauss-Markov model [10] as  $\xi_{i,j,u}(n) = \sqrt{1 - a^2}\xi_{i,j,u}(n - 1) + a\mathbf{v}_{i,j,u}(n)$ , where  $\mathbf{v}_{i,j,u}(n)$  follows  $\mathcal{CN}(\mathbf{0}, \mathbf{I}_{N_b})$ . Accordingly, the channel at time  $n$  becomes  $\mathbf{h}_{i,j,u}(n) = \sqrt{1 - a^2}\mathbf{h}_{i,j,u}(n - 1) + a\rho_{i,j,u}\mathbf{v}_{i,j,u}(n)$  where  $n \geq 1$  and  $0 < a < 1$ . I consider  $a = 0.9$ . Due to the time correlation, the solution attained for the previous channel can be a good initial point for the current channel, thereby achieving faster convergence as shown in Fig. 2.7(b).

### 2.5.3 Wideband OFDM Communications

I evaluate the proposed algorithm for the UL OFDM system. I assume that the channel delay spread is  $L = 3$  and the small scale fading of each channel tap is Rayleigh fading. The large scale fading model is the same as the one in the narrowband simulation.

Fig. 2.8 shows the OFDM results of the proposed algorithm for  $N_b = 16$ ,  $N_c = 2$ ,  $N_u = 2$ ,  $b \in \{2, 3, 4, \infty\}$ , and  $K = 64$  subcarriers. The proposed algorithm achieves the target SQINR within  $-0.4$  dB margin with reasonable total transmit power. Although the case of  $b = 2$  starts to diverge for high target SQINR, the other low-resolution ADC cases still show stable performance for high target SQINR. In addition, the differences in the total transmit power of low-resolution ADCs from the infinite bits are marginal. Therefore, the results demonstrate that the benefit of using low-resolution ADCs for improving energy efficiency of the wireless network.

## 2.6 Conclusion

This chapter investigated coordinated multipoint beamforming and power control for massive MIMO systems with low-resolution ADCs and DACs. I proved the strong duality between UL and DL total transmit power minimization problems under target SQINR constraints in low-resolution ADC and DAC systems based on the additive quantization noise model. Leveraging the duality, a fixed-point CoMP algorithm was proposed to jointly solve the UL and DL problems by incorporating the coarse quantization effect. The proposed algorithm provides optimal solutions for the UL and DL problems in an efficient and distributed manner without explicit inter-cell channel estimation. In addition, a deterministic approach provided a closed-form solution for the UL problem with the assumption of homogeneous transmit powers and SQINR targets within each cell. I proved that the derived results can be extended to wideband OFDM systems when optimizing a beamformer and transmit power for each user and subcarrier under coarse quantization. Via simulations, I showed that the proposed algorithm can achieve high target SQINRs without divergence of transmit power for low-resolution ADC and DAC systems, whereas the per-cell algorithm suffers from excessive power consumption even with infinite-resolution ADCs and DACs. I also observe that the deterministic method can achieve a reasonable trade-off between total transmit power and achieved SQINR. Overall, in massive MIMO systems integrated with coarse quantizer, the coordinated beamforming and power control offer spectrum- and power-efficient wireless communication systems. For future work, devel-

oping an algorithm with lower complexity and analyzing the impact of channel estimation error would be desirable.

## 2.7 Proof of Theorem 1

SQINR constraints of  $\mathcal{P}_2 1$  can be simplified by applying MMSE equalizers  $\mathbf{F}_i$  that maximize the SQINR. Let  $\mathbf{z}_{i,u}$  be the interference-plus-noise term of the UL quantized signal in (2.2) whose covariance matrix is expressed as

$$\begin{aligned} \mathbf{C}_{\mathbf{z}_{i,u}\mathbf{z}_{i,u}} &= \alpha^2 \sum_{(j,v) \neq (i,u)} \lambda_{j,v} \mathbf{h}_{i,j,v} \mathbf{h}_{i,j,v}^H + \alpha^2 \mathbf{I}_{N_b} \\ &\quad + \alpha(1 - \alpha) \text{diag}(\mathbf{H}_i \mathbf{\Lambda} \mathbf{H}_i^H + \mathbf{I}_{N_b}) \\ &= \alpha^2 \sum_{(j,v) \neq (i,u)} \lambda_{j,v} \mathbf{h}_{i,j,v} \mathbf{h}_{i,j,v}^H + \alpha \mathbf{I}_{N_b} \\ &\quad + \alpha(1 - \alpha) \text{diag}(\mathbf{H}_i \mathbf{\Lambda} \mathbf{H}_i^H). \end{aligned}$$

Then, the MMSE equalizer  $\mathbf{f}_{i,u}$  can be given as [92]

$$\mathbf{f}_{i,u} = \mathbf{C}_{\mathbf{z}_{i,u}\mathbf{z}_{i,u}}^{-1} \mathbf{h}_{i,i,u}. \quad (2.31)$$

Applying (2.31) to the UL SQINR in (2.6), the constraints in  $\mathcal{P}_2 1$  become  $\alpha^2 \lambda_{i,u} \mathbf{h}_{i,i,u}^H \mathbf{C}_{\mathbf{z}_{i,u}\mathbf{z}_{i,u}}^{-1} \mathbf{h}_{i,i,u} \geq \gamma_{i,u}$ . Then I multiply both sides with  $\mathbf{h}_{i,i,u}^H \mathbf{h}_{i,i,u}$  and rearrange as

$$\mathbf{h}_{i,i,u}^H (\alpha^2 \lambda_{i,u} \mathbf{h}_{i,i,u} \mathbf{h}_{i,i,u}^H \mathbf{C}_{\mathbf{z}_{i,u}\mathbf{z}_{i,u}}^{-1} - \gamma_{i,u} \mathbf{I}_{N_b}) \mathbf{h}_{i,i,u} \geq 0. \quad (2.32)$$

To satisfy (2.32), I need  $\alpha^2 \lambda_{i,u} \mathbf{h}_{i,i,u} \mathbf{h}_{i,i,u}^H \mathbf{C}_{\mathbf{z}_{i,u} \mathbf{z}_{i,u}}^{-1} - \gamma_{i,u} \mathbf{I}_{N_b} \succeq 0$ . Rearranging this condition, I can rewrite  $\mathcal{P}_2 1$  as

$$\min_{\lambda_{i,u}} \sum_{i,u} \lambda_{i,u} \quad (2.33)$$

$$\text{s.t. } \mathbf{K}_i(\boldsymbol{\Lambda}) \preceq \alpha \left(1 + \frac{1}{\gamma_{i,u}}\right) \lambda_{i,u} \mathbf{h}_{i,i,u} \mathbf{h}_{i,i,u}^H, \quad \forall i, u. \quad (2.34)$$

where  $\mathbf{K}_i(\boldsymbol{\Lambda}) = \mathbf{I}_{N_b} + \alpha \sum_{j,v} \lambda_{j,v} \mathbf{h}_{j,j,v} \mathbf{h}_{j,j,v}^H + (1 - \alpha) \text{diag}(\mathbf{H}_i \boldsymbol{\Lambda} \mathbf{H}_i^H)$ .

Now, I prove the duality between  $\mathcal{P}_2 1$  and  $\mathcal{P}_2 2$  by managing the quantization error term and by showing that (2.33) is equivalent to the Lagrangian dual problem of  $\mathcal{P}_2 2$  which is given as

$$\begin{aligned} \mathcal{L}(\mathbf{w}_{i,u}, \mu_{i,u}) &= \sum_{i,u} \alpha \mathbf{w}_{i,u}^H \mathbf{w}_{i,u} - \sum_{i,u} \mu_{i,u} \left( \alpha^2 \frac{|\mathbf{w}_{i,u}^H \mathbf{h}_{i,i,u}|^2}{\gamma_{i,u}} \right. \\ &\quad \left. - \alpha^2 \sum_{v \neq u} |\mathbf{w}_{i,v}^H \mathbf{h}_{i,i,u}|^2 - \alpha^2 \sum_{\substack{j \neq i \\ v}} |\mathbf{w}_{j,v}^H \mathbf{h}_{j,i,u}|^2 \right. \\ &\quad \left. + \alpha(1 - \alpha) \sum_j \mathbf{h}_{j,i,u}^H \text{diag}(\mathbf{W}_j \mathbf{W}_j^H) \mathbf{h}_{j,i,u} + 1 \right) \end{aligned} \quad (2.35)$$

where  $\mu_{i,u}$  is a Lagrangian multiplier. Rearranging and rewriting (3.46), the Lagrangian becomes

$$\begin{aligned} \mathcal{L}(\mathbf{w}_{i,u}, \mu_{i,u}) &= \sum_{i,u} \mu_{i,u} + \alpha \sum_{i,u} \mathbf{w}_{i,u}^H \left( \mathbf{I}_{N_b} - \alpha \left(1 + \frac{1}{\gamma_{i,u}}\right) \right. \\ &\quad \left. \times \mu_{i,u} \mathbf{h}_{i,i,u} \mathbf{h}_{i,i,u}^H + \alpha \sum_{j,v} \mu_{j,v} \mathbf{h}_{i,j,v} \mathbf{h}_{i,j,v}^H \right) \mathbf{w}_{i,u} \\ &\quad + \alpha(1 - \alpha) \sum_{i,u} \mu_{i,u} \sum_j \mathbf{h}_{j,i,u}^H \text{diag}(\mathbf{W}_j \mathbf{W}_j^H) \mathbf{h}_{j,i,u}. \end{aligned} \quad (2.36)$$

I need to rewrite the quantization error term in (2.36) to manipulate  $\mathbf{W}_j$  in the diagonal matrix. Let  $\mathbf{M}_i = \text{diag}(\mu_{i,1}, \dots, \mu_{i,N_u})$  and  $\mathbf{M} = \text{blkdiag}(\mathbf{M}_1, \dots, \mathbf{M}_{N_c}) \in$

$\mathbb{C}^{N_c N_u \times N_c N_u}$ . Changing the indices of  $\sum_{i,u} \mu_{i,u} \sum_j \mathbf{h}_{j,i,u}^H \text{diag}(\mathbf{W}_j \mathbf{W}_j^H) \mathbf{h}_{j,i,u}$  from  $(i, u, j)$  to  $(j, v, i)$ , I have

$$\begin{aligned}
& \sum_{j,v}^{N_c, N_u} \mu_{j,v} \sum_i^{N_c} \mathbf{h}_{i,j,v}^H \text{diag}(\mathbf{W}_i \mathbf{W}_i^H) \mathbf{h}_{i,j,v} \\
&= \sum_{i,u}^{N_c, N_u} \mathbf{w}_{i,u}^H \text{diag} \left( \sum_{j,v}^{N_c, N_u} \mu_{j,v} |h_{i,j,v,1}|^2, \dots, \sum_{j,v}^{N_c, N_u} \mu_{j,v} |h_{i,j,v,N_b}|^2 \right) \mathbf{w}_{i,u} \\
&= \sum_{i,u}^{N_c, N_u} \mathbf{w}_{i,u}^H \text{diag}(\mathbf{H}_i \mathbf{M} \mathbf{H}_i^H) \mathbf{w}_{i,u}, \tag{2.37}
\end{aligned}$$

where  $h_{i,j,v,n}$  and  $w_{i,u,n}$  are the  $n$ th entries of  $\mathbf{h}_{i,j,v}$  and  $\mathbf{w}_{i,u}$ , respectively, and  $\mathbf{H}_i = [\mathbf{H}_{i,1}, \dots, \mathbf{H}_{i,N_c}]$  as defined earlier. Applying (2.37) to (2.36), the Lagrangian becomes (2.38), which is on top of the next page.

The dual objective function is defined as  $g(\mu_{i,u}) = \min_{\mathbf{w}_{i,u}} \mathcal{L}(\mathbf{w}_{i,u}, \mu_{i,u})$ . To prevent an unbounded solution, I need  $\mathbf{I}_{N_b} - \alpha \left(1 + \frac{1}{\gamma_{i,u}}\right) \mu_{i,u} \mathbf{h}_{i,i,u} \mathbf{h}_{i,i,u}^H + \alpha \sum_{j,v} \mu_{j,v} \mathbf{h}_{i,j,v} \mathbf{h}_{i,j,v}^H + (1 - \alpha) \text{diag}(\mathbf{H}_i \mathbf{M} \mathbf{H}_i^H) \succeq 0$ . Accordingly, the Lagrangian dual problem of  $\mathcal{P}_2 2$  in (2.7) becomes equivalent to

$$\begin{aligned}
& \max_{\mu_{i,u}} \sum_{i,u}^{N_c, N_u} \mu_{i,u} \tag{2.39} \\
& \text{s.t. } \mathbf{K}_i(\mathbf{M}) \succeq \alpha \left(1 + \frac{1}{\gamma_{i,u}}\right) \mu_{i,u} \mathbf{h}_{i,i,u} \mathbf{h}_{i,i,u}^H, \quad \forall i, u
\end{aligned}$$

where  $\mathbf{K}_i(\mathbf{M}) = \mathbf{I}_{N_b} + \alpha \sum_{j,v} \mu_{j,v} \mathbf{h}_{i,j,v} \mathbf{h}_{i,j,v}^H + (1 - \alpha) \text{diag}(\mathbf{H}_i \mathbf{M} \mathbf{H}_i^H)$ .

Although the Lagrangian dual problem of  $\mathcal{P}_2 2$  in (2.39) and the UL problem in (2.33) have the opposite objectives (max vs. min) with the reversed inequality in the constraints, optimal solutions of  $\mathcal{P}_2 1$  and the Lagrangian dual problem is obtained with active constraints, and (2.39) and (2.33) have



the same optimal solutions with active constraints. Therefore, (2.39) and (2.33) become equivalent by replacing  $\mu_{i,u}$  in (2.39) with  $\lambda_{i,u}$ ,  $\forall i, u$ , i.e., the Lagrangian multiplier of  $\mathcal{P}_2 2$ ,  $\mu_{i,u}$ , is equivalent to the UL transmit power  $\lambda_{i,u}$  in  $\mathcal{P}_2 1$ . This completes the proof.

## 2.8 Proof of Corollary 1

I first show that (2.7) can be represented as a standard conic optimization problem. Let  $\mathbf{W}$  be defined as  $\mathbf{W} = [\mathbf{W}_1, \dots, \mathbf{W}_{N_c}]$ , then the DL problem (2.7) is rewritten as

$$\min_{\mathbf{W}, P_o} P_o \quad (2.40)$$

$$\text{s.t. } \Gamma_{i,u}^{\text{dl}} \geq \gamma_{i,u}, \quad \forall i, u \quad (2.41)$$

$$\text{Tr}(\mathbf{W}^H \mathbf{W}) \leq P_o \quad (2.42)$$

where  $P_o$  is a positive slack variable. As in [102, 106], I can take a diagonal phase scaling on the right of each precoder as  $\mathbf{W}_i \text{diag}(e^{j\phi_{i,1}}, \dots, e^{j\phi_{i,N_u}})$  for  $i = 1, \dots, N_c$ , without changing the objective nor the constraints, I can design the precoder to be  $\mathbf{w}_{i,u}^H \mathbf{h}_{i,i,u} \geq 0$ ,  $\forall i, u$ .

Using (2.37), I rewrite the quantization term in (2.8) as

$$\begin{aligned} \sum_j \mathbf{h}_{j,i,u}^H \mathbf{C}_{\mathbf{q}_j^{\text{dl}} \mathbf{q}_j^{\text{dl}}} \mathbf{h}_{j,i,u} &= \alpha(1 - \alpha) \sum_j \mathbf{h}_{j,i,u}^H \text{diag}(\mathbf{W}_j \mathbf{W}_j^H) \mathbf{h}_{j,i,u} \\ &= \alpha(1 - \alpha) \sum_{j,v} \mathbf{w}_{j,v}^H \text{diag}(\mathbf{h}_{j,i,u} \mathbf{h}_{j,i,u}^H) \mathbf{w}_{j,v}. \end{aligned} \quad (2.43)$$

Let  $\mathbf{D}_{j,i,u} = \text{diag}(\mathbf{h}_{j,i,u} \mathbf{h}_{j,i,u}^H)$ ,  $\mathbf{W}_{\text{BD}} = \text{blkdiag}(\mathbf{W}_1, \dots, \mathbf{W}_{N_c})$ , and  $\tilde{\mathbf{W}}_{\text{BD}} = \text{blkdiag}((\mathbf{I}_{N_b} \otimes \mathbf{W}_1), \dots, (\mathbf{I}_{N_b} \otimes \mathbf{W}_{N_c}))$ . Using (2.43), the SQINR constraints

in (2.41) can be rearranged as

$$\begin{aligned} & \alpha^2 \left(1 + \frac{1}{\gamma_{i,u}}\right) |\mathbf{w}_{i,u}^H \mathbf{h}_{i,i,u}|^2 \\ & \geq \left\| \frac{\alpha \mathbf{W}_{\text{BD}}^H \text{vec}(\mathbf{h}_{1,i,u}, \dots, \mathbf{h}_{N_c,i,u})}{\sqrt{\alpha(1-\alpha)} \tilde{\mathbf{W}}_{\text{BD}}^H \text{vec}(\mathbf{D}_{1,i,u}^{1/2}, \dots, \mathbf{D}_{N_c,i,u}^{1/2})} \right\|_1^2, \quad \forall i, u. \end{aligned} \quad (2.44)$$

Since I restrict the precoders to be  $\mathbf{w}_{i,u}^H \mathbf{h}_{i,i,u} \geq 0$ , I can take square root for (2.44). In addition, the power constraint (2.42) can be reformulated as  $\|\text{vec}(\mathbf{W})\| \leq \sqrt{P_o}$ . Using (2.44) and  $\|\text{vec}(\mathbf{W})\| \leq \sqrt{P_o}$ , the problem in (2.40) can be cast to the standard second order conic problem (SOCP) [102].

Next, (2.7) is strictly feasible because given a solution  $\mathbf{W}$ , it can be always scaled by a factor of  $c > 1$  satisfying the constraints. Thus, the strong duality holds between (2.5) and (2.7).  $\square$

## 2.9 Proof of Corollary 2

Here I use  $\lambda_{i,u}$  instead of  $\mu_{i,u}$  since I showed that they are equivalent. The derivative of the Lagrangian (2.38) with respect to  $\mathbf{w}_{i,u}$  is given as

$$\begin{aligned} \frac{\partial \mathcal{L}(\mathbf{w}_{i,u}, \lambda_{i,u})}{\partial \mathbf{w}_{i,u}} &= 2\alpha \left( \mathbf{I}_{N_b} - \alpha \left(1 + \frac{1}{\gamma_{i,u}}\right) \lambda_{i,u} \mathbf{h}_{i,i,u} \mathbf{h}_{i,i,u}^H \right. \\ & \left. + \alpha \sum_{j,v} \lambda_{j,v} \mathbf{h}_{i,j,v} \mathbf{h}_{i,j,v}^H + (1-\alpha) \text{diag}(\mathbf{H}_i \mathbf{\Lambda} \mathbf{H}_i^H) \right) \mathbf{w}_{i,u}. \end{aligned} \quad (2.45)$$

Setting (2.45) equal to zero, I derive (2.9). Accordingly,  $\lambda_{i,u}$ 's are the Lagrangian multipliers that satisfy the stationarity condition. In addition, at the optimal solution, all the constraints in  $\mathcal{P}_2$  are active, which satisfies the

complementary slackness condition. Therefore, (2.9) is the optimal Lagrangian multiplier, equivalently, optimal transmit power for  $\mathcal{P}_2$ .  $\square$

## 2.10 Proof of Corollary 3

To find the optimal  $\mathbf{w}_{i,u}$ , I set the derivative of the Lagrangian with respect to  $\mathbf{w}_{i,u}$  in (2.45) to zero, and solve it for  $\mathbf{w}_{i,u}$ . Then I have

$$\begin{aligned}\mathbf{w}_{i,u} &= \left( \alpha^2 \sum_{(j,v) \neq (i,u)} \lambda_{j,v} \mathbf{h}_{i,j,v} \mathbf{h}_{i,j,v}^H + \alpha(1-\alpha) \text{diag}(\mathbf{H}_i \boldsymbol{\Lambda} \mathbf{H}_i^H) \right. \\ &\quad \left. + \alpha \mathbf{I}_{N_b} \right)^{-1} \alpha^2 \left( 1 + \frac{1}{\gamma_{i,u}} \right) \lambda_{i,u} \mathbf{h}_{i,i,u} \mathbf{h}_{i,i,u}^H \mathbf{w}_{i,u} \\ &= \alpha^2 \left( 1 + \frac{1}{\gamma_{i,u}} \right) \lambda_{i,u} \mathbf{h}_{i,i,u}^H \mathbf{w}_{i,u} \mathbf{f}_{i,u}\end{aligned}$$

where  $\mathbf{f}_{i,u}$  is in (2.10). I consider  $\sqrt{\tau_{i,u}} = \alpha^2 \left( 1 + \frac{1}{\gamma_{i,u}} \right) \lambda_{i,u} \mathbf{h}_{i,i,u}^H \mathbf{w}_{i,u}$  and thus,  $\mathbf{w}_{i,u} = \sqrt{\tau_{i,u}} \mathbf{f}_{i,u}$ .

Based on the Lagrangian dual problem, the global optimum occurs when the constraints satisfy equality conditions, i.e., active constraints. By replacing  $\mathbf{w}_{i,u}$  in (2.8) with  $\sqrt{\tau_{i,u}} \mathbf{f}_{i,u}$ , the constraints of the primal DL problem

satisfy the following conditions:

$$\begin{aligned}
1 &= \frac{\alpha^2}{\gamma_{i,u}} |\mathbf{w}_{i,u}^H \mathbf{h}_{i,i,u}|^2 - \alpha^2 \sum_{v \neq u} |\mathbf{w}_{i,v}^H \mathbf{h}_{i,i,u}|^2 \\
&\quad - \alpha^2 \sum_{\substack{j \neq i \\ v}} |\mathbf{w}_{j,v}^H \mathbf{h}_{j,i,u}|^2 - \sum_j \mathbf{h}_{j,i,u}^H \mathbf{C}_{\mathbf{q}_j^{\text{d1}} \mathbf{q}_j^{\text{d1}}} \mathbf{h}_{j,i,u} \\
&\stackrel{(a)}{=} \frac{\alpha^2}{\gamma_{i,u}} |\mathbf{f}_{i,u}^H \mathbf{h}_{i,i,u}|^2 \tau_{i,u} - \alpha^2 \sum_{(j,v) \neq (i,u)} |\mathbf{f}_{j,v}^H \mathbf{h}_{j,i,u}|^2 \tau_{j,v} \\
&\quad - \alpha(1-\alpha) \sum_{j,v} \mathbf{f}_{j,v}^H \text{diag}(\mathbf{h}_{j,i,u} \mathbf{h}_{j,i,u}^H) \mathbf{f}_{j,v} \tau_{j,v} \tag{2.46}
\end{aligned}$$

for all  $i$  and  $u$  where (a) is from (2.43) and  $\mathbf{w}_{i,u} = \sqrt{\tau_{i,u}} \mathbf{f}_{i,u}$ . I express (2.46) for all  $i, u$  as a matrix form:  $\mathbf{1} = \mathbf{\Sigma} \boldsymbol{\tau}$ . Therefore,  $\tau_{i,u}$  can be obtained as  $\boldsymbol{\tau} = \mathbf{\Sigma}^{-1} \mathbf{1}$ .  $\square$

## 2.11 Proof of Corollary 4

The proof is based on the standard function approach [105]. Let us rewrite (2.13) as  $\lambda_{i,u}^{(n+1)} = \mathcal{F}_{i,u}(\boldsymbol{\Lambda}^{(n)})$ . I need to show that  $\mathcal{F}_{i,u}(\boldsymbol{\Lambda})$  is a standard function which satisfies the followings:

- (positivity) If  $\lambda_{i,u} \geq 0 \forall i, u$ , then  $\mathcal{F}_{i,u}(\boldsymbol{\Lambda}) > 0$ .
- (monotonicity) If  $\lambda_{i,u} \geq \lambda'_{i,u} \forall i, u$ , then  $\mathcal{F}_{i,u}(\boldsymbol{\Lambda}) \geq \mathcal{F}_{i,u}(\boldsymbol{\Lambda}')$ .
- (scalability) For  $\rho > 1$ ,  $\rho \mathcal{F}_{i,u}(\boldsymbol{\Lambda}) > \mathcal{F}_{i,u}(\rho \boldsymbol{\Lambda})$ .

It can be shown that  $\mathcal{F}_{i,u}(\boldsymbol{\Lambda}^{(n)})$  satisfies the properties by carefully following the proof in Appendix II in [102].  $\square$

## 2.12 Proof of Theorem 2

Let  $\mathbf{z}_{i,u}(k)$  be the interference-plus-noise term of (2.19) and  $\mathbf{F}_i(k)$  be the MMSE equalizer  $\mathbf{F}_i(k) = \mathbf{C}_{\mathbf{z}_{i,u}(k)\mathbf{z}_{i,u}(k)}^{-1} \mathbf{g}_{i,i,u}(k)$  where

$$\begin{aligned} \mathbf{C}_{\mathbf{z}_{i,u}(k)\mathbf{z}_{i,u}(k)} &= \alpha^2 \sum_{(j,v) \neq (i,u)} \lambda_{j,v}(k) \mathbf{g}_{i,j,v}(k) \mathbf{g}_{i,j,v}^H(k) + \alpha^2 \mathbf{I}_{N_b} \\ &+ \alpha(1-\alpha) \mathbf{\Psi}_{N_b}(k) \text{diag} \left( \sum_{j=1}^{N_c} \mathbf{H}_{i,j} \mathbf{\Psi}_{N_u}^H \mathbf{\Lambda}_j \mathbf{\Psi}_{N_u} \mathbf{H}_{i,j} + \mathbf{I}_{KN_b} \right) \mathbf{\Psi}_{N_b}^H(k). \end{aligned} \quad (2.47)$$

Noting that  $\mathbf{\Psi}_{N_b}^H \mathbf{G}_{i,j} = \mathbf{H}_{i,j} \mathbf{\Psi}_{N_u}^H$ , I first rewrite the diagonal matrix in (2.47) as

$$\begin{aligned} &\text{diag} \left( \sum_{j=1}^{N_c} \mathbf{H}_{i,j} \mathbf{\Psi}_{N_u}^H \mathbf{\Lambda}_j \mathbf{\Psi}_{N_u} \mathbf{H}_{i,j} + \mathbf{I}_{KN_b} \right) \\ &= \text{diag} \left( \mathbf{\Psi}_{N_b}^H \mathbf{G}_i \mathbf{\Lambda} \mathbf{G}_i^H \mathbf{\Psi}_{N_b} + \mathbf{I}_{KN_b} \right) \end{aligned} \quad (2.48)$$

where  $\mathbf{G}_i = [\mathbf{G}_{i,1}, \dots, \mathbf{G}_{i,N_c}]$  and  $\mathbf{\Lambda} = \text{blkdiag}(\mathbf{\Lambda}_1, \dots, \mathbf{\Lambda}_{N_c})$ . Following the same steps in the proof of Theorem 1 with (2.48) and  $\mathbf{\Psi}_{N_b}(k) \mathbf{\Psi}_{N_b}^H(k) = \mathbf{I}_{N_b}$ ,  $\mathcal{P}_2$  3 with the MMSE equalizer becomes

$$\begin{aligned} &\min \sum_{i,u,k} \lambda_{i,u}(k) \\ \text{s.t. } &\bar{\mathbf{K}}_{i,k}(\mathbf{\Lambda}) \preceq \alpha \left( 1 + \frac{1}{\gamma_{i,u}(k)} \right) \lambda_{i,u}(k) \mathbf{g}_{i,i,u}(k) \mathbf{g}_{i,i,u}^H(k), \forall i, u, k \end{aligned} \quad (2.49)$$

where

$$\begin{aligned} \bar{\mathbf{K}}_{i,k}(\mathbf{\Lambda}) &= \mathbf{I}_{N_b} + \alpha \sum_{j,v} \lambda_{j,v}(k) \mathbf{g}_{i,j,v}(k) \mathbf{g}_{i,j,v}^H(k) \\ &+ (1-\alpha) \mathbf{\Psi}_{N_b}(k) \text{diag} \left( \mathbf{\Psi}_{N_b}^H \mathbf{G}_i \mathbf{\Lambda} \mathbf{G}_i^H \mathbf{\Psi}_{N_b} \right) \mathbf{\Psi}_{N_b}^H(k). \end{aligned} \quad (2.50)$$

It is necessary to show that (2.49) is equivalent to the Lagrangian dual problem of  $\mathcal{P}_2 4$ . Similarly to the proof of Theorem 1, the Lagrangian of  $\mathcal{P}_2 4$  is given in the rearranged form as

$$\begin{aligned}
\bar{\mathcal{L}} &= \sum_{i,u,k} \mu_{i,u}(k) + \alpha(1-\alpha) \sum_{i,u,k} \mu_{i,u}(k) \sum_j \mathbf{g}_{j,i,u}^H(k) \mathbf{\Psi}_{N_b} \\
&\quad \times \text{diag}(\mathbf{\Psi}_{N_b}^H \mathbf{W}_j \mathbf{W}_j^H \mathbf{\Psi}_{N_b}) \mathbf{\Psi}_{N_b}^H \mathbf{g}_{j,i,u}(k) + \sum_{i,u,k} \mathbf{w}_{i,u}^H(k) \\
&\quad \times \left( \alpha \mathbf{I}_{N_b} - \alpha^2 \left( 1 + \frac{1}{\gamma_{i,u,k}} \right) \mu_{i,u}(k) \mathbf{g}_{i,i,u}(k) \mathbf{g}_{i,i,u}^H(k) \right. \\
&\quad \left. + \alpha^2 \sum_{j,v} \mu_{j,v}(k) \mathbf{g}_{i,j,v}(k) \mathbf{g}_{i,j,v}^H(k) \right) \mathbf{w}_{i,u}(k). \tag{2.51}
\end{aligned}$$

I rewrite the quantization error term in (2.51) to manipulate  $\mathbf{W}_j$  in the diagonal matrix. Let

$$\begin{aligned}
\text{QE}(i, u, k, j) &= \sum_{i,u,k} \mu_{i,u}(k) \\
&\quad \times \sum_j \mathbf{g}_{j,i,u}^H(k) \mathbf{\Psi}_{N_b} \text{diag}(\mathbf{\Psi}_{N_b}^H \mathbf{W}_j \mathbf{W}_j^H \mathbf{\Psi}_{N_b}) \mathbf{\Psi}_{N_b}^H \mathbf{g}_{j,i,u}(k).
\end{aligned}$$

Changing the indices of  $\text{QE}(i, u, k, j)$  from  $(i, u, k, j)$  to  $(j, v, \ell, i)$ , I have

$$\begin{aligned}
\text{QE}(j, v, \ell, i) &= \sum_{j,v,\ell,i} \mu_{j,v}(\ell) \mathbf{g}_{i,j,v}^H(\ell) \mathbf{\Psi}_{N_b} \\
&\quad \times \text{diag} \left( \sum_{u,k} |\boldsymbol{\psi}_{N_b,m}^H(n) \mathbf{w}_{i,u}(k)|^2, \forall m, n \right) \mathbf{\Psi}_{N_b}^H \mathbf{g}_{i,j,v}(\ell) \tag{2.52}
\end{aligned}$$

where  $\boldsymbol{\psi}_{N_b,m}(n)$  denotes the  $(m + (n-1)N_b)$ th column of  $\mathbf{\Psi}_{N_b}$ , i.e.,  $\boldsymbol{\psi}_{N_b,m}(n) = [\mathbf{w}_{\text{DFT},n} \otimes \mathbf{I}_{N_b}]_{:,m}$  for  $m = 1, \dots, N_b$ ,  $n = 1, \dots, K$ , and  $\mathbf{w}_{i,u}(k)$  is the  $(kN_u + u)$ th column of  $\mathbf{W}_j$ , i.e., the entire column of  $\mathbf{W}_i$  that corresponds to the precoder

for  $k$ th subcarrier of user  $u$ . Let  $\mathbf{M}_i(k) = \text{diag}(\mu_{i,1}(k), \dots, \mu_{i,N_u}(k))$ ,  $\underline{\mathbf{M}}_i = \text{blkdiag}(\mathbf{M}_i(0), \dots, \mathbf{M}_i(K-1))$ , and  $\underline{\mathbf{M}} = [\underline{\mathbf{M}}_1, \dots, \underline{\mathbf{M}}_{N_c}]$ . Recalling that  $\Psi_{N_b}(k) = ([\mathbf{W}_{\text{DFT}}]_{k+1,:} \otimes \mathbf{I}_{N_b})$  and  $\underline{\mathbf{G}}_i = [\underline{\mathbf{G}}_{i,1}, \dots, \underline{\mathbf{G}}_{i,N_c}]$ , (2.52) is rewritten as (2.53) which is on the top of the next page. Here (a) comes from  $\underline{\mathbf{w}}_{i,u}^H(k) \Psi_{N_b} = \mathbf{w}_{i,u}^H(k) \Psi_{N_b}(k)$  as  $\underline{\mathbf{w}}_{i,u}(k)$  has nonzero elements  $\mathbf{w}_{i,u}(k)$  only in the place that corresponds to the precoder for subcarrier  $k$ , and  $\underline{g}_{i,j,v,r}(\ell)$  and  $\psi_{N_b,m,r}(n)$  are the  $r$ th elements of  $\underline{\mathbf{g}}_{i,j,v}(\ell)$  and  $\psi_{N_b,m}(n)$ , respectively.

Applying (2.53) to the Lagrangian in (2.51), I have

$$\begin{aligned} \bar{\mathcal{L}} = & \sum_{i,u,k} \mu_{i,u}(k) + \sum_{i,u,k} \mathbf{w}_{i,u}^H(k) \left( \alpha \mathbf{I}_{N_b} - \alpha^2 \left( 1 + \frac{1}{\gamma_{i,u,k}} \right) \right. \\ & \times \mu_{i,u}(k) \mathbf{g}_{i,i,u}(k) \mathbf{g}_{i,i,u}^H(k) + \alpha^2 \sum_{j,v} \mu_{j,v}(k) \mathbf{g}_{i,j,v}(k) \mathbf{g}_{i,j,v}^H(k) \\ & \left. + \alpha(1-\alpha) \Psi_{N_b}(k) \text{diag}(\Psi_{N_b}^H \underline{\mathbf{G}}_i \underline{\mathbf{M}} \underline{\mathbf{G}}_i^H \Psi_{N_b}) \Psi_{N_b}^H(k) \right) \mathbf{w}_{i,u}(k). \end{aligned}$$

Following similar steps in the proof of Theorem 1, the Lagrangian dual problem of  $\mathcal{P}_2 4$  becomes

$$\begin{aligned} & \max_{\mu_{i,u}} \sum_{i,u,k} \mu_{i,u}(k) \tag{2.54} \\ \text{s.t. } & \bar{\mathbf{K}}_{i,k}(\underline{\mathbf{M}}) \succeq \alpha \left( 1 + \frac{1}{\gamma_{i,u,k}} \right) \mu_{i,u}(k) \mathbf{g}_{i,i,u}(k) \mathbf{g}_{i,i,u}^H(k) \end{aligned}$$

where

$$\begin{aligned} \bar{\mathbf{K}}_{i,k}(\underline{\mathbf{M}}) = & \mathbf{I}_{N_b} + \alpha \sum_{j,v} \mu_{j,v}(k) \mathbf{g}_{i,j,v}(k) \mathbf{g}_{i,j,v}^H(k) \\ & + (1-\alpha) \Psi_{N_b}(k) \text{diag}(\Psi_{N_b}^H \underline{\mathbf{G}}_i \underline{\mathbf{M}} \underline{\mathbf{G}}_i^H \Psi_{N_b}) \Psi_{N_b}^H(k). \end{aligned}$$

Since the problem in (2.54) has its optimal solution when the constraints are active, it is also equivalent to (2.49). This completes the proof.

### 2.13 Proof of Corollary 5

I use (2.53) to manipulate the precoders  $\mathbf{W}_i(k)$  in the diagonal matrix of the quantization term in the SQINR (2.25), and follow similar approach as the proof of Corollary 1. Then,  $\mathcal{P}_2 4$  can be cast to the SOCP. In addition,  $\mathcal{P}_2 4$  is strictly feasible. This completes the proof.  $\square$

### 2.14 Proof of Corollary 6

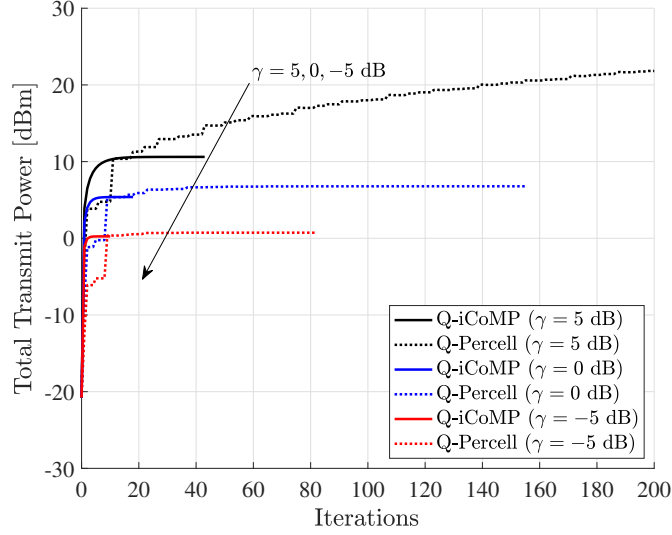
To satisfy the KKT stationarity condition with the DL constraint in (2.27), the SQINR of subcarrier  $k$  of user  $u$  in cell  $i$  needs to fulfill the target SQINR with equality. Let us define  $\mu_{i',u'}(n)$  where  $\mu_{i',u'}(n) = 1$  if  $i' = i$ ,  $u' = u$  and  $n = k$ , and  $\mu_{i',u'}(n) = 0$  otherwise. To compose the DL constraint in a



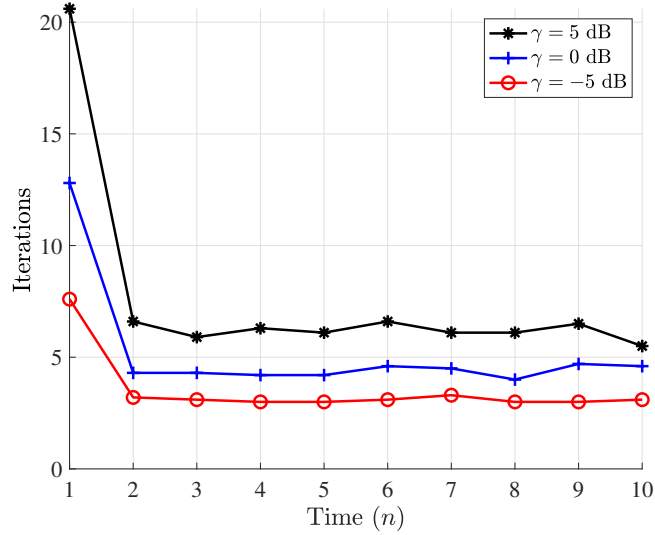
tractable form, I can rewrite the quantization error term in (2.25) as

$$\begin{aligned}
& \sum_{j=1}^{N_c} \underline{\mathbf{g}}_{j,i,u}^H(k) \underline{\Psi}_{N_b} \text{diag}(\underline{\Psi}_{N_b}^H \underline{\mathbf{W}}_j \underline{\mathbf{W}}_j^H \underline{\Psi}_{N_b}) \underline{\Psi}_{N_b}^H \underline{\mathbf{g}}_{j,i,u}(k) \\
&= \sum_{i',u',n,j} \mu_{i',u'}(n) \underline{\mathbf{g}}_{j,i',u'}^H(n) \underline{\Psi}_{N_b} \\
&\quad \times \text{diag}(\underline{\Psi}_{N_b}^H \underline{\mathbf{W}}_j \underline{\mathbf{W}}_j^H \underline{\Psi}_{N_b}) \underline{\Psi}_{N_b}^H \underline{\mathbf{g}}_{j,i',u'}(n) \\
&\stackrel{(a)}{=} \sum_{j,v,\ell} \underline{\mathbf{w}}_{j,v}^H(\ell) \underline{\Psi}_{N_b}(\ell) \text{diag}(\underline{\Psi}_{N_b}^H \underline{\mathbf{G}}_j \underline{\mathbf{M}} \underline{\mathbf{G}}_j^H \underline{\Psi}_{N_b}) \underline{\Psi}_{N_b}^H(\ell) \underline{\mathbf{w}}_{j,v}(\ell) \\
&\stackrel{(b)}{=} \sum_{j,v,\ell} \underline{\mathbf{w}}_{j,v}^H(\ell) \underline{\Psi}_{N_b}(\ell) \\
&\quad \times \text{diag}\left(\underline{\Psi}_{N_b}^H \underline{\mathbf{g}}_{j,i,u}(k) \underline{\mathbf{g}}_{j,i,u}^H(k) \underline{\Psi}_{N_b}\right) \underline{\Psi}_{N_b}^H(\ell) \underline{\mathbf{w}}_{j,v}^H(\ell), \tag{2.55}
\end{aligned}$$

where (a) comes from following the same steps in (2.52) and (2.53). Recalling the definition of  $\underline{\mathbf{M}}$  defined in the proof of Theorem 2 with slight abuse of notations, (b) follows from  $\underline{\mathbf{G}}_j \underline{\mathbf{M}} \underline{\mathbf{G}}_j^H = \underline{\mathbf{g}}_{j,i,u}(k) \underline{\mathbf{g}}_{j,i,u}^H(k)$ . Replacing  $\underline{\mathbf{w}}_{i,u}(n)$  with  $\sqrt{\mathcal{I}_{i,u}}(n) \underline{\mathbf{f}}_{i,u}(n)$  and using (2.55), the DL SQINR constraint in (2.27) can be rewritten, and the rest of the proof is similar to Corollary 3.  $\square$



(a) Total Power vs. Iterations



(b) Iterations vs. Time

Figure 2.7: Convergence results for  $N_b = 64$  antennas,  $N_c = 4$  cells,  $N_u = 3$  per cell, and  $b = 3$  quantization bits. (a) shows total transmit power with respect to the number of iterations and (b) shows the total number of iterations for convergence with respect to time for channel realization.

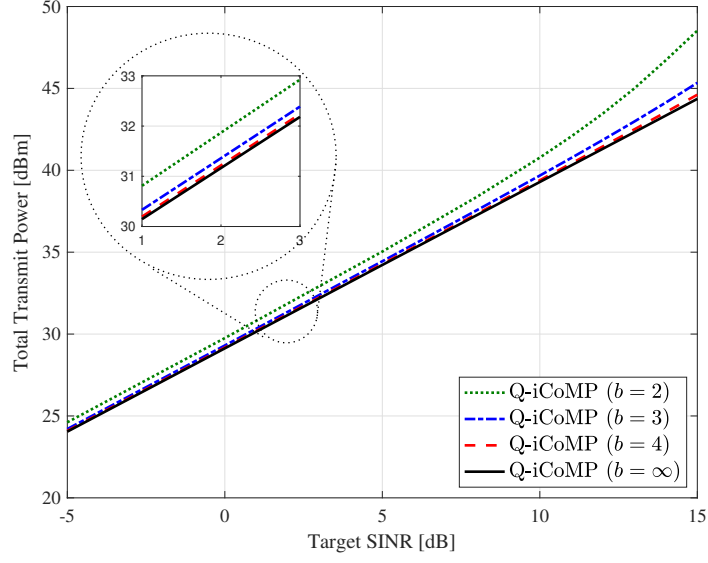


Figure 2.8: UL total transmit power versus the target SQINR for  $N_b = 16$  BS antennas,  $N_c = 2$  cells,  $N_u = 2$  users per cell,  $b \in \{2, 3, 4, \infty\}$  quantization bits, and 64 subcarriers.

$$\begin{aligned}
\mathcal{L}(\mathbf{w}_{i,u}, \mu_{i,u}) = & \sum_{i,u} \mu_{i,u} + \alpha \sum_{i,u} \mathbf{w}_{i,u}^H \left( \mathbf{I}_{N_b} - \alpha \left( 1 + \frac{1}{\gamma_{i,u}} \right) \mu_{i,u} \mathbf{h}_{i,i,u} \mathbf{h}_{i,i,u}^H \right. \\
& \left. + \alpha \sum_{j,v} \mu_{j,v} \mathbf{h}_{i,j,v} \mathbf{h}_{i,j,v}^H + (1-\alpha) \text{diag}(\mathbf{H}_i \mathbf{M} \mathbf{H}_i^H) \right) \mathbf{w}_{i,u}. \quad (2.38)
\end{aligned}$$


---

$$\begin{aligned}
& \sum_{j,v,\ell,i} \mu_{j,v}(\ell) \sum_{m,n} \left( \sum_{u,k} |\boldsymbol{\psi}_{N_b,m}^H(n) \underline{\mathbf{w}}_{i,u}(k)|^2 \times \right. \\
& \quad \left. \left( \sum_r \underline{g}_{i,j,v,r}^*(\ell) \psi_{N_b,m,r}(n) \right) \left( \sum_{r'} \underline{g}_{i,j,v,r'}(\ell) \psi_{N_b,m,r'}^*(n) \right) \right) \\
&= \sum_{i,u,k} \underline{\mathbf{w}}_{i,u}^H(k) \left( \sum_{m,n} \boldsymbol{\psi}_{N_b,m}(n) \times \right. \\
& \quad \left. \left( \sum_{j,v,\ell} \mu_{j,v}(\ell) \boldsymbol{\psi}_{N_b,m}^H(n) \underline{\mathbf{g}}_{i,j,v}(\ell) \underline{\mathbf{g}}_{i,j,v}^H(\ell) \boldsymbol{\psi}_{N_b,m}(n) \right) \boldsymbol{\psi}_{N_b,m}^H(n) \right) \underline{\mathbf{w}}_{i,u}(k) \\
&= \sum_{i,u,k} \underline{\mathbf{w}}_{i,u}^H(k) \left( \sum_{m,n} \boldsymbol{\psi}_{N_b,m}(n) \boldsymbol{\psi}_{N_b,m}^H(n) \underline{\mathbf{G}}_i \underline{\mathbf{M}} \underline{\mathbf{G}}_i^H \boldsymbol{\psi}_{N_b,m}(n) \boldsymbol{\psi}_{N_b,m}^H(n) \right) \underline{\mathbf{w}}_{i,u}(k) \\
&= \sum_{i,u,k} \underline{\mathbf{w}}_{i,u}^H(k) \boldsymbol{\Psi}_{N_b} \text{diag} \left( \boldsymbol{\Psi}_{N_b}^H \underline{\mathbf{G}}_i \underline{\mathbf{M}} \underline{\mathbf{G}}_i^H \boldsymbol{\Psi}_{N_b} \right) \boldsymbol{\Psi}_{N_b}^H \underline{\mathbf{w}}_{i,u}(k) \\
&\stackrel{(a)}{=} \sum_{i,u,k} \underline{\mathbf{w}}_{i,u}^H(k) \boldsymbol{\Psi}_{N_b}(k) \text{diag} \left( \boldsymbol{\Psi}_{N_b}^H \underline{\mathbf{G}}_i \underline{\mathbf{M}} \underline{\mathbf{G}}_i^H \boldsymbol{\Psi}_{N_b} \right) \boldsymbol{\Psi}_{N_b}^H(k) \underline{\mathbf{w}}_{i,u}(k). \tag{2.53}
\end{aligned}$$


---

## Chapter 3

# Coordinated Per-Antenna Maximum Power Minimization for Low-Resolution Systems

In this chapter<sup>1</sup>, I investigate multicell-coordinated beamforming for massive multiple-input-multiple-output (MIMO) orthogonal frequency division multiplexing (OFDM) communications with low-resolution data converters when the power restriction is added for a more realistic deployment. In particular, I aim to find the downlink (DL) beamformer that minimizes the maximum power on transmit antenna array of each BS under received signal-to-quantization-and-interference-plus-noise ratio (SQINR) constraints while minimizing per-antenna transmit power. The primary milestones of this work are (1) formulating the quantized DL OFDM antenna power minimax problem and deriving its associated dual problem, (2) showing strong duality and interpreting the dual as a virtual quantized uplink (UL) OFDM problem, and (3) developing an iterative minimax algorithm to identify a feasible solution

---

<sup>1</sup>This chapter is based on the following submitted paper: Y. Cho, J. Choi, and B. L. Evans, “Coordinated Per-Antenna Power Minimization for Multicell Massive MIMO Systems with Low-Resolution Data Converters,” submitted to *IEEE Transactions on Communications*, 2023. This work was published in part in the following conference paper: Y. Cho, J. Choi, and B. L. Evans, “Coordinated Beamforming in Quantized Massive MIMO Systems with Per-Antenna Constraints,” in *IEEE Wireless Communications and Networking Conference (WCNC)*, Apr. 10-13, 2022. This work was supervised by Prof. Brian L. Evans.

based on the dual problem with performance validation through simulations. Specifically, the dual problem requires joint optimization of virtual UL transmit power and noise covariance matrices. To solve the problem, I first derive the optimal dual solution of the UL problem for given noise covariance matrices. Then, I use the solution to compute the associated DL beamformer. Subsequently, using the DL beamformer, I update the UL noise covariance matrices via subgradient projection. Finally, I propose an iterative algorithm by repeating the steps for optimizing DL beamformers. Simulations evaluate the effectiveness of the proposed algorithm in terms of the maximum antenna transmit power and peak-to-average-power ratio which are directly related to hardware efficiency of large-scale MIMO OFDM communication systems..

### 3.1 Introduction

Massive MIMO techniques have drawn attention for future wireless communication systems because of its remarkable gain in spectral efficiency and capacity [56]. However, employing the massive number of power-hungry high-resolution analog-to-digital converters (ADCs) and digital-to-analog converters (DACs) attached to the antenna arrays results in prohibitively high power consumption. Accordingly, the adoption of low-resolution data converters in communication building blocks has gathered momentum as a promising power-efficient alternative and has been widely investigated [14, 15, 17–19, 22, 67, 89, 107].

In addition to power consumption, interference has emerged as a crit-

ical consideration in modern wireless systems. Consequently, intra-cell and inter-cell interference as well as quantization error must be carefully considered when analyzing and designing power-efficient multicell communication networks to achieve a desired performance. Moreover, for practical implementations, it is desirable to impose a per-antenna power constraint that restricts the transmit power of each antenna because the communication system can operate with more energy-efficient power amplifiers and prevent nonlinear distortion [23, 106]. In this regard, I investigate coordinated multipoint (CoMP) beamforming and power control problems in multicell and multiuser massive MIMO OFDM systems with low-resolution data converters and per-antenna level power and quality-of-service constraints.

### 3.1.1 Prior Work

Low-resolution ADC architectures have been the subject of extensive research in recent years to provide power-efficient communications [17–19, 22, 39, 69, 89, 97, 98, 104, 110]. In order to properly handle the severe nonlinearities in low-resolution ADCs, many studies have re-engineered essential wireless communication functions such as channel estimation and data detection [17, 22, 39, 89, 97, 98]. Since low-resolution data converters destroy the orthogonality of subcarriers in OFDM systems, novel OFDM channel estimation and symbol detection were developed and integrated into a turbo framework, justifying its feasibility and reliability in over-the-air experiments when using low-resolution ADCs [97, 98]. In [22], a near maximum likelihood channel estimation and

symbol detection were proposed for 1-bit ADCs while showing improved estimation accuracy compared to expectation-maximum estimators. Maximum a-posteriori detection and channel estimation with low-resolution ADCs showed that 4-bit ADCs are sufficient to achieve near-optimal performance in massive MIMO OFDM systems [89]. To facilitate the learning of likelihood probabilities in 1-bit ADC maximum likelihood data detector, a robust learning with artificial noise was presented in [17]. The authors in [53, 110] developed data detectors for mixed-ADC systems that assign either 1-bit or infinite-resolution depending on channel gain. In addition, a resolution-adaptive ADC system with a bit-allocation algorithm was proposed while outperforming the conventional fixed-precision low-resolution ADC systems in terms of both spectral and energy efficiency [18]. For analytic tractability, the severe non-linearity of the low-resolution quantizer was linearized using Bussgang decomposition [39] and the additive quantization noise model (AQNM) [15, 19, 69, 104], while producing useful algorithms and insightful analytical results.

For downlink transmission, a number of works have reduced power consumption and hardware cost using low-resolution DACs [38, 51, 71]. Using Bussgang decomposition, the authors in [38] demonstrated a marginal communication gap in achievable rates for linear precoders with 3 to 4-bit DACs compared to infinite-resolution DACs and further proposed a non-linear precoder in 1-bit DAC systems via relaxation and sphere precoding. The use of  $2.5\times$  more transmit antennas can compensate for the spectral efficiency loss brought on by the use of 1-bit DACs according to the analyzed rate of



the quantized downlink systems with matched-filter precoding [51]. Based on constructive interference and decision regions, low-complexity symbol-level precoding methods for 1-bit DAC systems were developed for quadrature-amplitude-modulation constellations in [71]. The authors in [83] proposed 1-bit and constant-envelope precoding methods. For quantized downlink OFDM systems, the authors in [40] derived a lower bound on achievable sum-rate using linear precoding and oversampling DACs. The authors in [108] considered massive MIMO relaying systems with mixed-DACs and mixed-ADCs at the relay and derived exact and closed-form expressions for the achievable rate which approach infinite-resolution performance using only 2-3 bits thanks to strong synergy with large-scale antenna arrays. For downlink communications with low-resolution DACs, Busgang decomposition that linearizes the low-resolution DAC system was adopted in [38, 51, 103] to develop precoders and analyze system performance. By applying AQNM to massive MIMO systems with millimeter wave channels, the authors in [78] introduced fully-connected and partially-connected hybrid beamforming architectures under low-resolution DACs which are more energy-efficient than conventional digital-only precoders.

As modern cellular communication systems are primarily limited by interference, research efforts and later standards supported CoMP to coordinate transmission by multiple base stations (BSs) in order to reduce inter-cell interference, thereby improving data rates and coverage [8, 23, 36, 44, 65, 76, 77, 85, 87]. The authors in [44] demonstrated that the synergy between CoMP and

massive MIMO is advantageous to 5G communication systems due to a more robust link, localized interference, and reduced backhaul overhead. The feasibility of CoMP was demonstrated for both UL and DL in physical testbeds with improved average throughput and cell edge throughput [36].

To improve data rate and satisfy demanding requirements of cellular systems, many papers have contributed to beamforming design [8, 65, 85]. The DL beamforming problem was cast as a semidefinite programming problem and efficiently solved via interior point methods [8]. Noting that signals from neighboring BSs have significant impact, the authors in [65] proposed a near-optimal distributed DL beamforming algorithm based on message passing between neighboring BSs without requiring centralized processing. To improve the data rate of cell-edge users, the CoMP beamforming problem based on interference alignment was also studied in a non-orthogonal multiple access system [85].

To further unleash the potential of CoMP systems, joint optimization of beamforming and power control has been proposed [76, 77, 87, 102]. For UL transmission, authors in [77] proposed a fixed-point algorithm that jointly solves beamforming and power control problems and proves the existence of at least one optimal solution. Authors in [76] formulated a virtual UL system model whose combiner and power control solutions are used to iteratively update the DL beamforming solution. For multiuser MIMO systems, linear programming UL–DL duality led to centralized and decentralized algorithms to efficiently solve the joint beamforming and power control problem [87]. Au-

thors in [102] derived an iterative algorithm that finds optimal UL power control and DL beamforming solutions based on Lagrangian theory and brought insights to [23] which generalized the algorithm to multicell multiuser MIMO systems.

Recently, a coarsely quantized CoMP beamforming and power control problem was studied for OFDM systems in [15]. The UL-DL beamforming duality was extended to the quantized OFDM systems, and an iterative algorithm for solving the DL total transmit power minimization problems was developed by leveraging the duality [15] without requiring explicit estimation of inter-cell interference. It was shown that the proposed algorithm can be performed in a distributed fashion by estimating the covariance matrix of the received signals at local BSs. The problem considered in [15] only focused on the power minimization with the quality-of-service constraints. However, it is necessary to minimize the transmit power consumed at each antenna to simplify the design of the power amplifier and avoid distortion from the non-linearity of the power amplifier in the high power regime. Therefore, lowering the peak power can help us scale up the multi-cell and multi-user communication network. Employing cell-free MIMO systems is considered as a scalable way to implement CoMP [35]; however, cell-free MIMO solutions are missing either per-antenna level power restriction or the joint optimization of DL beamformer and UL power control [9, 109]. Therefore, a thorough study on the quantized DL CoMP beamforming and UL power control for minimizing the transmit power with per-antenna power constraints would make a worthwhile

contribution toward a more practical CoMP deployment.

### 3.1.2 Contributions

In this work, I consider downlink multicell massive MIMO OFDM communications in which each BS with multiple antennas serves dedicated users with a single antenna. The BS are equipped with low-resolution data converters, i.e., DACs and ADCs, and cooperate for beamforming and PC. In such a system, I investigate a DL antenna power minimization problem with quality-of-service constraints. The contributions are summarized as follows:

- **Formulating the DL antenna power minimax problem and deriving its dual.** I aim to minimize the maximum transmit power over all transmit antennas and formulate the problem with individual SQINR constraints. As the main contribution of this chapter, I derive the Lagrangian dual of the primal DL OFDM problem, which can be considered as a virtual UL OFDM transmit power minimization problem with uncertain noise covariance matrices. This finding extends the previous DL-UL duality under per-antenna power constraints [106] to the quantized OFDM systems. By transforming the DL OFDM problem to a strictly feasible second-order cone program (SOCP), I show that strong duality holds between the primal DL OFDM problem and its associated dual, i.e., the virtual UL OFDM problem in this work.
- **Developing an iterative minimax algorithm to provide a feasible solution.** Leveraging the strong duality, I develop an iterative

algorithm to solve the primal DL OFDM beamforming problem; I first solve the dual UL OFDM problem for a fixed set of UL noise covariance matrices. I then compute the DL beamformer via linear transformation of the obtained UL solution. Using the DL beamformer, I update the UL noise covariance matrices via projected subgradient ascent method. Finally, I repeat the steps until the UL noise covariance matrices converge. Although the DL beamforming problem can be cast to a semidefinite programming, the proposed direct iterative updates are in general more efficient and insightful.

- **Validating the proposed algorithm through extensive simulations.** Simulation results validate the derived results and algorithm in both wideband and narrowband scenarios. The proposed algorithm outperforms approaches that do not impose per-antenna constraints in terms of the maximum antenna transmit power consumption. I further show the significant advantages of the proposed algorithm with per-antenna constraints by comparing peak-to-average-power ratio (PAPR) which is a paramount measure for the design of the power amplifiers and other nonlinear electronics in OFDM communication systems.

## 3.2 System Model

### 3.2.1 Network and Signal Model

I consider a wideband multicell and multiuser MIMO network with  $N_c$  cells,  $N_u$  single-antenna users per cell, and  $K$  subcarriers. All BSs are

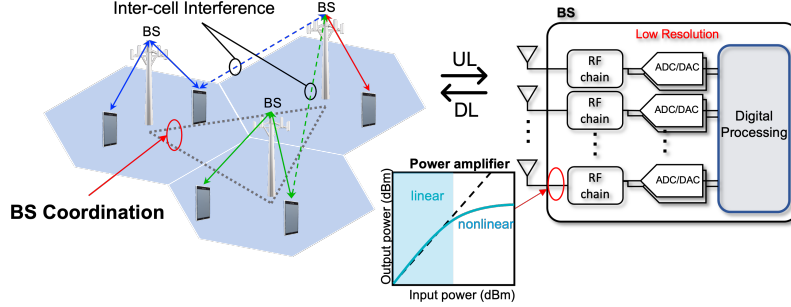


Figure 3.1: Multicell and multiuser MIMO communication configuration when each base station (BS) is equipped with low-resolution ADCs and DACs. The power amplifier causes nonlinear distortion in the high input power regime.

equipped with  $N_b$  antennas ( $N_b \gg N_u$ ). The BS in cell  $i$  is denoted as  $BS_i$  which serves  $N_u$  dedicated users in cell  $i$ . I assume the BSs for all  $N_c$  cells cooperate and are equipped with low-resolution DACs with the same number of DAC quantization bits  $b$  as shown in Fig. 3.1. Time-division duplexing (TDD) is assumed to exploit channel reciprocity. The BSs are considered to have perfect channel state information (CSI) for all channels as they cooperate with each other, whereas the users are assumed to have perfect CSI only for their own channel.

I consider a DL broadcast channel where the  $BS_i$  generates  $\mathbf{s}_i(k) \in \mathbb{C}^{N_u}$  that contains the dedicated symbols for  $N_u$  users in cell  $i \in \{1, \dots, N_c\}$  at subcarrier  $k \in \{0, \dots, K-1\}$ . In addition, I use  $\mathbf{W}_i(k) = [\mathbf{w}_{i,1}(k), \dots, \mathbf{w}_{i,N_u}(k)] \in \mathbb{C}^{N_b \times N_u}$  to denote the matrix of precoders, and the  $u$ th symbol in  $\mathbf{s}_i(k)$  is precoded via  $\mathbf{w}_{i,u}(k)$ . I then define the precoded frequency domain symbol for user  $u$  in cell  $i$  at subcarrier  $k$  as  $\mathbf{u}_i(k) = \mathbf{W}_i(k)\mathbf{s}_i(k)$ . Let  $\mathbf{x}_i(k) \in \mathbb{C}^{N_b}$  be the vector of OFDM symbols of  $N_u$  users in cell  $i$  at time  $k$ . I stack the OFDM symbol

vectors at BS<sub>*i*</sub> over  $K$  time slots as  $\underline{\mathbf{x}}_i = [\mathbf{x}_i^T(0), \dots, \mathbf{x}_i^T(K-1)]^T \in \mathbb{C}^{KN_b}$ , which is given as

$$\underline{\mathbf{x}}_i = (\mathbf{W}_{\text{DFT}}^H \otimes \mathbf{I}_{N_b}) \underline{\mathbf{u}}_i \quad (3.1)$$

$$= \mathbf{\Psi}_{N_b}^H \underline{\mathbf{W}}_i \underline{\mathbf{s}}_i, \quad (3.2)$$

where  $\mathbf{W}_{\text{DFT}} \in \mathbb{C}^{K \times K}$  represents a normalized discrete Fourier transform (DFT) matrix,  $\underline{\mathbf{u}}_i = [\mathbf{u}_i^T(0), \dots, \mathbf{u}_i^T(K-1)]^T \in \mathbb{C}^{KN_b}$ ,  $\mathbf{\Psi}_{N_b} = \mathbf{W}_{\text{DFT}} \otimes \mathbf{I}_{N_b}$ ,  $\underline{\mathbf{W}}_i = \text{blkdiag}(\mathbf{W}_i(0), \dots, \mathbf{W}_i(K-1)) \in \mathbb{C}^{KN_b \times KN_u}$ , and  $\underline{\mathbf{s}}_i = [\mathbf{s}_i^T(0), \dots, \mathbf{s}_i^T(K-1)]^T \in \mathbb{C}^{KN_u}$ .

Before transmitting the signals,  $\underline{\mathbf{x}}_i$  is quantized by the low-resolution DACs with  $b$  quantization bits. I adopt the AQNM [15, 69] to elicit a linearized approximation of the quantization process derived from assuming a scalar minimum-mean-squared-error (MMSE) quantizer with Gaussian signaling. The quantized signal vector of input  $\underline{\mathbf{x}}_i$  with the AQNM is represented as

$$Q(\underline{\mathbf{x}}_i) \approx \underline{\mathbf{x}}_{\text{q},i} = \alpha \underline{\mathbf{x}}_i + \underline{\mathbf{q}}_i \quad (3.3)$$

$$= [\mathbf{x}_{\text{q},i}^T(0), \dots, \mathbf{x}_{\text{q},i}^T(K-1)]^T \quad (3.4)$$

where  $Q(\cdot)$  is a data quantizer applied for real and imaginary parts,  $\underline{\mathbf{q}}_i = [\mathbf{q}_i^T(0), \dots, \mathbf{q}_i^T(K-1)]^T \in \mathbb{C}^{KN_b}$  denotes the stacked quantization noise vector at BS<sub>*i*</sub> with  $\mathbf{q}_i(k)$  denoting the quantization noise vector for the quantization input of  $\mathbf{x}_i(k)$ ,  $\mathbf{x}_{\text{q},i}(k) = \alpha \mathbf{x}_i(k) + \mathbf{q}_i(k)$  is the quantized signal transmitted by BS<sub>*i*</sub> at the  $k$ th time slot, and  $\alpha$  is the quantization gain defined as  $\alpha =$

$1 - \beta$  where the values of  $\beta$  are listed in Table 2.1 in Chapter 2 assuming  $\mathbf{s}_i(k) \sim \mathcal{CN}(\mathbf{0}_{N_u}, \mathbf{I}_{N_u}), \forall i, k$ . The lower the resolution of DACs, the smaller  $\alpha$  is triggered, reflecting more severe quantization effects. I assume that the quantization noise is uncorrelated with the quantization input and follows a complex Gaussian distribution, i.e.,  $\underline{\mathbf{q}}_i \sim \mathcal{CN}(\mathbf{0}, \mathbf{C}_{\underline{\mathbf{q}}_i \underline{\mathbf{q}}_i})$  which is the worst case in terms of the achievable rate. The covariance matrix  $\mathbf{C}_{\underline{\mathbf{q}}_i \underline{\mathbf{q}}_i}$  is computed as [15]

$$\mathbf{C}_{\underline{\mathbf{q}}_i \underline{\mathbf{q}}_i} = \alpha(1 - \alpha) \text{diag}(\underline{\Psi}_{N_b}^H \underline{\mathbf{W}}_i \underline{\mathbf{W}}_i^H \underline{\Psi}_{N_b}). \quad (3.5)$$

Because of the multicell broadcast channel,  $N_u$  users in cell  $i$  receive signals from all BSs. Stacking over  $K$  subcarriers after removing cyclic prefix and applying the DFT, the received signals at the users in cell  $i$  become [15]

$$\underline{\mathbf{y}}_i = \alpha \underline{\mathbf{G}}_{j,i}^H \underline{\mathbf{W}}_i \underline{\mathbf{s}}_i + \alpha \sum_{j \neq i}^{N_c} \underline{\mathbf{G}}_{j,i}^H \underline{\mathbf{W}}_j \underline{\mathbf{s}}_j + \underline{\tilde{\mathbf{q}}}_j + \underline{\tilde{\mathbf{n}}}_i \in \mathbb{C}^{KN_u}. \quad (3.6)$$

Here, the DL frequency domain channels combined accross all  $K$  subcarriers are defined as  $\underline{\mathbf{G}}_{j,i}^H = \text{blkdiag}(\mathbf{G}_{j,i}^H(0), \dots, \mathbf{G}_{j,i}^H(K-1)) \in \mathbb{C}^{KN_u \times KN_b}$ , where  $\mathbf{G}_{j,i}(k) = \sum_{\ell=0}^{L-1} \mathbf{H}_{j,i,\ell} e^{-\frac{j2\pi k\ell}{K}}$  is the individual UL frequency domain channel for the  $k$ th subcarrier between BS $_j$  and users in cell  $i$  (by channel reciprocity, which is an inherit feature of TDD systems,  $\mathbf{G}_{j,i}(k)$  can be interpreted as the UL frequency domain channel matrix),  $\mathbf{H}_{j,i,\ell}$  is the UL time domain channel between BS $_j$  and users in cell  $i$  for the  $\ell$ th channel tap, and  $L$  is the delay spread. In addition,  $\underline{\tilde{\mathbf{q}}}_j = [\tilde{\mathbf{q}}_j^T(0), \dots, \tilde{\mathbf{q}}_j^T(K-1)]^T = \sum_{j=1}^{N_c} \underline{\mathbf{G}}_{j,i}^H \underline{\Psi}_{N_b} \underline{\mathbf{q}}_j$  and  $\underline{\tilde{\mathbf{n}}}_i = [\tilde{\mathbf{n}}_i(0), \dots, \tilde{\mathbf{n}}_i(K-1)]^T = \underline{\Psi}_{N_u} \underline{\mathbf{n}}_i$  where  $\underline{\Psi}_{N_u} = \mathbf{W}_{\text{DFT}} \otimes \mathbf{I}_{N_u}$  and



$\underline{\mathbf{n}}_i = [\underline{\mathbf{n}}_i^T(0), \dots, \underline{\mathbf{n}}_i^T(K-1)]^T \sim \mathcal{CN}(\mathbf{0}_{KN_u}, \sigma^2 \mathbf{I}_{KN_u})$  denotes the stacked additive white Gaussian noise (AWGN) vector over  $K$  time slots for  $N_u$  users in cell  $i$ . I observe that the received signal at user  $u$  in cell  $i$  for subcarrier  $k$  is expressed as

$$y_{i,u}(k) = \alpha \mathbf{g}_{i,i,u}^H(k) \mathbf{w}_{i,u}(k) s_{i,u}(k) + \alpha \sum_{\substack{N_c, N_u \\ (j,v) \neq (i,u)}} \mathbf{g}_{j,i,u}^H(k) \mathbf{w}_{j,v}(k) s_{j,v}(k) + \tilde{q}_{i,u}(k) + \tilde{n}_{i,u}(k), \quad (3.7)$$

where  $\mathbf{g}_{j,i,u}(k)$  indicates the  $u$ th column of  $\mathbf{G}_{j,i}$  and  $s_{i,u}(k)$ ,  $\tilde{q}_{i,u}(k)$ , and  $\tilde{n}_{i,u}(k)$  represent the  $u$ th element of  $\mathbf{s}_i(k)$ ,  $\tilde{\mathbf{q}}_i(k)$ , and  $\tilde{\mathbf{n}}_i(k)$ , respectively.

### 3.2.2 Problem Formulation

Based on (3.5)-(3.7), the DL SQINR for user  $u$  in cell  $i$  at subcarrier  $k$  is represented as

$$\Gamma_{i,u}(k) = \frac{\alpha^2 |\mathbf{g}_{i,i,u}^H(k) \mathbf{w}_{i,u}(k)|^2}{\alpha^2 \sum_{\substack{N_c, N_u \\ (j,v) \neq (i,u)}} |\mathbf{g}_{j,i,u}^H(k) \mathbf{w}_{j,v}(k)|^2 + Q_{i,u}(k) + \sigma^2}, \quad (3.8)$$

whose first term in the denominator is interference and  $Q_{i,u}(k)$  is quantization error defined as

$$Q_{i,u}(k) = \sum_{j=1}^{N_c} \underline{\mathbf{g}}_{j,i,u}^H(k) \mathbf{\Psi}_{N_b} \mathbf{C}_{\mathbf{q}_j \mathbf{q}_j} \mathbf{\Psi}_{N_b}^H \underline{\mathbf{g}}_{j,i,u}(k). \quad (3.9)$$

Here,  $\underline{\mathbf{g}}_{j,i,u}(k)$  denotes the  $(kN_u + u)$ th column of  $\underline{\mathbf{G}}_{j,i}$ , i.e., the column of  $\underline{\mathbf{G}}_{j,i}$  which is the channel for subcarrier  $k$  of user  $u$ . Since BS $_i$  sends  $\mathbf{x}_{\mathbf{q},i}(k)$  at the  $k$ th time slot, the average transmit power of the  $m$ th antenna of BS $_i$  at the  $k$ th time slot is written as  $\left[ \mathbb{E}[\mathbf{x}_{\mathbf{q},i}(k) \mathbf{x}_{\mathbf{q},i}^H(k)] \right]_{m,m}$ . Using (3.8), the DL

OFDM transmit power minimization problem with per-antenna power for each antenna  $m$  and SQINR constraints is finally formulated as

$$\mathcal{P}_3 1 : \underset{\mathbf{w}_{i,u}(k), p_0}{\text{minimize}} \quad p_0 \quad (3.10)$$

$$\text{subject to} \quad \Gamma_{i,u}(k) \geq \gamma_{i,u}(k) \quad \forall i, u, k \quad (3.11)$$

$$\left[ \mathbb{E}[\mathbf{x}_{q,i}(k)\mathbf{x}_{q,i}^H(k)] \right]_{m,m} \leq p_0 \quad \forall i, k, m, \quad (3.12)$$

where  $p_0$  denotes the peak transmit power across  $N_b N_c$  BS antennas. Making  $p_0$  smaller results in a more precise and economical usage of the power amplifiers by limiting the dynamic range.

I aim to identify the DL beamformer  $\mathbf{w}_{i,u}(k)$  for all  $i, u, k$  that can minimize  $p_0$  while satisfying all SQINR constraints. Note that  $p_0$  is a free variable, the objective function in (3.10), and the upper limit in the constraint (3.12). As shown in (3.8)-(3.9), the fact that  $\Gamma_{i,u}(k)$  contains the quantization noise as well as  $\mathbf{w}_{i,u}(k)$  for all  $i, u, k$  makes the problem more challenging to solve. Since a closed-form algebraic solution is not available, I seek an efficient algorithm to find a numerical solution. Instead of solving the optimization problem directly, I first derive a Lagrangian dual and then solve the problem in the dual domain with an efficient solver. I will show that the DL beamforming solution is ultimately calculated by exploiting the dual solution.

### 3.3 Duality between Downlink and Uplink

In this section, I first introduce the corresponding uplink problem and then show that the uplink and downlink problems have strong duality. The

primary challenge in deriving a dual problem is the quantization noise terms coupled with both beamformers and OFDM modulation.

### 3.3.1 Dual UL OFDM Systems with Low-Resolution ADCs

Let  $\mathbf{s}_i^{\text{ul}}(k) \in \mathbb{C}^{N_u}$  denote the vector of symbols from  $N_u$  users in cell  $i$  at subcarrier  $k$  and let

$$\mathbf{u}_i^{\text{ul}}(k) = \mathbf{\Lambda}_i(k)^{1/2} \mathbf{s}_i^{\text{ul}}(k) \quad (3.13)$$

where  $\mathbf{\Lambda}_i(k) = \text{diag}(\lambda_{i,1}(k), \dots, \lambda_{i,N_u}(k))$  is the collection of transmit power. With  $\mathbf{x}_i^{\text{ul}}(k)$  denoting the vector of OFDM symbols of  $N_u$  users in cell  $i$  at time  $k$ , I stack the OFDM symbol vectors as  $\underline{\mathbf{x}}_i^{\text{ul}} = [\mathbf{x}_i^{\text{ul}}(0)^T, \dots, \mathbf{x}_i^{\text{ul}}(K-1)^T]^T$  which is written as

$$\underline{\mathbf{x}}_i^{\text{ul}} = (\mathbf{W}_{\text{DFT}}^H \otimes \mathbf{I}_{N_u}) \underline{\mathbf{u}}_i^{\text{ul}} \quad (3.14)$$

$$= \mathbf{\Psi}_{N_u}^H \underline{\mathbf{\Lambda}}_i^{1/2} \underline{\mathbf{s}}_i^{\text{ul}}, \quad (3.15)$$

where the stacked components are defined as

$$\mathbf{\Psi}_{N_u} = (\mathbf{W}_{\text{DFT}} \otimes \mathbf{I}_{N_u}), \quad (3.16)$$

$$\underline{\mathbf{u}}_i^{\text{ul}} = [\mathbf{u}_i^{\text{ul}}(0)^T, \dots, \mathbf{u}_i^{\text{ul}}(K-1)^T]^T, \quad (3.17)$$

$$\underline{\mathbf{s}}_i^{\text{ul}} = [\mathbf{s}_i^{\text{ul}}(0)^T, \dots, \mathbf{s}_i^{\text{ul}}(K-1)^T]^T, \quad (3.18)$$

$$\underline{\mathbf{\Lambda}}_i = \text{blkdiag}(\mathbf{\Lambda}_i(0), \dots, \mathbf{\Lambda}_i(K-1)). \quad (3.19)$$

I assume that the noise vector received at BS $_i$ , i.e.,  $\tilde{\mathbf{n}}_i^{\text{ul}}(k)$ , is unknown yet tunable by diagonal noise covariance  $\mathbf{D}_i$ , i.e.  $\tilde{\mathbf{n}}_i^{\text{ul}}(k) \sim \mathcal{CN}(\mathbf{0}_{N_b}, \mathbf{D}_i)$ . After

performing CP removal and applying DFT operation, the frequency-domain received signal at subcarrier  $k$  is then given as

$$\mathbf{y}_i^{\text{ul}}(k) = \alpha \mathbf{G}_{i,i}(k) \mathbf{\Lambda}_i(k) \mathbf{s}_i^{\text{ul}}(k) + \alpha \sum_{j \neq i}^{N_c} \mathbf{G}_{i,j}(k) \mathbf{\Lambda}_j(k) \mathbf{s}_j^{\text{ul}}(k) + \alpha \tilde{\mathbf{n}}_i^{\text{ul}}(k) + \tilde{\mathbf{q}}_i^{\text{ul}}(k). \quad (3.20)$$

The combined signal for user  $u$  at subcarrier  $k$  is now given as  $\mathbf{f}_{i,u}^H(k) \mathbf{y}_i^{\text{ul}}(k)$  where  $\mathbf{f}_{i,u}(k)$  is an equalizer of subcarrier  $k$  for user  $u$  in cell  $i$ .

Accordingly, the UL SQINR for user  $u$  in cell  $i$  at subcarrier  $k$  is computed as

$$\Gamma_{i,u}^{\text{ul}}(k) = \frac{\alpha^2 \lambda_{i,u}(k) |\mathbf{f}_{i,u}^H(k) \mathbf{g}_{i,i,u}(k)|^2}{\alpha^2 \sum_{(j,v) \neq (i,u)}^{N_c, N_u} \lambda_{j,v}(k) |\mathbf{f}_{i,u}^H(k) \mathbf{g}_{i,j,v}(k)|^2 + \alpha^2 |\mathbf{f}_{i,u}^H(k) \mathbf{D}_i \mathbf{f}_{i,u}(k)| + \mathbf{f}_{i,u}^H(k) \mathbf{C}_{\tilde{\mathbf{q}}_i^{\text{ul}}(k)} \mathbf{f}_{i,u}(k)}. \quad (3.21)$$

I then define  $\mathbf{\Psi}_{N_b}(k) = ([\mathbf{W}_{\text{DFT}}]_{k+1,:} \otimes \mathbf{I}_{N_b})$ ,  $\mathbf{G}_i = [\mathbf{G}_{i,1}, \dots, \mathbf{G}_{i,N_c}]$ , and  $\mathbf{\Lambda} = \text{blkdiag}(\mathbf{\Lambda}_1, \dots, \mathbf{\Lambda}_{N_c})$ . Since  $\mathbf{C}_{\tilde{\mathbf{q}}_i^{\text{ul}}(k)}$  by the AQNM is expressed as

$$\mathbf{C}_{\tilde{\mathbf{q}}_i^{\text{ul}}(k)} = \alpha(1 - \alpha) \mathbf{\Psi}_{N_b}(k) \text{diag}(\mathbf{\Psi}_{N_b}^H \mathbf{G}_i \mathbf{\Lambda} \mathbf{G}_i^H \mathbf{\Psi}_{N_b} + \mathbf{D}_i) \mathbf{\Psi}_{N_b}^H(k), \quad (3.22)$$

the UL SQINR can be rewritten as

$$\Gamma_{i,u}^{\text{ul}}(k) = \frac{\alpha^2 \lambda_{i,u}(k) |\mathbf{f}_{i,u}^H(k) \mathbf{g}_{i,i,u}(k)|^2}{\mathbf{f}_{i,u}^H(k) \mathbf{Z}_{i,u}(k) \mathbf{f}_{i,u}(k)}, \quad (3.23)$$

where

$$\begin{aligned} \mathbf{Z}_{i,u}(k) = & \alpha^2 \sum_{(j,v) \neq (i,u)} \lambda_{j,v}(k) \mathbf{g}_{i,j,v}(k) \mathbf{g}_{i,j,v}^H(k) + \alpha \mathbf{D}_i \\ & + \alpha(1 - \alpha) \mathbf{\Psi}_{N_b}(k) \text{diag}(\mathbf{\Psi}_{N_b}^H \mathbf{G}_i \mathbf{\Lambda} \mathbf{G}_i^H \mathbf{\Psi}_{N_b}) \mathbf{\Psi}_{N_b}^H(k). \end{aligned} \quad (3.24)$$

### 3.3.2 Downlink-Uplink Duality

In Theorem 3, I derive a dual problem of (3.10) which is a virtual UL OFDM problem with unknown noise covariance matrices.

**Theorem 3** (Duality). *The Lagrangian dual problem of the DL OFDM problem in (3.10) is equivalent to*

$$\mathcal{P}_3 2 : \max_{\mathbf{D}_i} \min_{\lambda_{i,u}(k)} \sum_{i,u,k}^{N_c, N_u, K} \lambda_{i,u}(k) \sigma^2 \quad (3.25)$$

$$\text{subject to } \max_{\mathbf{f}_{i,u}(k)} \Gamma_{i,u}^{\text{ul}}(k) \geq \gamma_{i,u}(k), \quad (3.26)$$

$$\mathbf{D}_i \succeq 0, \mathbf{D}_i \in \mathbb{R}^{N_b \times N_b} : \text{diagonal}, \quad (3.27)$$

$$\text{tr}(\mathbf{D}_i) \leq N_b \quad \forall i, u, k \quad (3.28)$$

*It is possible to consider the above problem as a virtual UL case where  $\lambda_{i,u}(k)$  is considered as UL transmit power of virtual user  $u$  in cell  $i$  at sub-carrier  $k$  and  $BS_i$  operates with unknown noise covariance matrix  $\mathbf{D}_i$ .*

*Proof.* See Appendix 3.7. □

I remark that the Lagrangian dual problem in (3.25) is considered to be an antenna power minimax problem with noise covariance constraints for the virtual UL OFDM system with low-resolution ADCs at the BSs shown in Theorem 3.

**Corollary 7** (Strong Duality). *There exists zero duality gap between the DL problem formulation and its associated dual problem.*

*Proof.* See Appendix 3.8. □

### 3.4 Proposed Solution for Joint Beamforming

In this section, I present the algorithm that can efficiently find the DL beamforming solution by leveraging the strong dual problem derived in Section 3.3. In particular, I separate the dual problem in Theorem 3 into the inner minimization and outer maximization problems and solve the problems in an alternating manner; upon obtaining the dual solution, I use the dual solution to identify the primal solution and repeat through proper update and projection onto feasible sets.

#### 3.4.1 Optimal Downlink Precoder

I first present the linear relationship between the optimal DL precoder and the dual solution, i.e., the virtual UL MMSE combiner in Corollary 8.

**Corollary 8** (Optimal DL Beamformer). *With coefficients  $\tau_{i,u}(k)$ 's, an optimal DL beamformer can be obtained by establishing a linear transformation of the UL MMSE receiver, i.e.,  $\mathbf{w}_{i,u}(k) = \sqrt{\tau_{i,u}(k)}\mathbf{f}_{i,u}(k) \forall i, u, k$ . Here,  $\tau_{i,u}(k)$ 's are derived from solving  $\underline{\boldsymbol{\tau}} = \underline{\boldsymbol{\Sigma}}^{-1}\mathbf{1}_{N_u N_c K}$ , where  $\underline{\boldsymbol{\tau}} = [\boldsymbol{\tau}^T(0), \dots, \boldsymbol{\tau}^T(K-1)]^T$  with  $\boldsymbol{\tau}(k) = [\boldsymbol{\tau}_1^T(k), \dots, \boldsymbol{\tau}_{N_c}^T(k)]^T$  and  $\boldsymbol{\tau}_i^T(k) = [\tau_{i,1}(k), \dots, \tau_{i,N_u}(k)]^T$ , and  $\underline{\boldsymbol{\Sigma}} = \text{blkdiag}(\boldsymbol{\Sigma}(0), \dots, \boldsymbol{\Sigma}(K-1))$  whose submatrix is defined as*

$$\boldsymbol{\Sigma}(k) = \begin{pmatrix} \boldsymbol{\Sigma}_{1,1}(k) & \cdots & \boldsymbol{\Sigma}_{1,N_c}(k) \\ \vdots & \ddots & \vdots \\ \boldsymbol{\Sigma}_{N_c,1}(k) & \cdots & \boldsymbol{\Sigma}_{N_c,N_c}(k) \end{pmatrix}, \quad (3.29)$$

and

$$[\boldsymbol{\Sigma}_{i,j}(k)]_{u,v} = \tag{3.30}$$

$$\begin{cases} \frac{\alpha^2}{\gamma_{i,u}(k)} |\mathbf{g}_{i,i,u}^H(k) \mathbf{f}_{i,u}(k)|^2 - \alpha(1-\alpha) \sum_{\ell} \mathbf{f}_{i,u}^H(\ell) \boldsymbol{\Psi}_{N_b}(\ell) \\ \quad \times \text{diag} \left( \boldsymbol{\Psi}_{N_b}^H \underline{\mathbf{g}}_{i,i,u}(k) \underline{\mathbf{g}}_{i,i,u}^H(k) \boldsymbol{\Psi}_{N_b} \right) \boldsymbol{\Psi}_{N_b}^H(\ell) \mathbf{f}_{i,u}(\ell), & \text{if } i = j, u = v, \\ -\alpha^2 |\mathbf{g}_{j,i,u}^H(k) \mathbf{f}_{j,v}(k)|^2 - \alpha(1-\alpha) \sum_{\ell} \mathbf{f}_{j,v}^H(\ell) \boldsymbol{\Psi}_{N_b}(\ell) \\ \quad \times \text{diag} \left( \boldsymbol{\Psi}_{N_b}^H \underline{\mathbf{g}}_{j,i,u}(k) \underline{\mathbf{g}}_{j,i,u}^H(k) \boldsymbol{\Psi}_{N_b} \right) \boldsymbol{\Psi}_{N_b}^H(\ell) \mathbf{f}_{j,v}(\ell), & \text{otherwise.} \end{cases}$$

*Proof.* See Appendix 3.9 □

By Corollary 8, the optimal DL precoder  $\mathbf{w}_{i,u}(k)$  can be derived by using the virtual UL MMSE combiner  $\mathbf{f}_{i,u}(k)$  with a scalar weight  $\sqrt{\tau_{i,u}(k)}$ . The virtual UL MMSE equalizer, however, is a function of the uncertain noise covariance matrix  $\mathbf{D}_i$  and UL transmit power  $\lambda_{i,u}(k)$  as shown in (3.39). Accordingly, I further need to find the optimal virtual noise covariance matrix and UL transmit power to update its corresponding UL MMSE equalizer and DL precoder.

### 3.4.2 Iterative Algorithm via Dual Uplink Solution

In this subsection, I characterize the virtual UL solutions by exploiting the strong duality and further adopt the fixed-point iteration with a projected subgradient ascent [23] to maximize the objective function with respect to the noise covariance matrix of the virtual UL problem.

Instead of directly solving the dual problem in (3.25), I can decouple it into outer maximization and inner minimization problems where the latter is

then written as

$$f(\mathbf{D}_i) = \min_{\lambda_{i,u}(k)} \sum_{i,u,k}^{N_c, N_u, K} \lambda_{i,u}(k) \sigma^2 \quad (3.31)$$

subject to  $\max_{\mathbf{f}_{i,u}(k)} \hat{\Gamma}_{i,u}(k) \geq \gamma_{i,u}(k) \quad \forall i, u, k.$

I notice that the above problem is interpreted as the inner optimization on  $\lambda_{i,u}(k)$  of the dual objective function  $g(\tilde{\mathbf{D}}_i, \lambda_{i,u}(k))$  where MMSE equalizer in (3.39) is used for computing  $\mathbf{f}_{i,u}(k)$ . The virtual UL power control solution of (3.31) derived in Corollary 9 is the solution of (3.31).

**Corollary 9.** *For given  $\mathbf{D}_i$ , the optimal power for the virtual UL transmit power minimization problem in (3.25) is derived as*

$$\lambda_{i,u}(k) = \frac{1}{\alpha \left(1 + \frac{1}{\gamma_{i,u}(k)}\right) \mathbf{g}_{i,i,u}^H(k) \mathbf{K}_{i,k}^{-1}(\underline{\mathbf{\Lambda}}) \mathbf{g}_{i,i,u}(k)}, \quad (3.32)$$

where  $\mathbf{K}_{i,k}(\underline{\mathbf{\Lambda}})$  is defined as

$$\mathbf{K}_{i,k}(\underline{\mathbf{\Lambda}}) = \mathbf{D}_i + \alpha \sum_{j,v} \lambda_{j,v}(k) \mathbf{g}_{i,j,v}(k) \mathbf{g}_{i,j,v}^H(k) + (1-\alpha) \Psi_{N_b}(k) \text{diag} \left( \Psi_{N_b}^H \underline{\mathbf{G}}_i \underline{\mathbf{\Lambda}} \underline{\mathbf{G}}_i^H \Psi_{N_b} \right) \Psi_{N_b}^H(k). \quad (3.33)$$

*Proof.* See Appendix 3.10. □

Since  $\mathbf{K}_{i,k}(\underline{\mathbf{\Lambda}})$  is a function of  $\lambda_{i,u}(k)$ , I iteratively update  $\lambda_{i,u}(k)$  until convergence. Convergence to an global optimal point is guaranteed [15] for given  $\mathbf{D}_i$ . Once I obtain the optimal  $\lambda_{i,u}(k)$  for the fixed covariance matrices, I further need to update  $\mathbf{D}_i$  by solving the outer maximization for a fixed  $\lambda_{i,u}(k)$  and alternate the inner and outer optimization until the solutions converge. I



note that the function  $f(\mathbf{D}_i)$  is concave in  $\mathbf{D}_i$ , which directly follows from that  $f(\mathbf{D}_i)$  is the objective function of a dual problem. Based on this observation, a projected subgradient ascent method is utilized in order to maximize the objective function while satisfying the constraints on  $\mathbf{D}_i$  in (3.27) and (3.28).

**Corollary 10** (Subgradient). *One of the subgradients of (3.31) in updating  $\mathbf{D}_i$  is obtained as*

$$\text{diag}\left(\sum_{u,k} \mathbf{w}_{i,k}(k)\mathbf{w}_{i,k}^H(k)\right). \quad (3.34)$$

*Proof.* See Appendix 3.11. □

I can finally assemble the inner minimization and outer maximization problems into the complete dual problem  $\mathcal{P}_3 2$  in (3.25). Recall that  $\mathcal{P}_3 2$  eventually becomes the minimax problem whose main objective is to maximize the concave  $f(\mathbf{D}_i)$  by updating  $\mathbf{D}_i$  while satisfying the constraints on  $\mathbf{D}_i$  and  $f(\mathbf{D}_i)$  wants to minimize the total transmit power of the virtual UL problem. Upon obtaining a solution of  $f(\mathbf{D}_i)$  for fixed  $\mathbf{D}_i$  as shown in Corollary 9, I update  $\mathbf{D}_i$  by taking a step in the direction of a positive subgradient to establish an increment in the objective function.

Let  $\mathbf{D}_i^{(n)}$  denote  $\mathbf{D}_i$  at the  $n$ th iteration. Then, the update of  $\mathbf{D}_i^{(n)}$  is performed as

$$\mathbf{D}_i^{(n+1)} = \mathbf{D}_i^{(n)} + \eta \text{diag}\left(\sum_{u,k} \mathbf{w}_{i,u}(k)\mathbf{w}_{i,u}^H(k)\right), \quad (3.35)$$

where  $\eta > 0$  is a real-valued step size. I remark that the subgradient ascent method is guaranteed to converge to an optimal point since the UL problem is convex. Since it is highly likely that  $\mathbf{D}_i^{(n+1)}$  escapes the feasible domain, I further project the updated  $\mathbf{D}_i$  onto the feasible set on  $\mathbf{D}_i$  in (3.27) and (3.28) as

$$\mathbf{D}_i^{(n+1)} = \frac{\left(\text{tr}\left(\mathbf{D}_i^{(n+1)}\right) - N_b\right)}{\|\mathbf{1}_{N_b}\|^2} \text{diag}(\mathbf{1}_{N_b}), \quad (3.36)$$

and

$$\mathbf{D}_i^{(n+1)} = \max\left(0, \mathbf{D}_i^{(n+1)}\right), \quad (3.37)$$

respectively, where  $\max(a, b)$  represents an element-wise max function. As discussed in [7], the alternating projection on (3.27) and (3.28) converges to the intersection of the convex sets if there exists any point in the intersection. For example,  $\mathbf{D}_i = \mathbf{I}_{N_b}$  is one of the points in the intersection, and thus, the intersection is not an empty set, thereby guaranteeing the convergence. I note that (3.27) and (3.28) need to be performed in an alternating manner until convergence. The proposed algorithm for the quantized CoMP beamforming under per-antenna power and SQINR constraints (Q-CoMP-PA) is described in Algorithm 1.

**Remark 1** (Narrowband Communications). The considered quantized MIMO OFDM system naturally reduces to a quantized MIMO narrowband system with  $K = 1$  subcarrier. Accordingly, the derived duality, optimal solutions, and algorithm still hold for the quantized MIMO narrowband communications

since the derived results and algorithm hold for an arbitrary  $K$ . In this case, I omit the subcarrier index  $k$  from the system parameters and variables in Algorithm 1.

### 3.4.3 Convergence of Sub-problems

The convergence of each sub-problem can be guaranteed as follows: regarding the inner minimization problem, the fixed-point iteration for given  $\mathbf{D}_i^{(n)}$  converges as shown in Corollary 11.

**Corollary 11.** *For any arbitrary initial points  $\lambda_{i,u}^{(0)}(k)$ ,  $\forall i, u, k$ , the proposed fixed-point algorithm converges to a unique fixed point at which objective function of inner problem is minimized.*

*Proof.* See Appendix 3.12. □

Therefore, the fixed-point iteration always converges to a unique fixed point that is the optimal solution of the inner optimization subproblem for a fixed covariance matrix.

Regarding the outer maximization problem, the iterative projection of  $\mathbf{D}_i^{(n)}$  converges for given  $\mathbf{w}_{i,u}(k)$  as discussed in [7]: the alternating projection on (3.27) and (3.28) converges to the intersection of the convex sets if there exists any point in the intersection. Since  $\mathbf{D}_i = \mathbf{I}_{N_b}$  belongs to the intersection, the intersection is not an empty set, thereby guaranteeing the convergence.

Accordingly, I theoretically show that each sub-problem can be solved

with guaranteed convergence. For the convergence of the entire algorithm, I provide the numerical validation in Section 3.6.

#### 3.4.4 Computational Complexity

The computational complexity of the proposed algorithm is governed by the computation of  $\lambda_{i,u}(k)$ , which is dominated by the matrix inversion of  $\mathbf{K}_{i,k}(\underline{\mathbf{A}})$ . For the matrix inversion, the number of floating point operations can be reduced by taking advantage of the Hermitian symmetric and positive semi-definite properties of  $\mathbf{K}_{i,k}(\underline{\mathbf{A}})$ . Consequently, the computational complexity of the per-cell and Q-CoMP algorithms are  $O(T_1KN_cN_uN_b^3)$  and  $O(T_2KN_cN_uN_b^3)$ , respectively, where  $T_1$  and  $T_2$  denote the number of iterations required for obtaining a converged  $\lambda_{i,u}(k)$  value. Likewise, the inner optimization loop of the Q-CoMP-PA algorithm with  $T_3$  iterations has computational complexity of  $O(T_3KN_cN_uN_b^3)$ . Since the proposed Q-CoMP-PA algorithm also requires an outer maximization loop with  $T_0$  iterations, the total computational complexity of the proposed algorithm is  $O(T_0T_3KN_cN_uN_b^3)$ .

### 3.5 Simulation Results

I evaluate the derived results of the proposed Q-CoMP-PA algorithm. I also simulate the quantization-aware CoMP algorithm (Q-CoMP) presented in Chapter 2 for comparison. Both methods utilize multicell coordination in designing DL precoders. However, Q-CoMP-PA minimizes the maximum antenna power whereas Q-CoMP minimizes the total transmit power without

considering the per-antenna power constraints. I compare the methods in terms of maximum transmit antenna power, dynamic range, and PAPR for wideband and narrowband systems. I assume the target SQINR  $\gamma$  is equal for all users and subcarriers.

### 3.5.1 Wideband OFDM Communications

I consider the wideband OFDM systems assuming the delay spread is  $L = 3$  and the small scale fading follows Rayleigh fading with zero mean and unit variance. I consider a 24 GHz carrier frequency with 100 MHz bandwidth. The adjacent BSs are 200 m apart and the minimum distance between any BS and user is 50 m. For large scale fading, I adopt the log-distance pathloss model in [1] with the 72 dB intercept, the pathloss exponent of 2.92, and the shadow fading whose shadowing variance is 8.7 dB. Noise power is computed with  $-174$  dBm/Hz power spectral density and 5 dB noise figure. I also use the sector antenna gain of 15 dB.

I evaluate the performance of the Q-CoMP-PA and Q-CoMP algorithms in wideband OFDM communication systems. I also simulate the quantization-aware per-cell based CoMP (Q-PerCell) algorithm as an additional benchmark by adapting the algorithm in [76] to the considered system. For the Q-PerCell algorithm, each BS first discovers its optimal solution by treating the inter-cell interference as noise and assuming that it is fixed. Once the BSs derive solutions for the given inter-cell interference, the BSs share the converged solutions to update the interference power and compute solutions again. These

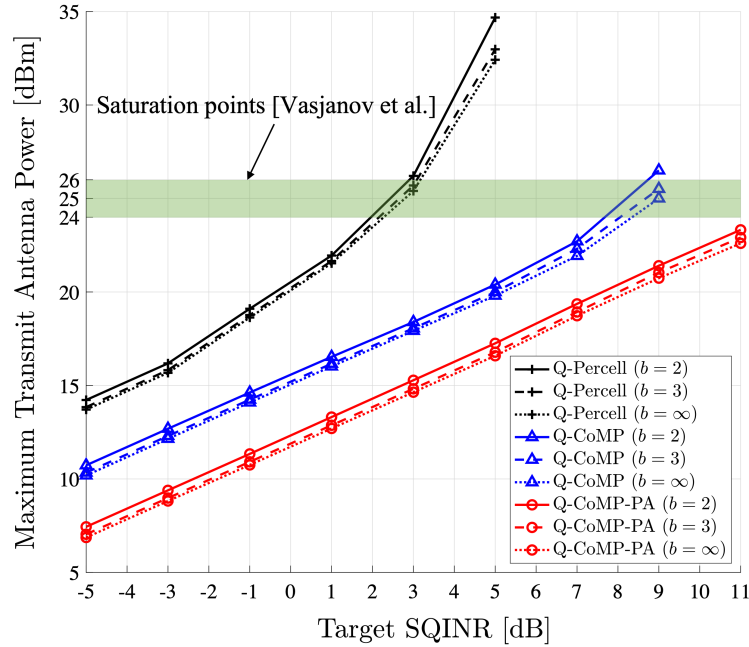


Figure 3.2: Maximum transmit antenna power versus the target SQINR for the multicell wideband network with  $N_b = 16$  BS transmit antennas,  $N_c = 4$  cells,  $N_u = 2$  users per cell,  $K = 32$  subcarriers, and  $b \in \{2, 3, \infty\}$  bits.

steps repeat until the solutions converge. Consequently, Q-Percell is expected to be far sub-optimal than the other algorithms.

In Fig. 3.2, I present the maximum transmit antenna power in DL direction across all  $N_c N_b$  transmit antennas which is  $p_0$  of the primal DL problem that I want to minimize for given target SQINRs. I consider  $N_b = 16$  antennas,  $N_c = 3$  cells,  $N_u = 2$  users per cell,  $K = 32$  subcarriers, and  $b \in \{2, 3, \infty\}$  DAC bits. I see that the Q-Percell method consumes much higher transmit power than the Q-CoMP method and proposed Q-CoMP-PA method and shows divergence in the maximum transmit power as the target SQINR increases. In

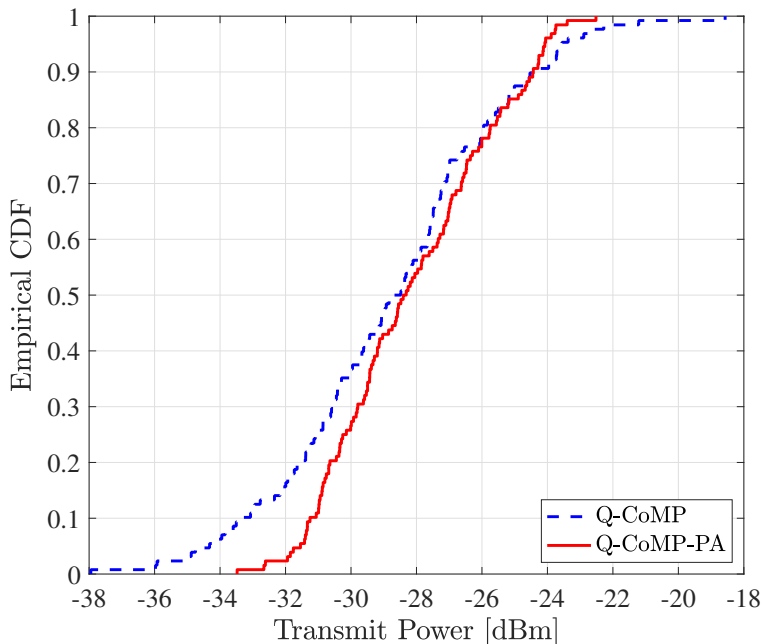


Figure 3.3: Empirical CDFs of BS antennas with respect to antenna transmit power in the multicell network with  $N_b = 32$  BS antennas,  $N_c = 4$  cells,  $N_u = 2$  users per cell,  $K = 64$  subcarriers,  $b = 3$  quantization bits, and  $\gamma = -1$  dB target SQINR.

contrast to the Q-Percell algorithm, the Q-CoMP and Q-CoMP-PA methods with multicell coordination scale linearly with the target SQINR without implausible power consumption or unfavorable divergence. Nevertheless, based on the primal objective of the Q-CoMP-PA, the proposed algorithm can limit the maximum transmit power providing around 3 dB reduction over the regular Q-CoMP. From both Q-CoMP and Q-CoMP-PA methods, when using infinite-resolution quantizers, I have lower peak power compared to the one with 2-bit or 3-bit data converters; however, the gap between  $b = 2$ ,  $b = 3$ ,

and  $b = \infty$  cases is marginal for both Q-CoMP and Q-CoMP-PA by properly taking the coarse quantization error and inter-cell interference into account.

I further note that transmit power higher than the saturation input triggers RF nonlinearity, thereby causing a substantial reduction in RF output power and many undesirable additional frequencies compared to the ideal linear amplification regime of RF power amplifiers. As most of the state-of-the-art RF power amplifiers introduced in [93] have the saturation input of between 24 dBm and 26 dBm, I can interpret from Fig. 3.2 that the per-cell and Q-CoMP methods escape the efficient amplification regime at around 3 dB and 8 dB target SQINR, respectively, while the proposed Q-CoMP-PA has stable and linear amplification at the simulated target SQINR values.

Fig. 3.3 shows the empirical cumulative density function (CDF) of the transmit power of all antennas by collecting the computed transmit power from all  $N_b N_c$  BS antennas. I employ a communication network with  $N_b = 32$ ,  $N_c = 4$ ,  $N_u = 2$ ,  $K = 64$ ,  $b = 3$ , and  $\gamma = -1$  dB. When comparing the peak power, the proposed Q-CoMP-PA method achieves around 4 dB lower maximum antenna power over Q-CoMP, which corresponds to the main purpose of the primal problem. Furthermore, the dynamic range defined as the gap between the minimum and maximum antenna power is narrower for Q-CoMP-PA compared to Q-CoMP, thereby showing more even power distribution across antennas. Therefore, the proposed method increases the efficiency of power-related components such as power amplifier.



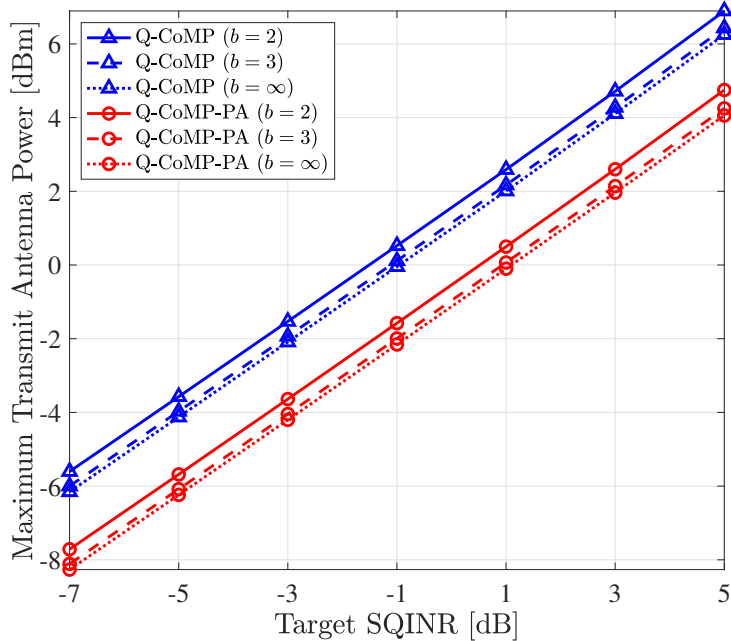


Figure 3.4: Maximum transmit antenna power versus target SQINR for the communication network with  $N_b = 32$  transmit antennas per BS,  $N_c = 4$  cells,  $N_u = 2$  users per cell,  $b \in \{2, 3, \infty\}$  bits, and  $K = 1$ .

### 3.5.2 Narrowband Communications

As a special case, I simulate over the narrowband channel, i.e.  $K = 1$ , as stated in Remark 1. I assume that the small scale fading of each channel fading coefficient also follows Rayleigh fading with zero mean and unit variance. For the large scale fading, I adopt the log-distance pathloss model in [27]. The distance between adjacent BSs is 2 km. The minimum distance between BS and user is 100 m. I consider a 2.4 GHz carrier frequency with 10 MHz bandwidth and use the same large scale fading model as the one used in Section 3.5.1

Fig. 3.4 illustrates the maximum transmit antenna power across  $N_c N_b$  transmit antennas. I consider  $N_b = 32$ ,  $N_c = 4$ ,  $N_u = 2$ , and  $b \in \{2, 3, \infty\}$  bits. The benefit of the proposed Q-CoMP-PA method identified in the wideband simulation can also be confirmed in the narrowband case. By properly incorporating the quantization noise and inter-cell interference in designing  $\mathbf{w}_{i,u}$ , the proposed Q-CoMP-PA method can achieve the 3 dB reduction over Q-CoMP in peak transmit power without experiencing undesirable divergence at the simulated target SQINR values.

Fig. 3.5 shows the CDF of the transmit power of all antennas. I use  $N_b = 32$ ,  $N_c = 5$ ,  $N_u = 2$ , and  $b = 3$ . Q-CoMP-PA achieves more than 3 dB reduction in the maximum transmit antenna power and operates with a much narrower dynamic range than Q-CoMP. This result validates that the proposed algorithm also outperforms Q-CoMP in minimizing the transmit antenna power under the quality-of-service constraints for the narrowband communication system.

### 3.5.3 Convergence

Fig. 3.6 shows progress in maximum transmit power with respect to the number of iterations of Q-CoMP-PA until the stopping condition is met considering  $\gamma \in \{-3, 0, 3\}$  dB,  $b = 3$ ,  $N_b = 32$ ,  $N_c = 2$ ,  $N_u = 3$ ,  $K = 64$ . It can be seen that more iterations are needed and the algorithm converges to a higher peak power as the target SQINR is raised. Since the curve is saturated after a certain number of iterations and the number of iterations is determined

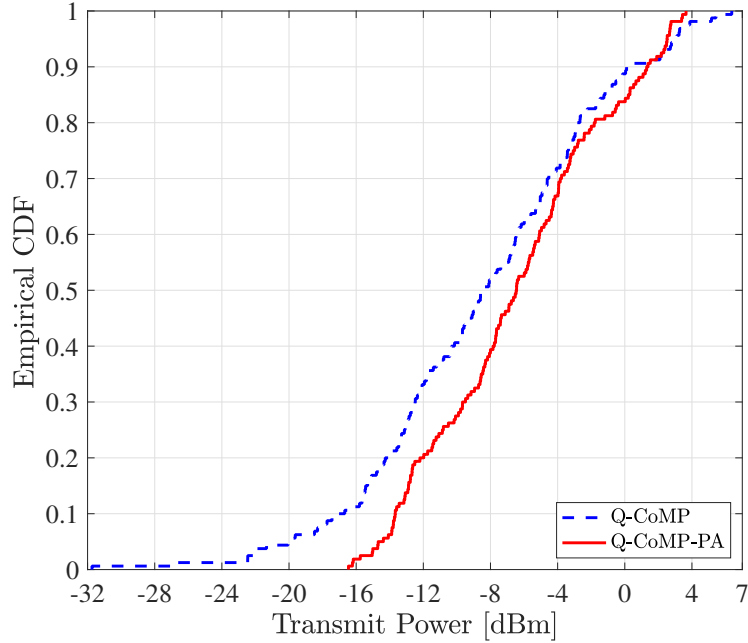


Figure 3.5: Empirical CDF of the transmit power of all BS transmit antennas in the network with  $N_b = 32$  transmit antennas per BS,  $N_c = 5$  cells,  $N_u = 2$  users per cell,  $b = 3$  quantization bits,  $\gamma = 2$  dB target SQINR, and  $K = 1$ .

by the stopping condition of the algorithm, I remark that the convergence can be faster by alleviating the stopping condition.

### 3.5.4 Channel Estimation Error

To assess the effects of channel estimation error, I employ a Gaussian channel estimation error model [96] that defines the estimated UL channel between BS  $i$  and user  $u$  in cell  $j$  as

$$\hat{\mathbf{h}}_{i,j,u} = \sqrt{(1 - e^2)} \mathbf{h}_{i,j,u} + e \mathbf{e}_{i,j,u}, \quad (3.38)$$

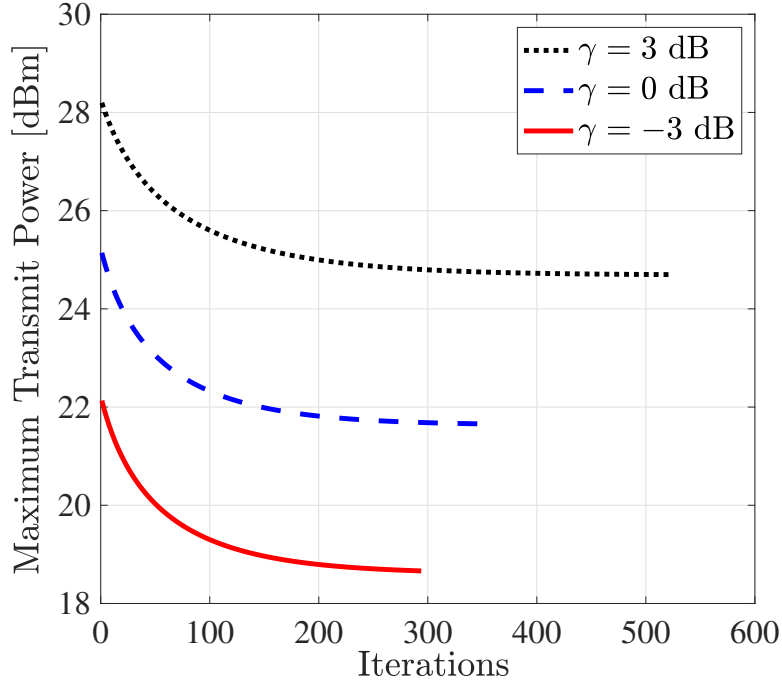


Figure 3.6: Convergence behavior for  $N_b = 32$  antennas,  $N_c = 2$  cells,  $N_u = 3$  users per cell,  $b = 3$  bits,  $K = 64$  subcarriers, and  $\gamma \in \{-3, 0, 3\}$  dB.

where  $e$  determines the degree of error, and  $\mathbf{e}_{i,j,u}$  is an error vector whose elements follow  $\mathcal{CN}(0, \rho_{i,j,u})$  in which  $\rho_{i,j,u}$  denotes large scale fading between  $\text{BS}_i$  and user  $u$  in cell  $j$ .

Fig. 3.7 shows CDFs of the achieved SQINR for channel estimation error factor  $e \in \{0, 0.1, 0.2\}$ ,  $\gamma = 3$  dB,  $b = 3$ ,  $N_b = 32$ ,  $N_c = 4$ , and  $N_u = 3$ . As  $e$  increases, the deviation from the target SQINR increases, resulting in less accurate performance in achieved SQINR. The Q-CoMP algorithm is more robust to the estimation error than the Q-Per-cell method, showing a smaller deviation from the target SQINR  $\gamma = 3$  dB.

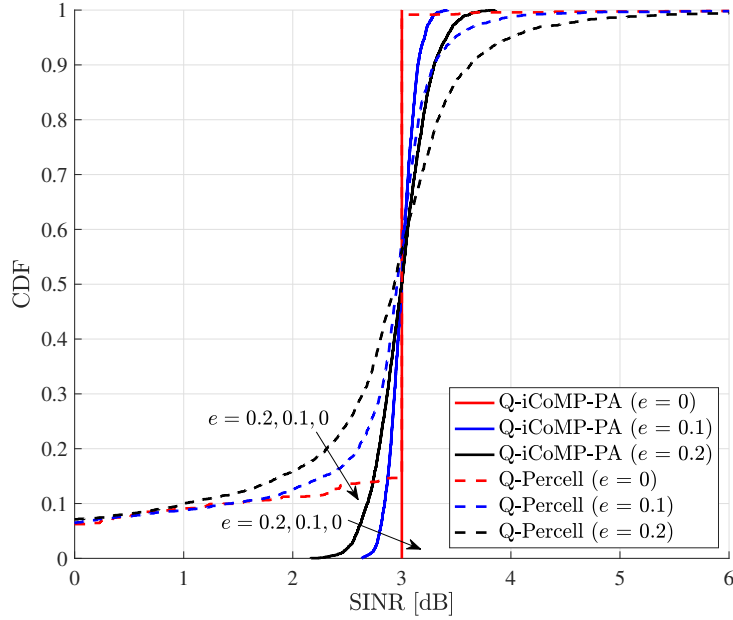


Figure 3.7: CDFs of the SQINRs of users in all cells for  $\gamma = 3$  dB target SQINR,  $b = 3$  quantization bits,  $N_b = 32$  BS antennas,  $N_c = 4$  cells, and  $N_u = 3$  users per cell with channel estimation error factor  $e \in \{0, 0.1, 0.2\}$ .

### 3.5.5 Peak-to-Average-Power Ratio (PAPR)

In this subsection, I simulate the PAPR of the transmitted signals. Since a large peak amplitude causes severe performance loss, reducing the PAPR is considered as one of the important topics in OFDM systems. In Table 3.1(a), I analyze a wideband communication network with  $N_b = 16$ ,  $N_c = 3$ ,  $N_u = 2$ ,  $K = 64$ , and  $b = 3$  over  $\gamma \in \{-5, 1\}$  dB. It is observed that Q-CoMP-PA achieves the lowest PAPR for the considered target SQINRs, reducing it by more than 2 dB and 5 dB from Q-CoMP and Q-Percell, respectively. Both Q-CoMP and Q-CoMP-PA methods exhibit more robust PAPR

performance for different target SQINRs than Q-Percell.

In Table 3.1(b), I consider a narrowband communication network with  $N_b = 32$ ,  $N_c \in \{2, 4, 6\}$ ,  $N_u = 2$ , and  $b = 3$  over  $\gamma \in \{-3, 2\}$  dB. As shown in Table 3.1(b), Q-CoMP-PA also achieves significant reduction in PAPR, showing more than 1.8 dB gain over Q-CoMP. Furthermore, it is shown that Q-CoMP-PA maintains similar PAPR over different SQINR targets or the different number of cells. Q-Percell with limited multicell coordination still demands the highest PAPR, which emphasizes the significance of taking multicell coordination into account since the decrease in PAPR is significant when employing the proposed Q-CoMP-PA. Therefore, Q-CoMP-PA is more favorable for communication systems by limiting the peak power of transmit antennas.

### 3.6 Conclusion

In this chapter, I investigated the DL OFDM CoMP beamforming problem with low-resolution data converters and employed per-antenna power constraints to give a more practical power-efficient solution. The DL antenna power minimization problem with SQINR constraints was formulated as a primal problem, and I derived the associated dual problem. I interpreted the dual problem as a virtual UL transmit power minimization problem with respect to the transmit power and noise covariance matrix. Subsequently, I showed that strong duality holds between the primal DL and dual UL problems. Inspired by the strong duality, I proposed an iterative DL beamforming algorithm. To this end, I addressed the inner and outer problems of the dual in

an alternating manner by solving the inner power control problem via fixed-point iteration and the outer noise covariance design problem via projected subgradient ascent. Then, the DL beamforming solutions were directly obtained from the UL beamforming solution through linear transformation. In simulation, I demonstrated the proposed Q-CoMP-PA algorithm is effective by reducing per-antenna transmit power while achieving target requirements over a wide variety of system settings. The derived duality can provide insight for designing power-efficient communication networks and the proposed method can contribute to realizing highly efficient and reliable future communication networks.

### 3.7 Proof of Theorem 3

Considering  $\mathbf{f}_{i,u}(k)$  as a combiner at subcarrier  $k$  for user  $u$  in cell  $i$ , I let  $\mathbf{f}_{i,u}(k)$  be the MMSE equalizer defined as

$$\mathbf{f}_{i,u}(k) = \mathbf{Z}_{i,u}^{-1}(k) \mathbf{g}_{i,i,u}(k). \quad (3.39)$$

Since the MMSE combiner maximizes SQINR, i.e.,  $\hat{\Gamma}_{i,u}(k)$ , applying (3.39) and  $\mathbf{\Psi}_{N_b}(k) \mathbf{\Psi}_{N_b}^H(k) = \mathbf{I}_{N_b}$  to (5.5) simplify the SQINR constraint into  $\alpha^2 \lambda_{i,u}(k) \mathbf{g}_{i,i,u}^H(k) \mathbf{Z}_{i,u}^{-1}(k) \mathbf{g}_{i,i,u}(k) \geq \gamma_{i,u}(k)$ . Therefore, multiplying both sides by  $\mathbf{g}_{i,i,u}^H(k) \mathbf{g}_{i,i,u}(k)$  and rearranging the terms give

$$0 \leq \mathbf{g}_{i,i,u}^H(k) \mathbf{g}_{i,i,u}(k) \left( \alpha^2 \lambda_{i,u}(k) \mathbf{g}_{i,i,u}^H(k) \mathbf{Z}_{i,u}^{-1}(k) \mathbf{g}_{i,i,u}(k) - \gamma_{i,u}(k) \mathbf{I}_{N_b} \right) \quad (3.40)$$

$$= \mathbf{g}_{i,i,u}^H(k) \left( \alpha^2 \lambda_{i,u}(k) \mathbf{g}_{i,i,u}(k) \mathbf{g}_{i,i,u}^H(k) \mathbf{Z}_{i,u}^{-1}(k) - \gamma_{i,u}(k) \mathbf{I}_{N_b} \right) \mathbf{g}_{i,i,u}(k). \quad (3.41)$$

I equivalently require  $\alpha^2 \lambda_{i,u}(k) \mathbf{g}_{i,i,u}(k) \mathbf{g}_{i,i,u}^H(k) \succeq \gamma_{i,u}(k) \mathbf{Z}_{i,u}(k)$ . Noting that  $\mathbf{Z}_{i,u}(k) = \alpha \mathbf{K}_{i,k}(\underline{\mathbf{\Lambda}}) - \alpha^2 \lambda_{i,u}(k) \mathbf{g}_{i,i,u}(k) \mathbf{g}_{i,i,u}^H(k)$  where  $\mathbf{K}_{i,k}(\underline{\mathbf{\Lambda}})$  is the covariance matrix of the received signal defined as

$$\begin{aligned} \mathbf{K}_{i,k}(\underline{\mathbf{\Lambda}}) = & \quad (3.42) \\ \mathbf{D}_i + \alpha \sum_{j,v} \lambda_{j,v}(k) \mathbf{g}_{i,j,v}(k) \mathbf{g}_{i,j,v}^H(k) + (1-\alpha) \Psi_{N_b}(k) \text{diag} \left( \Psi_{N_b}^H \underline{\mathbf{G}}_i \underline{\mathbf{\Lambda}} \underline{\mathbf{G}}_i^H \Psi_{N_b} \right) \Psi_{N_b}^H(k). \end{aligned}$$

Rearranging the above semidefinite condition allows rewriting the original problem as

$$\max_{\mathbf{D}_i} \min_{\lambda_{i,u}(k)} \sum_{i,u,k}^{N_c, N_u, K} \lambda_{i,u}(k) \sigma^2 \quad (3.43)$$

$$\text{subject to } \mathbf{K}_{i,k}(\underline{\mathbf{\Lambda}}) \preceq \alpha \left( 1 + \frac{1}{\gamma_{i,u}(k)} \right) \lambda_{i,u}(k) \mathbf{g}_{i,i,u}(k) \mathbf{g}_{i,i,u}^H(k), \quad (3.44)$$

$$\mathbf{D}_i \succeq 0, \mathbf{D}_i \in \mathbb{R}^{N_b \times N_b} : \text{diagonal},$$

$$\text{tr}(\mathbf{D}_i) \leq N_b \quad \forall i, u, k$$

Now, I show that (3.43) is equivalent to the Lagrangian dual of (3.10). To this end, I first rewrite the per-antenna constraint for antenna  $m$  in (3.12) as

$$\left[ \mathbb{E}[\mathbf{x}_{q,i}(k) \mathbf{x}_{q,i}^H(k)] \right]_{m,m} = \left[ \frac{\alpha}{K} \sum_{\ell=0}^{K-1} \mathbf{w}_i(\ell) \mathbf{w}_i^H(\ell) \right]_{m,m}. \quad (3.45)$$

I multiply the objective function in (3.10) by a scalar value,  $KN_c N_b$ , which does not change the fundamental of the primal problem. With Lagrangian multipliers  $\mu_{i,u}(k)$  and  $\nu_{i,m}(k)$ , the Lagrangian of the primal DL problem in



(3.10) is given as

$$\begin{aligned}
\mathcal{L}(\mathbf{w}_{i,u}(k), \mu_{i,u}(k), \nu_{i,m}(\ell)) &= KN_c N_b p_0 - \sum_{i,u,k} \mu_{i,u}(k) \left( \frac{\alpha^2 |\mathbf{w}_{i,u}^H(k) \mathbf{g}_{i,i,u}(k)|^2}{\gamma_{i,u}(k)} \right. \\
&\quad \left. - \alpha^2 \sum_{(j,v) \neq (i,u)}^{N_c, N_u} |\mathbf{g}_{j,i,u}^H(k) \mathbf{w}_{j,v}(k)|^2 - Q_{i,u}(k) - \sigma^2 \right) \\
&\quad + \sum_{i,m,\ell} \nu_{i,m}(\ell) \left( \left[ \frac{\alpha}{K} \sum_{\ell=0}^{K-1} \mathbf{W}_i(\ell) \mathbf{W}_i^H(\ell) \right]_{m,m} - p_0 \right). \tag{3.46}
\end{aligned}$$

To make the Lagrangian tractable, I start by rewriting  $\sum_{i,u,k} \mu_{i,u}(k) Q_{i,u}(k)$  in the Lagrangian to manipulate  $\underline{\mathbf{W}}_i$  which is deeply embedded in  $\mathbf{C}_{\mathbf{q}_j, \mathbf{q}_j}$  of  $Q_{i,u}(k)$ . By mapping the indices from  $(i, u, k, j)$  to  $(j, v, \ell, i)$ , I have

$$\begin{aligned}
\sum_{i,u,k} \mu_{i,u}(k) Q_{i,u}(k) &= \sum_{i,u,k} \mu_{i,u}(k) \sum_{j=1}^{N_c} \underline{\mathbf{g}}_{j,i,u}^H(k) \mathbf{\Psi}_{N_b} \mathbf{C}_{\mathbf{q}_j, \mathbf{q}_j} \mathbf{\Psi}_{N_b}^H \underline{\mathbf{g}}_{j,i,u}(k) \\
&= \sum_{j,v,\ell,i} \mu_{j,v}(\ell) \underline{\mathbf{g}}_{i,j,v}^H(\ell) \mathbf{\Psi}_{N_b} \text{diag} \left( \sum_{u,k} |\psi_{N_b,m}^H(n) \underline{\mathbf{w}}_{i,u}(k)|^2, \forall m, n \right) \mathbf{\Psi}_{N_b}^H \underline{\mathbf{g}}_{i,j,v}(\ell) \tag{3.47}
\end{aligned}$$

where  $\psi_{N_b,m}(n)$  denotes the  $(m + (n-1)N_b)$ th column of  $\mathbf{\Psi}_{N_b}$ , i.e.,  $\psi_{N_b,m}(n) = [\mathbf{w}_{\text{DFT},n} \otimes \mathbf{I}_{N_b}]_{:,m}$  for  $m = 1, \dots, N_b$ ,  $n = 1, \dots, K$ , and  $\underline{\mathbf{w}}_{i,u}(k)$  is the  $(kN_u + u)$ th column of  $\underline{\mathbf{W}}_i$ . Let  $\mathbf{M}_i(k) = \text{diag}(\mu_{i,1}(k), \dots, \mu_{i,N_u}(k))$ ,  $\underline{\mathbf{M}}_i = \text{blkdiag}(\mathbf{M}_i(0), \dots, \mathbf{M}_i(K-1))$ , and  $\underline{\mathbf{M}} = [\underline{\mathbf{M}}_1, \dots, \underline{\mathbf{M}}_{N_c}]$ . Recalling that  $\mathbf{\Psi}_{N_b}(k) = ([\mathbf{W}_{\text{DFT}}]_{k+1,:} \otimes \mathbf{I}_{N_b})$

and  $\underline{\mathbf{G}}_i = [\underline{\mathbf{G}}_{i,1}, \dots, \underline{\mathbf{G}}_{i,N_c}]$ , (3.47) is rewritten as

$$\begin{aligned}
& \sum_{j,v,\ell,i} \mu_{j,v}(\ell) \sum_{m,n} \left( \sum_{u,k} |\boldsymbol{\psi}_{N_b,m}^H(n) \underline{\mathbf{w}}_{i,u}(k)|^2 \left( \sum_r g_{i,j,v,r}^*(\ell) \psi_{N_b,m,r}(n) \right) \left( \sum_{r'} g_{i,j,v,r'}(\ell) \psi_{N_b,m,r'}^*(n) \right) \right) \\
&= \sum_{i,u,k} \underline{\mathbf{w}}_{i,u}^H(k) \left( \sum_{m,n} \boldsymbol{\psi}_{N_b,m}(n) \left( \sum_{j,v,\ell} \mu_{j,v}(\ell) \boldsymbol{\psi}_{N_b,m}^H(n) \underline{\mathbf{g}}_{i,j,v}(\ell) \underline{\mathbf{g}}_{i,j,v}^H(\ell) \boldsymbol{\psi}_{N_b,m}(n) \right) \boldsymbol{\psi}_{N_b,m}^H(n) \right) \underline{\mathbf{w}}_{i,u}(k) \\
&= \sum_{i,u,k} \underline{\mathbf{w}}_{i,u}^H(k) \boldsymbol{\Psi}_{N_b} \text{diag} \left( \boldsymbol{\Psi}_{N_b}^H \underline{\mathbf{G}}_i \underline{\mathbf{M}} \underline{\mathbf{G}}_i^H \boldsymbol{\Psi}_{N_b} \right) \boldsymbol{\Psi}_{N_b}^H \underline{\mathbf{w}}_{i,u}(k) \\
&\stackrel{(a)}{=} \sum_{i,u,k} \mathbf{w}_{i,u}^H(k) \boldsymbol{\Psi}_{N_b}(k) \text{diag} \left( \boldsymbol{\Psi}_{N_b}^H \underline{\mathbf{G}}_i \underline{\mathbf{M}} \underline{\mathbf{G}}_i^H \boldsymbol{\Psi}_{N_b} \right) \boldsymbol{\Psi}_{N_b}^H(k) \mathbf{w}_{i,u}(k). \tag{3.48}
\end{aligned}$$

Here, (a) comes from  $\underline{\mathbf{w}}_{i,u}^H(k) \boldsymbol{\Psi}_{N_b} = \mathbf{w}_{i,u}^H(k) \boldsymbol{\Psi}_{N_b}(k)$  since  $\underline{\mathbf{w}}_{i,u}(k)$  has nonzero elements  $\mathbf{w}_{i,u}(k)$  only in the position that corresponds to the precoder for subcarrier  $k$ , and  $g_{i,j,v,r}(\ell)$  and  $\psi_{N_b,m,r}(n)$  are the  $r$ th elements of  $\underline{\mathbf{g}}_{i,j,v}(\ell)$  and  $\boldsymbol{\psi}_{N_b,m}(n)$ , respectively.

Next, I define  $\tilde{\mathbf{D}}_i(k) = \text{diag}(\nu_{i,1}(k), \dots, \nu_{i,N_b}(k))$ . By switching the indices between  $k$  and  $\ell$ , I can cast  $\sum_{i,m,k} \nu_{i,m}(k) \left[ \sum_{\ell=0}^{K-1} \mathbf{W}_i(\ell) \mathbf{W}_i^H(\ell) \right]_{m,m}$  in (3.46) to

$$\begin{aligned}
\sum_{i,m,\ell} \nu_{i,m}(\ell) \left[ \sum_{u,k} \mathbf{w}_{i,u}(k) \mathbf{w}_{i,u}^H(k) \right]_{m,m} &= \sum_{i,m,\ell} \sum_{u,k} w_{i,u,m}^*(k) \nu_{i,m}(\ell) w_{i,u,m}(k) \\
&= \sum_{i,u,k} \mathbf{w}_{i,u}^H(k) \tilde{\mathbf{D}}_i \mathbf{w}_{i,u}(k), \tag{3.49}
\end{aligned}$$

where  $w_{i,u,m}(k)$  is the  $m$ th element of  $\mathbf{w}_{i,u}(k)$  and  $\tilde{\mathbf{D}}_i = \sum_{\ell=0}^{K-1} \tilde{\mathbf{D}}_i(\ell)$ . Further,  $\sum_{i,m,\ell} \nu_{i,m}(\ell) p_0$  in (3.46) can be redrafted as

$$p_0 \sum_{i,m,\ell} \nu_{i,m}(\ell) = p_0 \sum_{i=1}^{N_c} \text{tr}(\tilde{\mathbf{D}}_i). \tag{3.50}$$

By applying (3.48), (3.49), and (3.50) to the Lagrangian, I have the reformulated Lagrangian as

$$\begin{aligned}
\mathcal{L}(\mathbf{w}_{i,u}(k), \mu_{i,u}(k), \nu_{i,m}(\ell)) &= \sum_{i,u,k} \mu_{i,u}(k) \sigma^2 - p_0 \sum_i [\text{tr}(\tilde{\mathbf{D}}_i) - KN_b] \quad (3.51) \\
&+ \sum_{i,u,k} \mathbf{w}_{i,u}^H(k) \left( \frac{\alpha}{K} \tilde{\mathbf{D}}_i - \alpha^2 \left( 1 + \frac{1}{\gamma_{i,u}(k)} \right) \lambda_{i,u}(k) \mathbf{g}_{i,i,u}(k) \mathbf{g}_{i,i,u}^H(k) \right. \\
&+ \alpha^2 \sum_{j,v} \lambda_{j,v}(k) \mathbf{g}_{i,j,v}(k) \mathbf{g}_{i,j,v}^H(k) \\
&\left. + \alpha(1-\alpha) \Psi_{N_b}(k) \text{diag}(\Psi_{N_b}^H \mathbf{G}_i \mathbf{\Lambda} \mathbf{G}_i^H \Psi_{N_b}) \Psi_{N_b}^H(k) \right) \mathbf{w}_{i,u}(k).
\end{aligned}$$

Define the dual objective function as

$$g(\mu_{i,u}(k), \nu_{i,m}(\ell)) = \min_{\mathbf{w}_{i,u}(k), p_0} \mathcal{L}(\mathbf{w}_{i,u}(k), \mu_{i,u}(k), \nu_{i,m}(\ell)) \quad (3.52)$$

and let  $\mathbf{D}_i = \frac{1}{K} \tilde{\mathbf{D}}_i$ . To avoid an unbounded objective function, the required conditions are  $\text{tr}(\mathbf{D}_i) \leq N_b$  and

$$\begin{aligned}
\mathbf{K}_{i,k}(\mathbf{M}) &= \\
\mathbf{D}_i + \alpha \sum_{j,v} \mu_{j,v}(k) \mathbf{g}_{i,j,v}(k) \mathbf{g}_{i,j,v}^H(k) + (1-\alpha) \Psi_{N_b}(k) \text{diag}(\Psi_{N_b}^H \mathbf{G}_i \mathbf{M} \mathbf{G}_i^H \Psi_{N_b}) \Psi_{N_b}^H(k) \\
&\succeq \alpha \left( 1 + 1/\gamma_{i,u}(k) \right) \mu_{i,u}(k) \mathbf{g}_{i,i,u}(k) \mathbf{g}_{i,i,u}^H(k). \quad (3.53)
\end{aligned}$$

Consequently, the Lagrangian dual problem of (3.10) can be formulated as

$$\max_{\mathbf{D}_i} \max_{\mu_{i,u}(k)} \sum_{i,u,k}^{N_c, N_u, K} \mu_{i,u}(k) \sigma^2 \quad (3.54)$$

$$\text{subject to } \mathbf{K}_{i,k}(\mathbf{M}) \succeq \alpha \left( 1 + \frac{1}{\gamma_{i,u}(k)} \right) \mu_{i,u}(k) \mathbf{g}_{i,i,u}(k) \mathbf{g}_{i,i,u}^H(k), \quad (3.55)$$

$$\mathbf{D}_i \succeq 0, \mathbf{D}_i \in \mathbb{R}^{N_b \times N_b} : \text{diagonal},$$

$$\text{tr}(\mathbf{D}_i) \leq N_b \quad \forall i, u, k.$$

The differences between (3.43) and (3.54) are the opposite objective problems with respect to  $\lambda_{i,u}(k)$  and  $\mu_{i,u}(k)$ , i.e., min vs. max, and the reversed SQINR inequality conditions in (3.44) and (3.55). Since (3.43) and (3.54) obtain optimal solutions when the SQINR constraints satisfy equality conditions, the solutions for both problems are indeed equivalent to each other with the active SQINR constraints. Therefore, (3.43) and (3.54) are equivalent, and  $\lambda_{i,u}(k)$  and  $\mu_{i,u}(k)$  are interchangeable. This completes the proof.  $\square$

### 3.8 Proof of Corollary 7

First of all, the identity in (3.45) allows the primal DL problem in (3.10) to be rewritten as

$$\min_{\mathbf{w}_{i,u}(k), p_o} p_o \quad (3.56)$$

$$\text{s.t. } \Gamma_{i,u}(k) \geq \gamma_{i,u}(k), \quad \forall i, u, k \quad (3.57)$$

$$\left[ \frac{\alpha}{K} \sum_{\ell=0}^{K-1} \mathbf{W}_i(\ell) \mathbf{W}_i^H(\ell) \right]_{m,m} \leq p_o. \quad (3.58)$$

Let  $\mathbf{W}_{\text{BD}}(k) = \text{blkdiag}(\mathbf{W}_1(k), \dots, \mathbf{W}_{N_c}(k))$ ,  $\tilde{\mathbf{W}}_{\text{BD}}(k) = \text{blkdiag}((\mathbf{I}_{KN_b} \otimes \mathbf{W}_1(k)), \dots, (\mathbf{I}_{KN_b} \otimes \mathbf{W}_{N_c}(k)))$ ,  $\tilde{\mathbf{W}}_{\text{BD}} = \text{blkdiag}(\tilde{\mathbf{W}}_{\text{BD}}(0), \dots, \tilde{\mathbf{W}}_{\text{BD}}(K-1))$ ,  $\tilde{\Psi}_{N_b}(k) = \mathbf{I}_{KN_b} \otimes \Psi_{N_b}(k)$ ,  $\tilde{\Psi}_{N_b} = \text{blkdiag}(\tilde{\Psi}_{N_b}(0), \dots, \tilde{\Psi}_{N_b}(K-1))$ ,  $\mathbf{E}_{j,i,u}(k) = \text{diag}(\Psi_{N_b} \mathbf{g}_{j,i,u} \mathbf{g}_{j,i,u}^H \Psi_{N_b}^H)$ , and  $\mathbf{E}_{i,u}(k) = \mathbf{1}_K \otimes \text{vec}(\mathbf{E}_{1,i,u}^{1/2}(k), \dots, \mathbf{E}_{N_c,i,u}^{1/2}(k))$ . The

SQINR constraints in (3.57) can be re-interpreted as

$$\alpha^2 \left( 1 + \frac{1}{\gamma_{i,u}(k)} \right) |\mathbf{w}_{i,u}^H(k) \mathbf{g}_{i,i,u}|^2 \quad (3.59)$$

$$\geq \left\| \begin{array}{c} \alpha \mathbf{W}_{\text{BD}}^H(k) \text{vec}(\mathbf{g}_{1,i,u}, \dots, \mathbf{g}_{N_c,i,u}) \\ \sqrt{\alpha(1-\alpha)} \tilde{\mathbf{W}}_{\text{BD}}(0) \tilde{\Psi}_{N_b}(0) \text{vec}(\mathbf{E}_{1,i,u}^{1/2}(k), \dots, \mathbf{E}_{N_c,i,u}^{1/2}(k)) \\ \vdots \\ \sqrt{\alpha(1-\alpha)} \tilde{\mathbf{W}}_{\text{BD}}(K-1) \tilde{\Psi}_{N_b}(K-1) \text{vec}(\mathbf{E}_{1,i,u}^{1/2}(k), \dots, \mathbf{E}_{N_c,i,u}^{1/2}(k)) \end{array} \right\|^2 + \sigma^2 \quad (3.60)$$

$$= \left\| \frac{\alpha \mathbf{W}_{\text{BD}}^H(k) \text{vec}(\mathbf{g}_{1,i,u}, \dots, \mathbf{g}_{N_c,i,u})}{\sqrt{\alpha(1-\alpha)} \tilde{\mathbf{W}}_{\text{BD}} \tilde{\Psi}_{N_b} \mathbf{E}_{i,u}(k)} \right\|^2 + \sigma^2, \quad (3.61)$$

for all  $i$ ,  $u$ , and  $k$ . In addition, the per-antenna constraint in (3.58) is rewritten as

$$\left[ \frac{\alpha}{K} \sum_{\ell=0}^{K-1} \mathbf{W}_i(\ell) \mathbf{W}_i^H(\ell) \right]_{m,m} = \frac{\alpha}{K} \left\| \text{vec}(\mathbf{e}_m^H \mathbf{W}_i(0), \dots, \mathbf{e}_m^H \mathbf{W}_i(K-1)) \right\|^2 \quad (3.62)$$

for all  $m$ . Accordingly, the primal DL problem in (3.10) can be cast to the SOCP. Since (3.10) is strictly feasible and convex, strong duality holds between (3.10) and (3.25).  $\square$

### 3.9 Proof of Corollary 8

I first find the derivative of the Lagrangian in (3.51) with respect to  $\mathbf{w}_{i,u}(k)$  as

$$\begin{aligned} \frac{\partial \mathcal{L}(\mathbf{w}_{i,u}(k), \lambda_{i,u}(k), \nu_{i,m}(\ell))}{\partial \mathbf{w}_{i,u}(k)} &= 2 \left( \frac{\alpha}{K} \tilde{\mathbf{D}}_i - \alpha^2 \left( 1 + \frac{1}{\gamma_{i,u}(k)} \right) \lambda_{i,u}(k) \mathbf{g}_{i,i,u}(k) \mathbf{g}_{i,i,u}^H(k) \right. \\ &+ \alpha^2 \sum_{j,v} \lambda_{j,v}(k) \mathbf{g}_{i,j,v}(k) \mathbf{g}_{i,j,v}^H(k) \\ &\left. + \alpha(1 - \alpha) \Psi_{N_b}(k) \text{diag}(\Psi_{N_b}^H \underline{\mathbf{G}}_i \underline{\mathbf{\Lambda}} \underline{\mathbf{G}}_i^H \Psi_{N_b}) \Psi_{N_b}^H(k) \right) \mathbf{w}_{i,u}(k). \end{aligned} \quad (3.63)$$

I then set the derivative of the Lagrangian to zero, and solve it for  $\mathbf{w}_{i,u}(k)$  as

$$\begin{aligned} \mathbf{w}_{i,u}(k) &= \left( \alpha^2 \sum_{(j,v) \neq (i,u)} \lambda_{j,v}(k) \mathbf{g}_{i,j,v}(k) \mathbf{g}_{i,j,v}^H(k) \right. \\ &\left. + \alpha(1 - \alpha) \Psi_{N_b}(k) \text{diag}(\Psi_{N_b}^H \underline{\mathbf{G}}_i \underline{\mathbf{\Lambda}} \underline{\mathbf{G}}_i^H \Psi_{N_b}) \Psi_{N_b}^H(k) + \alpha \mathbf{D}_i \right)^{-1} \times \\ &\quad \frac{\alpha^2}{\gamma_{i,u}(k)} \lambda_{i,u}(k) \mathbf{g}_{i,i,u}(k) \mathbf{g}_{i,i,u}^H(k) \mathbf{w}_{i,u}(k) \end{aligned} \quad (3.64)$$

$$\stackrel{(a)}{=} \frac{\alpha^2}{\gamma_{i,u}(k)} \lambda_{i,u}(k) \mathbf{g}_{i,i,u}^H(k) \mathbf{w}_{i,u}(k) \mathbf{f}_{i,u}(k) \quad (3.65)$$

where (a) comes from  $\mathbf{f}_{i,u}(k)$  given in (3.39). As a result, I argue  $\mathbf{w}_{i,u}(k) = \sqrt{\tau_{i,u}(k)} \mathbf{f}_{i,u}(k)$  with properly computed  $\tau_{i,u}(k)$ .

To satisfy the Karush–Kuhn–Tucker stationarity condition with the DL constraint in (3.11),  $\Gamma_{i,u}(k)$  has to meet the target SQINR constraint with strict equality. For given  $i, u, k$ , define  $\xi_{i',u'}(n) = 1$  if  $(i', u', n) = (i, u, k)$ , and  $\xi_{i',u'}(n) = 0$  otherwise. I collect  $\xi_{i,u}$ 's as  $\Xi_i(k) = \text{diag}(\xi_{i,1}(k), \dots, \xi_{i,N_u}(k))$ ,  $\Xi(k) = \text{blkdiag}(\Xi_1, \dots, \Xi_{N_c})$ , and  $\underline{\Xi} = \text{blkdiag}(\Xi(0) \dots, \Xi(K-1))$ . I then

rewrite the quantization error term in (3.8) in a tractable form as

$$\begin{aligned}
Q_{i,u}(k) &\stackrel{(a)}{=} \alpha(1-\alpha) \sum_{j=1}^{N_c} \mathbf{g}_{j,i,u}^H(k) \Psi_{N_b} \text{diag}(\Psi_{N_b}^H \mathbf{W}_j \mathbf{W}_j^H \Psi_{N_b}) \Psi_{N_b}^H \mathbf{g}_{j,i,u}(k) \\
&= \alpha(1-\alpha) \sum_{i',u',n,j} \xi_{i',u'}(n) \mathbf{g}_{j,i',u'}^H(n) \Psi_{N_b} \text{diag}(\Psi_{N_b}^H \mathbf{W}_j \mathbf{W}_j^H \Psi_{N_b}) \Psi_{N_b}^H \mathbf{g}_{j,i',u'}(n) \\
&= \alpha(1-\alpha) \sum_{j,v,\ell} \mathbf{w}_{j,v}^H(\ell) \Psi_{N_b}(\ell) \text{diag}(\Psi_{N_b}^H \mathbf{G}_j \Xi \mathbf{G}_j^H \Psi_{N_b}) \Psi_{N_b}^H(\ell) \mathbf{w}_{j,v}(\ell) \\
&\stackrel{(b)}{=} \alpha(1-\alpha) \sum_{j,v,\ell} \mathbf{w}_{j,v}^H(\ell) \Psi_{N_b}(\ell) \text{diag}(\Psi_{N_b}^H \mathbf{g}_{j,i,u}(k) \mathbf{g}_{j,i,u}^H(k) \Psi_{N_b}) \Psi_{N_b}^H(\ell) \mathbf{w}_{j,v}(\ell),
\end{aligned} \tag{3.66}$$

where (a) is obtained by substituting (3.5) into (3.9) and (b) comes from the fact that  $\mathbf{G}_j \Xi \mathbf{G}_j^H = \mathbf{g}_{j,i,u}(k) \mathbf{g}_{j,i,u}^H(k)$  since  $\Xi$  can activate the  $(kN_u + u)$ th column of  $\mathbf{G}_j$  only.

Accordingly, the active DL SQINR constraint is rewritten as follows:

$$\begin{aligned}
\sigma^2 &= \frac{\alpha^2}{\gamma_{i,u}(k)} |\mathbf{g}_{i,i,u}^H(k) \mathbf{w}_{i,u}(k)|^2 - \alpha^2 \sum_{(j,v) \neq (i,u)}^{N_c, N_u} |\mathbf{g}_{j,i,u}^H(k) \mathbf{w}_{j,v}(k)|^2 - Q_{i,k}(k) \\
&\stackrel{(a)}{=} \frac{\alpha^2}{\gamma_{i,u}} |\mathbf{g}_{i,i,u}^H(k) \mathbf{f}_{i,u}(k)|^2 \tau_{i,u}(k) - \alpha^2 \sum_{(j,v) \neq (i,u)} |\mathbf{g}_{j,i,u}(k) \mathbf{f}_{j,v}^H(k)|^2 \tau_{j,v}(k) \\
&\quad - \alpha(1-\alpha) \sum_{j,v,\ell} \tau_{j,v}(\ell) \mathbf{f}_{j,v}^H(\ell) \Psi_{N_b}(\ell) \text{diag}(\Psi_{N_b}^H \mathbf{g}_{j,i,u}(k) \mathbf{g}_{j,i,u}^H(k) \Psi_{N_b}) \Psi_{N_b}^H(\ell) \mathbf{f}_{j,v}(\ell),
\end{aligned} \tag{3.67}$$

for all  $i, u, k$  where (a) is from (3.66) and  $\mathbf{w}_{i,u}(k) = \sqrt{\tau_{i,u}(k)} \mathbf{f}_{i,u}(k)$ . Representing (3.67) for all  $i, u, k$  gives  $\sigma^2 \mathbf{1} = \underline{\Sigma} \underline{\boldsymbol{\tau}}$ , thereby having  $\tau_{i,u}(k)$  by solving  $\underline{\boldsymbol{\tau}} = \sigma^2 \underline{\Sigma}^{-1} \mathbf{1}$ .  $\square$

### 3.10 Proof of Corollary 9

(3.32) is obtained by setting the Lagrangian in (3.63) to zero, solving for  $\lambda_{i,u}(k)$ , and replacing  $\frac{\alpha}{K}\tilde{\mathbf{D}}_i$  with  $\mathbf{D}_i$ . Thus, the solution of  $\lambda_{i,u}(k)$  satisfies the stationary condition, and I further observe that the UL SQINR constraint in (3.12) is active at the solution satisfying the complementary slackness condition. Therefore, (3.32) is optimal solution of the UL OFDM problem.  $\square$

### 3.11 Proof of Corollary 10

Using the beamforming duality between UL and DL problems shown in [23] and [15],  $f(\mathbf{D}_i)$  in (3.31) for fixed  $\mathbf{D}_i$  can be transformed to the following DL beamforming problem:

$$f(\mathbf{D}_i) = \min_{\mathbf{w}_{i,u}(k)} \sum_{u,k}^{N_u, K} \mathbf{w}_{i,u}^H(k) \mathbf{D}_i \mathbf{w}_{i,u}(k) \quad (3.68)$$

subject to  $\Gamma_{i,u}(k) \geq \gamma_{i,u}(k) \quad \forall i, u, k.$

I introduce two arbitrary diagonal covariance matrices  $\mathbf{D}_i$  and  $\mathbf{D}'_i$  whose associated optimal solution of (3.68) is denoted as  $\mathbf{w}_{i,u}(k)$  and  $\mathbf{w}'_{i,u}(k)$ , respectively.

I can then discover the following inequality on the objective function:

$$\begin{aligned} f(\mathbf{D}'_i) - f(\mathbf{D}_i) &= \sum_{u,k} \mathbf{w}'_{i,u}{}^H(k) \mathbf{D}'_i \mathbf{w}'_{i,u}(k) - \sum_{u,k} \mathbf{w}_{i,u}^H(k) \mathbf{D}_i \mathbf{w}_{i,u}(k) \\ &\stackrel{(a)}{\leq} \sum_{u,k} \mathbf{w}_{i,u}^H(k) \mathbf{D}'_i \mathbf{w}_{i,u}(k) - \sum_{u,k} \mathbf{w}_{i,u}^H(k) \mathbf{D}_i \mathbf{w}_{i,u}(k) \\ &\stackrel{(b)}{=} \text{tr} \left( \text{diag} \left( \sum_{u,k} \mathbf{w}_{i,k}(k) \mathbf{w}_{i,k}^H(k) \right) (\mathbf{D}'_i - \mathbf{D}_i) \right), \quad (3.69) \end{aligned}$$



where (a) holds because associating  $\mathbf{D}'_i$  with  $\mathbf{w}_{i,u}(k)$  cannot decrease the objective function from  $\mathbf{w}'_{i,u}(k)$ , and (b) follows because  $(\mathbf{D}'_i - \mathbf{D}_i)$  is diagonal. From the definition of a subgradient:  $\mathbf{A}$  is a subgradient if  $f(\mathbf{D}'_i) \leq f(\mathbf{D}_i) + \text{tr}(\mathbf{A}(\mathbf{D}'_i - \mathbf{D}_i))$ , (3.34) is a subgradient of  $f(\mathbf{D}_i)$ .  $\square$

### 3.12 Proof of Corollary 11

*Proof.* The proof is based on the standard function approach presented in [15, 23, 105]. Let us rewrite (3.32) as  $\lambda_{i,u}^{(n+1)}(k) = \mathcal{F}_{i,u,k}(\underline{\mathbf{\Lambda}}^{(n)})$ . I need to show that  $\mathcal{F}_{i,u,k}(\underline{\mathbf{\Lambda}})$  is a standard function which satisfies the followings:

- (Positivity) If  $\lambda_{i,u}(k) \geq 0 \forall i, u, k$ , then  $\mathcal{F}_{i,u,k}(\underline{\mathbf{\Lambda}}) > 0$ .

*Proof.* By limiting  $\lambda_{i,u}^{(n+1)}(k)$  to be non-negative, I have  $\mathbf{K}_{i,k}(\underline{\mathbf{\Lambda}}) \succ 0$ ; hence  $\mathbf{K}_{i,k}^{-1}(\underline{\mathbf{\Lambda}}) \succ 0$ . This makes the denominator of (3.32) strictly positive.  $\square$

- (Monotonicity) If  $\lambda_{i,u}(k) \geq \lambda'_{i,u}(k) \forall i, u, k$ , then  $\mathcal{F}_{i,u,k}(\underline{\mathbf{\Lambda}}) \geq \mathcal{F}_{i,u,k}(\underline{\mathbf{\Lambda}}')$ .

*Proof.* For the sake of brevity, I define the signal and quantization noise part of the covariance matrix as

$$\mathbf{R}(\underline{\mathbf{\Lambda}}) = \alpha \sum_{j,v} \lambda_{j,v}(k) \mathbf{g}_{i,j,v}(k) \mathbf{g}_{i,j,v}^H(k) + (1-\alpha) \Psi_{N_b}(k) \text{diag} \left( \Psi_{N_b}^H \underline{\mathbf{G}}_i \underline{\mathbf{\Lambda}} \underline{\mathbf{G}}_i^H \Psi_{N_b} \right) \Psi_{N_b}^H(k). \quad (3.70)$$

Leveraging the fact that  $\underline{\mathbf{\Lambda}}$  is a diagonal matrix, the covariance matrix of the received signal is then rewritten as

$$\mathbf{K}_{i,k}(\underline{\mathbf{\Lambda}}) = \mathbf{D}_i + \mathbf{R}(\underline{\mathbf{\Lambda}}) \quad (3.71)$$

$$= \mathbf{D}_i + \mathbf{R}(\underline{\mathbf{\Lambda}}') + \mathbf{R}(\underline{\mathbf{\Lambda}} - \underline{\mathbf{\Lambda}}'). \quad (3.72)$$

Since I assume  $\lambda_{i,u}(k) \geq \lambda'_{i,u}(k)$ , I can notice that  $\mathbf{R}((\underline{\mathbf{\Lambda}} - \underline{\mathbf{\Lambda}}')) \succeq 0$ . In addition, I know  $\mathbf{D}_i + \mathbf{R}(\underline{\mathbf{\Lambda}}) \succeq 0$  and  $\mathbf{g}_{i,i,u}^H(k)$  is in the range of  $\mathbf{D}_i + \mathbf{R}(\underline{\mathbf{\Lambda}}')$ . By Proposition 4 of [102], the following relationship holds:

$$\mathcal{F}_{i,u,k}(\underline{\mathbf{\Lambda}}) = \frac{1}{\alpha \left(1 + \frac{1}{\gamma_{i,u}(k)}\right) \mathbf{g}_{i,i,u}^H(k) \left(\mathbf{D}_i + \mathbf{R}(\underline{\mathbf{\Lambda}}') + \mathbf{R}(\underline{\mathbf{\Lambda}} - \underline{\mathbf{\Lambda}}')\right)^{-1} \mathbf{g}_{i,i,u}(k)} \quad (3.73)$$

$$\geq \frac{1}{\alpha \left(1 + \frac{1}{\gamma_{i,u}(k)}\right) \mathbf{g}_{i,i,u}^H(k) \left(\mathbf{D}_i + \mathbf{R}(\underline{\mathbf{\Lambda}}')\right)^{-1} \mathbf{g}_{i,i,u}(k)} \quad (3.74)$$

$$= \mathcal{F}_{i,u,k}(\underline{\mathbf{\Lambda}}') \quad (3.75)$$

□

- (Scalability) For  $\rho > 1$ ,  $\rho \mathcal{F}_{i,u,k}(\underline{\mathbf{\Lambda}}) > \mathcal{F}_{i,u,k}(\rho \underline{\mathbf{\Lambda}})$ .

*Proof.* I have  $(\rho - 1)\mathbf{D}_i$  is still a semidefinite matrix. By Proposition 4 of [102], the following relationship holds:

$$\rho \mathcal{F}_{i,u,k}(\underline{\mathbf{\Lambda}}) = \frac{1}{\alpha \left(1 + \frac{1}{\gamma_{i,u}(k)}\right) \mathbf{g}_{i,i,u}^H(k) \left((\rho - 1)\mathbf{D}_i + \mathbf{D}_i + \rho \mathbf{R}(\underline{\mathbf{\Lambda}})\right)^{-1} \mathbf{g}_{i,i,u}(k)} \quad (3.76)$$

$$\geq \frac{1}{\alpha \left(1 + \frac{1}{\gamma_{i,u}(k)}\right) \mathbf{g}_{i,i,u}^H(k) \left(\mathbf{D}_i + \rho \mathbf{R}(\underline{\mathbf{\Lambda}})\right)^{-1} \mathbf{g}_{i,i,u}(k)} \quad (3.77)$$

$$= \mathcal{F}_{i,u,k}(\rho \underline{\mathbf{\Lambda}}) \quad (3.78)$$

Since equality holds when  $\rho(\rho - 1)\mathbf{D}_i(\mathbf{D}_i + \mathbf{R}(\underline{\Lambda}))^{-1} \mathbf{g}_{i,i,u}(k) = \mathbf{0}$ . Since multiplying by  $\mathbf{g}_{i,i,u}(k)^H \mathbf{D}_i^{-1}$  on the left side yields

□

Combining the three proofs completes the proof of Corollary

□

---

**Algorithm 1:** Quantization-aware iterative CoMP with per-antenna constraints (Q-CoMP-PA)

---

**1 Initialize**  $\lambda_{i,u}^{(0)}(k)$ ,  $\forall i, u, k$  and  $\mathbf{D}_i^{(0)}$ ,  $\forall i$ .  
**2 while**  $|\mathbf{D}_i^{(n)} - \mathbf{D}_i^{(n-1)}| \geq \epsilon_{\mathbf{D}}$ ,  $\forall i$  **do**  
**3     while**  $|\lambda_{i,u}^{(t)}(k) - \lambda_{i,u}^{(t-1)}(k)| \geq \epsilon_{\lambda}$ ,  $\forall i, u, k$  **do**  
**4**Compute  $\mathbf{K}_{i,k}(\underline{\mathbf{\Lambda}}^{(t)})$  according to (3.42) using  $\lambda_{i,u}^{(t)}(k)$  and  $\mathbf{D}_i^{(n)}$ .  
**5**Update  $\lambda_{i,u}^{(t+1)}(k)$  according to (3.32) as  
**6**
$$\lambda_{i,u}^{(t+1)}(k) \leftarrow \frac{1}{\alpha \left(1 + \frac{1}{\gamma_{i,u}(k)}\right) \mathbf{g}_{i,i,u}^H(k) \mathbf{K}_{i,k}^{-1}(\underline{\mathbf{\Lambda}}^{(t)}) \mathbf{g}_{i,i,u}(k)}, \quad \forall i, u, k,$$
  
**7** $t \leftarrow t + 1$ .  
**8     end**  
**9**Find the UL MMSE equalizer  $\mathbf{f}_{i,u}(k)$  in (3.39) with  $\mathbf{D}_i^{(n)}$  and  $\lambda_{i,u}^{(t)}(k)$ .  
**10**Compute the DL precoder  $\mathbf{w}_{i,u}(k)$  from Corollary 8.  
**11**Update  $\mathbf{D}_i^{(n+1)}$  using a subgradient ascent method as  

$$\mathbf{D}_i^{(n+1)} \leftarrow \mathbf{D}_i^{(n)} + \eta \operatorname{diag} \left( \sum_{u,k} \mathbf{w}_{i,u}(k) \mathbf{w}_{i,u}^H(k) \right), \forall i.$$
  
**12**Project  $\mathbf{D}_i^{(n+1)}$  onto the feasible set (3.27)-(3.28) until converges as  

$$\mathbf{D}_i^{(n+1)} \leftarrow \max \left( 0, \frac{\left( \operatorname{tr} \left( \mathbf{D}_i^{(n+1)} \right) - N_b \right)}{\|\mathbf{1}_{N_b}\|^2} \operatorname{diag}(\mathbf{1}_{N_b}) \right), \forall i.$$
  
**13** $n \leftarrow n + 1$ .  
**14 end**  
**15 return**  $\mathbf{w}_{i,u}(k)$ ,  $\forall i, u, k$ .

---

Table 3.1: Comparison of peak-to-average power ratio (PAPR) for selected target SQINR values  $\gamma$ .

$\gamma$ [dB]	Q-Percell	Q-CoMP	<b>Q-CoMP-PA</b>
1	8.21 dB	4.98 dB	<b>2.96 dB</b>
-5	7.99 dB	4.93 dB	<b>2.88 dB</b>

- (a) PAPR of the wideband OFDM system with  $N_b = 32$  antennas,  $N_c = 3$  cells,  $N_u = 2$  users per cell,  $b = 3$  bits, and  $K = 64$  subcarriers.

$\gamma$ [dB]	$N_c = 2$ cells		
	Q-Percell	Q-CoMP	<b>Q-CoMP-PA</b>
2	4.02 dB	2.96 dB	<b>2.18 dB</b>
-3	3.97 dB	2.94 dB	<b>2.07 dB</b>

$\gamma$ [dB]	$N_c = 4$ cells		
	Q-Percell	Q-CoMP	<b>Q-CoMP-PA</b>
2	5.35 dB	4.21 dB	<b>2.25 dB</b>
-3	5.58 dB	4.42 dB	<b>2.55 dB</b>

$\gamma$ [dB]	$N_c = 6$ cells		
	Q-Percell	Q-CoMP	<b>Q-CoMP-PA</b>
2	5.49 dB	4.57 dB	<b>2.51 dB</b>
-3	5.96 dB	4.81 dB	<b>3.02 dB</b>

- (b) PAPR of the narrowband system with  $N_b = 32$  antennas,  $N_c \in \{2, 4, 6\}$  cells,  $N_u = 2$  users per cell, and  $b = 3$  bits.

## Chapter 4

# Learning-Based Maximum Likelihood Detection with One-Bit ADCs

In this chapter<sup>1</sup>, I propose a learning-based detection framework for uplink massive multiple-input-multiple-output (MIMO) systems with one-bit analog-to-digital converters (ADCs). The learning-based detection only requires counting the occurrences of the quantized outputs of -1 and +1 for estimating a likelihood probability at each antenna. Accordingly, the key advantage of this approach is to perform maximum likelihood detection without explicit channel estimation which has been one of the primary challenges of one-bit quantized systems. The learning in the high signal-to-noise ratio (SNR) regime, however, needs excessive training to estimate the extremely small likelihood probabilities. To address this drawback, I propose a dither-and-learning technique to estimate likelihood functions from dithered signals. First, I add a dithering signal to artificially decrease the SNR and then infer the likelihood

---

<sup>1</sup>This chapter is based on the following submitted paper: Y. Cho, J. Choi, and B. L. Evans, “Adaptive Learning-Based Maximum Likelihood and Channel-Coded Detection for Massive MIMO Systems with One-Bit ADCs,” submitted to *IEEE Transactions on Vehicular Technologies*, 2023. This work was published in part in the following conference paper: J. Choi, Y. Cho, and B. L. Evans, “Robust Learning-Based ML Detection for Massive MIMO Systems with One-Bit Quantized Signals,” in *IEEE Global Communications Conference (GLOBECOM)*, Dec. 9-13, 2019. This work was supervised by Prof. Brian L. Evans.

function from the quantized dithered signals by using an SNR estimate derived from an deep neural network-based offline estimator. I extend the dithering technique by developing an adaptive dither-and-learning method that updates the dithering power according the patterns observed in the quantized dithered signals. The proposed framework is also applied to state-of-the-art channel-coded MIMO systems by computing a bit-wise and user-wise log-likelihood ratio (LLR) from the refined likelihood probabilities. Simulation results validate the detection performance of the proposed methods in both uncoded and coded systems.

## 4.1 Introduction

Massive MIMO systems for sub-6 GHz wireless communications [46, 66] and millimeter wave (mmWave) communications [3, 33, 74, 75] have been considered as one of the emerging technologies for future communications because of the outstanding gain in spectral efficiency and capacity [56]. As wireless communication systems continue to grow in popularity and importance, there is a need to investigate communications systems that are not only reliable and high-performing, but also energy-efficient for various future wireless applications such as vehicle-to-everything, internet-of-things, extended reality, and smart grid [25, 79]. Because of the small wavelength of mmWave signals and small antenna spacing, the mmWave system allows the installation of more antennas per unit area, each of which is connected to a RF chain with a pair of high-precision data converters.

However, the use of a large number of high-resolution ADCs at receivers results in prohibitively huge power consumption, which becomes the main bottleneck in the practical deployment because a high-resolution ADC is particularly power-hungry as the power consumption of an ADC tends to scale up exponentially with the number of quantization bits. To overcome the circuit power issue, deploying low-precision ADCs has been considered as a low-power solution over the past years [16, 18, 20, 89, 101]. As an extreme case of the low-resolution data converters, the use of one-bit data converters has emerged and become particularly attractive due to the ability to enhance power efficiency, lower hardware cost, and simplify analog processing of receivers [14, 21, 22, 58, 62, 63, 71, 100]. Because of the strong nonlinearity, data detection and channel estimation with one-bit data converters become more challenging; however, the use of massive antenna arrays can alleviate the performance loss [51, 84]. Nevertheless, when conventional signal processing algorithms are applied directly to low-resolution systems, significant performance losses can be experienced due to the severe nonlinear distortions that low-resolution ADCs cause.

#### 4.1.1 Prior Works

State-of-the-art one-bit detection, oversampling, beamforming, and channel estimation techniques have been developed in the recent decades [14, 21, 22, 39, 55, 71, 100]. Low-complexity symbol-level beamforming methods for one-bit quantized systems were developed for quadrature-amplitude-modulation



(QAM) constellations [71]. Taking into account the heavily quantized signals and antenna correlations, an iterative multiuser detection by using a message-passing de-quantization algorithm was devised in [100]. In [21], a high-complexity one-bit ML detection and low-complexity zero-forcing (ZF)-type detection methods were developed. In terms of MIMO detectors, by converting the ML estimation problem in [21] to convex optimization, the optimal maximum-likelihood (ML) detector was introduced and the near-ML detector was also proposed by transforming the ML detection problem into a tractable convex optimization problem [22]. Successive-interference-cancellation one-bit receivers that can be applied to modern channel coding techniques was presented in [14]. However, such detection methods require the estimation of channel state information (CSI), which is unrealistic with one-bit quantized signals. Machine learning techniques were also employed for one-bit detection [5, 67, 68]. It was shown in [68] that support vector machines can be used for efficient channel estimation and data detection with one-bit quantized observations. In [5], the conventional orthogonal frequency division multiplexing precoder and decoder are replaced with artificial neural networks to enable unsupervised autoencoder-based detection. [67] combined a linear estimator based on the Bussgang decomposition and a model-based deep neural network approach to make data detection with one-bit ADCs adaptive to the current channel. It was shown in [64] that employing oversampling of one-bit ADCs at the receiver can unlock the improved energy efficiency. The oversampling technique was further applied to downlink precoding to compensate the loss

caused by the receiver's one-bit ADCs. [57]

Accordingly, various channel estimation methods were developed such as least-square (LS), ML, ZF, and Bussgang decomposition-based methods [22, 52]. Combined with antenna-wise non-zero thresholding for one-bit quantizers, the majorization-minimization-based ML channel estimator was proposed in [55]. In [39], it was shown that Bussgang decomposition-based channel estimator with linear equalizers can provide reliable performance for high-order constellations in one-bit ADC systems. Supervised deep learning in learning a mapping from the one-bit quantized measurements to the channels was utilized in [111]. Such channel estimation schemes with one-bit quantized signals, however, still suffer degradation in estimation accuracy compared with high-precision ADC systems. However, such methods are heavily influenced by channel estimation accuracy. In this regard, I investigate a learning-based detection that replaces one-bit channel estimation with a likelihood probability learning process.

Learning-based data detection techniques have recently been investigated [41–43, 70]. The authors in [42] applied sphere decoding to the one-bit quantized system and showed that the detection complexity is reduced while achieving near-optimal performance. Viewing the one-bit ADC systems as a classification problem, various supervised-learning-based data detection techniques were provided by estimating effective channels and learning the non-linear system response [41]. In [43], however, a channel estimation was done to initialize likelihood functions for ML detection, and a learning-based likelihood

function was used for post-update of the likelihood functions. In contrast, the authors in [70] used an estimated channel to generate a noisy training pilots and developed an expectation-maximization algorithm that facilitates the likelihood probability learning process. Unlike previous learning-based approaches that focused on developing detection mechanisms based on estimation channels, I rather focus on applying one-bit ML detection and learning likelihood functions to overcome the problem of the learning process with the limited amount of training.

#### 4.1.2 Contributions

In this chapter, I propose a learning-based ML detection approach that replaces a one-bit channel estimation stage with a counting-based learning process for an uplink multiuser MIMO systems with one-bit ADCs. The main aim of this work is to estimate the likelihood probability with an acceptable amount of training by utilizing known dithering noise signals. The contributions of this work are summarized as follows:

- I propose the dithering and learning technique to infer likelihood functions from dithered signals. Such an approach significantly reduces the number of zero-valued likelihood functions whereas naive learning-based one-bit detection suffers from a number of zero-valued likelihood functions. After the dithering process, I obtain a preferable statistical pattern in the one-bit quantized output sequences with moderate sign changes thanks to the reduced SNR. Then a denoising phase retrieves the actual

likelihood functions without the impact of the dithering noise. The proposed method allows estimating the likelihood functions with a reasonable training length by drawing meaningful sign patterns in the quantized output sequence.

- To further improve the learning accuracy, I develop a adaptive dithering and learning for adjusting each antenna element's dithering power based on feedback. Since the performance of the proposed dithering-based learning algorithm is affected by the dithering power, the proposed feedback-based adaptive algorithm effectively adjusts the dithering noise power depending on the pattern of the one-bit quantized outputs. A deep neural network-based offline SNR estimation method is also developed to enable the denoising phase of the dithering-based learning in the practical systems.
- In order to further apply the learning-based scheme to modern communication frameworks rather than being limited to hard-output detection, I compute the log-likelihood ratio (LLR), i.e., soft output, which is fed into a channel-decoder. Noting that the LLR needs to be defined for an individual binary bit of each user, I separate the index set of all possible symbol vectors into two disjoint subgroups and compare the sum of the likelihood probabilities over the two subgroups.
- Simulation results validate that, in contrast to the conventional learning-based one-bit ML detectors and other channel estimation-based one-bit

detectors, the proposed learning-based one-bit detector can achieve comparable performance to the optimal one-bit ML detection that requires perfect CSI and exhibit more reliable detection performance in both uncoded and coded simulations.

## 4.2 System Model

### 4.2.1 Signal Model

Uplink multiuser MIMO communication systems are considered where the base station (BS) equipped with  $N_r$  receive antennas concurrently communicates with  $N_u$  single-antenna users. I suppose  $N_r \gg N_u$  in the context of massive MIMO systems. Each antenna element has its own dedicated RF chain as well as individual in-phase and quadrature one-bit ADCs. I assume a block fading channel model whose channel matrix is invariant for  $N_c$  coherent time slots. I then split the uplink transmission into a training phase with  $N_t$  time slots and a data transmission phase with  $N_d$  slots, i.e.,  $N_c = N_t + N_d$ . During the training phase, each user transmits up to  $N_t$  pilot symbols. I use  $K$  to denote the number of possible pilot symbol combinations of  $N_u$  users, e.g.,  $K = 2^{N_u}$  for binary phase shift keying at all  $N_u$  users. I also use  $N_{\text{tr}}$  to represent the number of transmissions of each combination. This implies  $N_t \geq KN_{\text{tr}}$  to learn the characteristics of all possible combinations.

Let  $\mathbb{Q}_M$  denote the set of constellation points of  $M$ -ary QAM scheme from which  $\bar{s}_u[t]$  is generated where  $\bar{s}_u[t]$  is the complex-valued data symbol of user  $u$  at time  $t$ . I assume  $\bar{s}_u[t] \in \mathbb{Q}_M$  to have zero mean and unit variance, i.e.,

$\mathbb{E}[\bar{s}_u] = 0$  and  $\mathbb{E}[|\bar{s}_u[t]|^2] = 1$ . A symbol vector  $\bar{\mathbf{s}}[t] = [\bar{s}_1[t], \dots, \bar{s}_{N_u}[t]]^T \in \mathbb{Q}_M^{N_u}$ ,  $t \in \{1, \dots, N_c\}$  denotes the collection of the transmitted signals from  $N_u$  users at time  $t$ . I consider each user to adopt  $M$ -ary QAM constellation and thus, the number of possible symbol vectors  $\bar{\mathbf{s}}[t]$  becomes  $K = M^{N_u}$ . Assuming that the symbols from users are concurrently received and jointly processed at the BS, the received analog complex baseband signal vector at time  $t$  is represented as

$$\bar{\mathbf{r}}[t] = \sqrt{\rho} \bar{\mathbf{H}}^T \bar{\mathbf{s}}[t] + \bar{\mathbf{z}}[t], \quad (4.1)$$

where  $\bar{\mathbf{H}} \in \mathbb{C}^{N_u \times N_r}$  is the complex-valued channel matrix between the BS and  $N_u$  users, whose  $i$ th column vector, i.e.,  $\bar{\mathbf{h}}_i$ , indicates the channel vector defined between all user and the  $i$ th antenna element of the BS. The transmit power is denoted as  $\rho$ , and the additive white complex Gaussian noise vector  $\bar{\mathbf{z}}[t]$  follows  $\bar{\mathbf{z}}[t] \sim \mathcal{CN}(\mathbf{0}_{N_r}, N_0 \mathbf{I}_{N_r})$ . Here, I define the SNR as

$$\gamma = \rho/N_0. \quad (4.2)$$

Then, each real and imaginary component of the received signals in (4.1) is quantized with one-bit ADCs which only reveal the sign of the signals, i.e., either  $+1$  or  $-1$ . The quantized signal can be represented as

$$\bar{\mathbf{y}}[t] = \mathcal{Q}(\text{Re}\{\bar{\mathbf{r}}[t]\}) + j\mathcal{Q}(\text{Im}\{\bar{\mathbf{r}}[t]\}) \quad (4.3)$$

where  $\mathcal{Q}(a) = (-1)^{1\{a \leq 0\}} \in \{-1, +1\}$  is an element-wise one-bit quantizer which returns  $+1$  if the input is positive, or  $-1$  otherwise. The received signal

in the complex-vector expression  $\bar{\mathbf{r}}[t]$  can be rewritten in a real-valued vector representation as

$$\mathbf{r}[t] = \begin{bmatrix} \text{Re}\{\bar{\mathbf{r}}[t]\} \\ \text{Im}\{\bar{\mathbf{r}}[t]\} \end{bmatrix} = \sqrt{\rho}\mathbf{H}^T \mathbf{s}[t] + \mathbf{z}[t] \quad (4.4)$$

where

$$\mathbf{H}^T = \begin{bmatrix} \text{Re}\{\bar{\mathbf{H}}^T\} & -\text{Im}\{\bar{\mathbf{H}}^T\} \\ \text{Im}\{\bar{\mathbf{H}}^T\} & \text{Re}\{\bar{\mathbf{H}}^T\} \end{bmatrix}, \quad (4.5)$$

$$\mathbf{s}[t] = \begin{bmatrix} \text{Re}\{\bar{\mathbf{s}}[t]\} \\ \text{Im}\{\bar{\mathbf{s}}[t]\} \end{bmatrix}, \quad (4.6)$$

$$\mathbf{z}[t] = \begin{bmatrix} \text{Re}\{\bar{\mathbf{z}}[t]\} \\ \text{Im}\{\bar{\mathbf{z}}[t]\} \end{bmatrix}. \quad (4.7)$$

where  $\mathbf{z}[t] \sim \mathcal{N}(\mathbf{0}_{2N_r}, \frac{N_0}{2}\mathbf{I}_{2N_r})$ . Accordingly, I also rewrite the quantized signal in a real-vector form as

$$\mathbf{y}[t] = \mathcal{Q}(\mathbf{r}[t]) \quad (4.8)$$

$$= \mathcal{Q}(\sqrt{\rho}\mathbf{H}^T \mathbf{s}[t] + \mathbf{z}[t]), \quad (4.9)$$

which is composed of  $2N_r$  real-valued observations of either  $-1$  or  $+1$ . Throughout this chapter, I consider to have  $2N_r$  antennas to denote the real-valued ports for ease of notation, i.e., the  $i$ th antenna in the real-value representation corresponds to  $y_i[t]$ .

#### 4.2.2 One-Bit ML Detection with CSI

I first introduce the conventional one-bit ML detection with the full CSI. I define the index set of all possible symbol vectors as  $\mathcal{K} = \{1, \dots, K\}$  and use  $\mathbf{s}_k$  to denote the  $k$ th pilot symbol vector in a real-vector form. Let  $\mathbf{P}^{(\beta)} \in$

$[0, 1]^{K \times 2N_r}$  with  $\beta \in \{-1, +1\}$  denote the matrix of likelihood probabilities whose  $\mathbf{P}_{k,i}^{(\beta)}$  means the probability that the  $i$ th antenna component receives  $\beta$  when the users transmit the  $k$ th symbol vector  $\mathbf{s}_k$ . Assuming uncorrelated antennas, the likelihood probability of the one-bit quantized signal vector  $\mathbf{y}[t]$  for a given channel  $\mathbf{H}$  and transmit symbol vector  $\mathbf{s}_k$  is given as

$$\mathbb{P}(\mathbf{y}[t]|\mathbf{H}, \mathbf{s}_k) = \prod_{i=1}^{2N_r} \mathbf{P}_{k,i}^{(y_i[t])}. \quad (4.10)$$

I remark that the likelihood function for the  $i$ th antenna element of an observation  $y_i[t] \in \{-1, +1\}$  with the perfect CSI can be computed as

$$\mathbf{P}_{k,i}^{(y_i[t])} = \mathbb{P}(y_i[t]|\mathbf{h}_i, \mathbf{s}_k) \quad (4.11)$$

$$= \Phi(y_i[t]\psi_{k,i}), \quad (4.12)$$

where

$$\psi_{k,i} = \sqrt{\frac{\rho}{N_0/2}} \mathbf{h}_i^T \mathbf{s}_k \quad (4.13)$$

is the effective output of the  $i$ th antenna in real-value representation when transmitting the  $k$ th symbol vector, and  $\Phi(x) = \int_{-\infty}^x \frac{1}{\sqrt{2\pi}} e^{-\tau^2/2} d\tau$  is the cumulative distribution function of a standard Gaussian distribution. Based on (4.10), the one-bit ML detection rule is given as

$$k^*[t] = \arg \max_{k \in \mathcal{K}} \prod_{i=1}^{2N_r} \mathbf{P}_{k,i}^{(y_i[t])}. \quad (4.14)$$

The detected real-valued symbol vector is then defined as  $\hat{\mathbf{s}}[t] = \mathbf{s}_{k^*[t]}$  which can be mapped to  $\hat{\mathbf{s}}[t] \in \mathbb{Q}_M^{N_\nu}$  as detected QAM symbols by performing the reverse



operation of (4.6). Assuming an equal probability for each pilot symbol vector, (4.14) provides the optimal detection. I note that the ML detection in (4.14) requires full CSI for computing (4.11). The channel estimation, however, can be greatly burdensome in massive MIMO systems and much less accurate for receivers employing one-bit ADCs. In this regard, it is desirable to perform the optimal detection without requiring explicit channel estimation in one-bit massive MIMO systems.

### 4.3 Preliminary: Naive One-bit ML Detection without CSI

Now, I outline a direct learning-based one-bit ML detection strategy that does not require channel estimation. Although this approach still requires  $N_{\text{tr}}$  training sequences, the learning principle is greatly simpler than the one-bit channel estimation, thereby providing robust detection performance. Each pilot symbol vector  $\mathbf{s}_k \in \mathbb{Q}_M^{N_u}$  is transmitted  $N_{\text{tr}}$  times throughout the pilot transmission of length  $N_t$ . The BS aims to approximate the true likelihood probability  $\mathbf{P}_{k,i}^{(\beta)}$  by observing the frequency of  $y_i[t] = +1$  and  $y_i[t] = -1$  during the transmission as

$$\hat{\mathbf{P}}_{k,i}^{(\beta)} = \begin{cases} \hat{\mathbf{P}}_{k,i}^{(+1)} = \frac{1}{N_{\text{tr}}} \sum_{t=1}^{N_{\text{tr}}} \mathbb{1}\{y_i[(k-1)N_{\text{tr}} + t] = +1\} \\ \hat{\mathbf{P}}_{k,i}^{(-1)} = 1 - \hat{\mathbf{P}}_{k,i}^{(+1)} \end{cases} \quad (4.15)$$

where  $\beta \in \{+1, -1\}$ . The operation in (4.15) measures the number of +1's at the  $i$ th antenna element out of the  $N_{\text{tr}}$  observations triggered by  $\mathbf{s}_k$ . After learning the likelihood functions, the BS obtains the estimate of the likelihood

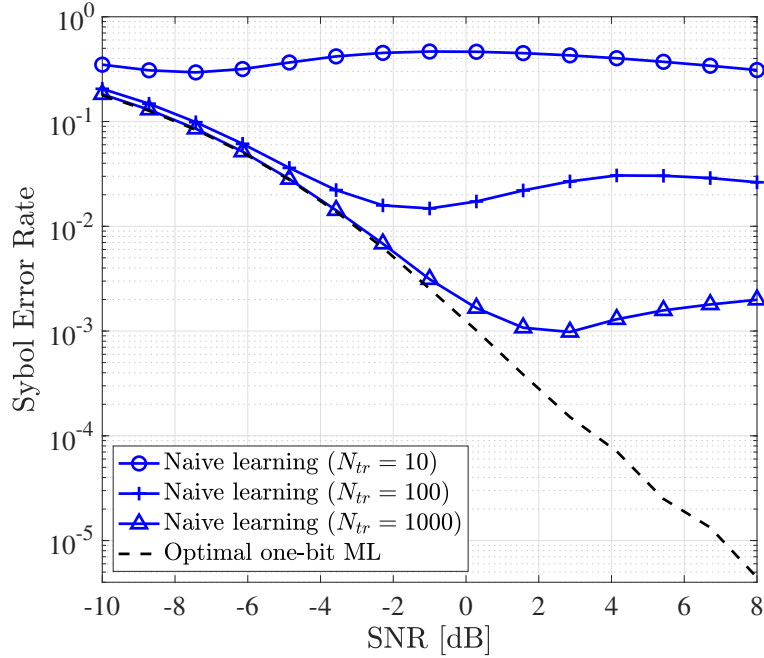


Figure 4.1: Symbol error rate simulation results of the optimal one-bit ML detection with full CSI against naive learning-based one-bit ML detection for  $N_r = 32$  receive antennas,  $N_u = 3$  users, 4-QAM, and  $N_{tr} \in \{10, 100, 1000\}$  pilot signals.

probability for a given data signal  $\mathbf{y}[t]$  as

$$\mathbb{P}(\mathbf{y}[t]|\mathbf{H}, \mathbf{s}_k) \approx \prod_{i=1}^{2N_r} \left( \hat{\mathbf{P}}_{k,i}^{(+1)} \mathbb{1}\{y_i[t] = +1\} + \hat{\mathbf{P}}_{k,i}^{(-1)} \mathbb{1}\{y_i[t] = -1\} \right), \quad (4.16)$$

and the receiver can perform the ML detection in (4.14) by searching the best index that maximizes (4.16) over the  $K$  possible symbol vectors.

Although such one-bit ML approaches can provide a near-optimal detection performance with simple function learning, they may suffer from crit-

ical performance degradation due to a limited amount of training as stated in the following remark:

**Remark 2** (Under-trained likelihood functions). At the high SNR, the  $N_{\text{tr}}$  quantized output of each antenna is repeatedly observed to be either all +1's or all -1's due to the low power of the aggregate noise. This phenomenon results in obtaining a number of zero-valued empirical likelihood functions in (4.15), e.g.,  $\hat{\mathbf{P}}_{k,i}^{(\beta)} = 0$  because the one-bit quantized observations at the high SNR regime become quasi-deterministic such that it is difficult to observe a change in the sign of the quantized output sequences during the  $N_{\text{tr}}$  transmissions of the symbol vector  $\mathbf{s}_k$ . Such a zero-valued likelihood function, called under-trained likelihood function, completely ruins the ML detection rule since the ML computation in (4.16) can be completely negated by any zero probability.

Fig. 4.1 shows the symbol error rates (SERs) of the optimal one-bit ML detection and the naive approach with the number of training samples  $N_{\text{tr}} \in \{10, 100, 1000\}$  for  $N_r = 32$  receive antennas,  $N_u = 3$  users and 4-QAM modulation with respect to the SNR. It is observed that although I increase the number of pilot signals, the naive approach starts to suffer at the medium to high SNR since the under-trained likelihood functions start to appear more frequently as the SNR increases. Therefore, such a critical drawback of the naive learning-based approach needs to be resolved to deploy the one-bit ADC systems in practice.

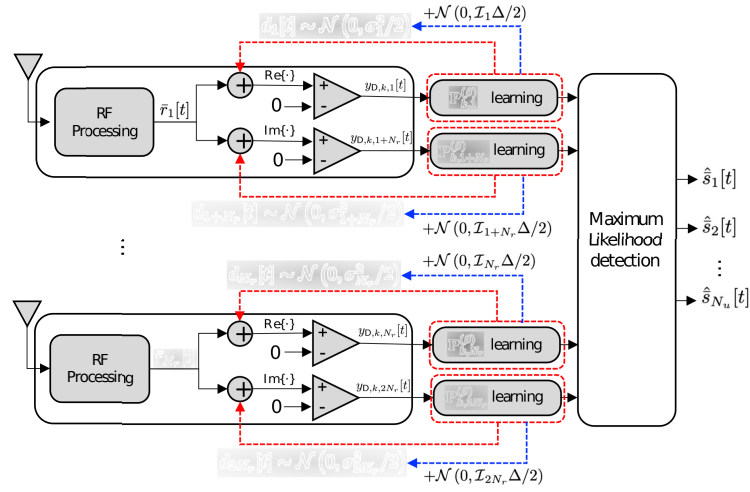


Figure 4.2: A receiver architecture for the pilot transmission phase with dithering signal added before quantization. Based on the feedback information, the variance of the dithering signal is updated.

#### 4.4 Adaptive Statistical Learning without CSI

In this section, I present an adaptive learning-based ML detection method for one-bit ADC systems in order to closely achieve the optimal CSI-aware ML detection performance without suffering the error floor of the naive learning approach observed in Fig. 4.1 and without requiring explicit estimation of channels. Being identical to the maximum a posteriori estimation, the ML estimation is optimal in minimizing the probability of detection error when all possible transmit symbols have an equal probability of being transmitted. Accordingly, the proposed method can achieve the detection performance close to optimal without explicit channel estimation.

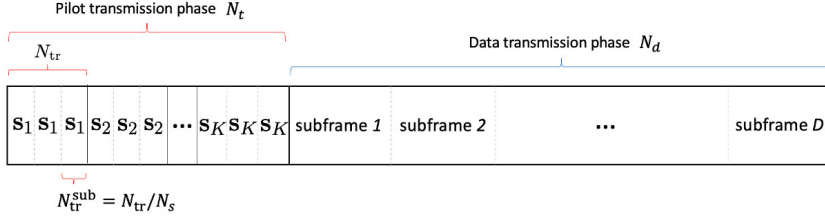


Figure 4.3: Communication data frame with a pilot transmission and a data transmission phases.

#### 4.4.1 Dithering-and-Learning

To resolve the problem of the under-trained likelihood functions, I propose the dither-and-learning method that can learn the likelihood functions with a reasonable training length  $N_{tr}$ . As shown in Fig. 4.2, the BS appends antenna-wise dithering signals  $d_i[t]$  to the analog baseband received signal  $r_i[t]$  during the training phase. After dithering, the quantization input for transmitted symbol  $\mathbf{s}_k$  in the real-vector form becomes

$$\mathbf{r}_{D,k}[t] = \mathbf{r}_k[t] + \mathbf{d}[t] \quad (4.17)$$

$$= \sqrt{\rho}\mathbf{H}\mathbf{s}_k + \mathbf{z}[t] + \mathbf{d}[t]. \quad (4.18)$$

I let  $\sigma_i^2/2$  denote the variance of the real-valued dithering signal at the  $i$ th antenna and consider  $\mathbf{d}[t] \sim \mathcal{N}(\mathbf{0}_{2N_r}, \mathbf{\Sigma})$  where  $\mathbf{\Sigma} = \text{diag}(\sigma_1^2/2, \dots, \sigma_{2N_r}^2/2)$ . The distribution of the dithering signal is controlled at the BS. The dithered and quantized signal associated with the  $k$ th symbol vector becomes

$$\mathbf{y}_{D,k}[t] = \mathcal{Q}(\sqrt{\rho}\mathbf{H}\mathbf{s}_k + \mathbf{z}[t] + \mathbf{d}[t]) \in \{+1, -1\}^{2N_r}. \quad (4.19)$$

As a next step, the BS computes the estimated likelihood function for the dithered signals  $\hat{\mathbf{P}}_{D,k,i}^{(\beta)}$  as in (4.15) for  $\beta \in \{+1, -1\}$ . Without loss of

generality, let us fix  $\beta = +1$  for ease of explanation. Then,  $\hat{\mathbf{P}}_{\mathbf{D},k,i}^{(+1)}$  offers an estimate of the actual likelihood functions as shown in (4.12) with increased noise power:

$$\hat{\mathbf{P}}_{\mathbf{D},k,i}^{(+1)} \approx \Phi \left( \sqrt{\frac{2\rho}{N_0 + \sigma_i^2}} \mathbf{h}_i^T \mathbf{s}_k \right). \quad (4.20)$$

Assuming  $N_0$  (equivalently, SNR) is known at the BS, the BS can find the estimate of  $\psi_{k,i}$  in (4.13) by leveraging (4.20). Such denoising is computed as

$$\hat{\psi}_{k,i} = \sqrt{1 + \frac{\sigma_i^2}{N_0}} \Phi^{-1} \left( \hat{\mathbf{P}}_{\mathbf{D},k,i}^{(+1)} \right) \quad (4.21)$$

Finally, the BS uses  $\hat{\psi}_{k,i}$  to approximate the true (non-dithered) likelihood function  $\mathbf{P}_{k,i}^{(+1)}$  as

$$\tilde{\mathbf{P}}_{k,i}^{(+1)} = \Phi \left( \hat{\psi}_{k,i} \right). \quad (4.22)$$

Since the likelihood function of the dithered signal  $\hat{\mathbf{P}}_{\mathbf{D},k,i}^{(+1)}$  in (4.20) is much less likely to have zero probability compared with that of the non-dithered case, the BS can learn the majority of the likelihood functions  $\tilde{\mathbf{P}}_{k,i}^{(+1)}$  with a reasonable training length. When I observe zero likelihood functions after the dither-and-learning process, I set a very small probability that is lower than any of the non-zero likelihood functions, i.e.,

$$\tilde{\mathbf{P}}_{k,i}^{(\beta)} = p_{\min}, \quad \forall i \in \mathcal{A}_k^0(\beta), \quad (4.23)$$

where  $p_{\min,k} < \min_{j \in \mathcal{A}_k^{\text{nz}}(\beta)} \tilde{\mathbf{P}}_{k,j}^{(\beta)}$ ,  $\forall \beta$ ,  $\mathcal{A}_k^0(\beta)$  indicates the index set of zero likelihood functions for  $\mathbf{s}_k$  and  $\beta$ , and  $\mathcal{A}_k^{\text{nz}}(\beta)$  is the index set of non-zero likelihood functions for  $\mathbf{s}_k$  and  $\beta$ .

For the proposed dither-and-learning method, intuitively, the power of dithering signals affects the learning performance as stated in Remark 3.

**Remark 3.** The level of dithering power is important as low dithering power continues to trigger under-trained likelihood functions, and high dithering power hinders recovering the symbol information, leading noise term dominant.

Based on Remark 3, I further propose an adaptive dithering power update method in the following section.

#### 4.4.2 Adaptive Dithering Power Update

Fixing dithering variance does not suitably adjust the dithering power, and this behavior can cause two fundamental problems: 1) when the dithering power is low and the SNR remains high, it is highly probable to have undesirably many under-trained likelihood functions and 2) for high dithering power, although the dither-and-learning procedure successfully prevents the under-trained likelihood functions, the estimate of the effective output in (4.21) cannot be accurate due to the large randomness of the dithering signals. In this respect, the BS has to properly determine dithering power considering the system environment. To this end, I empirically update the dithering power by leveraging feedback based on the behavior of received observations and propose the adaptive dither-and-learning (ADL) method that fits the dithering power into a suitable range.

As shown in Fig. 4.3, I first divide the  $N_{\text{tr}}$  signals of each pilot symbol  $\mathbf{s}_k$  into  $N_s$  disjoint sub-blocks in which each sub-block accommodates  $N_{\text{tr}}^{\text{sub}} = N_{\text{tr}}/N_s$  training samples where  $N_{\text{tr}}$  is assumed to be a multiple of  $N_s$ . Then, the  $n$ th dithered and quantized sub-block observed at the  $i$ th antenna when transmitting  $\mathbf{s}_k$  can be represented as

$$\begin{aligned} \tilde{\mathbf{y}}_{\text{D},k,i,n} = & \left\{ y_{\text{D},k,i}[(k-1)N_{\text{tr}} + (n-1)N_{\text{tr}}^{\text{sub}} + 1], \right. \\ & \left. \dots, y_{\text{D},k,i}[(k-1)N_{\text{tr}} + nN_{\text{tr}}^{\text{sub}}] \right\}^T \in \{+1, -1\}^{N_{\text{tr}}^{\text{sub}}}, \end{aligned} \quad (4.24)$$

where  $n \in \{1, \dots, N_s\}$  and  $y_{\text{D},k,i}[t]$  denotes the dithered observation at the  $i$ th antenna at time  $t$  for the  $k$ th pilot symbol vector  $\mathbf{s}_k$ . When the received training sequence is either  $\tilde{\mathbf{y}}_{\text{D},k,i,n} = +\mathbf{1}_{N_{\text{tr}}^{\text{sub}}}$  or  $\tilde{\mathbf{y}}_{\text{D},k,i,n} = -\mathbf{1}_{N_{\text{tr}}^{\text{sub}}}$  for antenna  $i$ , the dither power is regarded to be lower than the desirable dithering power for  $\mathbf{s}_k$  at antenna  $i$  in the current system. In such a case, I increase the dithering noise variance of the  $i$ th antenna for the next sub-block by  $\Delta$ , i.e.,

$$\sigma_i^2 \leftarrow \sigma_i^2 + \mathcal{J}_i \Delta, \quad (4.25)$$

where  $\mathcal{J}_i$  is the indicator function defined for the  $i$ th antenna, i.e.,  $\mathcal{J}_i = 1$  if  $\tilde{\mathbf{y}}_{\text{D},k,i,n} = +\mathbf{1}_{N_{\text{tr}}^{\text{sub}}}$  or  $\tilde{\mathbf{y}}_{\text{D},k,i,n} = -\mathbf{1}_{N_{\text{tr}}^{\text{sub}}}$ , and  $\mathcal{J}_i = 0$  otherwise. This allows that the subsequent training sequence is more likely to observe the sign change within  $N_{\text{tr}}^{\text{sub}}$  quantized outputs thanks to the increased perturbation.

Upon completing all sub-blocks, the likelihood probability of symbol vector  $k$  is determined by computing the mean of the likelihood probabilities for all  $N_s$  sub-blocks associated with symbol vector  $\mathbf{s}_k$ . Algorithm 2 summarizes the adaptive dithering-and-learning (ADL) process. I note that the fixed



---

**Algorithm 2:** Adaptive Dithering-and-Learning (ADL)

---

```

1 Initialize  $\tilde{\mathbf{P}}_{k,i}^{(+1)} = 0 \quad \forall k, i$ 
2 Fix the increment of the dithering variance,  $\Delta$ .
3 for  $k = 1$  to  $K$  do
4     Initialize  $\sigma_i^2 = \sigma^2$  and  $J_i = 0 \quad \forall i$ .
5     for  $n = 1$  to  $N_s$  do
6         for  $i = 1$  to  $2N_r$  do
7             Observe  $\tilde{\mathbf{y}}_{D,k,i,n}$  (4.24) during  $N_{tr}^{\text{sub}}$  slots
8             Compute  $\hat{\mathbf{P}}_{D,k,i}^{(\beta)}$  of  $\tilde{\mathbf{y}}_{D,k,i,n}$  using (4.15)
9             Compute  $\hat{\psi}_{k,i}$  in (4.21)
10             $\tilde{\mathbf{P}}_{k,i}^{(+1)} \leftarrow \tilde{\mathbf{P}}_{k,i}^{(+1)} + \frac{1}{N_s} \Phi(\hat{\psi}_{k,i})$ 
11             $J_i \leftarrow \mathbb{1}\{\tilde{\mathbf{y}}_{D,k,i,n} = +\mathbf{1}_{N_{tr}^{\text{sub}}}\} + \mathbb{1}\{\tilde{\mathbf{y}}_{D,k,i,n} = -\mathbf{1}_{N_{tr}^{\text{sub}}}\}$ 
12             $\sigma_i^2 \leftarrow \sigma_i^2 + J_i \Delta$ 
13        end
14    end
15 end
16 return  $\tilde{\mathbf{P}}^{(+1)}$  and  $\tilde{\mathbf{P}}^{(-1)} = \mathbf{1} - \tilde{\mathbf{P}}^{(+1)}$ .

```

---

dithering-and-learning method in Section 4.4.1 is the special case of the ADL method with  $N_s = 1$ . I also remark that the ADL method prevents not only the under-trained likelihood functions but also the undesirably large fluctuations of the received signals since the dithering power update is supervised by the BS to fit into the appropriate SNR region based on the observations.

#### 4.4.3 SNR Estimation

In spite of the properly managed dithering power, the computation of likelihood probabilities using the denoising process in (4.21) requires the perfect knowledge of the SNR  $\gamma$  or equivalently, the AWGN noise variance  $N_0$ .

In this work, I also perform the SNR estimation via offline supervised learning using the deep neural network as shown in Fig. 4.4. The offline training first collects training data points  $\{\mathbf{y}[j]; \gamma[j]\}$  where  $\mathbf{y}[j] \in \{+1, -1\}^{2N_r}$  is the  $j$ th one-bit quantized observations and  $\gamma[j]$  is the true SNR at time  $j$ . Once sufficient samples are collected, the BS selects a portion of the data points as training samples and performs the supervised offline learning with  $\mathbf{y}[j]$  as inputs and  $\gamma[j]$  as outputs to be estimated. Assuming that there exist  $L$  hidden layers, the estimated SNR is represented as the scalar output of the neural network expressed as

$$\hat{\gamma}[j] = \mathbf{w}_L^T \mathbf{a}_{L-1} + b_L, \quad (4.26)$$

where each intermediate vector is defined as  $\mathbf{a}_\ell = \phi(\mathbf{W}_\ell \mathbf{a}_{\ell-1} + \mathbf{b}_\ell)$  for  $\ell \in \{1, \dots, L-1\}$  with the initial point  $\mathbf{a}_0 = \mathbf{y}[j]$  when  $\phi(\cdot)$  is the element-wise activation function such as rectified linear unit or sigmoid functions. The deep neural network is updated by minimizing the estimation error, e.g.,  $(\gamma[j] - \hat{\gamma}[j])^2$ , and hence estimates the SNR by extracting meaningful information of the one-bit observations such as statistical pattern and the number of +1's or -1's.

## 4.5 Extension to Channel Coding

Even though the one-bit ML detection has attractive aspects, I are still confined to the uncoded hard-decision scenarios. Modern communication frameworks should be paired with channel coding that exhibits an impressive

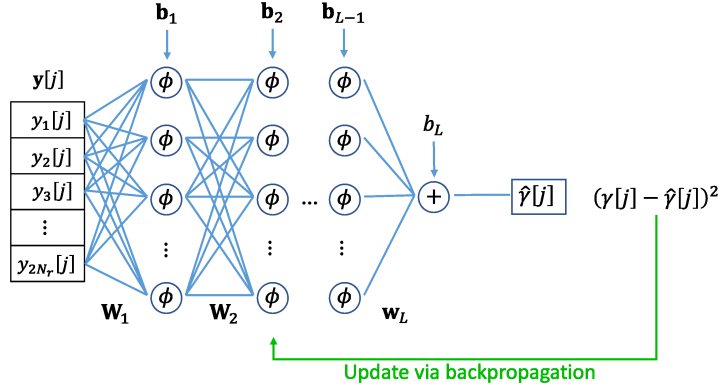


Figure 4.4: Illustration of the SNR offline training via deep neural networks.

gain and performance calibration; however, soft outputs are needed for the decoding perspective. In this section, I first introduce a frame structure to use channel coding, after that I describe how to generate soft metrics from the previously trained likelihood functions.

#### 4.5.1 Frame Structure

For a channel-coded communication framework, I first assume that a  $(\kappa, \eta)$  binary code with the code rate of  $\kappa/\eta$  is used throughout this chapter. At the beginning of the framework, each user  $u$  then generates uncoded binary messages of length  $\kappa$ , e.g.,  $\mathbf{m}_u \in \{0, 1\}^\kappa$ . Encoding with the pre-arranged channel coding scheme, I have the codeword for  $\mathbf{m}_u \in \{0, 1\}^\kappa$ , denoted as  $\mathbf{c}_u \in \{0, 1\}^\eta$ . As the last step, each user combines  $q (= \log_2 M)$  pieces of information together to map the binary bits into an  $M$ -ary QAM symbol, and then the transmitted symbol of the  $u$ th user at time slot  $t$  is represented as

$$\bar{s}_u[t] = f_M(\{c_u[(t-1)q+1], \dots, c_u[tq]\}) \quad (4.27)$$

where  $f_M : \{0, 1\}^q \rightarrow \mathbb{Q}_M$  is the constellation mapping function from  $q$  binary bits to  $M$ -ary QAM symbols and  $t \in \{1, \dots, \eta/q\}$  where  $\eta/q$  means the number of channel uses for a data subframe of each user by mapping  $q$  bits into a symbol. The overall communication structure is illustrated in Fig. 4.3. Each subframe of the data transmission phase is composed of the  $N_d^{\text{sub}} = \eta/q$  channel uses, and the data transmission phase consists of the  $D$  subframes, i.e.,  $N_d = DN_d^{\text{sub}}$ .

#### 4.5.2 Soft Metric

In Section 4.4, I produced a posteriori probabilities (APPs) utilizing the repeated transmissions with  $N_{\text{tr}}$  pilot signals per possible symbol vector and the ADL technique. Furthermore, from the calculated APPs which are the likelihood probabilities, I can compute a likelihood ratio for a given observation  $\mathbf{y}_d[t]$ .

I note that the one-bit observation at the  $t$ th time slot is held accountable for the LLR computation of the  $q$  positions of each user; as a result, the LLR needs to be calculated based on the user-wise and bit-wise operation. To this end, for the  $\ell$ th bit of the QAM symbol of user  $u$ , I separate the index set of all possible symbol vectors into two non-overlapping subgroups as follows:

$$\mathcal{S}_{\ell,b}^u = \{k \mid \bar{s}_{k,u} = f_M(\{c_1, \dots, c_q\}), c_\ell = b, k \in \mathcal{K}\}, \quad (4.28)$$

where  $b \in \{0, 1\}$  and  $\bar{s}_{k,u}$  denotes the  $u$ th element of  $\bar{\mathbf{s}}_k$  which is the QAM symbol of user  $u$ . Consequently, each subset in (4.28) is crafted to separate

$K$  indices into two disjoint sets in terms of the  $\ell$ th bit of the  $u$ th user's bit sequence that corresponds to  $\bar{s}_{k,u}$ . By the definition of (4.28), I have  $\mathcal{S}_{\ell,0}^u \cap \mathcal{S}_{\ell,1}^u = \emptyset$  and  $\mathcal{S}_{\ell,0}^u \cup \mathcal{S}_{\ell,1}^u = \mathcal{K}$  for any  $\ell$  and  $u$ . Note that the subsets are defined regardless of current observations and computed only once when the set of system parameters is configured.

Leveraging the two separated subgroups and the likelihood probabilities for the given observation, the corresponding LLR of the  $\ell$ th bit of the  $u$ th user at time  $t$  can be represented as

$$\begin{aligned}
\Lambda_{(t-1)q+\ell}^u(\mathbf{y}_d[t]|\mathbf{H}) &\stackrel{(a)}{=} \log \frac{\mathbb{P}(c_u[(t-1)q+\ell] = 0|\mathbf{y}_d[t], \mathbf{H})}{\mathbb{P}(c_u[(t-1)q+\ell] = 1|\mathbf{y}_d[t], \mathbf{H})} \\
&\stackrel{(b)}{=} \log \frac{\mathbb{P}(\mathbf{y}_d[t]|c_u[(t-1)q+\ell] = 0, \mathbf{H})}{\mathbb{P}(\mathbf{y}_d[t]|c_u[(t-1)q+\ell] = 1, \mathbf{H})} \\
&\stackrel{(c)}{=} \log \frac{\sum_{k \in \mathcal{S}_{\ell,0}^u} \mathbb{P}(\mathbf{y}_d[t]|\mathbf{s}_k, \mathbf{H})\mathbb{P}(\mathbf{s}_k)}{\sum_{k \in \mathcal{S}_{\ell,1}^u} \mathbb{P}(\mathbf{y}_d[t]|\mathbf{s}_k, \mathbf{H})\mathbb{P}(\mathbf{s}_k)} \\
&\stackrel{(d)}{=} \log \frac{\sum_{k \in \mathcal{S}_{\ell,0}^u} \prod_{i=1}^{2N_r} \mathbf{P}_{k,i}^{(y_i[t])}}{\sum_{k \in \mathcal{S}_{\ell,1}^u} \prod_{i=1}^{2N_r} \mathbf{P}_{k,i}^{(y_i[t])}}, \tag{4.29}
\end{aligned}$$

where  $\ell \in \{1, \dots, q\}$ ,  $t \in \{1, \dots, \eta/q\}$ , (a) is from the definition of LLR, (b) is from Bayes' rule with the equiprobability of  $\mathbf{y}_d$  and  $\mathbf{c}_u$ , (c) comes from the definition of sets defined in (4.28), and (d) is from the equiprobability of  $\mathbf{s}_k$  and the ML detection rule in (4.10). Finally, the collected LLRs associated with the  $u$ th user, i.e.,  $\{\Lambda_1^u, \dots, \Lambda_\eta^u\}$ , are conveyed to a channel decoder to recover the message  $\mathbf{m}_u \in \{0, 1\}^\kappa$ . Therefore, the ADL-based estimates of the likelihood functions can be successfully used for computing the LLR of the channel decoder.

## 4.6 Simulation Results

In this section, I evaluate the performance of the proposed learning-based method in terms of the number of under-trained likelihood functions, the symbol error probability (SER) for uncoded systems, and the frame error probability (FER) for coded systems. I consider Rayleigh fading model  $\bar{\mathbf{H}}$  whose each element follows  $\mathcal{CN}(0, 1)$ . I initialize the dithering variance as  $\sigma_i^2 = \rho/2$  and the increment as  $\Delta = \rho/3$  for all BS antennas in the ADL case.

### 4.6.1 Under-trained Likelihood Functions

Fig. 4.5 shows the average number of under-trained likelihood functions, i.e.,  $\hat{\mathbf{P}}_{k,i}^{(b)} = 0$ , out of  $2N_r$  antennas over the wide range of simulated SNR levels. For the learning-based detectors, I use  $N_{\text{tr}} = 45$  and compare the naive learning and the ADL methods with  $N_s \in \{1, 3, 5\}$ . Recall that the ADL method with  $N_s = 1$  reduces to the case that uses identical and fixed dithering power without adaptation. As the SNR increases, the number of under-trained likelihood functions for the non-dithering case rapidly approaches  $2N_r$ . For the ADL case with  $N_s = 1$ , i.e., fixed dithering power, however, the number of under-trained likelihood functions much slowly increases with the SNR and converges to around 20 thanks to the dithering effect. In addition, for the ADL method with non-trivial split factor, the number of under-trained likelihood functions increases only to 17 and 9 when  $N_s = 3$  and  $N_s = 5$ , respectively. Since the ADL method decides whether to increase the dithering noise depending on the realization of each sub-block, I can further optimize the learning procedure in

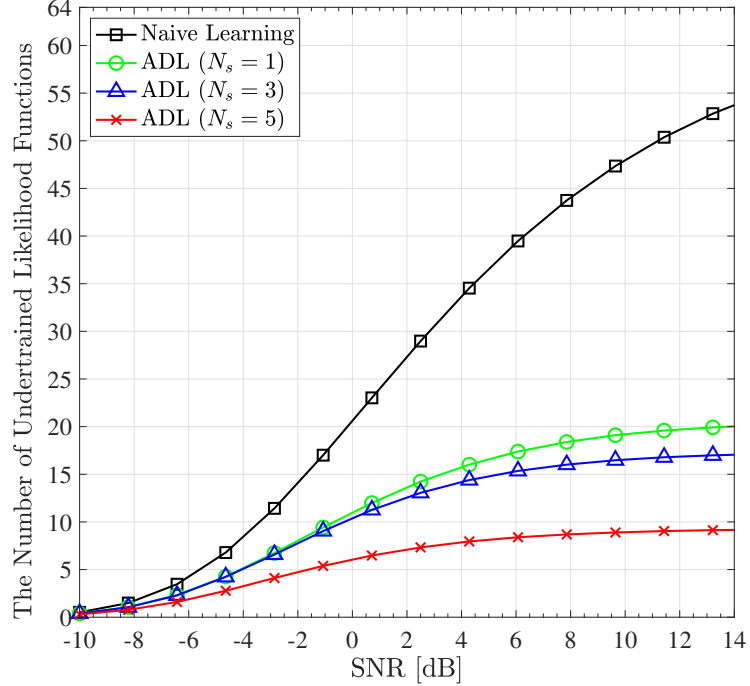


Figure 4.5: The number of under-trained likelihood functions among  $2N_r$  likelihood functions for  $N_u = 4$  users, 4-QAM,  $N_r = 32$  antennas, and  $N_{tr} = 45$  pilot signals with Rayleigh channels. The proposed adaptive dither-and-learning (ADL) method divides the training period into  $N_s \in \{1, 3, 5\}$  sub-blocks for the feedback-driven update of dithering power.

terms of the number of under-trained likelihood functions. If  $N_s$  is properly increased, each antenna is more likely to avoid zero-valued likelihood functions. As a result, with the adaptive dithering the proposed algorithm can estimate much more valid likelihood functions, thereby increasing the detection accuracy.

#### 4.6.2 Uncoded System: Symbol Error Rate

To evaluate the data detection performance of the proposed methods in the multiuser massive MIMO system, I compare the following detection methods:

1. Naive learning-based one-bit ML
2. ADL-based one-bit ML (proposed)
3. ADL-based one-bit ML with estimated SNR (proposed)
4. Minimum-Center-Distance (MCD) [41]
5. One-bit ZF with perfect CSI [21]
6. One-bit ML with perfect CSI (optimal one-bit detection)
7. One-bit ML with estimated CSI
8. Infinite-bit ML with perfect CSI (optimal detection)

I note that the learning-based methods: 1) Naive one-bit ML, 2) ADL one-bit ML, 3) ADL one-bit ML with estimated SNR, and 4) MCD, do not require explicit channel estimation; however, the other methods either assume perfect CSI or estimate CSI at the BS. The learning-based methods transmit  $N_{\text{tr}}$  pilot signals per each training symbol vector, which requires  $KN_{\text{tr}}$  pilot signals in total. Accordingly, I consider that the conventional one-bit ML detection with an estimated channel also uses  $KN_{\text{tr}}$  pilot signals to estimate the



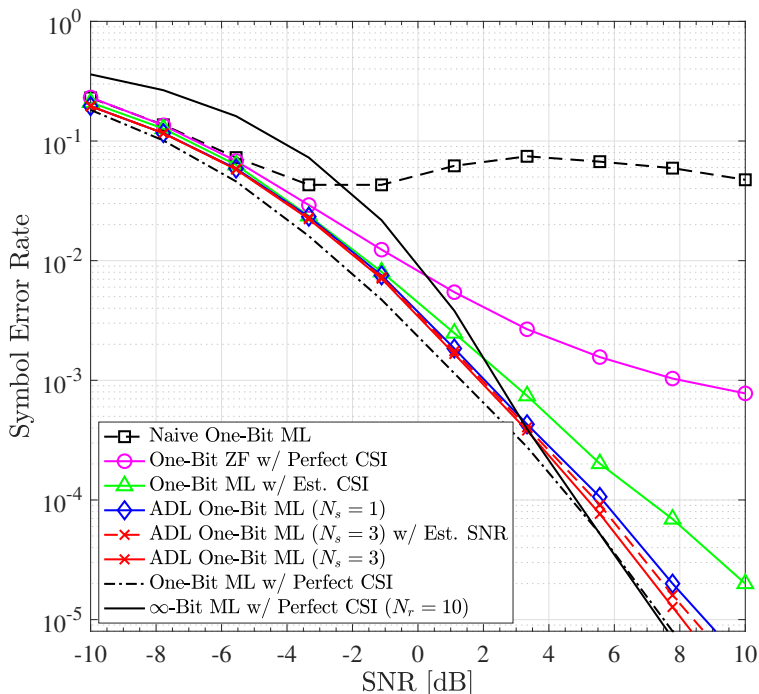


Figure 4.6: Symbol error rate results with  $N_u = 4$  users,  $N_r = 32$  BS antennas,  $N_{tr} = 45$  pilot signals, and 4-QAM constellation. The proposed adaptive dither-and-learning (ADL) uses  $N_s \in \{1, 3\}$  split factors.

channel. In the simulations, the one-bit channel estimation method developed in [22] is adopted to provide the estimated CSI. For readability of the curves, I compare MCD for the 16-QAM case shown in Fig. 4.8.

Fig. 4.6 presents the SER results for  $N_r = 32$  antennas,  $N_u = 4$  users,  $N_{tr} = 45$  pilot signals, and 4-QAM. As expected from Fig. 4.5, the naive-learning approach shows the catastrophic result from the medium to high SNR due to the large number of zero-valued likelihood functions. The one-bit ZF detection that applies the pseudo-inverse matrix of the perfectly-known channel

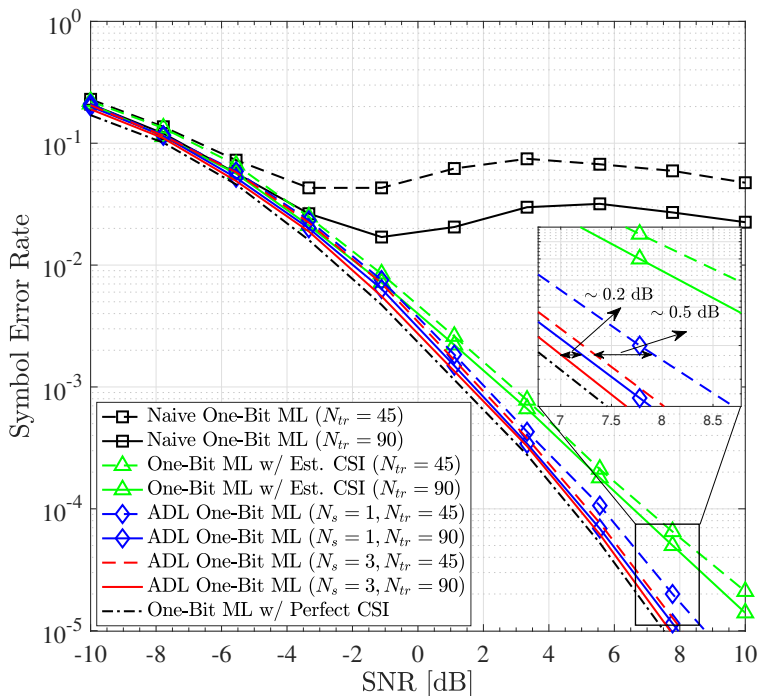


Figure 4.7: Symbol error rate results with  $N_u = 4$  users,  $N_r = 32$  BS antennas,  $N_{tr} \in \{45, 90\}$  pilot signals, and 4-QAM constellation. The proposed adaptive dither-and-learning (ADL) uses  $N_s \in \{1, 3\}$  split factors.

matrix onto the one-bit observations shows the large performance degradation with the error floor at the medium and high SNR regime. The one-bit ML detection with the one-bit estimated channels shows a larger deviation from the optimal one-bit ML detection with perfect CSI as the SNR increases due to the channel estimation error. Unlike the above benchmarks, the proposed ADL one-bit ML methods closely follow the SER performance curve of the optimal one-bit ML case by avoiding under-trained likelihood functions as shown in Fig. 4.5 and learning the likelihood functions with high accuracy. In addition,

the proposed ADL method with  $N_s = 3$  has around 1.0 dB gain over the ADL method with fixed dithering power, i.e.,  $N_s = 1$ , which demonstrates the gain of adaptive dithering based on the feedback. I can also notice that the performance gap between the ADL method with the perfect SNR and the ADL with the estimated SNR is marginal. This observation validates the fact that the offline supervised SNR learning can successfully capture the observation pattern to estimate the SNR required for the de-noising phase in the ADL method. Lastly, it is observed that the optimal one-bit ML detection with  $N_r = 32$  achieves similar target SER, e.g.,  $10^{-4}$  to  $10^{-5}$ , as the infinite-resolution ML detection with  $N_r = 10$  antennas. By deploying  $\sim 3\times$  more antennas with the simple one-bit ADCs, it is possible to compensate for the severe non-linearity loss caused by one-bit ADCs and to achieve higher detection performance than the infinite-bit ADC system in the low to medium SNR regime.

Fig. 4.7 shows the SER performance of the one-bit ML algorithms for different training length,  $N_{\text{tr}} \in \{45, 90\}$  with  $N_r = 32$  BS antennas,  $N_u = 4$  users, and 4-QAM. I first observe that both the naive learning-based one-bit ML and the conventional one-bit ML with the estimated channel still show the noticeable performance degradation from the proposed methods for both the short and long training lengths,  $N_{\text{tr}} \in \{45, 90\}$ . This implies that to achieve the optimal one-bit ML performance, it is necessary to use a great number of training symbols for the naive learning-based one-bit ML and the conventional one-bit ML with estimated channels. In contrast, the proposed ADL-based one-bit ML detection offers robust performance in terms of training

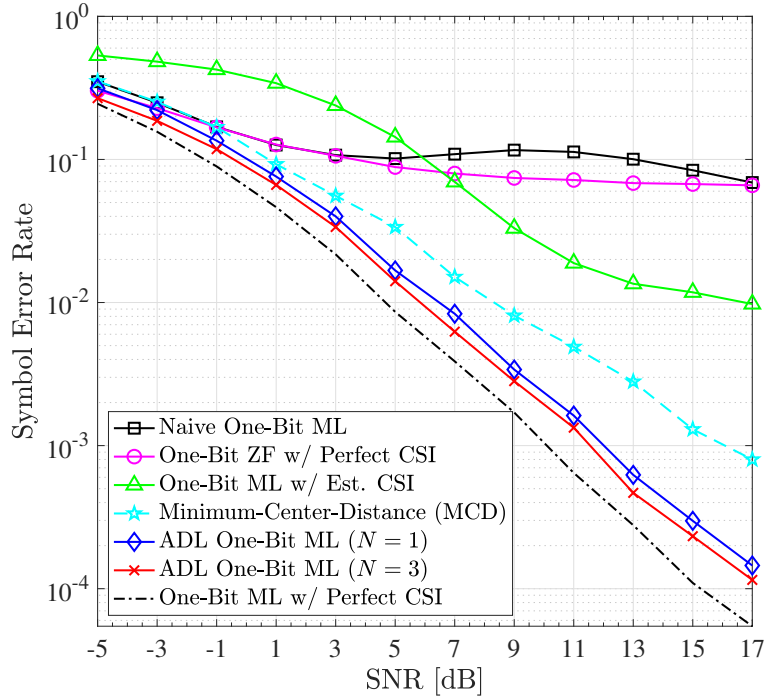


Figure 4.8: Symbol error rate results with  $N_u = 3$  users,  $N_r = 64$  BS antennas,  $N_{tr} = 45$  pilot signals, and 16-QAM constellation. The proposed adaptive dither-and-learning (ADL) method divides the training period into  $N_s \in \{1, 3\}$  sub-blocks.

length. In particular, the SER improvement of increasing  $N_s = 1$  to  $N_s = 3$  for the ADL method with  $N_{tr} = 90$  is about 0.2 dB which is small compared with that for the ADL method with  $N_{tr} = 45$ . Therefore, I can claim that the proposed ADL method is more beneficial for the system with the limited amount of pilot signals, and using proper adaptation stages further improves the detection performance. I can also find out that the ADL case with  $N_s = 3$  and  $N_{tr} = 45$  achieves almost the same performance as the case  $N_s = 1$  and

$N_{\text{tr}} = 90$ , which emphasizes that adaptive learning can effectively reduce the amount of training sequences.

Fig. 4.8 shows the SER performance curves for  $N_r = 64$  BS antennas,  $N_u = 3$  users, and 16-QAM. I use  $N_{\text{tr}} = 45$  training length for the learning-based approaches. It is remarkable that the proposed ADL method still offers a robust detection performance whereas the one-bit ZF with perfect CSI and the one-bit ML with the estimated CSI present largely degraded detection performance. Although the MCD method shows the lower SER than the other benchmarks, the performance gap from the proposed method is not trivial and increases with the SNR. In this regard, the simulation results demonstrate that the proposed method outperforms the state-of-the-art one-bit detection methods, is more robust to communication environments, and requires shorter training sequences.

#### 4.6.3 Coded System: Frame Error Rate

I consider the MIMO system with  $N_r = 32$ ,  $N_u = 4$ , and 4-QAM. As a sophisticated channel coding, I adopt a rate-1/2 polar code of length 128, i.e.,  $(\kappa, \eta) = (64, 128)$  and a list decoding with list size 8 is used for the decoding method of the polar code. In the coded system, I also extend the naive learning-based one-bit ML detection to the coded system and compare the following methods:

1. Naive learning-based one-bit ML

2. ADL-based one-bit ML (proposed)
3. One-bit successive cancellation soft-output (OSS) [14]

For the ADL methods, I allocate  $N_{\text{tr}} = 45$  pilot signals to each symbol vector. Unlike the learning-based methods, the OSS detector assumes perfect CSI to compute LLRs. Accordingly, it can be regarded as an FER lower bound, and I include it for providing the performance guideline. Recall that to use state-of-the-art channel codes, I calculate LLRs using the likelihood probabilities derived by each method.

Fig. 4.9 illustrates the frame error rate (FER) of the channel-coded systems. The naive learning one-bit detection no longer experiences the tragic reverse trend shown in the uncoded systems; however, the performance gap from the proposed method grows up as SNR increases. In addition, the FER of the ADL method with  $N_s = 3$  is placed between that of the OSS detector and the ADL method with  $N_s = 1$ , thereby showing the advantage over the ADL with fixed dithering power. Again, the improvement achieved by the ADL method with  $N_s = 3$  is because the ADL method can accurately learn the likelihood probabilities by avoiding zero-valued likelihood functions even with the limited amount of training sequences. In summary, although the performance of the naive learning-based approach is devastated by the under-trained probabilities in the uncoded system, the likelihood probability in (4.16) is still capable of being computed with the under-trained likelihood functions for the LLR defined in (4.29) for the coded systems. Regarding the probability

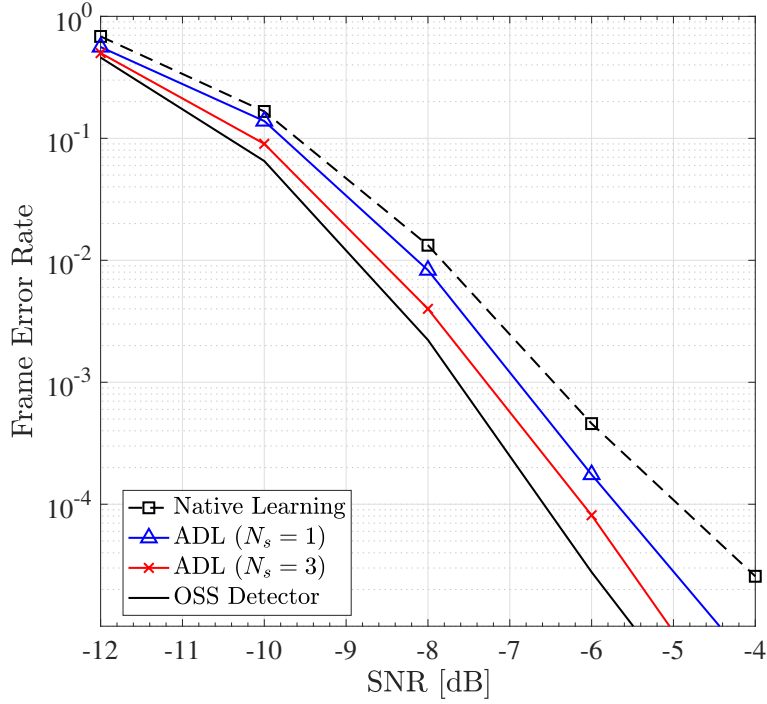


Figure 4.9: Frame error rate results for  $N_u = 4$  users,  $N_r = 32$  BS antennas,  $N_{tr} = 45$ , 4-QAM constellation, and a polar code of rate  $1/2$  where  $(\kappa, \eta) = (64, 128)$ . The proposed adaptive dither-and-learning (ADL) method learns the likelihood probability with split factor  $N_s \in \{1, 3\}$ . The one-bit successive-cancellation soft-output (OSS) detector is valid in case of perfect CSI.

learning accuracy, however, the proposed ADL method can perform better than the naive learning approach, thereby increasing the performance gap with the SNR.

## 4.7 Conclusion

In this chapter, I proposed the statistical learning-based ML detection method for uplink massive MIMO communication systems with one-bit ADCs. Since the performance of learning-based one-bit detection approaches can be severely degraded when the number of training samples is insufficient, the proposed method handled such challenges by injecting dithering noise to facilitate the acquisition of statistical patterns. Without requiring explicit channel knowledge, the dithering-and-learning method performed one-bit ML detection through learning likelihood functions at each antenna. The proposed method was more robust to the number of training symbols because the adaptive randomness triggers moderate fluctuation in the change of signs of the training sequence, thereby successfully extracting the statistical pattern of one-bit quantized signals. I further adapted dithering power to fit the BS into the appropriate SNR region in accordance with observations. In addition, deep neural network-based SNR estimation for denoising and extension to channel-coded systems were also proposed for more practical scenarios. Simulation results validated the detection performance of the proposed method. Therefore, the proposed method can be a potential low-power and low-complexity multiuser communication solution for 6G applications.



## Chapter 5

# Joint Hybrid Beamforming and Power Control Using Deep Reinforcement Learning

In this chapter<sup>1</sup>, I investigate a deep reinforcement learning (DRL)-based solution for joint hybrid beamforming (HB) and power control problems in case that multiple base stations (BSs) equipped with a massive number of antennas communicate with multiple user devices in the uplink millimeter wave band. Unlike the traditional digital-only method, the HB necessitates both digital and analog beamformers. Analog beamformers employ discrete phase shifters to project the high-dimensional observation onto the low-dimensional vector and scale down the number of radio frequency (RF) chains; however, the inclusion of analog beamformers results in non-convexity which makes the problem difficult to solve via existing efficient algorithms. In multicell uplink communication systems, I aim to jointly design the HB at each base station and transmit power control of the associated users while ensuring that the received signal-to-interference-and-noise ratio (SINR) constraints. Considering the use of the DRL-based approach and the primal problem, I formulate the

---

<sup>1</sup>This chapter is based on the following paper: Y. Cho, C. Dick, and B. L. Evans, “Joint Hybrid Beamforming and Power Control for Multicell Millimeter Wave Massive MIMO Systems Using Deep Reinforcement Learning,” to be submitted to *IEEE Access*, 2023. This work was supervised by Dr. Chris Dick and Prof. Brian L. Evans.

fundamentals to enable reinforcement learning (RL). To synthesize the mixture of discrete and continuous entries, I use deep deterministic policy gradient (DDPG) RL whose actor network outputs a valid action that can form a one-to-one mapping to the design factors. In particular, to unlock the full potential of phase shifters that constitute the analog beamformer, I aim to individually control each phase shifter by introducing an intermediate vector and applying a differentiable argmax function which estimates the phase angle index. Via simulation results, I evaluate the proposed method in terms of the achieved SINR.

## 5.1 Introduction

With growing demand for higher data rate, millimeter wave (mmWave) systems have been extensively researched for many years as an essential facilitator of modern and future wireless communication systems. A mmWave spectrum extends up to 300 GHz to provide a remarkable increment in both data rates and capacity [4, 91]. Due to the small wavelength of mmWave signals and small antenna spacing, the mmWave system allows the installation of more antennas per unit area. Therefore, massive MIMO systems that achieve significant gain in spectral efficiency and capacity [56] have been naturally coupled with mmWave systems. However, increasing the number of antennas and RF chains results in a prohibitively huge power consumption, which becomes the main bottleneck of the realistic deployment. Unlike the conventional digital-only beamforming that connects a separate RF chain per each antenna

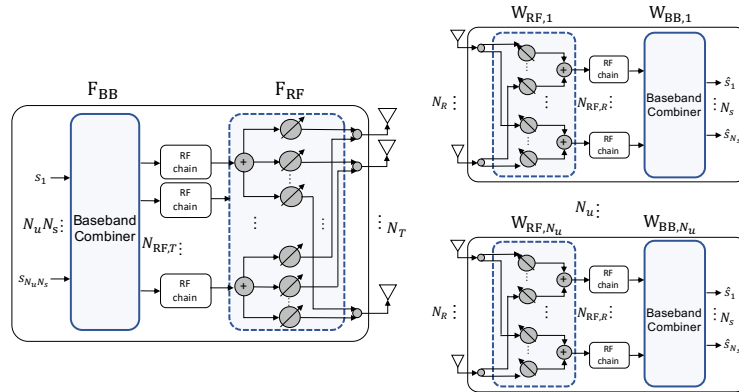


Figure 5.1: Illustration of hybrid beamforming architecture in a cell.

and hence employs a plethora of power-hungry RF chains, the hybrid beamforming architecture combines high-dimensional analog RF beamforming and low-dimensional digital beamforming to reduce the number of power-hungry RF chains (see Fig. 5.1).

## 5.2 Prior Works

Many literatures were published to analyze and solve the hybrid beamforming architecture. Leveraging the sparse nature of mmWave channels, the hybrid architecture design was interpreted as a sparsity-constrained matrix reconstruction and solved in an alternating fashion [26]. The sparse nature of the mmWave channel was also used in [2] to develop a low-complexity yet efficient hybrid precoding using a small training and feedback overhead. For MIMO uplink communications, the authors in [49] developed the Gram-Schmidt-based analog combiner while still using the minimum mean square error (MMSE) beamforming for the digital combiner. The authors in [86] showed that the

hybrid beamforming architecture can achieve the same performance as the conventional digital-only beamforming when the number of RF chains is sufficient. A near optimal analog combining solution in hybrid MIMO systems with low-resolution data converters was developed by introducing the two-stage analog combiner that performs channel gain aggregation and spreading functions separately [19]. For a wideband multiuser MIMO systems, the authors in [12] developed the hybrid transmit precoding by leveraging the long-term channel covariance matrix and the angle-of-departure information.

Recently, the disruptive role of machine learning techniques has been seen on the design of the hybrid beamforming architecture or power control. [34, 47, 50, 59, 82, 112] Deep Q-Network (DQN)-based deep reinforcement learning (DRL) frameworks have been used in designing the analog beamformer of the hybrid beamforming architecture by selecting codebook index [59, 82]. The authors in [50] proposed a novel neural network that jointly performs the channel compressive sensing and the prediction of analog beams. For the 2-tier beam search, supervised learning was utilized in designing a probing codebook with wide beams to adapt to a particular environment [34]. Relying only on receive power measurements and using Deep Deterministic Policy Gradient (DDPG) [54], the authors in [112] suggested how to optimize the beam codebooks to adapt to current communication layout. However, these works are limited to the analog-only beamforming and the codebook-based grid-of-beams (GoB) beamforming. Using the spatial features in channel gain, the authors in [47] developed a frame work based on convolutional neural network

to learn the autonomous power control scheme.

In this work, I investigate joint hybrid beamforming and power control problems in multicell multiuser networks with BSs equipped with a large number of antenna arrays. Accordingly, the non-negligible inter-cell interference needs to be taken into account as modern cellular systems operate on the interference-limited regime [15]. Unlike other approaches that optimize the digital and analog beamformers in an alternating manner, this approach jointly design the two beamformers. Instead of using a GoB-based method, this approach individually control each phase shifter, i.e., non-grid-of-beams (NGoB), to unlock the full potential of phase shifters. Considering the design factors, I present the fine-tuned reward function that aims to satisfy target SINR. Numerical results show that the proposed approach can satisfy a pre-determined target SINR.

### 5.3 Preliminaries

I consider multi-cell MIMO uplink networks with  $N_c$  cells where each BS in the cell center is equipped with  $N_r$  receive antennas and  $BS_c$  denotes the BS in the  $c$ th cell. Each BS also employs  $N_{\text{RF}}$  RF chains, each of which is connected to  $N_r$  receive antennas via fully-connected analog combiner. There exist  $N_u$  single-antenna user devices per cell, which communicate with the dedicated BS, i.e., users in cell  $c$  are served by  $BS_c$ .

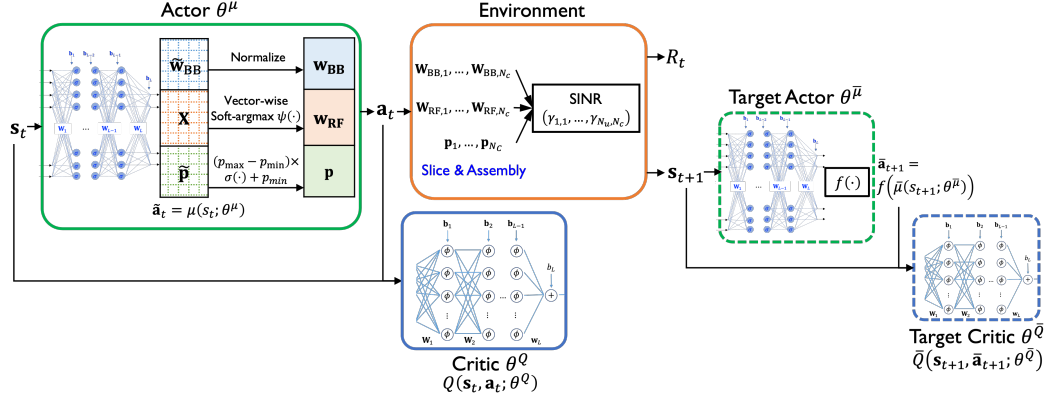


Figure 5.2: Illustration of deep reinforcement learning frame work via deep deterministic policy gradient approach.

### 5.3.1 Signal Model

The transmit power  $p_{u,c}$  and the information source  $s_{u,c}$  are assigned to the  $u$ th user device in cell  $c$ , thereby transmitting signal  $\sqrt{p_{u,c}}s_{u,c}$  over a wireless channel. The uplink wireless channel vector propagated from user  $u$  in cell  $\bar{c}$  to  $BS_c$  is represented as  $\mathbf{h}_{c,\bar{c},u} \in \mathbb{C}^{N_r}$ . Then, the received signal at  $BS_c$  is written as

$$\mathbf{r}_c = \mathbf{H}_{c,c} \mathbf{P}_c^{1/2} \mathbf{s}_c + \sum_{\substack{c=1 \\ \bar{c} \neq c}}^{N_c} \mathbf{H}_{c,\bar{c}} \mathbf{P}_{\bar{c}}^{1/2} \mathbf{s}_{\bar{c}} + \mathbf{n}_c \quad (5.1)$$

where  $\mathbf{H}_{c,\bar{c}} = [\mathbf{h}_{c,\bar{c},1}, \dots, \mathbf{h}_{c,\bar{c},N_u}] \in \mathbb{C}^{N_r \times N_u}$  is the complex-valued channel matrix between  $BS_c$  and users in cell  $\bar{c}$ ,  $\mathbf{s}_c = [s_{c,1}, \dots, s_{c,N_u}]^T \in \mathbb{C}^{N_u}$  is the dedicated symbol vector of the  $N_u$  users in cell  $c$ ,  $\mathbf{P}_c = \text{diag}(p_{c,1}, \dots, p_{c,N_u})$  is the the transmit power matrix of the users in cell  $c$ , and  $\mathbf{n}_c \in \mathbb{C}^{N_r}$  is the additive white Gaussian noise (AWGN) vector at  $BS_c$ . I assume that each user device needs to satisfy the minimum power  $p_{\min}$  and maximum power  $p_{\max}$

constraints, i.e.,  $p_{u,c} \in [p_{\min}, p_{\max}]$ . Throughout this chapter, I consider a normalized variance for AWGN without loss of generality, i.e.,  $\mathbf{n}_c \sim \mathcal{CN}(\mathbf{0}_{N_r}, \mathbf{I}_{N_r})$ . I further consider that  $\mathbf{s}_c$  is uncorrelated and has a zero mean and unit variance, i.e.,  $\mathbf{s}_c \sim \mathcal{CN}(\mathbf{0}_{N_u}, \mathbf{I}_{N_u})$ .

I consider the deployment of the hybrid beamforming architecture at  $\text{BS}_c$  whose digital beamformer and analog beamformer are denoted as  $\mathbf{W}_{\text{BB},c}$  and  $\mathbf{W}_{\text{RF},c}$ , respectively. Unlike the conventional digital-only beamforming that connects a separate RF chain per each antenna and hence employs a plethora of RF chains, the hybrid beamforming architecture combines high-dimensional analog RF beamforming and low-dimensional digital beamforming to reduce the number of RF chains. To produce high beamforming gain and immunize against large free-space pathloss, the analog beamformer  $\mathbf{W}_{\text{RF},c} \in \mathbb{P}^{N_{\text{RF}} \times N_r}$  manipulates directional propagation paths via unit-modulus phase shifters, where  $\mathbb{P} = \{e^{j\pi\phi} | \phi \in \{-1, -1 + \frac{2}{M}, \dots, +1 - \frac{2}{M}\}\}$  denotes the set of feasible phase shifters with  $M$  possible discrete phase angles. The analog beamformer comprises passive microwave devices used to change the phase angle of an RF signal. The analog beamformer projects the high-dimensional antenna ports into the low-dimensional logical RF ports to directly scale down the number of RF chains. Afterwards, the digital beamformer  $\mathbf{W}_{\text{BB},c} \in \mathbb{C}^{N_u \times N_{\text{RF}}}$  performs multi-stream baseband processing with low-dimensional input. Therefore, the combined signal at  $\text{BS}_c$  is processed as

$$\mathbf{y}_c = \mathbf{W}_{\text{BB},c}^H \mathbf{W}_{\text{RF},c}^H \mathbf{r}_c. \quad (5.2)$$

By defining the hybrid beamforming vector associated with user  $u$  in cell  $c$  as  $\mathbf{w}_{u,c} = \mathbf{W}_{\text{RF}} [\mathbf{W}_{\text{BB},c}]_u$ , the uplink SINR of user  $u$  in cell  $c$  from  $\mathbf{y}_c$  is computed as

$$\gamma_{u,c} = \frac{p_{u,c} |\mathbf{w}_{u,c}^H \mathbf{h}_{c,c,u}|^2}{\sum_{(\bar{u}, \bar{c}) \neq (c,u)}^{(N_c, N_u)} p_{\bar{c}, \bar{u}} |\mathbf{w}_{u,c}^H \mathbf{h}_{c,\bar{c}, \bar{u}}|^2 + \|\mathbf{w}_{u,c}\|^2}. \quad (5.3)$$

I note that the digital combiners, the analog combiners, and transmission powers are complicatedly intertwined in  $\gamma_{u,c}$ . Based on the design factors, the primary problem can be formulated as

$$\mathcal{P}_5 1 : \min_{\mathbf{W}_{\text{RF},c}, \mathbf{W}_{\text{BB},c}, \mathbf{p}_c \forall c} \sum_{u,c} p_{u,c} \quad (5.4)$$

$$\text{subject to } \gamma_{u,c} \geq \bar{\gamma} \quad (5.5)$$

$$\mathbf{W}_{\text{BB},c} \in \mathbb{C}^{N_{\text{RF}} \times N_u} \quad \forall c \quad (5.6)$$

$$\mathbf{W}_{\text{RF},c} \in \mathbb{P}^{N_r \times N_{\text{RF}}} \quad \forall c \quad (5.7)$$

$$\mathbf{p}_c \in [p_{\min}, p_{\max}]^{N_u} \quad \forall c, \quad (5.8)$$

where  $\bar{\gamma}$  is the target SINR requirement for all users. The primal problem aims to satisfy the target SINR for all users while consuming the minimum total transmit power. The analog and digital beamformers need to be jointly optimized to maximize communication performance metrics. However, because of the unit-modulus and discreteness constraints in (5.7), the entire system is neither a convex nor a concave function [32].

### 5.3.2 Channel Model

I adopt a geometric channel model whose channel delay spread is  $L$ . Noting that  $L$  is typically small since mmWave signals have high path loss



and less reflections to the surrounding environment [32], the mmWave channel propagated from user  $u$  in cell  $\bar{c}$  to  $\text{BS}_c$  is expressed as

$$\mathbf{h}_{c,\bar{c},u} = \sqrt{\gamma_{c,\bar{c},u}} \sum_{\ell=1}^L \alpha_{c,\bar{c},u}(\ell) \mathbf{u}(\phi_{c,\bar{c},u}(\ell), N_r), \quad (5.9)$$

where  $\gamma_{c,\bar{c},u}$  denotes the large-scale fading gain that counts propagation attenuation, shadowing, and noise figure between  $\text{BS}_c$  and the  $u$ th user in the  $\bar{c}$ th cell; therefore, the mean of  $\gamma_{c,\bar{c},u}$  tends to be smaller when  $c \neq \bar{c}$  compared to the case of  $c = \bar{c}$ .

The  $\ell$ th path between  $\text{BS}_c$  and the  $u$ th user in cell  $\bar{c}$  is synthesized by  $\phi_{c,\bar{c},u}(\ell) \in [-\frac{\pi}{2}, \frac{\pi}{2}]$  which is the azimuth angle of arrival (AoA) and  $\alpha_{c,\bar{c},u}(\ell) \sim \mathcal{CN}(0, 1)$  that corresponds to the complex path gain.

Parametrized by an azimuth angle  $\phi$ ,  $\mathbf{u}(\phi, N)$  is the ULA which is the collection of  $N$  evenly spaced phase shifts defined as

$$\mathbf{u}(\phi, N) = \frac{1}{\sqrt{N}} \left[ 1, e^{-j\pi \frac{2d}{\lambda} \sin \phi}, \dots, e^{-j\pi(N-1) \frac{2d}{\lambda} \sin \phi} \right], \quad (5.10)$$

where  $\lambda$  denotes the signal wavelength and  $d$  is the antenna spacing.

### 5.3.3 Deep Reinforcement Learning

I consider a DRL framework that allows a DRL agent to learn in an interactive yet unknown environment by using experiences and feedback without any labeled data. The sequential decisions and interactions in the reinforcement learning approach are described by the crucial components [90] defined as follows:

- *State*: A state  $s_t$  is the representative of the current situation of the given task at time step  $t$ .
- *Action*: An action  $a_t$  is what the DRL agent decides to perform at time step  $t$  after observing the state  $s_t$ .
- *Policy*: A policy  $\mu(\cdot) : s_t \mapsto a_t$  is either stochastic or deterministic mapping that consists of the valid actions that the DRL agent is required to take for every possible state to tell which action to take from each state.
- *Reward*: A reward  $R_t$  is feedback from the environment when the agent takes an action for a given state at time step  $t$ . The DRL agent does not have direct control over the reward, however, can choose the best action expected to maximize the reward at its best knowledge.
- *Return*: A return at time step  $t$  is the sum of the discounted rewards from the current state defined as  $G_t = \sum_{i=0}^{\infty} \mu^i R_{t+i}$  where  $\mu \in [0, 1]$  is the discount factor.
- *Action value function*: An action value function  $Q(s, a)$  is the expected return from current state by taking specific action. One of the key goals of DRL is to approximate  $G_t$  using a  $Q$ -function.

At each time step  $t$ , the agent interacting with the environment observes a state  $s_t$ , selects an action  $a_t$  from the policy, receives an immediate reward,  $R_t$ , and advances toward a next state  $s_{t+1}$ .

## 5.4 Hybrid Beamforming and Power Control via Reinforcement Learning: Action Space

Based on the primary problem and the fundamental components of the hybrid beamforming architecture, a valid action can be defined as the concatenated vector that can make the one-to-one mapping to the digital beamformers, the analog beamformers, and transmission powers across all cells. In this section, I explain how each component is designed via RL and then combine all things together to create a valid action.

### 5.4.1 Digital Beamformer

The complex-valued digital beamformer can be decomposed into real and imaginary parts, i.e.,  $\mathbf{W}_{\text{BB},c} = \text{Re}(\mathbf{W}_{\text{BB},c}) + j\text{Im}(\mathbf{W}_{\text{BB},c})$ , so that an action contains  $2N_c$  real-valued vectorized matrices  $\text{vec}(\text{Re}(\mathbf{W}_{\text{BB},c}))$  and  $\text{vec}(\text{Im}(\mathbf{W}_{\text{BB},c}))$  for all  $c \in \{1, \dots, N_c\}$ . Therefore, I can combine the decomposed digital beamformers from all  $N_c$  BSs as

$$\tilde{\mathbf{w}}_{\text{BB}} = \text{vec} \left( \left[ \begin{array}{l} \text{vec}(\text{Re}(\mathbf{W}_{\text{BB},1})), \text{vec}(\text{Im}(\mathbf{W}_{\text{BB},1})), \\ \dots, \text{vec}(\text{Re}(\mathbf{W}_{\text{BB},N_c})), \text{vec}(\text{Im}(\mathbf{W}_{\text{BB},N_c})) \end{array} \right] \right). \quad (5.11)$$

After that,  $\tilde{\mathbf{w}}_{\text{BB}}$  is normalized to  $\mathbf{w}_{\text{BB}}$  in order to achieve a better convergence.

### 5.4.2 Analog Beamformer

Taking into account that each phase shifter employs one of  $M$  distinct phases that can be picked evenly from  $[-\pi, +\pi)$ ,  $\text{BS}_c$  is equipped with the

grid-free analog beamformer constructed as

$$\mathbf{W}_{\text{RF},c} = e^{j\pi\Phi_c} \quad (5.12)$$

where  $\Phi_c$  is the NGoB matrix of phase angles at the  $\text{BS}_c$  defined as

$$\Phi_c = \begin{pmatrix} \phi_{1,1,c} & \cdots & \phi_{1,N_{\text{RF}},c} \\ \vdots & \ddots & \vdots \\ \phi_{N_r,1,c} & \cdots & \phi_{N_r,N_{\text{RF}},c} \end{pmatrix}, \quad (5.13)$$

where  $\phi_{i,j,c} \in \{-1, -1 + \frac{2}{M}, \dots, +1 - \frac{2}{M}\}$  denotes the normalized reception phase of the phase shifter connected between the  $i$ th antenna and the  $j$ th RF chain at  $\text{BS}_c$ . Rather than using a codebook-based GoB approach, I attempt to individually regulate the phase shifters to unleash the full potential of employing a plethora of phase shifters. Since phase angles and analog beamformers form one-to-one correspondence, encompassing  $\phi_{i,j,c}$  for all  $i, j, c$  suffices to reconstruct the analog combiner.

However, directly guessing restricted yet discrete  $\phi_{i,j,c}$ 's from a neural net output is challenging because 1) neural networks have inconsistent output range and 2) generation of discrete output is via quantization is not differentiable. To resolve the issue, I represent phase element  $\phi_{i,j,c}$  by the intermediate vector of length  $M$ , i.e.,  $\mathbf{x}_{i,j,c} \in \mathbb{R}^M$ , and then apply the soft-argmax function defined as

$$\psi(\mathbf{x}) = \sum_{m=0}^{M-1} \frac{m}{M} \frac{e^{\beta x_m}}{\sum_{\ell=0}^{M-1} e^{\beta x_\ell}}, \quad (5.14)$$

which is differentiable and obtains the same output as the regular argmax with a sufficiently large  $\beta$  where  $\mathbf{x}$  has  $M$  real-valued entries. In other words,

$\mathbf{x}$  represents each phase element and  $\psi(\cdot)$  takes  $M$ -dimensional input  $\mathbf{x}$  to return the index of the maximum value, thereby connecting the index with the discrete phase angle. Note that  $\psi(\mathbf{x}) = \frac{m^*}{M}$  with a sufficiently large  $\beta$  where  $m^*$  denotes the index of the largest entry in  $\mathbf{x}$ . I then define the collection of intermediate vectors for the  $c$ th cell as

$$\mathbf{X}_c = \begin{pmatrix} \mathbf{x}_{1,1,c} & \cdots & \mathbf{x}_{1,N_{\text{RF}},c} \\ \vdots & \ddots & \vdots \\ \mathbf{x}_{N_r,1,c} & \cdots & \mathbf{x}_{N_r,N_{\text{RF}},c} \end{pmatrix}. \quad (5.15)$$

I further gather all the intermediate vectors as

$$\mathbf{X} = [\mathbf{X}_1, \dots, \mathbf{X}_{N_c}]. \quad (5.16)$$

To make valid phase indices, I can then unite the phase angles of the analog beamformers from all  $N_c$  BSs by applying the vector-wise soft argmax as

$$\mathbf{w}_{\text{RF}} = \text{vec} \left( \left[ \text{vec}(\Phi_1), \dots, \text{vec}(\Phi_{N_c}) \right] \right), \quad (5.17)$$

where  $\Phi_c$  is extracted as

$$\Phi_c = \psi(\mathbf{X}_c) \quad (5.18)$$

$$= \begin{pmatrix} \psi(\mathbf{x}_{1,1,c}) & \cdots & \psi(\mathbf{x}_{1,N_{\text{RF}},c}) \\ \vdots & \ddots & \vdots \\ \psi(\mathbf{x}_{N_r,1,c}) & \cdots & \psi(\mathbf{x}_{N_r,N_{\text{RF}},c}) \end{pmatrix}. \quad (5.19)$$

For the inference stage during the practical deployment, the soft-argmax function can be replaced with the regular argmax since no further update is needed.

### 5.4.3 Power Control

Based on the signal model in (5.1), the allocated transmit powers for  $N_u$  users in cell  $c$  are collected in  $\mathbf{P}_c$ . Likewise, I combine the transmit power across all cells and users as

$$\tilde{\mathbf{p}} = \text{vec} \left( \left[ \text{diag}(\mathbf{P}_1), \dots, \text{diag}(\mathbf{P}_{N_c}) \right] \right). \quad (5.20)$$

To guarantee that the power constraint in (5.8) is met,  $\tilde{\mathbf{p}}$  is post-processed as

$$\mathbf{p} = (p_{\max} - p_{\min}) \sigma(\tilde{\mathbf{p}}) + p_{\min}, \quad (5.21)$$

where  $\sigma(\cdot) = 1/(1 + e^{-x}) \in (0, 1)$  is the regular sigmoid function.

### 5.4.4 Action Vector

All things considered, the concatenation of the digital beamformers, the analog beamformers, and transmit powers associated across all cells is committed to establishing an action vector represented as

$$\mathbf{a} = \text{vec} \left( \left[ \mathbf{w}_{\text{BB}}, \mathbf{w}_{\text{RF}}, \mathbf{p} \right] \right). \quad (5.22)$$

Upon handing over the action to the environment, the action vector is sliced and each BS assembles the HB components associated with the dedicated cell. Note that the action needs to be valid in terms of the constraints.

## 5.5 Hybrid Beamforming and Power Control via Reinforcement Learning: State and Reward

### 5.5.1 State Space

Since the state is the only measure that the DRL agent relies on in taking an action, the state needs to include sufficiently rich information on the environment. I define the current state at the  $t$ th iteration, i.e.,  $\mathbf{s}_t$ , as a concatenated vector of achieved individual SNRs and the previously refined action.  $\mathbf{s}_t = [\gamma_{1,1}, \dots, \gamma_{N_c, N_u}, \mathbf{a}_{t-1}^T]^T$ . Note that adding the information on current users' locations can potentially improve the performance of the DRL approach since the state can attain a richer representation of the current situation.

### 5.5.2 Reward

A reward is feedback from the environment when the DRL agent takes an action in a given state. The DRL agent does not have a direct control on the reward; however the DRL agent aims to choose the best action that can maximize the reward at its best knowledge. Therefore, the reward should be related with the primal problem  $\mathcal{P}_5 1$  defined in (5.4)-(5.8). Based on the objective of the target problem, I define a reward at the  $t$ th iteration, i.e.,  $R_t$ , as a function of the currently achieved SINR  $\gamma_{u,c}^{(t)}$  as follows:

$$\begin{aligned}
R_t = & \delta_1 \prod_{c=1}^{N_c} \prod_{u=1}^{N_u} \mathbb{1}_{\{\gamma_{u,c}^{(t)} \geq \bar{\gamma}\}} + \delta_2 \left( 1 - \prod_{c=1}^{N_c} \prod_{u=1}^{N_u} \mathbb{1}_{\{\gamma_{u,c}^{(t)} < \bar{\gamma}\}} \right) \\
& + \delta_3 \prod_{c=1}^{N_c} \prod_{u=1}^{N_u} \mathbb{1}_{\{\gamma_{u,c}^{(t)} \geq \gamma_{u,c}^{(t-1)}\}} - \delta_4 \sum_{c=1}^{N_c} \sum_{u=1}^{N_u} p_{u,c}
\end{aligned} \tag{5.23}$$

where the first term is the ultimate goal for all  $\gamma_{u,c}$ 's to be higher than the target SINR, the second term is the intermediate goal activated when at least one SINR is higher than or equal to the target, the third term is also the intermediate goal triggered when all  $\gamma_{u,c}$ 's at time  $t$  are improved compared with the previous time frame, and the last term is the sum-power penalty which is proportional to the total transmit power to be minimized. Here, I enable hierarchical RL that decomposes the challenging goal-oriented RL tasks into simpler subtasks, thereby accelerating the convergence and improving the overall performance in practice [72]. The associated weights are described as  $\delta_1$ ,  $\delta_2$ ,  $\delta_3$ , and  $\delta_4$ , where  $\delta_1$  and  $\delta_4$  are chosen to be significantly greater than the other weights. Accordingly, the DRL agent eventually updates the policy in a way that all the SINRs are maintained above the target while minimizing the total transmit power.

## 5.6 Policy Gradient Deep Reinforcement Learning

Recently, Deep Q-Network (DQN) has been used in designing the analog beamformer of the hybrid beamforming architecture by selecting beam index or codebook index [59, 82]. However, because of the value-based nature



and policy, DQN which aims to find the best action over all possible action-value pairs of a given state is only able to address a low-dimensional yet discrete action space even with high-dimensional observation spaces [60]. Considering the massive MIMO systems, the output dimension of DQN eventually goes up when deploying a more complicated architecture with many antennas and RF chains, thereby becoming an infeasible scheme.

DDPG, in contrast to DQN, employs a policy-based actor-critic approach that directly predicts a deterministic action for a given state. Since an output of an actor is considered as an action, DDPG can support a mixture of high-dimensional continuous and discrete elements. The main building blocks of DDPG include an actor network that generates an action based on the state input and a critic network that evaluates the pair of the state and the output taken by the actor network, thereby concurrently learning the policy and the Q-function. The DDPG can handle the RL components as shown in Fig. 5.2.

### 5.6.1 Critic Network

The critic network is an approximator of the Q-function that takes in the state and action as input and outputs the estimated Q-value of the associated state-action pair. The output of the critic network is written as  $Q(\mathbf{s}_t, \mathbf{a}_t; \theta^Q)$ . Then, the critic network is updated to minimize the gap between the true return obtained from interacting with the DRL environment, i.e.,  $G_t$  and the approximated value  $Q(\mathbf{s}_t, \mathbf{a}_t; \theta^Q)$ .

### 5.6.2 Actor Network

The actor network parametrized by  $\phi^\mu$  maintains the deterministic policy that directly computes the action for a given state instead of outputting the probability distribution across a discrete action space. The output of the actor network is written as  $\mathbf{a}_t = \mu(\mathbf{s}_t; \theta^\mu)$ . The actor network is updated in a way that the output of the critic network, i.e.,  $Q(\mathbf{s}_t, \mathbf{a}_t; \theta^Q)$ , is maximized via gradient ascent algorithms.

### 5.6.3 Replay Buffer

In order to remove the correlation between training samples and hence achieve stable convergence and improvement, DDPG borrows the notion of replay buffer from DQN. The replay buffer  $\mathcal{R}$  collects up to  $N_{max}$  training samples over time and discards a random sample if data is overflowing. At each time step  $i$ , the buffer memorizes the footprint of the interaction between the DRL agent and the environment. To be specific, based on the given state  $\mathbf{s}_i$ , I choose  $\mathbf{a}_t$  from the policy, and the current reward  $r_i$  and next state  $\mathbf{s}_{i+1}$  are determined. Afterwards, one complete experience, i.e.,  $(\mathbf{s}_i, \mathbf{a}_i, r_i, \mathbf{s}_{i+1})$ , is added to  $\mathcal{R}$ . After collecting sufficiently many data points, I randomly take  $B$  samples from  $\mathcal{R}$  to train the actor and critic networks.

### 5.6.4 Network Update

DDPG trains a deterministic policy in an off-policy way. Because the policy is deterministic, if the agent were to explore on-policy, in the beginning,

it would probably not try a wide enough variety of actions to find useful learning signals. To make DDPG policies explore better, I add noise to their actions at training time.

DDPG employs the use of off-policy data and the Bellman equation to learn the  $Q$ -function which is in turn used to derive and learn the policy.

$$\theta^\mu \leftarrow \theta^\mu + \alpha \nabla_{\phi^\mu} \frac{1}{B} \sum_{b=1}^B Q^{\phi^Q}(\mathbf{s}_{t(b)}, \mu(\mathbf{s}_{t(b)}; \theta^\mu)), \quad (5.24)$$

$$\theta^Q \leftarrow \theta^Q - \beta \nabla_{\phi^Q} \frac{1}{B} \sum_{b=1}^B \left( R_{t(b)} + \gamma Q^{\theta^{\bar{Q}}}(\mathbf{s}_{t(b+1)}, \mathbf{a}_{t(b+1)}^{\theta^{\bar{\mu}}}) - Q^{\phi^Q}(\mathbf{s}_{t(b)}, \mathbf{a}_{t(b)}^{\theta^\mu}) \right)^2, \quad (5.25)$$

where  $t(b)$  denotes the index of the  $b$ th sampled experience from the replay buffer. Note that the actor network is updated by (5.24) to maximize  $Q$ -function via gradient ascent algorithms and the critic network is updated by (5.25) to minimize the gap between the approximated one-step  $G_t$  and the approximated  $Q$ -function.

To improve the stability during the training step and relieve the moving target problem, I borrow the notion of target networks on both the actor and critic networks. The target networks have the same structure and dimension as the main behavior networks; however, the target networks contain different neural network parameters  $\theta^{\bar{\mu}}$  and  $\theta^{\bar{Q}}$  for the target actor and the target critic networks, respectively. The target networks in DDPG are delayed compared

to the main behavior networks and updated gradually and continuously in the following soft-update fashion:

$$\theta^{\bar{\mu}} \leftarrow \tau\theta^{\bar{\mu}} + (1 - \tau)\theta^{\mu} \quad (5.26)$$

$$\theta^{\bar{Q}} \leftarrow \tau\theta^{\bar{Q}} + (1 - \tau)\theta^Q \quad (5.27)$$

where the soft-update rate  $\tau$  is chosen to be close to 1, e.g., 0.99, in this work.

## 5.7 Simulation Results

In this section, I validate the proposed DRL-based method in terms of the achieved SINR. I consider the mmWave communication system assuming a 24 GHz carrier frequency with 100 MHz bandwidth. The adjacent BSs are 100 m apart and the minimum distance between any BS and user is 10 m. For large scale fading, I adopt the log-distance pathloss model in [1] with the 72 dB intercept, the pathloss exponent of 2.92, and the shadow fading whose shadowing variance is 8.7 dB. Noise power is computed with  $-174$  dBm/Hz power spectral density and 5 dB noise figure. I also use the sector antenna gain of 15 dB.

Fig. 5.3 presents the progress of the achieved SINRs and the reward. I consider  $N_r = 16$  BS antennas,  $N_{\text{RF}} = 2$  RF chains at each BS,  $N_c = 2$  cells, and  $N_u = 2$  users per cell. Each phase shifter of RF chains can take one of  $M = 32$  equally spaced phase angles. The power constraint of each user is specifies as  $p_{\min} = 10$  dBm and  $p_{\max} = 30$  dBm. The homogeneous SINR target of  $\bar{\gamma} = 2$  dB is required for all users. For the reward function,

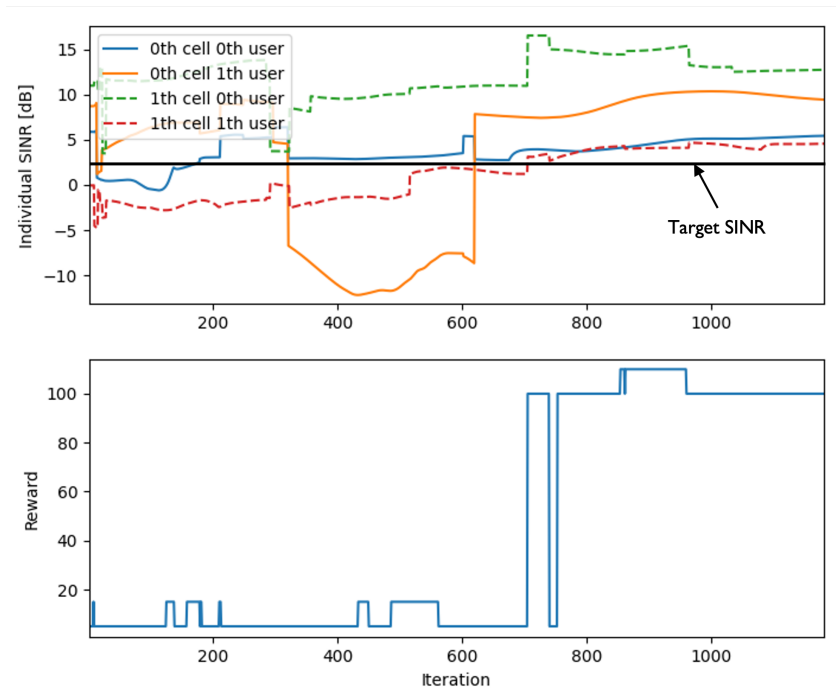


Figure 5.3: The progress of the achieved SINRs and the reward.

the reward weights are determined as  $\{\delta_1, \delta_2, \delta_3, \delta_4\} = \{100, 5, 10, 1\}$ , which means that the positive reward of 100 is provided if all users are satisfied. As shown in the figure, the progress of the achieved SINRs and the reward discloses that the DDPG-based approach can satisfy all  $N_c N_u$  users' achieved SINR after training 700 iterations. Because of the intermediate rewards, the DRL agent aims to make an effort to make advancement. Even though the DRL agent fails to achieve the target slightly at around the 750th iteration, the shock is quickly recovered and the DRL agent can consistently achieve the pre-determined target SINR.

## 5.8 Conclusion

In this chapter, I investigated the DRL-based method for jointly designing the hybrid beamformers and power control in multicell mmWave MIMO systems. Specifically, the aim was to develop a strategy for determining the hybrid beamformers and transmission power control for users at each base station in multicell uplink communication systems while minimizing transmit power and satisfying SINR constraints. To tackle the challenge posed by the non-convex conditions arising from the analog beamformers and achieve the aforementioned objective, I introduced a DRL-based methodology that leverages the DDPG algorithm. This approach effectively addresses the integration of both discrete and continuous inputs and generates an appropriate action that aligns with the desired design factors. To elaborate further, my approach involved individual control of each phase shifter via an intermediate vector and a differentiable soft-argmax function to estimate the phase angle index. Accordingly, the actor network can be trained continually and the action vector was able to construct the beamformers and transmission power values properly. The effectiveness of this method was assessed by evaluating the achieved SINR, which was determined through simulation results.

## Chapter 6

### Concluding Remarks

This chapter concludes the dissertation with a summary of contributions in Section 6.1 and potential future research directions in Section 6.2

#### 6.1 Summary and contributions

In this dissertation, I investigated the power-efficient and intelligent algorithms to re-engineer crucial communication functions when the communication systems adopt one of the following two low-power architectures: low-resolution data converters and the HB architecture. Because either the quantization error of low-resolution data converters or the non-convexity and non-linearity of the HB cannot be disregarded, the existing methods cannot be directly applied to the low-power systems. Therefore, it is crucial to develop advanced power-efficient and intelligent communication techniques that have the ability to satisfy demanding requirements and improve key performance metrics even in the presence of severe distortion and non-linearity caused by low-power architectures.

First of all, I developed a joint beamforming and power control design for the coordinated multicell MIMO systems with low-resolution converters.

After formulating the uplink and downlink problems, I showed the uplink-downlink strong duality which facilitates the problem-solving. It was shown that the derived results also work for the wideband OFDM systems. I used the derived results to devise an iterative algorithm that can jointly design beamforming and power control design to minimize the total power consumption. Under homogeneous user requirements, I also proposed a deterministic solution that can compute the uplink powers immediately. I showed that the proposed algorithms outperform the existing methods in terms of total transmit power, target achievement rate, and convergence.

Hereafter, I extended the first contribution in a way that maximum transmit power is minimized to raise the power efficiency of power-related components. For a more practical, I formulated the downlink antenna power minimization problem with target SQINR constraints as a primal problem, and I derived the associated dual problem which is interpreted as the uplink problem with known yet controllable noise covariance matrices. Leveraging the strong duality devised for this particular problem, I addressed the inner and outer problems of the dual uplink problem in an alternating manner by solving the inner power control problem via fixed-point iteration and the outer noise covariance design problem via projected subgradient ascent. The converged uplink solution is then used for computing the primal downlink problem by using the linear transformation. It was shown that the proposed algorithms outperform the existing methods in terms of maximum transmit power, PAPR, and convergence.



The third part of this dissertation discussed the learning-based ML detection method for uplink massive MIMO communication systems with one-bit ADCs. To handle the performance loss of learning-based one-bit detection when the number of training samples is insufficient, I proposed how to effectively place dithering noise to facilitate the acquisition of statistical patterns. The proposed method was more robust to the number of training symbols because the adaptive randomness induces moderate fluctuations in the sign changes of the training sequence, thereby successfully extracting the statistical pattern of one-bit quantized signals. The deep neural network-based SNR estimator also effectively worked for the denoising stage. I further adjusted the dithering power to match the appropriate SNR range. It was shown that the learning-based ML detection achieves optimal performance and outperforms other approaches by a large gap. Further, the derived likelihood probabilities are used for computing the soft LLR and the simulation results demonstrate the superiority of the proposed algorithm.

Lastly, I developed the DRL-based approach for jointly designing the hybrid beamformers and power control in case of multicell mmWave MIMO systems. In multicell uplink communication systems, I intended to devise the HB at each BS and the transmission power control for the corresponding users while consuming the minimal transmit power and ensuring that the SINR constraints are met. To accomplish this goal while considering the non-convex conditions caused by the analog beamformers, I proposed the DRL-based approach that utilizes the DDPG algorithm to handle the combination

of discrete and continuous inputs and output a suitable action that corresponds to the design factors. Specifically, I controlled each phase shifter individually using an intermediate vector and a differentiable argmax function to estimate the phase angle index. The performance of the proposed method was evaluated based on the achieved SINR through simulation results.

## 6.2 Future work

I present the following future directions related to the topics addressed in this dissertation.

- **Multicell Coordination in Case of Imperfect CSI**

The multicell CoMP designs proposed in Chapter 2 and Chapter 3 outperformed the benchmarks in case of imperfect CSI; however, the proposed algorithms require full CSI and showed the deviation from the target SQINR when the channel estimation error becomes non-trivial. A more advanced beamforming and power control design needs to take the channel estimation error into account as well. Using orthogonal pilot sequences, the MMSE estimation of  $\mathbf{h}_{j,i,u}$  introduces the estimation failure error of  $\mathbf{f}_{j,i,u} = \mathbf{h}_{j,i,u} - \hat{\mathbf{h}}_{j,i,u}$  whose statistics can be known. With considering the estimated channel via MMSE estimator,  $\mathbf{h}_{j,i,u}$  is replaced with  $\hat{\mathbf{h}}_{j,i,u} + \mathbf{f}_{j,i,u}$  and the received signal with the impact of imperfect

CSI can be written as

$$\begin{aligned} \tilde{y}_{i,u}^{\text{dl}} = & \alpha (\hat{\mathbf{h}}_{i,i,u} + \mathbf{f}_{i,i,u})^H \mathbf{w}_{i,u} s_{i,u}^{\text{dl}} + \alpha \sum_{\substack{(j,v) \neq (i,u) \\ (j,v) \in (N_c, N_u)}} (\hat{\mathbf{h}}_{j,i,v} + \mathbf{f}_{j,i,v})^H \mathbf{w}_{j,v} s_{j,v}^{\text{dl}} \quad (6.1) \\ & + \sum_{j=1}^{N_c} (\hat{\mathbf{h}}_{j,i,u} + \mathbf{f}_{j,i,u})^H \mathbf{q}_j^{\text{dl}} + n_{i,u}^{\text{dl}}. \end{aligned}$$

In this case, since the channel estimation error is not known at the BS, the approaches I proposed in Chapter 2 and Chapter 3 cannot be directly applied. Given that the statistics of  $\mathbf{f}_{i,i,u}$  are known, i.e., error covariance matrices, it is possible to rewrite the SQINR expression in terms of the error covariance matrices, not the error itself, and hence the solutions can take into account the channel estimation successfully.

- **Oversampling of One-Bit ADCs**

The proposed one-bit ML detection with artificial dithering noise allows to train the likelihood functions with an acceptable amount of training sequences. However, the amount can still be considered as a huge overhead. One can oversample the one-bit observations in time. In this way, the receiver takes a very limited amount of pilot signals and generates many randomly dithered realizations to virtually increase the number of observations. This method requires a more thorough calibration of dithering signals.

- **Adaptive Change to Decision Threshold of One-Bit ADCs**

So far, one-bit ADCs have a fixed decision threshold of zero. Rather than adding artificial dithering noise at the receiver, one can adaptively

change the decision threshold so that the one-bit observations can sign changes within an acceptable amount of training. Based on the fact that the one-bit observation at the  $i$ th antenna is defined as

$$y_i[t] = \mathcal{Q}(\sqrt{\rho}\mathbf{h}_i^T \mathbf{s}[t] + z_i[t]), \quad (6.2)$$

it is easily noticed that the unquantized version is centered at  $\sqrt{\rho}\mathbf{h}_i^T \mathbf{s}[t]$ . Then, one-bit ADCs aim to set the comparator with decision threshold  $\sqrt{\rho}\mathbf{h}_i^T \mathbf{s}[t]$  by an adaptive update as a function of one-bit realizations. This method will help the receiver see  $+1$  and  $-1$  equally likely.

- **Online Learning Based Joint Design of Hybrid Architecture**

The joint design of hybrid architectures across multiple BSs needs to take into account the variant dynamics of the channel; however, implementing real-time learning is very challenging. Here, online learning can come into play. Online learning is a subset of machine learning in which fresh data samples arrive sequentially and the prediction model is continually updated to adapt to the new data as quickly as possible. However, a majority of online learning algorithms are based on convex problems. Therefore, an intelligent idea to apply non-convex online learning to the multicell hybrid beamforming problems is needed.

- **Spectral Efficiency Maximization via Deep Reinforcement Learning Based Reconfigurable Intelligent Surfaces**

To address the challenging behaviors of the mmWave spectrum and the

demanding requirements of the future 6G and beyond wireless networks, a brand-new technology called reconfigurable intelligent surfaces (RIS) has been brought to the attention of the wireless research community in recent years. The RIS shown in Fig. 6.1 is a programmable man-made structure that can be used to control the propagation of electromagnetic waves by changing the electric and magnetic properties of the surface. By placing these surfaces in a wireless environment, the properties of radio channels can be reconfigured, thereby improving the quality of signals.

The RIS structure is defined as

$$\mathbf{R} = e^{j2\pi \text{diag}(\phi_1, \dots, \phi_{N_{RIS}})}, \quad (6.3)$$

and the main aim is to dynamically adjust the reflecting panels of the RIS, where each  $\phi_n$  takes one of  $M$  possible normalized discrete angles as

$$\phi_n \in \left\{0, \frac{1}{M}, \dots, \frac{M-1}{M}\right\}. \quad (6.4)$$

Each diagonal entry of  $\mathbf{R}$  in (6.3) needs to satisfy the non-convex unit-modulus constraint, i.e.,  $|\mathbf{R}_{n,n}| = 1$ . Because of this restriction and (6.4), it is challenging to find a solution of the RIS-aided system efficiently. Therefore, the DRL-based approach can come into play. Especially, the notion of intermediate vectors and soft-argmax function used to control the phase shifter of the analog beamformers in Chapter 5 can be utilized in this problem.

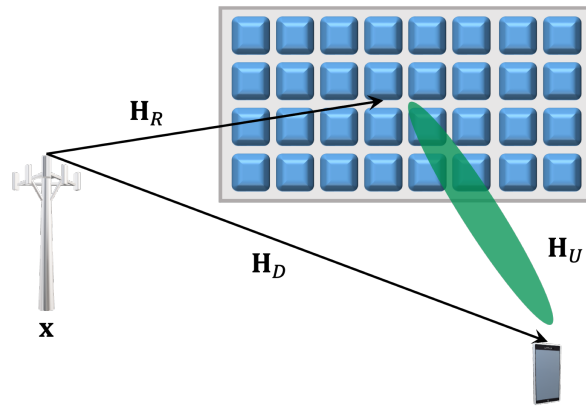


Figure 6.1: System model with reconfigurable intelligent surfaces.

## Bibliography

- [1] Mustafa Riza Akdeniz, Yuanpeng Liu, Mathew K Samimi, Shu Sun, Sundeeep Rangan, Theodore S Rappaport, and Elza Erkip. Millimeter wave channel modeling and cellular capacity evaluation. *IEEE J. Sel. Areas in Commun.*, 32(6):1164–1179, 2014.
- [2] Ahmed Alkhateeb, Geert Leus, and Robert W Heath. Limited feedback hybrid precoding for multi-user millimeter wave systems. *IEEE Trans. Wireless Commun.*, 14(11):6481–6494, 2015.
- [3] Jeffrey G Andrews, Stefano Buzzi, Wan Choi, Stephen V Hanly, Angel Lozano, Anthony CK Soong, and Jianzhong Charlie Zhang. What will 5G be? *IEEE Journal Sel. Areas in Commun.*, 32(6):1065–1082, 2014.
- [4] Tianyang Bai, Ahmed Alkhateeb, and Robert W Heath. Coverage and capacity of millimeter-wave cellular networks. *IEEE Commun. Mag.*, 52(9):70–77, 2014.
- [5] Eren Balevi and Jeffrey G Andrews. One-bit ofdm receivers via deep learning. *IEEE Trans. on Communications*, 67(6):4326–4336, 2019.
- [6] Elyes Balti and Brian L. Evans. A unified framework for full-duplex massive mimo cellular networks with low resolution data converters. *IEEE Open Journal of the Commun. Society*, 4:1–28, 2023.

- [7] Heinz H Bauschke and Jonathan M Borwein. On projection algorithms for solving convex feasibility problems. *SIAM Review*, 38(3):367–426, 1996.
- [8] Mats Bengtsson and Björn Ottersten. Optimal downlink beamforming using semidefinite optimization. In *Allerton Conf. on Commun., Control, and Computing*, pages 987–996, 1999.
- [9] Emil Björnson and Luca Sanguinetti. Scalable cell-free massive MIMO systems. *IEEE Trans. Commun.*, 68(7):4247–4261, 2020.
- [10] Rong-Rong Chen, Bruce Hajek, Ralf Koetter, and Upamanyu Madhok. On fixed input distributions for noncoherent communication over high-SNR Rayleigh-fading channels. *IEEE Trans. Info. Theory*, 50(12):3390–3396, 2004.
- [11] Runhua Chen, Jeffrey G Andrews, Robert W Heath, and Arunabha Ghosh. Uplink power control in multi-cell spatial multiplexing wireless systems. *IEEE Trans. Wireless Commun.*, 6(7):2700–2711, 2007.
- [12] Yun Chen, Da Chen, Tao Jiang, and Lajos Hanzo. Channel-covariance and angle-of-departure aided hybrid precoding for wideband multiuser millimeter wave mimo systems. *IEEE Transactions on Communications*, 67(12):8315–8328, 2019.
- [13] Yunseong Cho, Jinseok Choi, and Brian L Evans. Coordinated beamforming in quantized massive MIMO systems with per-antenna con-



- straints. In *IEEE Wireless Commun. and Networking Conf.*, pages 2512–2517, 2022.
- [14] Yunseong Cho and Song-Nam Hong. One-Bit Successive-Cancellation Soft-Output (OSS) Detector for Uplink MU-MIMO Systems with One-Bit ADCs. *IEEE Access*, 2019.
- [15] J. Choi, Y. Cho, and B. L. Evans. Quantized Massive MIMO Systems with Multicell Coordinated Beamforming and Power Control. *IEEE Trans. on Commun.*, 69(2):946–961, 2021.
- [16] Jinseok Choi, Yunseong Cho, and Brian L. Evans. Quantized massive mimo systems with multicell coordinated beamforming and power control. *IEEE Trans. Communications*, 69(2):946–961, 2021.
- [17] Jinseok Choi, Yunseong Cho, Brian L Evans, and Alan Gatherer. Robust learning-based ML detection for massive MIMO systems with one-bit quantized signals. In *IEEE Global Commun. Conf.*, pages 1–6, 2019.
- [18] Jinseok Choi, Brian L Evans, and Alan Gatherer. Resolution-adaptive hybrid MIMO architectures for millimeter wave communications. *IEEE Trans. Signal Process.*, 65(23):6201–6216, 2017.
- [19] Jinseok Choi, Gilwon Lee, and Brian L Evans. Two-stage analog combining in hybrid beamforming systems With low-resolution ADCs. *IEEE Trans. Signal Process.*, 67(9):2410–2425, 2019.

- [20] Jinseok Choi, Junmo Sung, Brian L Evans, and Alan Gatherer. Antenna Selection for Large-Scale MIMO Systems with Low-Resolution ADCs. *IEEE Int. Conf. Acoustics, Speech, and Signal Process.*, 2018.
- [21] Junil Choi, David James Love, D Richard Brown III, and Mireille Boutin. Quantized Distributed Reception for MIMO Wireless Systems Using Spatial Multiplexing. *IEEE Trans. Signal Process.*, 63(13):3537–3548, 2015.
- [22] Junil Choi, Jianhua Mo, and Robert W Heath. Near maximum-likelihood detector and channel estimator for uplink multiuser massive MIMO systems with one-bit ADCs. *IEEE Trans. Commun.*, 64(5):2005–2018, 2016.
- [23] Hayssam Dahrouj and Wei Yu. Coordinated beamforming for the multicell multi-antenna wireless system. *IEEE Trans. Wireless Commun.*, 9(5):1748–1759, 2010.
- [24] Jianxin Dai, Juan Liu, Jiangzhou Wang, Junxi Zhao, Chonghu Cheng, and Jin-Yuan Wang. Achievable rates for full-duplex massive MIMO systems with low-resolution ADCs/DACs. *IEEE Access*, 7:24343–24353, 2019.
- [25] Chamitha De Alwis, Anshuman Kalla, Quoc-Viet Pham, Pardeep Kumar, Kapal Dev, Won-Joo Hwang, and Madhusanka Liyanage. Survey on 6G frontiers: Trends, applications, requirements, technologies and future research. *IEEE Open J. of Commun. Society*, 2:836–886, 2021.

- [26] Omar El Ayach, Sridhar Rajagopal, Shadi Abu-Surra, Zhouyue Pi, and Robert W Heath. Spatially sparse precoding in millimeter wave MIMO systems. *IEEE Trans. Wireless Commun.*, 13(3):1499–1513, 2014.
- [27] Vinko Erceg, Larry J Greenstein, Sony Y Tjandra, Seth R Parkoff, Ajay Gupta, Boris Kulic, Arthur A Julius, and Renee Bianchi. An empirically based path loss model for wireless channels in suburban environments. *IEEE J. Sel. Areas in Commun.*, 17(7):1205–1211, 1999.
- [28] Li Fan, Shi Jin, Chao-Kai Wen, and Haixia Zhang. Uplink achievable rate for massive MIMO systems with low-resolution ADC. *IEEE Commun. Lett.*, 19(12):2186–2189, October 2015.
- [29] Alyson K Fletcher, Sundeep Rangan, Vivek K Goyal, and Kannan Ramchandran. Robust predictive quantization: Analysis and design via convex optimization. *IEEE J. Sel. Topics in Signal Process.*, 1(4):618–632, 2007.
- [30] Gerard J Foschini and Zoran Miljanic. A simple distributed autonomous power control algorithm and its convergence. *IEEE Trans. Veh. Technol.*, 42(4):641–646, 1993.
- [31] Allen Gersho and Robert M Gray. *Vector quantization and signal compression*. Springer, 2012.
- [32] Robert W Heath, Nuria Gonzalez-Prelcic, Sundeep Rangan, Wonil Roh, and Akbar M Sayeed. An overview of signal processing techniques for

- millimeter wave MIMO systems. *IEEE J. Sel. Topics in Signal Process.*, 10(3):436–453, February 2016.
- [33] Robert W Heath Jr and Angel Lozano. *Foundations of MIMO Communication*. Cambridge University Press, 2018.
- [34] Yuqiang Heng, Jianhua Mo, and Jeffrey G. Andrews. Learning site-specific probing beams for fast mmwave beam alignment. *IEEE Transactions on Wireless Communications*, 21(8):5785–5800, 2022.
- [35] Giovanni Interdonato, Emil Björnson, Hien Quoc Ngo, Pål Frenger, and Erik G Larsson. Ubiquitous cell-free massive mimo communications. *EURASIP J. Wireless Commun. and Networking*, 2019(1):1–13, 2019.
- [36] R. Irmer, H. Droste, P. Marsch, M. Grieger, G. Fettweis, S. Brueck, H. Mayer, L. Thiele, and V. Jungnickel. Coordinated multipoint: Concepts, performance, and field trial results. *IEEE Commun. Mag.*, 49(2):102–111, 2011.
- [37] Christian Isheden, Zhijiat Chong, Eduard Jorswieck, and Gerhard Fettweis. Framework for link-level energy efficiency optimization with informed transmitter. *IEEE Transactions on Wireless Communications*, 11(8):2946–2957, 2012.
- [38] S. Jacobsson, G. Durisi, M. Coldrey, T. Goldstein, and C. Studer. Quantized precoding for massive MU-MIMO. *IEEE Trans. Commun.*, 65(11):4670–4684, 2017.

- [39] S. Jacobsson, G. Durisi, M. Coldrey, U. Gustavsson, and C. Studer. Throughput Analysis of Massive MIMO Uplink With Low-Resolution ADCs. *IEEE Trans. Wireless Commun.*, 16(6):4038–4051, 2017.
- [40] S. Jacobsson, G. Durisi, M. Coldrey, and C. Studer. Linear precoding With low-resolution DACs for massive MU-MIMO-OFDM downlink. *IEEE Trans. Wireless Commun.*, 18(3):1595–1609, 2019.
- [41] Yo-Seb Jeon, Song-Nam Hong, and Namyoon Lee. Supervised-Learning-Aided Communication Framework for MIMO Systems with Low-Resolution ADCs. *IEEE Trans. on Veh. Technol.*, 2018.
- [42] Yo-Seb Jeon, Namyoon Lee, Song-Nam Hong, and Robert W Heath. One-bit sphere decoding for uplink massive MIMO systems with one-bit ADCs. *IEEE Trans. Wireless Commun.*, 17(7):4509–4521, 2018.
- [43] Yo-Seb Jeon, Minji So, and Namyoon Lee. Reinforcement-learning-aided ML detector for uplink massive MIMO systems with low-precision ADCs. In *IEEE Wireless Commun. and Networking Conf.*, pages 1–6, 2018.
- [44] V. Jungnickel, K. Manolakis, W. Zirwas, B. Panzner, V. Braun, M. Losow, M. Sternad, R. Apelfröjd, and T. Svensson. The role of small cells, coordinated multipoint, and massive MIMO in 5G. *IEEE Commun. Mag.*, 52(5):44–51, 2014.

- [45] Aravindh Krishnamoorthy and Deepak Menon. Matrix inversion using cholesky decomposition. In *Signal Processing: Algorithms, Architectures, Arrangements, and Applications*, pages 70–72, 2013.
- [46] Erik G Larsson, Ove Edfors, Fredrik Tufvesson, and Thomas L Marzetta. Massive MIMO for next generation wireless systems. *IEEE Commun. Mag.*, 52(2):186–195, 2014.
- [47] Woongsup Lee, Minhoe Kim, and Dong-Ho Cho. Deep power control: Transmit power control scheme based on convolutional neural network. *IEEE Communications Letters*, 22(6):1276–1279, 2018.
- [48] A. Li, F. Liu, C. Masouros, Y. Li, and B. Vucetic. Interference exploitation 1-Bit massive MIMO precoding: A partial branch-and-bound solution with near-optimal performance. *IEEE Trans. Wireless Commun.*, pages 1–1, 2020.
- [49] Jiahui Li, Limin Xiao, Xibin Xu, and Shidong Zhou. Robust and low complexity hybrid beamforming for uplink multiuser mmwave mimo systems. *IEEE Communications Letters*, 20(6):1140–1143, 2016.
- [50] Xiaofeng Li and Ahmed Alkhateeb. Deep learning for direct hybrid precoding in millimeter wave massive mimo systems. In *2019 53rd Asilomar Conference on Signals, Systems, and Computers*, pages 800–805, 2019.

- [51] Y. Li, C. Tao, A. Lee Swindlehurst, A. Mezghani, and L. Liu. Down-link Achievable Rate Analysis in Massive MIMO Systems With One-Bit DACs. *IEEE Commun. Lett.*, 21(7):1669–1672, 2017.
- [52] Yongzhi Li, Cheng Tao, Gonzalo Seco-Granados, Amine Mezghani, A. Lee Swindlehurst, and Liu Liu. Channel estimation and performance analysis of one-bit massive mimo systems. *IEEE Trans. Signal Processing*, 65(15):4075–4089, 2017.
- [53] Ning Liang and Wenyi Zhang. Mixed-ADC massive MIMO. *IEEE J. Sel. Areas in Commun.*, 34(4):983–997, Mar. 2016.
- [54] Timothy P Lillicrap, Jonathan J Hunt, Alexander Pritzel, Nicolas Heess, Tom Erez, Yuval Tassa, David Silver, and Daan Wierstra. Continuous control with deep reinforcement learning. *arXiv preprint arXiv:1509.02971*, 2015.
- [55] Fangqing Liu, Xiaolei Shang, and Heng Zhu. Efficient majorization-minimization-based channel estimation for one-bit massive mimo systems. *IEEE Trans. Wireless Commun.*, 20(6):3444–3457, 2021.
- [56] T. L. Marzetta. Noncooperative Cellular Wireless with Unlimited Numbers of Base Station Antennas. *IEEE Trans. Wireless Commun.*, 9(11):3590–3600, 2010.
- [57] Diana M. V. Melo, Lukas T. N. Landau, Rodrigo C. De Lamare, Peter F. Neuhaus, and Gerhard P. Fettweis. Zero-crossing precoding techniques

for channels with 1-bit temporal oversampling adcs. *IEEE Transactions on Wireless Communications*, pages 1–1, 2023.

- [58] Amine Mezghani and Josef A Nossek. On ultra-wideband MIMO systems with 1-bit quantized outputs: Performance analysis and input optimization. In *IEEE Int. Symp. Inform. Theory*, pages 1286–1289. IEEE, 2007.
- [59] Faris B Mismar, Brian L Evans, and Ahmed Alkhateeb. Deep reinforcement learning for 5g networks: Joint beamforming, power control, and interference coordination. *IEEE Transactions on Communications*, 2019.
- [60] Volodymyr Mnih, Koray Kavukcuoglu, David Silver, Andrei A Rusu, Joel Veness, Marc G Bellemare, Alex Graves, Martin Riedmiller, Andreas K Fidjeland, Georg Ostrovski, et al. Human-level control through deep reinforcement learning. *Nature*, 518(7540):529–533, 2015.
- [61] Jianhua Mo, Ahmed Alkhateeb, Shadi Abu-Surra, and Robert W Heath. Hybrid architectures with few-bit ADC receivers: Achievable rates and energy-rate tradeoffs. *IEEE Trans. Wireless Commun.*, 16(4):2274–2287, 2017.
- [62] Jianhua Mo and Robert W Heath. Capacity analysis of one-bit quantized MIMO systems with transmitter channel state information. *IEEE Trans. Signal Process.*, 63(20):5498–5512, 2015.



- [63] Christopher Mollén, Junil Choi, Erik G Larsson, and Robert W Heath Jr. Uplink Performance of Wideband Massive MIMO With One-Bit ADCs. *IEEE Trans. Wireless Commun.*, 16(1):87–100, 2017.
- [64] Peter Neuhaus, Martin Schlüter, Christoph Jans, Meik Dörpinghaus, and Gerhard Fettweis. Enabling energy-efficient tbit/s communications by 1-bit quantization and oversampling. In *2021 Joint European Conference on Networks and Communications & 6G Summit (EuCNC/6G Summit)*, pages 84–89. IEEE, 2021.
- [65] Boon Loong Ng, Jamie S Evans, Stephen V Hanly, and Defne Aktas. Distributed downlink beamforming with cooperative base stations. *IEEE Trans. Inform. Theory*, 54(12):5491–5499, 2008.
- [66] Hien Quoc Ngo, Erik G Larsson, and Thomas L Marzetta. Energy and spectral efficiency of very large multiuser MIMO systems. *IEEE Trans. Commun.*, 61(4):1436–1449, 2013.
- [67] Ly V Nguyen, A Lee Swindlehurst, and Duy HN Nguyen. Linear and deep neural network-based receivers for massive mimo systems with one-bit adcs. *IEEE Trans. Wireless Commun.*, 20(11):7333–7345, 2021.
- [68] Ly V Nguyen, A Lee Swindlehurst, and Duy HN Nguyen. Svm-based channel estimation and data detection for one-bit massive mimo systems. *IEEE Trans. Signal Processing*, 69:2086–2099, 2021.

- [69] Oner Orhan, Elza Erkip, and Sundeep Rangan. Low power analog-to-digital conversion in millimeter wave systems: Impact of resolution and bandwidth on performance. In *IEEE Info. Theory and Appl. Work.*, pages 191–198, February 2015.
- [70] Jinsung Park, Namyoon Lee, Song-Nam Hong, and Yo-Seb Jeon. Learning from noisy labels for mimo detection with one-bit adcs. *IEEE Wireless Communications Letters*, 12(3):456–460, 2023.
- [71] Sungyeal Park, Yunseong Cho, and Songnam Hong. Construction of 1-bit transmit signal vectors for downlink mu-miso systems: Qam constellations. *IEEE Trans. Vehicular Tech.*, 70(10):10065–10076, 2021.
- [72] Shubham Pateria, Budhitama Subagdja, Ah-hwee Tan, and Chai Quek. Hierarchical reinforcement learning: A comprehensive survey. *ACM Computing Surveys (CSUR)*, 54(5):1–35, 2021.
- [73] Ture Peken, Sudarshan Adiga, Ravi Tandon, and Tamal Bose. Deep learning for svd and hybrid beamforming. *IEEE Transactions on Wireless Communications*, 19(10):6621–6642, 2020.
- [74] Zhouyue Pi and Farooq Khan. An introduction to millimeter-wave mobile broadband systems. *IEEE Commun. Mag.*, 49(6), 2011.
- [75] Theodore S Rappaport, Shu Sun, Rimma Mayzus, Hang Zhao, Yaniv Azar, Kevin Wang, George N Wong, Jocelyn K Schulz, Mathew Samimi,

- and Felix Gutierrez. Millimeter wave mobile communications for 5G cellular: It will work! *IEEE Access*, 1:335–349, May 2013.
- [76] Farrokh Rashid-Farrokhi, KJ Ray Liu, and Leandros Tassiulas. Transmit beamforming and power control for cellular wireless systems. *IEEE J. Sel. Areas in Commun.*, 16(8):1437–1450, 1998.
- [77] Farrokh Rashid-Farrokhi, Leandros Tassiulas, and KJ Ray Liu. Joint optimal power control and beamforming in wireless networks using antenna arrays. *IEEE Trans. Commun.*, 46(10):1313–1324, 1998.
- [78] Lucas N Ribeiro, Stefan Schwarz, Markus Rupp, and André LF de Almeida. Energy efficiency of mmWave massive MIMO precoding with low-resolution DACs. *IEEE J. of Sel. Topics in Signal Process.*, 12(2):298–312, 2018.
- [79] Walid Saad, Mehdi Bennis, and Mingzhe Chen. A vision of 6G wireless systems: Applications, trends, technologies, and open research problems. *IEEE Network*, 34(3):134–142, 2019.
- [80] Amichai Sanderovich, Oren Somekh, and Shlomo Shamai. Uplink macro diversity with limited backhaul capacity. In *IEEE Int. Symp. Info. Theory*, pages 11–15, 2007.
- [81] Philipp Schulz, Andreas Traßl, André Noll Barreto, and Gerhard Fettweis. Efficient and reliable wireless communications via multi-connectivity using rateless codes in single-and multi-user scenarios. *IEEE Transactions on Wireless Communications*, 20(9):5714–5729, 2021.

- [82] Rubayet Shafin, Hao Chen, Young Han Nam, Sooyoung Hur, Jeongho Park, Jianzhong Zhang, Jeffrey Reed, and Lingjia Liu. Self-tuning sectorization: Deep reinforcement learning meets broadcast beam optimization. *IEEE Transactions on Wireless Communications*, 2020.
- [83] Mingjie Shao, Qiang Li, Wing-Kin Ma, and Anthony Man-Cho So. A framework for one-bit and constant-envelope precoding over multiuser massive MISO channels. *IEEE Trans. on Signal Process.*, 67(20):5309–5324, 2019.
- [84] Zhichao Shao, Rodrigo C de Lamare, and Lukas TN Landau. Iterative detection and decoding for large-scale multiple-antenna systems with 1-bit adcs. *IEEE Wireless Commun. Letters*, 7(3):476–479, 2017.
- [85] W. Shin, M. Vaezi, B. Lee, D. J. Love, J. Lee, and H. V. Poor. Coordinated beamforming for multi-cell MIMO-NOMA. *IEEE Commun. Lett.*, 21(1):84–87, 2017.
- [86] Foad Sohrabi and Wei Yu. Hybrid digital and analog beamforming design for large-scale antenna arrays. *IEEE Journal of Selected Topics in Signal Processing*, 10(3):501–513, 2016.
- [87] Bongyong Song, Rene L Cruz, and Bhaskar D Rao. Network duality for multiuser MIMO beamforming networks and applications. *IEEE Trans. Commun.*, 55(3):618–630, 2007.

- [88] Rickard Stridh, Mats Bengtsson, and Björn Ottersten. System evaluation of optimal downlink beamforming with congestion control in wireless communication. *IEEE Trans. Wireless Commun.*, 5(4):743–751, 2006.
- [89] Christoph Studer and Giuseppe Durisi. Quantized massive mu-mimo-ofdm uplink. *IEEE Trans. Commun.*, 64(6):2387–2399, 2016.
- [90] Richard S Sutton and Andrew G Barto. *Reinforcement learning: An introduction*. MIT press, 2018.
- [91] Lee A. Swindlehurst, Ender Ayanoglu, Payam Heydari, and Filippo Capolino. Millimeter-wave massive MIMO: The next wireless revolution? *IEEE Commun. Mag.*, 52(9):56–62, Sep. 2014.
- [92] David Tse and Pramod Viswanath. *Fundamentals of wireless communication*. Cambridge university press, 2005.
- [93] Aleksandr Vasjanov and Vaidotas Barzdenas. A review of advanced cmos rf power amplifier architecture trends for low power 5g wireless networks. *Electronics*, 7(11):271, 2018.
- [94] Robert H Walden. Analog-to-digital converter survey and analysis. *IEEE Journal on selected areas in communications*, 17(4):539–550, 1999.
- [95] C. Wang, C. Wen, S. Jin, and S. Tsai. Finite-alphabet precoding for massive MU-MIMO With low-resolution DACs. *IEEE Trans. Wireless Commun.*, 17(7):4706–4720, 2018.

- [96] Cheng Wang and Ross D Murch. Adaptive downlink multi-user mimo wireless systems for correlated channels with imperfect csi. *IEEE Trans. Wireless Comm.*, 5(9):2435–2446, 2006.
- [97] Hanqing Wang, Wan-Ting Shih, Chao-Kai Wen, and Shi Jin. Reliable OFDM receiver with ultra-low resolution ADC. *IEEE Trans. Commun.*, 67(5):3566–3579, 2019.
- [98] Hanqing Wang, Chao-Kai Wen, and Shi Jin. Bayesian optimal data detector for mmWave OFDM system with low-resolution ADC. *IEEE J. Sel. Areas in Commun.*, 35(9):1962–1979, 2017.
- [99] Shengchu Wang, Yunzhou Li, and Jing Wang. Multiuser detection in massive spatial modulation MIMO with low-resolution ADCs. *IEEE Trans. Wireless Commun.*, 14(4):2156–2168, 2014.
- [100] Shengchu Wang, Yunzhou Li, and Jing Wang. Multiuser detection in massive spatial modulation MIMO with low-resolution ADCs. *IEEE Trans. Wireless Commun.*, 14(4):2156–2168, 2015.
- [101] Chao-Kai Wen, Chang-Jen Wang, Shi Jin, Kai-Kit Wong, and Pagan Ting. Bayes-optimal joint channel-and-data estimation for massive MIMO with low-precision ADCs. *IEEE Trans. Signal Process.*, 64(10):2541–2556, 2016.
- [102] Ami Wiesel, Yonina C Eldar, and Shlomo Shamai. Linear precoding via conic optimization for fixed MIMO receivers. *IEEE Trans. Signal*

- Process.*, 54(1):161–176, 2005.
- [103] J. Xu, W. Xu, J. Zhu, D. W. K. Ng, and A. Lee Swindlehurst. Secure massive MIMO communication With low-resolution DACs. *IEEE Trans. Commun.*, 67(5):3265–3278, 2019.
- [104] L. Xu, X. Lu, S. Jin, F. Gao, and Y. Zhu. On the uplink achievable rate of massive MIMO system with low-resolution ADC and RF impairments. *IEEE Commun. Lett.*, 23(3):502–505, March 2019.
- [105] Roy D. Yates. A framework for uplink power control in cellular radio systems. *IEEE J. Sel. Areas in Commun.*, 13(7):1341–1347, 1995.
- [106] Wei Yu and Tian Lan. Transmitter optimization for the multi-antenna downlink with per-antenna power constraints. *IEEE Trans. Signal process.*, 55(6):2646–2660, 2007.
- [107] Jide Yuan, Qi He, Michail Matthaiou, Tony Q. S. Quek, and Shi Jin. Toward Massive Connectivity for IoT in Mixed-ADC Distributed Massive MIMO. *IEEE Internet of Things Journal*, 7(3):1841–1856, 2020.
- [108] J. Zhang, L. Dai, Z. He, B. Ai, and O. A. Dobre. Mixed-ADC/DAC multipair massive MIMO relaying systems: Performance analysis and power optimization. *IEEE Trans. Commun.*, 67(1):140–153, 2019.
- [109] Jiayi Zhang, Linglong Dai, Ziyang He, Bo Ai, and Octavia A Dobre. Mixed-adc/dac multipair massive mimo relaying systems: Performance

- analysis and power optimization. *IEEE Trans. Commun.*, 67(1):140–153, 2018.
- [110] Ti-Cao Zhang, Chao-Kai Wen, Shi Jin, and Tao Jiang. Mixed-ADC massive MIMO detectors: Performance analysis and design optimization. *IEEE Trans. Wireless Commun.*, 15(11):7738–7752, 2016.
- [111] Yu Zhang, Muhammad Alrabeiah, and Ahmed Alkhateeb. Deep learning for massive mimo with 1-bit adcs: When more antennas need fewer pilots. *IEEE Wireless Commun. Letters*, 9(8):1273–1277, 2020.
- [112] Yu Zhang, Muhammad Alrabeiah, and Ahmed Alkhateeb. Reinforcement learning of beam codebooks in millimeter wave and terahertz mimo systems. *IEEE Transactions on Communications*, 70(2):904–919, 2022.



# Vita

Yunseong Cho received his B.S. degree in Electrical and Computer Engineering from Ajou University, South Korea in 2018 and his M.S. degree in Electrical and Computer Engineering from the University of Texas at Austin in 2020. He is now pursuing a Ph.D. degree in Electrical and Computer Engineering at the University of Texas at Austin under the supervision of Prof. Brian L. Evans. He is a member of the Embedded Signal Processing Laboratory (ESPL), Wireless Networking and Communications Group (WNCG), and 6G@UT. He completed four internships at Futurewei Technologies, Mavenir, Qualcomm, and Nvidia in 2019, 2020, 2021, and 2022, respectively. His research focuses on massive MIMO, low-resolution data converters, and machine learning approaches for wireless communication systems.

Permanent address: 3367 Lake Austin Blvd. APT C  
Austin, Texas 78703  
yscho@utexas.edu

This dissertation was typeset with  $\text{\LaTeX}^\dagger$  by the author.

---

<sup>†</sup> $\text{\LaTeX}$  is a document preparation system developed by Leslie Lamport as a special version of Donald Knuth's  $\text{\TeX}$  Program.